

Investigating the Relationship between Surface Water and Dengue Fever Incidence

A Case Study: Vientiane Capital, Laos

By

Palamy Changleuxai

Thesis

Submitted to Flinders University

for the degree of

Master of Geospatial Information Science

College of Science and Engineering

02 November 2019

CONTENTS

LIST OF FIGURES	V
LIST OF TABLES.....	VIII
LIST OF ACRONYMS	X
SUMMARY	XIII
DECLARATION.....	XIV
ACKNOWLEDGEMENTS.....	XV
CHAPTER ONE: INTRODUCTION AND LITERATURE REVIEW.....	1
1.1. Background of Study.....	1
1.2. The Association Between Water Bodies and Dengue Fever	2
1.2.1. Methods.....	2
1.2.2. Results.....	3
1.2.3. Discussion.....	13
1.2.4. Conclusion.....	15
1.3. Geographic Information System and Remote Sensing in Epidemiology	15
1.3.1. Remote Sensing Sensors.....	16
1.3.2. Remote Sensing used for Water Bodies Detection.....	18
1.3.3. Spectral Water Indices used for Water Bodies Extraction.....	20
1.4. Aims and Objectives	22
1.5. Research Questions.....	22
1.6. Hypothesis	22
1.7. Scope of the Study.....	22
1.8. Study Area	23
1.8.1. Dengue Incidence Situations.....	23
1.8.2. Location	24
CHAPTER TWO: RESEARCH METHODS.....	28
2.1. Ethics Approval.....	28
2.2. Data Collection.....	28
2.2.1. Image Dataset Selection for Surface Water Extraction.....	28

2.2.2. Dengue Incidence Data.....	40
2.2.3. Meteorological Data	41
2.3. Software Used	42
2.3.1. Earth Resource Data Analysis System (ERDAS) Imagine 2018.....	42
2.3.2. ArcGIS Version 10.6	42
2.3.3. Google Earth Pro	43
2.3.4. Statistical Package for the Social Sciences (SPSS)	43
2.4. Areas of Interest (AOI)	43
2.5. Image Correction	44
2.5.1. Atmospheric Correction.....	44
2.5.2. Haze Reduction	48
2.5.3. Cloud Masking	49
2.5.4. Mosaicking.....	51
2.6. Water Body Extraction	52
2.6.1. Multi-band Spectral Relationship Method.....	53
2.6.2. Normalized Difference Vegetation Index (NDVI)	54
2.6.3. Normalized Difference Water Index (NDWI).....	55
2.6.4. Normalized Difference Moisture Index (NDMI)	56
2.6.5. Threshold Values	57
2.7. Post-Image Analysis	58
2.8. Accuracy Assessment.....	59
2.9. Association of Surface Water and Dengue Incidence.....	61
2.9.1. Spatial Distribution of Dengue Cases.....	61
2.9.2. Analysis of Dengue Incidence Associated with Water Bodies	63
CHAPTER THREE: RESULTS.....	67
3.1. Pre-processing of Image Analysis.....	67
3.1.1. Atmospheric Correction.....	67
3.1.2. Haze Reduction	71
3.1.3 Cloud Masking	73
3.2. Surface Water Extraction	74

3.2.1. Multi-band Spectral Relationship Method	74
3.2.2. Normalized Difference Vegetation Index (NDVI)	75
3.2.3. Normalized Difference Water Index (NDWI) and Normalized Moisture Index (NDMI)	77
3.3. Accuracy Assessment.....	81
3.4. Association between Surface Water and Dengue Incidence	82
3.4.1. The Spatial Distribution of Dengue Cases	82
3.4.2. Analysis of Dengue Incidence Associated with Surface Water	84
CHAPTER FOUR: DISCUSSION AND CONCLUSION	90
4.1. Analysis of Dengue Fever Occurrence	90
4.1.1. Spatial Distribution of Dengue Incidence	90
4.1.2. Analysis of the Association of Dengue Incidence and Water Bodies	92
4.1.3. Analysis of the Association between Dengue Incidence and Rainfall	94
4.2. Image Correction	94
4.2.1. Atmospheric Correction.....	94
4.2.2. Haze Reduction	96
4.2.3. Cloud Removal	97
4.3. Surface Water Extraction	98
4.3.1. Normalized Difference Water Index (NDWI)	98
4.3.2. Normalized Difference Moisture Index (NDMI)	99
4.3.3. Optimum Thresholds for Indices Methods	100
4.4. Accuracy Assessment.....	101
4.5. Factors affecting Surface Water Results	102
4.6. Aspects to be Considered When Applying RS and GIS in Dengue Epidemic	104
4.7. Limitations.....	106
4.8. Areas of Further Investigation	107
4.9. Conclusion	107
4.9.1. Key Findings	107
4.9.2. Recommendation	108
REFERENCE LIST	110
APPENDICES	124

Appendix 1: Field Survey Collection Data.....	124
Appendix 2: Survey 123 ArcGIS Form used for field surveying.....	124
Appendix 3: Surveillance System, Institut Pasteur du Laos	125
Appendix 4: Georeferenced Points of Dengue Incidence.....	126
Appendix 5: Ground Reference	134
Appendix 6: Average Nearest Neighbour Summary	145
Appendix 7: Rainfall Data 2017	146

LIST OF FIGURES

Figure 1.1: Active and Passive Remote Sensors.....	17
Figure 1.2: Electromagnetic spectrum.....	17
Figure 1.3: <i>Aedes aegypti</i> and <i>Aedes albopictus</i> adults collected in the Centre of Vientiane	24
Figure 1.4: Vientiane Capital classified by urbanised regions.....	25
Figure 1.5: Dengue Incidence in 2017.....	26
Figure 1.6: Current Dengue Epidemic (29/12/2018 to 01/07/2019) by Province	27
Figure 2.1: Flowchart method process of extracting surface water data.....	29
Figure 2.2: Sentinel-2 MSI in true-colour composite with radiometry adjust—Equalised Percentage (March 2018-left) and Histogram Equalisation (October 2018-right).....	31
Figure 2.3: Either/Or Function used in Spatial Model	31
Figure 2.4: Cloud removal model	32
Figure 2.5: Cloud masked image in March 2018 displayed in true-colour composite.....	32
Figure 2.6: Original image of SAR from amplitude VV (left) and VH (right).....	34
Figure 2.7: Red, Green, Blue image channels.....	35
Figure 2.8: A combination of VH-dB, VH-dB, VV-dB Lee filter 3x3 (left) and 5x5 (right) displayed in RGB.....	35
Figure 2.9: Ground point data collected from Survey 123 overlaid on Open Street Map.....	37
Figure 2.10: Monthly precipitation data from 2016 to 2018.....	42
Figure 2.11: Area of interest and dengue incidence in the study site overlaid on PlanetScope image in January displayed in true-colour composite.....	44
Figure 2.12: Spectral radiance at the Earth’s surface	45
Figure 2.13: Spatial model of atmospheric correction to obtain TOA reflectance.....	47
Figure 2.14: Spatial model of dark object subtraction to obtain BOA.....	47
Figure 2.15: Atmospheric correction spatial model used to correct atmospheric effect on RapidEye	48
Figure 2.16: 5 x 5 Convolution Kernel	49
Figure 2.17: Haze reduction spatial model	49
Figure 2.18: Spatial model for cloud and shadow masking multiplied with image data	50

Figure 2.19: Spatial model for cloud masking image obtained from a single band threshold method	50
Figure 2.20: Combining cloud masked binary image produced from classification method with the cloud mask image from a single band threshold method.....	51
Figure 2.21: PlanetScope image tiles displayed in true-colour composite	51
Figure 2.22: RapidEye image tiles displayed in true-colour composite	52
Figure 2.23: PlanetScope spectral profile.....	53
Figure 2.24: RapidEye spectral profile	53
Figure 2.25: Spatial model of multi-band spectral relationship method.....	54
Figure 2.26: NDVI spatial model	55
Figure 2.27: NDWI spatial model	56
Figure 2.28: NDMI spatial model.....	57
Figure 2.29: Spectral histogram	57
Figure 2.30: Conditional function used to classify surface and non-surface water	58
Figure 2.31: Reclassify function	59
Figure 2.32: Extract by Mask	59
Figure 2.33: An illustration of data distribution pattern.....	62
Figure 2.34: Average Nearest Neighbour analysis	63
Figure 2.35: <i>Aedes</i> mosquito life cycle.....	64
Figure 2.36: The estimated time of patients contracting the disease (Lg2), and the estimated time of mosquitoes developing into adults (Lag1) based on the onset time.....	64
Figure 3.1: Histogram showing data values for January images in band 1 (Blue) with non-atmospheric correction (left) and with atmospheric correction (right).....	68
Figure 3.2: Histogram showing data values for January images in band 4 (NIR) with non-atmospheric correction (left) and with atmospheric correction (right).....	68
Figure 3.3: Water areas spots for pixel values inspection.....	70
Figure 3.4: Histograms showing the minimum and maximum values of Blue band, before the correction (a), and after the correction (b); and NIR band, before the correction (c), and after the correction (d).....	71
Figure 3.5: PlanetScope image in February before haze reduction (a) and after haze reduction (b) displayed in false-colour composite (RGB: band 4, band 3, band 2)	72

Figure 3.6: Cloud masking image from unsupervised classification (a), a single band threshold (b) and the combination of classification and a single band threshold methods (c) displayed in true-colour composite.....	74
Figure 3.7: Multi-band spectral relationship method compared with NDWI and NDMI.....	75
Figure 3.8: PlanetScope image (a) displayed in false-colour (RGB: 4,3,2), and indices of vegetation (b), moisture (c), and water (d) images displayed in the same colour ramp.....	76
Figure 3.9: Comparison of NDVI (a) and NDMI (b) used to extract water features	77
Figure 3.10: Surface water extraction from NDWI and NDMI	79
Figure 3.11: NDWI and NDMI results displayed in stretched colour ramp	80
Figure 3.12: Surface water extraction in percentage	81
Figure 3.13: Frequency of dengue incidence spread in Easting	82
Figure 3.14: Frequency of dengue incidence spread in Northing.....	82
Figure 3.15: Dengue incidence compared with rainfall	84
Figure 3.16: Dengue incidence compared with surface water	85
Figure 3.17: Surface water compared with Lag2 counts.....	85
Figure 3.18: Surface water compared with Lag1 counts.....	86
Figure 3.19: Surface water compared with <i>Aedes</i> mosquito population	86
Figure 4.1: Study area by number of populations.....	91
Figure 4.2: Population density per square kilometre.....	92
Figure 4.3: The effects of cloud and shadow removal on other ground surface features, PlanetScope displayed in true-colour composite.....	98
Figure 4.4: Ground reference on aerial imagery, Google Earth Pro, displayed in true-colour composite	102
Figure 4.5: PlanetScope displayed in false-colour (RGB: 4,3,2), (a) shows water channel blocked by vegetation, and (b) small stream mixed with vegetation	103
Figure 4.6: Rainfall data in 2017	104
Figure 4.7: Dengue incidence in 2014 to 2018.....	105

LIST OF TABLES

Table 1.1: Search results from PubMed and Web of Science databases	4
Table 1.2: Characteristics of studies on association of dengue fever, dengue haemorrhagic fever with water bodies	4
Table 1.3: Major regions of the electromagnetic spectrum	18
Table 1.4: Common water indices used to extract water features	21
Table 2.1: Sentinel-2 satellite sensor specifications	30
Table 2.2: Sentinel-2 MSI image dataset	31
Table 2.3: Sentinel-1C band, Interferometric Wide swath mode nominal measurement modes	33
Table 2.4: PlanetScope 3B analytic ortho tile product attributes	38
Table 2.5: RapidEye analytic ortho tile products attribute	39
Table 2.6: PlanetScope and RapidEye sensor specifications	39
Table 2.7: Image datasets used in this study	40
Table 2.8: Reflectance coefficient of 04 January and 16 January 2017	46
Table 2.9: Variation observation	60
Table 2.10: Interpretation of Kappa coefficient	61
Table 2.11: Sample datasets	65
Table 2.12: Range of strength relationship and squared correlation	66
Table 3.1: Statistical values of NDWI and water values obtained from TOA and non-TOA	68
Table 3.2: Dark pixel values used for dark object subtraction	69
Table 3.3: Statistical information of PlanetScope satellite image derived from DOS	69
Table 3.4: Statistical values of NDWI with non-DOS and with DOS and water pixel values	70
Table 3.5: Statistical values of NDWI before and after Rapid atmospheric correction	71
Table 3.6: Statistical information for February image data	72
Table 3.7: NDWI statistical values of non-haze and haze reduction images in February	73
Table 3.8: NDWI, NDMI Statistical information before and after de-haze of RapidEye image	73
Table 3.9: Threshold values used to detect cloud and shadow	74
Table 3.10: Statistical information for NDVI, NDWI, NDMI, and optimal threshold values	75

Table 3.11: Threshold values used to extract surface water from water index images	77
Table 3.12: Confusion matrix derived from Kappa statistics	81
Table 3.13: F-Test two-sample for variances	83
Table 3.14: Average Nearest Neighbour analysis information	83
Table 3.15: Spearman' s correlation coefficient analysis	87
Table 3.16: Association between lag1 counts and surface water and rainfall from Multivariate Linear Regression.....	88
Table 3.17: Association between lag2 counts and surface water and rainfall from Multivariate Linear Regression.....	88
Table 3.18: Association between <i>Aedes</i> mosquito counts and surface water, rainfall, and lag1 counts from Multivariate Linear Regression	88

LIST OF ACRONYMS

μm	Micrometre
<i>A. aegypti</i>	<i>Aedes aegypti</i>
<i>A. albopictus</i>	<i>Aedes albopictus</i>
AVHRR	Advanced Very High-Resolution Radiometer
ANN	Average Nearest Neighbour
AOI	Area of Interest
AWEI	Automated Water Extraction Index
BOA	Bottom of Atmosphere
dB	Decibel
DEM	Digital Elevation Model
DF	Dengue Fever
DHF	Dengue Haemorrhagic Fever
DN	Digital Number
DOS	Dark Object Subtraction
ECOMORE	Economic development, Ecosystem Modifications, and emerging infectious diseases Risk Evaluation
ERDAS	Earth Resource Data Analysis System
ESA	European Space Agency
ESRI	Environmental System Research Institute
EW	Extra Wide
GCP	Ground Control Point
GDP	Gross Domestic Product
GHz	Gigahertz
GIS	Geographic Information System
GPS	Global Positioning System
GRD	Ground Range Detected
HH	Horizontal transmit, Horizontal receive

HV	Horizontal transmit, Vertical receive
IBM	International Business Machines
ID	Identification
IPL	Institut Pasteur du Laos
IW	Interferometric Wide
KAP	Knowledge, Attitudes and Practices
MIR	Mid-Infrared
mm	Millimetre
MNDWI	Modified Normalized Difference Water Index
MoNRE	Ministry of Natural Resource and Environment
MSI	Multispectral Instrument
NCLE	National Centre of Lab and Epidemiology
NDMI	Normalized Difference Moisture Index
NDPI	Normalized Difference Pond Index
NDVI	Normalized Difference Vegetation Index
NDWI	Normalized Difference Water Index
NIR	Near-Infrared
nm	Nanometre
NOAA	National Oceanic and Atmosphere Administration
NS	Non-Structural
OA	Overall Accuracy
PA	Producer Accuracy
Pacs	Pathogen Asset Control System
PCA	Principal Component Analysis
RADAR	Radio Detection and Ranging
RGB	Red, Green, Blue
RMES	Root Mean Square Error
RS	Remote Sensing
RT-PCR	Reverse Transcription Polymerase Chain Reaction

SAR	Synthetic Aperture Radar
SBREC	Social and Behavioural Research Ethics Committee
SLC	Single Look Complex
SM	Strip Map
SNAP	Sentinel Application Platform
SPOT	Satellite Pour l'Observation de la Terre
SPSS	Statistical Package for the Social Sciences
SRTM	Shuttle Radar Topography Mission
Std.Dev	Standard Deviation
SWIR	Short-Wave Infrared
TCT	Tasselled Cap Transformation
TM	Thematic Mapper
TOA	Top of Atmosphere
UA	User Accuracy
UTM	Universal Transverse Mercator
VH	Vertical transmit, Horizontal receive
VV	Vertical transmit, Vertical receive
WGS	World Geodetic System
WHO	World Health Organization
WV	Wave

SUMMARY

Dengue fever is a mosquito-borne disease caused by the dengue virus, with a high global incidence. More than 70 % of the world's population are living in areas that are vulnerable to dengue fever, and most of them are in tropical regions. One of the most affected regions is Southeast Asia, where cases of dengue fever and deaths associated with dengue fever account for 40% of global reported dengue fever cases (data from 2010 to 2013). Vientiane, the capital of Laos, has a long history of dengue disease, with the first report of dengue fever in 1983, and large outbreaks recorded in 1985, 1987, 1995, 1996, 1998, 2003, 2010, 2013, 2017 and the present (2019), with over 1,000 cases. The emergence of this increasing incidence is presumably associated with several factors, one of them is likely to be surface water, including both artificial and natural water bodies. Water bodies act as an important component in the number of dengue mosquitos – *Aedes aegypti*, and *Aedes albopictus*. Several previous studies have found that water bodies, a vector breeding site, tend to result in dengue mosquito proliferation under favourable conditions of temperature and rainfall. Vientiane is a mix of urban and rural areas and is surrounded by plenty of standing water and streams. During rainy seasons, many areas encounter poor water drainage, and this has caused marshland development. Given the nature of dengue disease mosquito vectors, small surface water bodies are likely to facilitate the expansion of mosquito populations.

In this study, freely available satellites images were used to derive surface water throughout the year 2017. Before selecting the suitable images, a process of selecting satellite imageries was conducted. Sentinel-1 SAR, Sentinel-2, PlanetScope, and RapidEye were assessed. A field survey was also conducted in order to observe the sites within the study area, focusing on water body size and vectors breeding sites. Three main datasets were used in this project; the satellite imageries – PlanetScope, and RapidEye, dengue incidence in 2017, and rainfall data. Surface water extraction, normalized difference water index (NDWI), and normalized difference moisture index (NDMI) were the main methods used to detect water areas.

To determine the relationship between surface water and dengue incidence, Spearman correlation and regression was used. As surface water acts as the breeding habitats for the dengue virus carriers, expected mosquito life development time was defined from the onset date of dengue fever symptoms. Estimated surface water extracted from satellite images showed a relationship with dengue incidence, at significant level, but many aspects may need to be considered. Rainfall data was also compared with dengue incidence and showed a positive correlation with the disease cases, however surface water and rainfall were found not to associate with dengue vector populations.

DECLARATION

I, Palamy Changleuxai, declare that this thesis is produced by my best efforts under supervision of my supervisors. All previous studies, and data that have been used as the reference in this research project have been well acknowledged. I certify that this thesis does not incorporate without acknowledgement any material previously submitted for a degree or diploma in any university, and it does not contain any material previously published or written by another person except where due reference has been made in the text.

Signature Palamy Changleuxai

Date 31 October 2019

ACKNOWLEDGEMENTS

Many special individuals and institutes have contributed to this work along the pathway to completion. First of all, I would like to express my sincere gratitude to my supervisors Dr. Kirstin Ross, Professor Richard Woodman, and Mr. Rob Keane of Flinders University, who kindly guided me from the beginning of the research project until the completed stage. Their efforts in assisting me to complete this thesis were an enormous help and a great support, if it is not because of their guidance, this thesis would never be accomplished.

I must thank Ms. Clare Pollock, a GIS and RS tutor, and a student of Master of Geospatial Information Science, Flinders University for her kindness in helping me with accessing the satellite image data needed to be used in this research project when my quota of image download was limited.

Other persons I must never forget to acknowledge are Dr. Paul Brey, the director of Institut Pasteur du Laos (IPL) for giving me a great opportunity to work with the laboratory teams – Arbovirus and Emerging viral disease, and Medical Entomology and Biology of disease vectors.

A special thanks to ECOMORE 2 project, IPL for allowing me to use data which was necessary for this project, and for inviting me to present my research in the National Stakeholder Conference held on 29 November 2019. This great opportunity fulfils my intention of coming here to Australia to gain new knowledge to make contributions to my communities, my home country.

My deep sincere thanks to Dr. Marc Grandadam, head of Arbovirus and Emerging viral disease lab, a co-supervisor of this project, who tirelessly explained and answered all the requests related to the emergence of dengue fever to me and helped broaden my understanding of the disease biodiversity. Importantly, I need to thank Ms. Somphavanh Somlor, a team member of the lab who assisted me during the processes of collecting and verifying dengue incidence data.

My thanks to Dr. Olivier Telle, and Dr. Marc Choisy, without their support of directing me in correcting dengue data used in this research project since the beginning, I would never be able to deal with the issues found in collecting spatial data of dengue cases. With this help, I was able to decide which data I should consider to be used in this research.

I would to also like to express my deep gratitude to Dr. Sebastien Marcombe, a head of Medical Entomology and Biology of disease vectors lab, as well as his team members, especially Ms. Phoutmany Thammavong who organised the field data collection with a demonstration of data collecting process.

My deepest appreciation goes to those who mentally supported me, and those who always stay next to me when I entered difficulties during my study time.

CHAPTER ONE: INTRODUCTION AND LITERATURE REVIEW

1.1. Background of Study

Dengue fever is an infectious disease transmitted to humans by mosquitoes (Ebi & Nealon 2016) that is spread around the world, especially in tropical and subtropical regions. According to the World Health Organization (2011) and Gubler (2011) more than 70% of the global population live in vulnerable regions and most are in tropical areas. From 2010 to 2013, it was reported that the number of cases of dengue fever had increased from 2.4 million to over 3 million people. This increase was seen primarily in three affected regions including the Americas, Southeast Asia, and the Western Pacific, under tropical climate (Murray, Quam & Wilder-Smith 2013). Around 1.3 million of those at risk are in the Southeast Asia (SEA) region (World Health Organization 2011).

The virus is carried by *Aedes aegypti* and *Aedes albopictus* female mosquitoes and transmitted by the mosquito biting an infected person and transmitting it to a healthy person. The *A. aegypti* is originally from Africa, while *A. albopictus* is from Asia, and they have, over 50 years, expanded their ranges through many ways. This includes increased transportation, human mobility and the rapid growth of urbanisation (Murray, Quam & Wilder-Smith 2013). There are two forms of the virus causing dengue 1) dengue fever (DF) and 2) dengue haemorrhagic fever (DHF) – which can develop severe symptoms (Derouich, Boutayeb & Twizell 2003). There are four types of dengue virus, or serotypes, DENV-1, -2, -3, and -4. These serotypes develop differently and have differing levels of severity. The recovery from infection by one of them provides lifelong immunity, however, the immunity will only be against such type not for other serotypes. Cross-immunity to the other type of serology could happen partially and temporally, but this secondary infection will heighten the risk of developing severe dengue (M Grandadam 2019, personal communication, 18 August). The virus stemmed from *Aedes mosquitoes* which is clinically more efficient than other mosquito vectors such as *A. albopictus* regarding the infectious symptoms and reactions on protection (World Health Organization 1986). Regarding factors influencing the distribution of dengue fever, climate, environment, and geographical aspects as well as population growth are likely to be critically associated with the disease occurrence. As the mosquito vector spreading dengue virus is climate dependent, the changes of climate, an increased average global temperature and humidity will increase the epidemic potential of dengue (Hales et al. 2002; Hii et al. 2009; Murray, Quam & Wilder-Smith 2013). Although it appears that the changes of climate would have an impact on dengue incidence, temperature and humidity which are the main drivers of disease incidence are varied due to topographical characteristic patterns. Geographical factors have an indirect influence (Hii et al. 2009) on temperature, precipitation and relative humidity which in turn impact on mosquito development. For instance, high humidity during rainy seasons facilitates longer mosquito survival and growth (Jetten & Focks 1997). Similarly, temperatures higher than 20°C provide favourable

conditions for *Aedes aegypti* mosquitoes (Gould 1998). Some studies also show that temperature, humidity, and precipitation provide appropriate conditions to the survival of mosquitoes (Banu et al. 2011; Murray, Quam & Wilder-Smith 2013). An example of this was a study of higher temperatures affecting dengue fever transmission in Taiwan. This study estimated that for every 1°C increase, the incidence of dengue fever transmission, especially in urban areas, could be up to 1.95 times (Wu et al. 2009). This is supported by a study that showed a relationship between higher temperature and higher population of mosquitoes at 28°C – 36°C (Nasir et al. 2017). In addition to climatic influence, the physical environment, such as land use and land cover are also considered as crucial variables for analysis of dengue occurrence (Nakhapakorn & Tripathi 2005).

Water bodies, including artificial and natural surface water, are one of physical environmental factors that play an important role in the spread of dengue. The areas that have reported an outbreak of dengue cases are likely to occur nearby water sources including rivers, streams, coastlines, lakes, ponds, and standing water bodies (Halstead et al. 1965; Hsueh, Lee & Beltz 2012; Nakhapakorn & Tripathi 2005; Qi et al. 2015; Raghavendra, Sharma & Dash 2008). Water bodies are breeding sites for mosquitoes to undergo part of their life cycle, from egg laying to hatching stage (Bowatte et al. 2013). With favourable conditions, including temperature, larval development in water takes a shorter time, and increases capacity to produce offspring (Githeko et al. 2000).

Examining the factors that influence the distribution of dengue fever by investigating the temperature and other environmental aspects might help predict the potential areas where an outbreak could happen (Wu et al. 2009). However, exploring the association of physical environment, land use/land cover types, especially surface water, and life cycle of mosquito vectors would help understand the vector's natural behaviour as it is regarded to be a critical indicator in epidemiology (Cheong, Leitão & Lakes 2014; Li et al. 2017; Nasir et al. 2017).

1.2. The Association Between Water Bodies and Dengue Fever

A systematic literature review was conducted in order to find out how water bodies and dengue incidence are correlated. This was divided into four sections which includes the method used to systematically search for the relevant literature and selection criteria, results of searching – study inclusion and the analysis of the relationship between water bodies and the vector, discussion, and conclusion.

1.2.1. Methods

Searching Strategy and Selection Criteria

PubMed and Web of Science databases were used to obtain studies on the association between dengue incidence and water bodies. The key words used to search for related studies were “dengue fever”, “dengue haemorrhagic fever”, “environment”, “tropical climate”, “water bodies”, “river”,

“stream”, “dam”, “physical environment”. The search focussed on two aspects. First, the studies reporting dengue cases that occurred near rivers or streams or other water bodies. Second, studies that emphasised water bodies or surface water as one of the influences on dengue incidence.

Selection Criteria

The search had no restrictions in geographical characteristics, but only English language and published journal articles were considered. In addition, reviews were included in the search, but for use in the discussion section of this paper only. The studies were limited to those published from 1960 until the present. The terms “dengue fever”, and “dengue haemorrhagic fever” were initially applied in the search system. However, using these terms, seemed to be too broad and plenty of irrelevant articles were selected as a result of that. Hence, to narrow the search to the specific field of interest, terms such as “physical environment”, “water bodies and streams”, “land-use/land-cover”, and “tropical climate” were added (Table 1.1).

The search was restricted by excluding studies of dengue fever, or dengue incidence that focussed on clinical aspects, serological examinations, surveillance, and vaccination. The articles which were written by reviewing and summarising related literature were not included since they were unlikely to provide sufficient information, such as the methods used in individual studies. However, some of them (Githeko et al. 2000; Morin, Com & Ernst 2013; Sutherst 2004; Tabachnick 2010) will be used as additional information to support the selected articles. The studies highlighting climatic factors were considered in this search as temperature and relative humidity are conditions that support an increase in mosquito populations.

1.2.2. Results

Study Inclusion

The search categories were divided into six different groups according to the terms used (as presented in Table 1.1). However, for the second to the fourth category; the focus is about surface water so that they were grouped together. The search found 148 articles related to dengue fever and dengue haemorrhagic fever in tropical climate regions in PubMed and Web of Science, with 26 identical articles. There were 81 articles (26 from PubMed, 55 from Web of Science) which contained the information on water bodies, rivers, and streams as the concerned aspects influencing dengue fever and dengue haemorrhagic fever, with nine similar articles. The articles highlighting physical environment, and land-use/land-cover as one of the factors contributing to dengue disease were found from PubMed (16) Web of Science (23).

Only 21 articles were selected out of these search results (see Table 1.2) as they cover all needed aspects such as tropical climate, the occurrence of dengue disease, physical environment, as well as types of land-use/land cover. The focus of these articles was their major findings which were

divided into two categories – dengue incidence in the regions where either surface water, rivers or streams are located, and the influence of dengue prevalence associated with climatic conditions such as precipitation, temperature and humidity. All articles in the final selection were published between 1965 and 2019. Five of the studies were in China, two each were in Sri Lanka, India, Malaysia, Taiwan, Thailand and Vietnam, and one each was in Indonesia, Pakistan, Cuba, and Australia.

Table 1.1: Search results from PubMed and Web of Science databases

Terms used	Results of search		
	PubMed	Web of Science	Similarity
Dengue fever, dengue haemorrhagic fever, tropical climate	59	89	26
Dengue fever, dengue haemorrhagic fever, water bodies	2	9	1
Dengue fever, dengue haemorrhagic fever, river	18	43	6
Dengue fever, dengue haemorrhagic fever, stream	6	3	2
Dengue fever, dengue haemorrhagic fever, physical environment	10	15	3
Dengue fever, dengue haemorrhagic fever, land-use/land-cover	6	8	3

Table 1.2: Characteristics of studies on association of dengue fever, dengue haemorrhagic fever with water bodies

Study	Location	Methods	Findings
Nakhapakorn and Tripathi (2005)	Thailand	Multiple regression Bayesian classifier	Built-up areas have the highest spatial risk factors for dengue. Agricultural areas were shown to have the second level of high risk. Water bodies showed a positive relationship with three districts, among those, only one district in which water bodies was determined by the authors of the study to present a significant risk.
Hsueh, Lee and Beltz (2012)	Taiwan	Weighted regression	Density of population has a stronger correlation with dengue fever than the comparison of the incidence with

Study	Location	Methods	Findings
		Moran's index	<p>population counts. In five years (2003 to 2007), the spatial distribution of dengue fever was different in each year.</p> <p>With the distance from DF cases to roads, the large majority of incidence was found within 1.0 km in 2004 and 2007. However, many cases occurred around 1.75 km away in 2006.</p> <p>About 75% of dengue incidence occurred within 1.5 km from a river. The greater the distance from roads and rivers, the smaller number of dengue fever cases was found.</p>
Raju and Sokhi (2008)	India	<p>Correlation and regression analysis</p> <p>Invert distance weighing (IDW) interpolation</p>	<p>Uncommon connections in urban area could limit the flight ranges of <i>Aedes aegypti</i>. The connectivity of the houses had a negative correlation with dengue incidence.</p> <p>Drainage where water is collected, and overflow of tank water in household sites are suitable sites for the <i>Aedes</i> to breed.</p>
Nasir et al. (2017)	Pakistan	<p>Logistic regression model</p> <p>Chi-square</p>	<p><i>Aedes aegypti</i> mosquitoes were collected from 810 water containers in urban and rural areas (83 sites). Population of the <i>Aedes aegypti</i> was found to be positive with high variation in the density of mosquitoes found in all seasons. 52.4% of total collected population in rainy season due to high temperature (28°C to 36°C), and high humidity up to 75%. In summer, 41.7% of total mosquitoes were found, while there was 5.9% in winter.</p> <p>Water quality had a significant influence on mosquito population density. They were found in turbid water (46.1%), turbid foul (33.8%), and clear and clear foul with 17.4% and 2.7% respectively. Most of the population was found in standing water (97.8%), while flowing water had only 2.2%.</p> <p>Abiotic factors (temperature and relative humidity) had a significant impact on <i>Aedes aegypti</i> population, as more rain fell, and more floods, increased relative humidity. This resulted in an increase of the population.</p>

Study	Location	Methods	Findings
			<p>Artificial containers were the major breeding habitats for <i>Aedes aegypti</i> mosquitoes as 44.8% were found in tyres, 37.8% in tanks and cans, while 17.4% of the total collected mosquitoes were found in water bodies, and none in natural tree holes.</p> <p>Most of the population of mosquitoes were found in urban areas (78.1%), the rest were found in rural areas (21.9%).</p> <p>The rainy season was shown to play a significant role in <i>Aedes aegypti</i> population dynamics compared with the summer time.</p>
Spiegel et al. (2007)	Cuba	Logistic regression Chi-square test	<p>Water pipe leaks, deposits of water as a result of uncovered tanks were not a significant risk factor of dengue incidence.</p> <p>Poor condition of houses was a highly significant risk factor – perhaps due to the accumulation of water leakages inside houses.</p>
Sirisena et al. (2017)	Sri Lanka	Autoregressive moving average (ARIMA) Correlation analysis R studio	<p>Dengue incidence was found in both wet and dry zones where there was a high human population number.</p> <p>An increase in the average rainfall had a positive correlation with dengue incidence, while temperature had no relationship with dengue incidence. Humidity was significantly correlated with the disease incidence.</p> <p>During heavy rain, there was not a strong correlation between dengue fever and rainfall, but when the rainfall decreased, and the area was flooded, there was a positive correlation.</p> <p>The occurrence of dengue fever was associated with water storage practices undertaken due to the scarcity of water.</p>
Schmidt et al. (2011)	Vietnam	Poisson regression— space-time scan statistics Ross-MacDonald model	<p>In rural areas, a high rate of dengue fever was also found – as high as in the urban areas. A high density of population in rural areas with lack of piped water supply experienced higher risk of dengue than in urban areas where there was adequate water supply.</p>

Study	Location	Methods	Findings
Bi et al. (1998)	China	Correlation and multiple linear regression analyses	<p>Higher incidence rates of dengue disease were associated with lower levels of precipitation, and with less inundation of farmland around the lake.</p> <p>Difference of water level in the Huai River was significantly correlated with the incidence rate.</p>
Angel and Joshi (2009)	India	Descriptive Analysis Mosquitoes collected from urban, rural, peri-urban, in which three zones were divided into desert, forest and river, semi-arid. All mosquitoes were subjected to the Indirect fluorescence antibody test (IFAT).	<p>In urban areas, desert zone showed highest mosquito infectivity (21.6%), while that was found 7.1% in forest and river area, and the least was in semi-arid area (3.2%).</p> <p>In rural areas, desert areas showed the highest natural infection in mosquitoes (25%) in semi-arid areas, it was 24.1%.</p> <p>In peri-urban areas, one of total mosquitoes (11) collected in this area showed positive IFA test in desert area, and no mosquito infectivity was found in the non-desert area.</p>
Qi et al. (2015)	China	Generalized additive model (GAM) Spline smooth	<p>Dengue incidence was clustered in the middle of the area of interest (Pearl River Delta economic zone).</p> <p>DF incidence showed a significant positive correlation with boundary, and urban and rural areas in study areas, which indicated an association of dengue fever with people living in urban areas.</p> <p>Population density with 30,000 to 40,000 people per square kilometre was found to have lower risk than areas with higher or lower population densities.</p> <p>Road density and risk of dengue fever were positive correlated, which indicated that high accessibility can increase the incidence.</p> <p>The increase of normalized difference vegetation index values showed a decline in risk of dengue fever.</p> <p>Higher GDP per capita appeared to be related to lower risk of dengue occurrence, while lower GDP in poorer areas was related to high risk of dengue infection</p>

Study	Location	Methods	Findings
Zheng et al. (2019)	China	Generalized additive model (GAM)	<p>Socioeconomic and environmental factors were tested and compared in two regions, and it was found that socioeconomic factors such as population, and urban land ratio showed the largest variance in regional epidemics.</p> <p>Normalized difference vegetation index (NDVI), and temperature as environmental factors showed a slight difference of variance compared with socioeconomic factors.</p> <p>Dengue fever was more severe in areas with temperatures greater than 17.8°C, at moderate level of rainfall of 170 to 190 mm, or water bodies with ratio of approximately 0.15 to 0.2.</p>
Wijayanti et al. (2016)	Indonesia	Bayesian Poisson spatial analysis	<p>Employment and education level in each village showed a positive correlation with the risk of dengue fever.</p> <p>Distance to hospital was negatively correlated to the risk of dengue cases.</p> <p>The increase of dengue infection risk was up to 28% in the area with temperature at night time between 10°C and 15°C, and that increased by 64% in the areas with night temperatures below 10°C.</p> <p>Urban areas contained breeding sites for mosquitoes like buckets, water storage containers, traditional bath tubs.</p> <p>Rural areas, in this study, showed comparable numbers of adult <i>Aedes aegypti</i> during the rainy season.</p>
Shang et al. (2010)	Taiwan	Logistic and Poisson regression model	<p>Lower rainfall and relative humidity were significantly related to dengue cases.</p> <p>Drier conditions may facilitate dengue transmission due to an increase of water storage behaviour, this results in creating breeding sites for mosquitoes <i>Aedes aegypti</i>, particularly in the areas without a reliable water supply.</p>
Li et al. (2017)	China	Meta-analysis Correlation analysis	Dengue incidence and weather factors such as temperature, humidity, and rainfall show different lagged relationships.

Study	Location	Methods	Findings
		Generalized additive model (GAM)	<p>It was found that mean temperature, maximum temperature, and minimum temperature at lags of 0-3 months had positive correlations with monthly dengue occurrence.</p> <p>Mean relative humidity and precipitation were strongly correlated with dengue fever cases but not significant.</p> <p>Dengue fever cases were shown to be higher, which was assumed to be due to the construction project of the artificial lake in the study site. Since this project was implemented, water areas in the city have been expanded.</p>
Tian et al. (2016)	China	Bayesian Markov Chain Monte Carlo	<p>Mosquito population sizes may vary according to water areas, especially the larger water area may lead to higher virus relative diversity.</p> <p>Surface water areas and dengue epidemics: the number of DF cases was found to be associated with the surface water as the study site had largest surface area in history, and a large dengue outbreak occurred.</p> <p>Rainfall significantly influenced surface water as heavy rainfall caused an increase of surface water.</p> <p>The lake construction project in the study site had disturbed the surface water. Although the amount of rainfall decreased, the surface water still increased.</p> <p>It was speculated that the larger surface water area could provide more breeding sites for <i>Aedes albopictus</i> mosquitoes, which possibly leads to a high chance of disease contact.</p>
Dickin, Schuster-Wallace and Elliott (2013)	Malaysia	Descriptive analysis – Water associated disease index (WADI)	<p>Each region in Malaysia has different patterns of dengue distribution. This is due to the changing climate patterns. For instance, the eastern coast of Malaysia had low exposure to dengue fever as it is affected by the monsoon season which brings heavy rain to the area. Heavy rainfall washed away mosquito breeding sites, while in drier months, moderate rainfall provides favourable conditions for</p>

Study	Location	Methods	Findings
			<p>mosquitoes to breed in so that large mosquito populations were found during this time.</p> <p>Low vulnerability of dengue fever was observed in areas with dense vegetation and forest as they are not favourable for <i>Aedes</i> vectors.</p> <p>Low temperature is not suitable for mosquitoes to survive.</p> <p>Water use and behaviour relate to the susceptibility to the disease as it can create sources for vector survival both indoors and outdoors.</p> <p>Regions without proper piped water supply showed high risk of dengue fever due to the need to store water.</p>
Tiong et al. (2015)	Malaysia	Spearman's rank order	For land cover type, large water bodies did not appear to influence dengue prevalence. Large water bodies were not suggested to be an indicator of dengue prevalence as most of them are located further away from human settlements.
Tun-Lin, Burkot and Kay (2000)	Queensland, Australia	Descriptive analysis	<p>Survival to adulthood of mosquitoes was found to be 88-98% of the total at 20-30°C, and that was reduced to 67% at 35°C, and to 23.5% at 15°C. All immature mosquitoes died at temperatures of 10°C and 40°C.</p> <p>Larval development was found to vary according to water temperature and water level.</p> <p>Food supply such as organic matter was an important component that affects the density of mosquito <i>Aedes aegypti</i>.</p>
Phuanukoonnon, Brough and Bryan (2006)	Thailand	Descriptive Analysis	<p>Water-holding bodies and volume and other characteristics of water like cleanliness were found to be significant impacts on the breeding sites of mosquitoes.</p> <p>Numbers of mosquitoes increased dramatically when water supply and electricity were available in the study areas. This leads to the successive use of water, which resulted in water disposal leading to ground surface water and drains which are favourable for mosquitoes.</p>

Study	Location	Methods	Findings
Bowatte et al. (2013)	Sri Lanka	ANOVA Analysis	<p>Water with tadpoles was favourable for mosquitoes to lay eggs as tadpoles provide food, while water with no tadpoles was found to have a smaller number of eggs.</p> <p>Hatching pattern of eggs found to be different in water with tadpoles and no tadpoles. Hatching percentage of mosquito eggs from water with no tadpoles was higher than that of in water with tadpoles. This indicates that female mosquitoes prefer to lay eggs in water with tadpoles, but during the hatching, the tadpoles destroyed larvae.</p> <p>For isolated water bodies it is suggested considering biological control such as tadpoles.</p>
Halstead et al. (1965)	Vietnam	Descriptive Analysis	<p>DF occurred in south Vietnam along the Mekong delta. This incidence was found in the area where there was a high population density despite the small size of villages. In addition, the effect of traffic between neighbouring countries such as Cambodia and Vietnam were suspected of assisting the spread, but this was not assessed.</p> <p>Numbers of <i>Aedes aegypti</i> were presented in the study site along Mekong River.</p>

The association analysis between dengue incidence and water bodies

From this searching, studies evaluated the relationship between dengue incidence and water bodies (Bi et al. 1998; Bowatte et al. 2013; Morin, Comrie & Ernst 2013; Nasir et al. 2017; Schmidt et al. 2011; Tian et al. 2016), however, among these studies, only one, a review article, discussed the mosquito life cycle (Morin, Comrie & Ernst 2013), and three of them included water bodies as one of the major dengue risk factors (Bowatte et al. 2013; Nasir et al. 2017; Tian et al. 2016). Of 21 published studies, fifteen studies have examined the dengue cases occurring in the outbreak areas and mention water resources as another potential factor in dengue distribution. Other published journal articles reviewed the correlation of climatic conditions and dengue transmission (Morin, Comrie & Ernst 2013), the effects of environment on vector borne disease, as well as human vulnerability to the disease (Githeko et al. 2000; Sutherst 2004; Tabachnick 2010). These have

outlined how water, in conjunction with climate – temperature, precipitation – can influence dengue incidence in tropical and sub-tropical regions.

The main variables assessed in these studies (Table 1.2) are the number of dengue cases and their distribution, and mosquito density. Most studies collected climatic data including temperature, precipitation and relative humidity (Bi et al. 1998; Dickin, Schuster-Wallace & Elliott 2013; Li et al. 2017; Nakhapakorn & Tripathi 2005; Nasir et al. 2017; Phuanukoonnon, Brough & Bryan 2006; Raju & Sokhi 2008; Shang et al. 2010; Sirisena et al. 2017; Tian et al. 2016; Zheng et al. 2019). Several used non-climatic factors such as house patterns, land use types, house cleaning and maintenance management (Raju & Sokhi 2008), topography (Bi et al. 1998), economic conditions and vegetation index as environmental variables. Population density, road density and land use/land cover are designated as social factors (Qi et al. 2015; Zheng et al. 2019) and are regarded as independent variables. Three studies assessed land cover, but focussed on developed land, vegetation, water bodies such as lakes, wetland, rivers and seas (Hsueh, Lee & Beltz 2012; Tian et al. 2016; Tiong et al. 2015), water supply (Schmidt et al. 2011), and water level (Bi et al. 1998). Two studies included night time surface temperature as environmental factors, sunshine hours, water vapour, evaporation and mean wind speed as weather factors (Li et al. 2017), as well as employment types, and health service accessibility in the assessment of dengue occurrence (Wijayanti et al. 2016).

Water samples were collected from ponds, sewage, rain water (Nasir et al. 2017), rivers, and wetlands where inundation is likely to occur during rainy seasons (Bowatte et al. 2013; Nasir et al. 2017; Tun-Lin, Burkot & Kay 2000) to test for nutrients and organic carbon and to compare with dengue prevalence.

Studies have collected serum, clinical data, (Halstead et al. 1965), serotype of dengue virus (Shang et al. 2010; Tiong et al. 2015), and gene sequences (Tian et al. 2016).

Different methods were used to evaluate the association between observed variables and dengue incidence, or vector borne disease. For instance, spatial analysis was used to identify land use/land cover type, and examine the incidence of spatial distribution and climatic factors (Nakhapakorn & Tripathi 2005; Raju & Sokhi 2008; Sirisena et al. 2017; Tiong et al. 2015; Zheng et al. 2019). There were five descriptive analyses (Angel & Joshi 2009; Dickin, Schuster-Wallace & Elliott 2013; Halstead et al. 1965; Phuanukoonnon, Brough & Bryan 2006; Tun-Lin, Burkot & Kay 2000). Regression methods, such as multiple regression, regression predictive model, logistic regression, weighted regression, and logistic and passion regression, were applied to evaluate dengue risk factors and predict future disease transmission. These regression models are used to analyse weather variables, the distributions of population density and dengue incidence. They were also used to assess the relationship between other risk factors which can be used to generate predictive models of dengue incidence. A generalized additive model (GAM) was used to identify potential contributing factors affecting dengue distribution patterns, and autoregressive moving average

(ARIMA) was used to predict future dengue outbreaks (Li et al. 2017; Qi et al. 2015; Sirisena et al. 2017). Other statistical approaches, including spline smooth, and Bayesian statistics, were applied to evaluate the socioeconomic and environmental effects on dengue cases (Qi et al. 2015), to quantify risk factors (Wijayanti et al. 2016), and to assess the temperature effect on probability of disease transmission (Tian et al. 2016).

1.2.3. Discussion

In this systematic review, the focus was an association between dengue incidence and water bodies which include surface water, rivers, ponds, and other open water areas. The previous reviews have revealed that there is a clear connection between dengue transmission and water areas, despite the fact that only one-third of recent studies considered water bodies as one of the main risk factors of dengue incidence. Water bodies such as ponds, and isolated surface water appear to play a role as a provider of breeding sites for proliferation vectors since the beginning of egg laying to hatching stages (Bowatte et al. 2013). This finding is supported by the studies from Nasir et al. (2017) which revealed that 97.8% of mosquitoes were found in standing water, and only 2.2% in flowing water. Tian et al. (2016) found that dengue cases are associated with surface water as it is likely to have an impact on mosquito population size, however that the presence of water bodies alone might not provide favourable sites for breeding of mosquitoes. Bi et al. (1998) stated that a relationship between incident rates of disease occurring in a particular region may relate to the system of surface water, rivers, or streams. Additionally, water quality, and nutrition in water are significant factors in contributing to mosquito population levels (Morin, Comrie & Ernst 2013; Nasir et al. 2017). Organic matter in water, for example, is important for the expansion of mosquito populations, and can provide conditions for shorter life cycle development, and higher survival rates as a result (Tun-Lin, Burkot & Kay 2000). This is also found in a review from Morin, Comrie and Ernst (2013) noting that although rainfall, one of the essential aspects to favour dengue incidence, can exacerbate the influence on density of mortality, it is relatively low when compared to nutrients in water. Nutrients in water provide suitable conditions which is a key to supporting larval development and therefore mosquito survival. The size of water areas is considered to have an impact on mosquito development. It has been found that large water areas can potentially limit the effect of the vector and pathogen as within these the light from the sun is limited and the oxygen can be reduced. These are likely to create unfavourable conditions for mosquito development (M Grandadam 2019, personal communication, 09 August). This is consistent with a study in Malaysia which showed that there was no connection between large water bodies – rivers, coasts – and dengue prevalence because larger water bodies have less influence on the incidence (Tabachnick 2010; Tiong et al. 2015). In contrast with these studies, it has also been reported that surface water areas, especially large surface water, seems to be associated with large epidemics (Tian et al. 2016). To add to this, Li et al. (2017) conducted research about dengue infection in Guangzhou, China to find out the factors which caused the issue. From

this study, it was found that the incidence seemed to relate to the artificial lake which was recently created in the study areas, because before the lake was there, there was no outbreak in the area.

Water temperature and humidity critically influence host and vector distribution (Githeko et al. 2000; Tabachnick 2010). When the temperature rises, larvae will take a shorter time to mature, and will have a higher capacity of producing vectors. A study in Punjab, Pakistan, showed that populations of mosquitoes were found to be up to 52.4% higher than at other times at temperatures between 28°C to 36°C, and humidity of 75% in the rainy season (Nasir et al. 2017). However, Shang et al. (2010) pointed out that higher temperatures may not cause an increase of dengue transmission but only supports mosquito proliferation, unlike precipitation.

Rainfall appears to be significantly related to dengue prevalence as the number of dengue cases increases when there is an increase of rainfall (Shang et al. 2010), however this contrasts with a study in Sri Lanka which reported that heavy rain has a negative correlation with the dengue incidence because eggs and larvae are washed away by heavy rain (Sirisena et al. 2017). Decline in rainfall creating drier conditions has been found to have a positive correlation with dengue transmission. Low precipitation creates less inundation and low water levels, especially in wetlands (Bi et al. 1998).

Apart from the factors such as precipitation and humidity that link to vector's breeding sites, some other components may need to be considered. It was highlighted that poor management of water supply and house condition have a connection to dengue cases to some extent (Schmidt et al. 2011; Spiegel et al. 2007). Lack of water supply in highly populated areas tends to increase the rate of dengue disease transmission, especially in rural areas. This is assumed to be because water deposition on the surface due to leaking water pipes, and poor management of water drainage systems may assist the capacity of mosquito development.

Geographical and topographical patterns also affect the emergence of dengue incidence. For example, a study in Malaysia found that dengue distributions showed different patterns in each region across the country due to the changing of climate patterns (Dickin, Schuster-Wallace & Elliott 2013). Likewise, a study in Yingshang County, China, also showed that low land and wetland within 100 metres above sea level and under mild ecological conditions were at high risk of epidemic (Bi et al. 1998; Nasir et al. 2017).

Some evidence has been reported that road density or transportation is one of the risk factors of dengue incidence as they are assumed to facilitate infected commuters who travel from place to place (Zheng et al. 2019). A study in the Pearl River Delta, China showed that a semi-urban area where the transportation was extensively linked is likely to be at higher risk of dengue disease than the urban area (Qi et al. 2015). None of the previous studies, however, have mentioned the distance from outbreak sites to water bodies such as rivers, lakes, ponds, irrigation, wetland, deltaic areas,

regardless of the fact that most dengue occurred in the regions where water areas are located (Angel & Joshi 2009; Bi et al. 1998; Halstead et al. 1965; Qi et al. 2015).

There are several limitations to this study that should be considered. First, strong evidence to show the correlation between water bodies and dengue incidence has not been clearly identified even though water bodies, the breeding habitats for larval development, were predominantly mentioned in the discussion. Most of the previous studies have provided some clues that water area might have the potential to affect dengue transmission and it should be the focus of further studies. Second, although socioeconomic and environmental factors are considered to be important factors in dengue distribution, it has not been identified which of them should be the major focus, whereas this was under climatic factors in a numbers of studies (Nakhapakorn & Tripathi 2005). Third, statistical methods were applied differently among the studies in finding out dengue distribution patterns and future anticipation without mentioning the restrictions or limitations. It may be useful for further studies if the tools used in the field of public health, like dengue incidence in terms of predicting disease and distribution patterns are compared to find the better fit models in this particular field.

1.2.4. Conclusion

This study aimed to assess the influence of water areas on dengue incidence through previous studies. Water bodies are essential for mosquito proliferation as they provide breeding sites for mosquitoes from egg laying and larval development to maturity stage. Temperature, precipitation and relative humidity are also crucial conditions that favour mosquito development. Study sites in the studies that have experienced dengue outbreaks are mostly located close to water areas. However, in some regions, there is no connection between water areas and dengue incidence particularly larger surface waters such as rivers, streams and lakes. Organic materials and nutrients in water might also have an impact on dengue incidence. To assess this, apart from climatic factors, further studies need to consider ecological domains on which mosquitos rely as breeding sites as an important aspect in order to understand the disease prevalence.

1.3. Geographic Information System and Remote Sensing in Epidemiology

Geographic information systems (GIS) and remote sensing (RS) technologies have been widely applied in the field of infectious diseases to study spatial and temporal distribution patterns. Epidemiology which is tightly associated with spatial data could help in determining disease risk by connecting locations to disease. GIS, Remote Sensing, and spatial analysis in epidemiology have been developed for over 25 years with the increasing capability of storage, retrieval, analysis and display of spatial data (Graham, Atkinson & Danson 2004). It has previously been suggested that utilising spatial analysis could aid the examination of the factors that influence the distribution of dengue incidence by investigating the climatic and environmental aspects which can not only predict

the potential areas but also identify the risk factors of dengue cases (Wu et al. 2009). Remote sensing and GIS have been applied in the field of infectious disease, with an emphasis on vector borne diseases. For instance, the use of satellite images has been largely used to determine the distribution of diseases and their variations through time. Particularly, when diseases correlate with environmental data such as climate, vegetation, land-use, these can be used as the indicators to forecast the emergence of diseases through predictive models (De La Rocque et al. 2004), and help prepare and develop effective early warning systems (Kitron 2002). Additionally, georeferenced data, which is processed through GIS software, can assist remotely sensed technologies to enhance public health surveillance. For example, high resolution satellite imageries provided timely and detailed in digital form to represent land formation and landscape can classify and identify the correlation between disease host and vector habitats (Croner, Sperling & Broome 1996).

Several studies have used remote sensing and GIS to investigate the relationship between the emergence of dengue incidence and specific factors in order to search for risk factors and to predict future risk. For instance, Khormi and Kumar (2011) created their model of dengue fever risk by using GIS and remote sensing. High resolution satellite images were used to examine the density of houses in different neighbourhoods in each district, while GIS was applied as a tool to predict risk level of dengue fever victims. Similarly, Zheng et al. (2019) investigated the factors that influenced dengue fever epidemics in China based on environmental factors such as vegetation index, and socioeconomic factors by applying GIS and satellite imageries (Qi et al. 2015).

Notably, it is clearly seen in previous studies that integrating GIS and remote sensing techniques in the epidemic field to investigate disease prevalence, factors causing the incidence can be identified as well as future risk model developed. However, concerning the availability of high resolution remotely sensed data and the high precision data seem to be the main challenge to some countries, like Laos, in obtaining highly accurate results.

1.3.1. Remote Sensing Sensors

Remote sensing systems have a long history of development since 1972 when the first satellite – Landsat-1— was launched. From that time onward, many satellites have been developed with an improvement of high resolution and sensors which can detect more accurate ground feature information (Joseph 2005). Regarding the availability of sensors, two sensor systems which are optical sensors and radio detection and ranging (RADAR) have presented high spatial resolution with the development of hyperspectral sensors which can obtain genuine world data (Donoghue 2000). Ground information is provided by the measurement of the sensor boarded on satellites which extract data from the electromagnetic radiation. The quality of this information detection would be varied depending on wavelength, polarisation, direction and intensity (Zhu et al. 2018). Two types of remote sensing sensors have been used, active sensor and passive sensor (Figure 1.1). Active remote sensor basically relies on its source of energy to measure the ground objects' illumination.

The wavelength range of this sensor type ranges from visible spectrum (400 nm – 700 nm) and near-infrared (700 nm – 2500 nm), and radar waves (Joseph 2005) (see Figure 1.2). Passive remote sensor, on the other hand, depends on solar energy as a radiance to measure the reflectance from earth surface illumination (Zhu et al. 2018). Basically, the wavelength ranges from visible to near-infrared electromagnetic spectrum (430 nm – 720 nm, and 750 nm – 950 nm respectively), however, some satellite sensors have provided a long wavelength up to 1580 nm – 1750 nm (mid-infrared) to derive more accurate information from surface information.

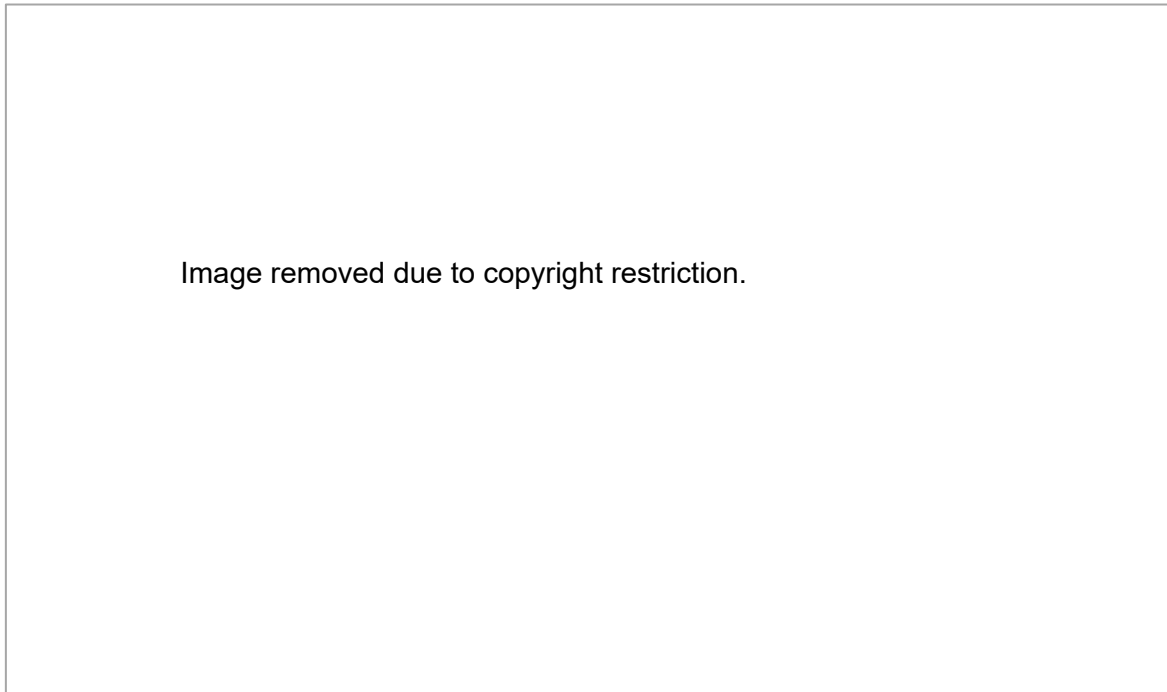


Figure 1.1: Active and Passive Remote Sensors

Source: http://www.gisresources.com/passive_and_active_remote_sensing

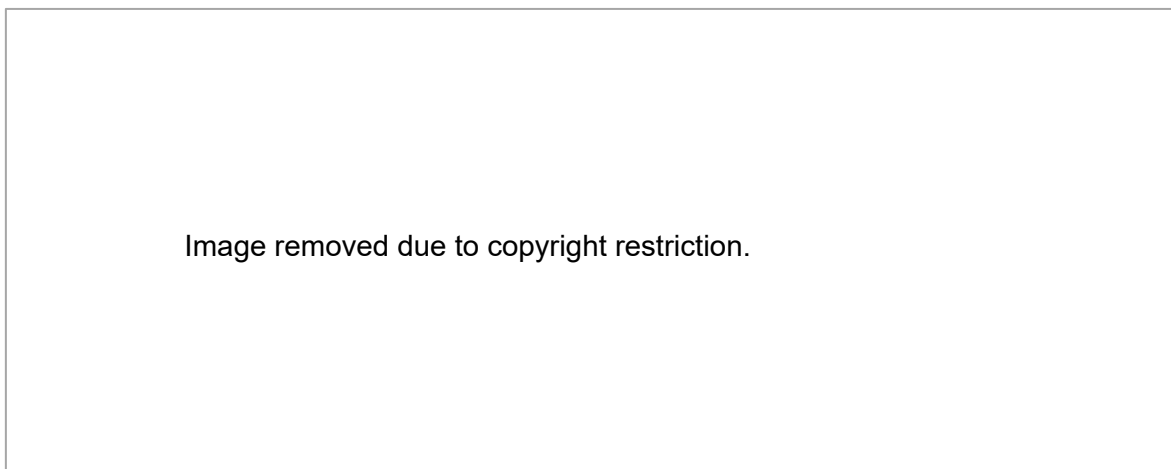


Figure 1.2: Electromagnetic spectrum

Source: Hexagon (n.d)

Table 1.3: Major regions of the electromagnetic spectrum

Region Name	Wavelength	Comments
Gamma Ray	< 0.03 nm	Entirely absorbed by the Earth's atmosphere and not available for remote sensing.
X-ray	0.03 to 30 nm	Entirely absorbed by the Earth's atmosphere and not available for remote sensing.
Ultraviolet ray	0.03 to 0.4 μ n	Wavelengths from 0.03 to 0.3 micrometres absorbed by ozone in the Earth's atmosphere.
Visible	0.4 to 0.7 μ n	Available for the Earth remote sensing. Surface objects can be imaged with cameras and sensors.
Near and Mid-Infrared	0.7 to 3.0 μ n	Available for the Earth remote sensing. Surface objects can be imaged with cameras and sensors.
Thermal-Infrared	< 0.7 to 3.0 μ n	Available for the Earth remote sensing. This wavelength cannot be captured by film cameras. Specific sensors are used to image this wavelength band.
Microwave or Radar	0.1 to 100 centimetres	Longer wavelengths of this band can pass through clouds, fog, and rain. Images using this band can be made with sensors that actively emit microwaves.
Radio	>100 centimetres	Not normally used for the Earth remote sensing

Adopted from Baumann (2010)

1.3.2. Remote Sensing used for Water Bodies Detection

Remotely sensed imageries and its allied techniques – Geographic Information System – have been widely used to observe water bodies for many years for two main reasons. Firstly, the need to assess the existing water resources and the changes of these resources due to the scarcity of water resources and issues related to water. Secondly, the effects caused by the changes in climate which influence the change of water cycling. Applying these technologies to study water bodies, might help develop feasible ways to mitigate the water related problems (Nath & Deb 2010).

To map open surface water, several methods have been used, for instance, using synthetic aperture radar (SAR) imagery to map out open fresh water areas in large regions; applying remote sensing

and GIS to identify type of land cover (Prakash & Gupta 1998), as well as a model developed based on EOS/MODIS model to extract water bodies called normalized difference water index (NDWI) or NDVI (Zhang, Wang & Shinohara 2007). The decision tree and programming method are also used for detecting water body information from flood affected areas (Gouveia & DaCamara 2006; Hu, Gong & Zhu 2007), and using semi-automated methods to extract water features from satellite images such as IKONOS and other high resolution satellite images to investigate temporal water changes (Di et al. 2003; Sharma, Mioc & Anton 2007).

To acquire more accurate results of surface water features, several remote sensing sensors which actively and passively detect the information have been developed. For example, optical sensors which cover visible, infrared channels of electromagnetic spectrum and thermal infrared radiance (optical systems), and active remote sensing like radars which use microwave pulses and record the received signals (Nath & Deb 2010). Although these two sensor systems have been developed for a better ground feature detection, each of them has some limitations which need to be considered. Passive remote sensing is claimed to detect water bodies well, however, under poor weather conditions such as cloud cover, and dense vegetation canopy, extracting water information becomes an issue. In contrast, active remote sensing or active microwave sensors, such as synthetic aperture radar (SAR) can penetrate darkness, cloud coverage and tree canopies at the longer wavelength. Synthetic aperture radar has become an important source of remotely sensed data to detect flood and to monitor surface water. SAR data have been acquired by many instruments such as RADARSAT, Envisat ASAR, PALSAR, with a provision of different areas of observations over the globe. Using SAR data for mapping surface water bodies is thought to be suitable in the tropical areas and forest zones with satisfactory performance up to 90% at local and regional levels, but in terms of freely access data and global observation seem to be a main limitation (Pham, Prigent & Aires 2017). Some SAR data could be freely obtained such as Sentinel-1, the active sensor radar imageries, which has been created with the ability to quantify the spatial and temporal variation of surface features under all weather and day and night. This Sentinel-1 SAR funded by the European Space Agency (ESA) is designed to capture the highly dynamic nature of several aquatic habitats with a wide swath of 250 km, high geometric, radiometric resolution, and six days revisit cycle (Zeng et al. 2017). Surface water can be detected by using SAR backscatter as open water bodies are relatively smooth so that they can be distinguished from other land cover types (Hardy et al. 2019; Huang et al. 2018). A number of studies have been carried out applying Sentinel-1 C bands to detect water bodies, for instance, Huang et al. (2018) employed Sentinel-1 data IW mode, GRD format cooperating with Landsat optical data to extract water extent by using automated extraction. Similarly, Hardy et al. (2019) used Sentinel-1 with Sentinel-2 and Pleiades optical imageries to help detect open and vegetated water bodies to map African malaria vector mosquito breeding habitats. Also, Cazals et al. (2016) deployed Sentinel-1A with C bands sensor to acquire data retrieved from GRD mode at dual polarisation (VV/VH) to map and characterise hydrological dynamics in a coastal marsh. However, under some conditions such as wind-induced waves, or surface water roughened

by vegetation, SAR seems to be limited to discriminating water features. Passive microwave measurements can detect water areas through dense cloud cover and vegetation, but spatial resolution seems to be a main challenge to extracting small water areas. Despite cloud cover issues, some passive remote sensing technology, especially the use of freely available high spatial resolution optical satellite data, such as Landsat series, Advanced Spaceborne Thermal Emission and Reflectance Radiometer (ASTER) and Sentinel2 multispectral imageries are widely applied to achieveably extract surface water bodies (Chen et al. 2018) – lakes (Bhardwaj et al. 2015), rivers (Jiang et al. 2014), coastlines (Li & Gong 2016), and water bodies in rural areas (McFeeters 1996). Regardless of the ability of mapping surface water, when dealing with urban and peri-urban water areas, this type of sensor is likely to encounter the issues of heterogeneous and mixed ground features caused by built-up areas which typically introduce shadow (Zhou et al. 2014). In addition, some water regions are covered by small grasses and trees which could limit the potential of satellite imageries to detect the edge of the water because vegetation could potentially be classified as part of water bodies so that water body under canopy is hard to be detect (Pham, Prigent & Aires 2017).

1.3.3. Spectral Water Indices used for Water Bodies Extraction

Different methods used to detect water features have been developed. Many of them are widely applied, for example, thematic classification method, Linear unmixing model, single-band thresholding method, spectral water index methods (Ji, Zhang & Wylie 2009), and classification methods (Yan et al. 2018). Of these methods, water index is currently accepted due to its ability of differentiating water features from other features based on the combination of two or more spectral bands in different formulas (see Table 1.4). The typical water index that has been developed is the normalized difference water index (NDWI). This renowned approach has used two or more spectral bands with an appropriate threshold of the index to detect water bodies from other land-cover types: for example, applying of near- infrared (NIR) reflectance of the NOAA/AVHRR satellite to delineate lakes, and the use of positive values of the modification of normalized difference water index (MNDWI) to detect surface water bodies (Bryant & Rainey 2002; Crétaux et al. 2011; McFeeters 1996; Xu 2006). The basic principle of the water index is based on the absorption of water bodies at near-infrared (NIR) and shortwave-infrared (SWIR) wavelengths as these areas are highly absorbed by water (Ji, Zhang & Wylie 2009). This normalized difference water index (NDWI) (Equation 1.2) was primarily adopted from the normalized difference vegetation index (NDVI) (Equation 1.1) by McFeeters (1996), where Green and NIR are the reflectance of green and near-infrared bands respectively. The values of NDWI range from -1 to +1 with the threshold value at zero: $NDWI > 0$ if the cover type is water, and for the non-water type $NDWI \leq 0$. Gao (1996) then developed a new form of NDWI by using NIR and SWIR (Equation 1.3) to extract water content from vegetation canopy. This water index was later defined as normalized difference moisture index (NDMI) (Equation 1.6) by Xu (2006). Rogers and Kearney (2004) had generated the use of Red and SWIR bands based on Landsat TM as another formula of NDWI to detect water information (Equation 1.4).

Xu (2006) discovered that previous NDWI was not able to thoroughly distinguish water areas from built-up features so he proposed another form of water index (Equation 1.5) which can improve the water index discovered by McFeeters (1996). This water index based on Landsat TM was introduced as the modified NDWI (MNDWI). Instead of using NIR, SWIR is used because the NIR appears as lower reflectance than the Green reflectance which results in overestimating built-up areas to be water areas. This modification helps improve the separability of built-up areas. Apart from these water indices, Lacaux et al. (2007) has created a normalized difference pond index (NDPI) based on SPOT-5 satellite. This index was developed in a study in West Africa as an attempt to identify ponds. This index makes use of the Green reflectance band and SWIR (Equation 1.7). The MNDWI and NDPI are found to be similar but the threshold used is different, for instance, if $NDPI < \text{threshold } 1$ and $SWIR < \text{threshold } 2$, the cover is identified as pond.

Despite the use of these different methods and indices, the accuracies of water body extraction results can vary because most of these methods were tested with a particular sensor and in specific areas so that specific methods used and threshold in a particular study site may require to be examined (Zhou et al. 2017).

Table 1.4: Common water indices used to extract water features

Algorithm based on index used	Algorithm	Values	Threshold	
NDVI	$\frac{NIR - Red}{NIR + Red}$	-1 to +1	< 0	Equation 1.1
NDWI	$\frac{Green - NIR}{Green + NIR}$	-1 to +1	> 0	Equation 1.2
NDWI	$\frac{NIR - SWIR}{NIR + SWIR}$	-1 to +1	> 0	Equation 1.3
NDWI	$\frac{Red - SWIR}{Red + SWIR}$	-1 to +1	> 0	Equation 1.4
MNDWI	$\frac{Green - SWIR}{Green + SWIR}$	-1 to +1	> 0	Equation 1.5
NDMI	$\frac{NIR - SWIR}{NIR + SWIR}$	-1 to +1	> 0	Equation 1.6
NDPI	$\frac{SWIR - Green}{SWIR + Green}$	$NDPI < 1$	< 1	Equation 1.7

1.4. Aims and Objectives

This study aimed to answer the following research questions:

1. What are the better methods used to extract surface water from satellite images?
2. Is there any relationship between water bodies and dengue incidence?

In order to answer these questions, there were two objectives that needed to be accomplished:

- 1). Extracting water bodies including natural water and artificial water bodies by applying freely available remotely sensed data analysis tools. The image data, and methods for surface water extraction were evaluated.
- 2). To determine the lag time of a mosquito developing into an adult, and the lag time of disease infection based on the onset date. These lag times were used in the statistical analysis to compare with surface water in order to find out the relationship between them.

1.5. Research Questions

The questions in this research aimed to answer are:

- 1). What are the suitable free-of-charge satellite image analysis tools that can be used to extract small surface water areas in urban and peri-urban areas like the study site in this research?
- 2). What is the method used in the image analysis tools to identify small surface water images?
- 3). What are the factors that affect this surface water extraction?
- 4). Does surface water correlate with dengue incidence?

1.6. Hypothesis

This study hypothesised that surface water is likely to have a relationship with dengue incidence.

1.7. Scope of the Study

This study attempted to examine the relationship between surface water and dengue incidence in Vientiane, the capital of Laos using 2017 data. To achieve this, the changes in surface water in that year were investigated by using satellite image datasets of PlanetScope and RapidEye in different time series (rainy season – May to November, and dry season – December to April). These image data were used to detect water information at the study site. Water features investigated in this research project included both natural and artificial surface water such as ponds, fish farms, lakes, rivers, streams, and water deposited on the ground. Rainfall data in 2017 obtained from Department of Meteorology, Ministry of Natural Resource and Environment (MoNRE), Laos, was also used to compare with the association between surface water and dengue incidence. Dengue fever data in the 2017 dataset were georeferenced – derived from Economic development, Ecosystem

Modifications, and emerging infectious diseases Risk Evaluation project (ECOMORE), Institut Pasteur du Laos (IPL). These data were statistically compared with the surface water generated from satellite image data. For this comparison, the two were analysed using Spearman's correlation coefficient to determine relationships between the changes in water bodies throughout different times and changes in disease incidence.

This research will contribute to the study of dengue incidence in Laos, especially in Vientiane, which has been affected by the disease each year. This contribution shows how rainfall and the changes of surface water have an impact on dengue. It will also help related organisations understand better the picture of the disease emergence and this may help current surveillance systems to actively and effectively act before the disease occurs.

1.8. Study Area

1.8.1. Dengue Incidence Situations

Laos is one of the Mekong basin nations which has been affected by dengue fever with less knowledge of the recent epidemiological profile of this disease (Van Panhuis, Guha-Sapir & Oshitani 2005). Specifically, in Vientiane, there are two types of vector-borne disease – *Aedes aegypti* and *Aedes albopictus*. The dominant species which is commonly found in central Vientiane is the *A. aegypti* which naturally breed in household water containers such as jars, tanks and drums and mostly are found in urban areas, whereas *A. albopictus* species is found in peri-urban areas (Vallée et al. 2009). However, it can be observed that the nature of these vectors has been changed due to the changes of environment. According to a survey conducted by the Entomological and Biological team, ECOMORE 2, IPL, since 2016 until now, both dengue vectors species have been found not just in urban but also in peri-urban areas (S Marcombe 2019, personal communication, 26 July). Figure 1.3 shows the numbers of dengue mosquito vectors adults collected in 2017 derived from the Medical Entomology and Biology of disease vectors laboratory team, IPL, in central Vientiane. A high number of dengue mosquitoes were found from January, the dry season time, before the rate dropped at the beginning of the rainy season (April to May). There was a considerable number of adult dengue vectors found during the wet season toward the onset of the dry season (June to December).

According to the World Health Organization (2007), prevalence of dengue fever stems from the rapid growth of urban development with inappropriate planning, and most of the cases are associated with poor management of sanitation and water storage. Laos, like other developing countries has many regions which are in transition from rural to urban areas so that there are still many places which mixed urban and peri-urban areas are. Dengue infection has become an epidemic since 1983 in Vientiane, where there were 1,759 cases of dengue haemorrhagic fever (DHF) (Fukunaga et al. 1994). Since then, dengue disease has been at an epidemic level across the country (Vallée et al. 2009). Major epidemics were reported in 1987 and again almost a decade later in 1995, 1996, 1998

and 2003 with more than 7,000 cases reported in hospitals annually (World Health Organization 2008). The outbreaks also occurred in 2010 and 2013, but were even larger than before with more than 22,000 cases (46 deaths), and 44,171 cases (95 deaths) respectively (National Centre of Laboratory and Epidemiology 2010; World Health Organization n.d-a).

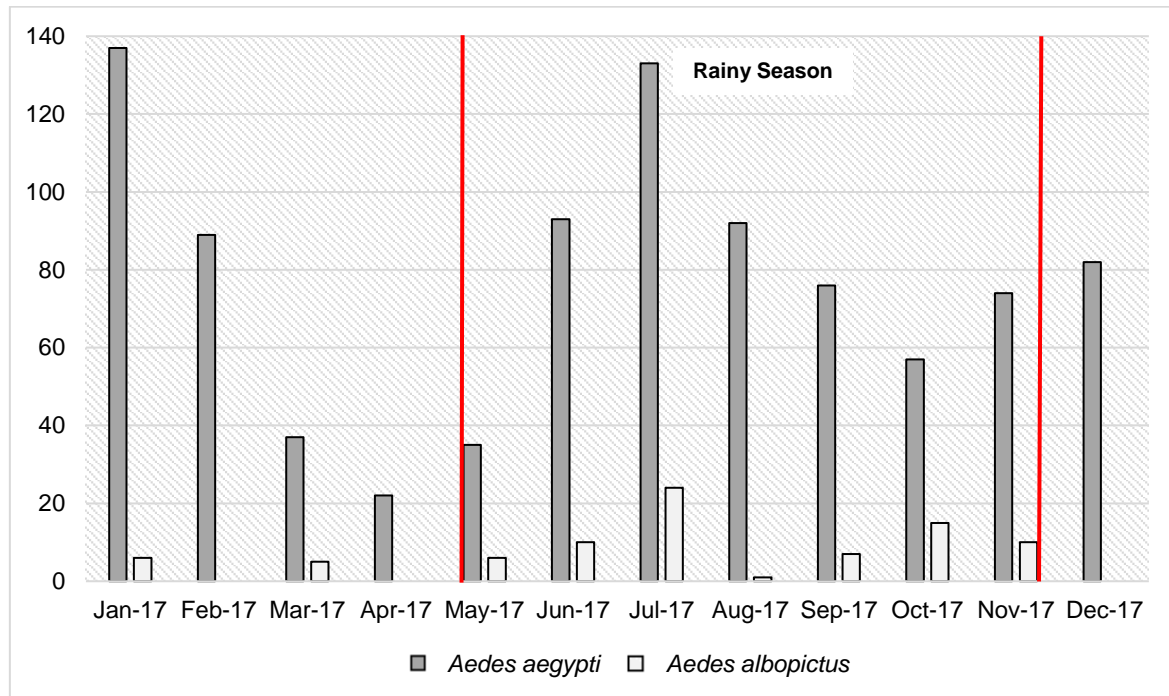


Figure 1.3: *Aedes aegypti* and *Aedes albopictus* adults collected in the Centre of Vientiane

Source: Medical Entomology and Biology of Disease Vectors Laboratory, IPL

1.8.2. Location

Vientiane is the capital of Laos which is rapidly growing due to ongoing urbanisation. It is located in the centre of the country on the left bank of the Mekong River (Rafiqui & Gentile 2009). As it is still in the ongoing transition from rural to urban areas, more than 50% of the region is still rural and peri-urban. The total area of Vientiane is 3,583 square kilometres, consisting of nine districts: Chanthabouly, Sikhottabong, Xaysetha, Sisattanak, Naxaithong, Xaythany, Hadxaifong, Sangthong, and Mayparkngum. Among these, only four districts are considered to be urbanised (Chanthabouly, Sikhottabong, Xaysetha, Sisattanak) (see Figure 1.4), whereas the rest are highly irrigated to supply agricultural activities (Sharifi et al. 2014). The area is characterised by a tropical climate which influences weather. There are two seasons: the rainy season from May to November, and the dry season from December to April. The average annual temperature (30-year period) ranges from 22.73C (min) to 31.05C (max) with average annual precipitation of 1660.5 mm (World Meteorological Organization 2019). Many areas in Vientiane are prone to flooding during the rainy season, and several areas are wetland with poor drainage systems where water typically is deposited during the wet season which has caused major floods in recent times (Comte 2009).

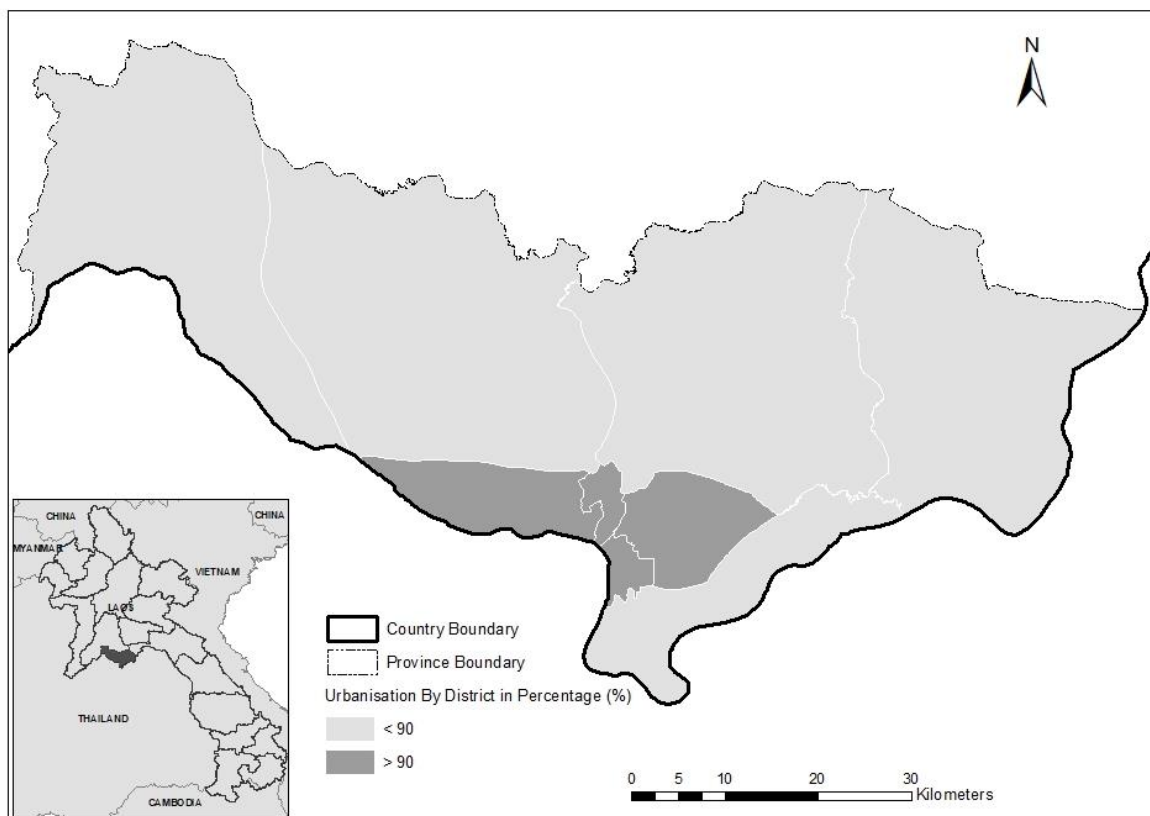


Figure 1.4: Vientiane Capital classified by urbanised regions

Source: Administrative boundary data retrieved from <http://www.decide.la/>. Urban index and population data retrieved from Lao Census 2015

The total population in Vientiane is 820,940 with 209 people per square kilometre which indicates that Vientiane is the most urbanised area in the country according to the Population and Household Census Report in 2015. The density of population in this area combined with a rapid growth of urbanisation which is likely to be associated with dengue disease (World Health Organization 2007), therefore it is no wonder that Vientiane has the second highest prevalence of the disease in Laos. In 2017, there were over 1,695 suspected cases 1,076 cases were confirmed as dengue fever, with 603 proving to be negative cases, and 16 cases were likely to contract the disease (see Figure 1.5).

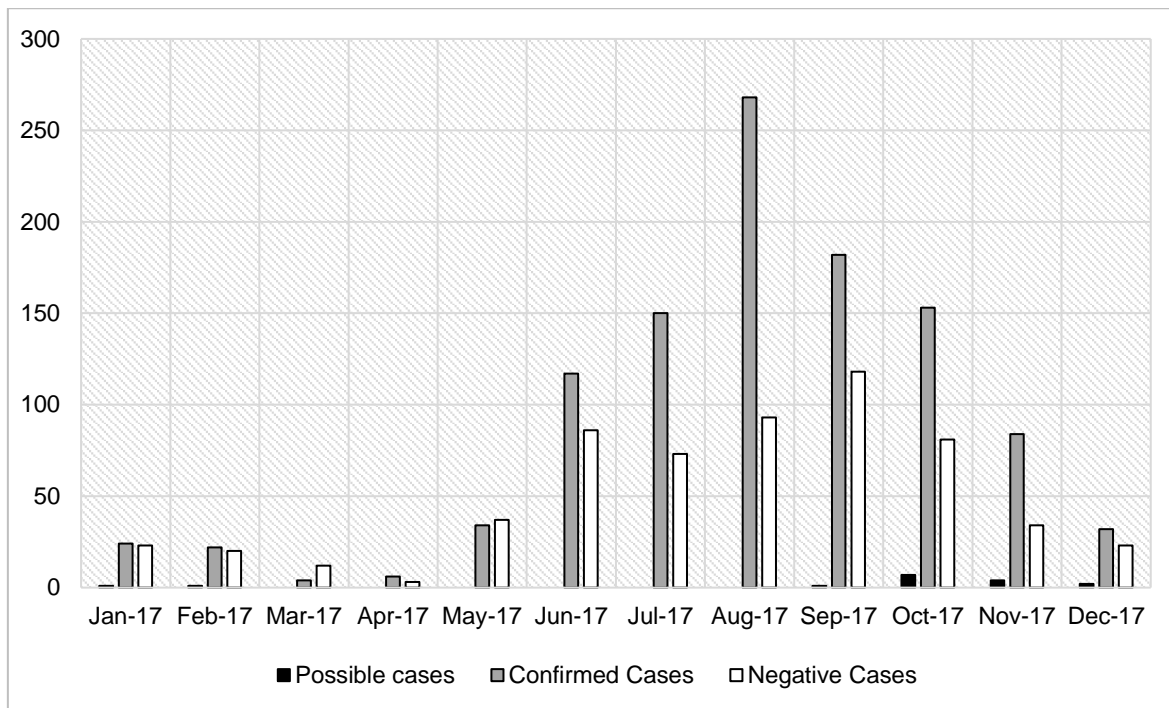


Figure 1.5: Dengue Incidence in 2017

Source: ECOMORE 2, IPL

Later in 2018, more than 1,200 cases were reported to be at risk of dengue fever and 705 people were confirmed to be infected. Earlier this year (2019), according to an unofficial report from the Ministry of Public Health, it was reported that since the beginning of 2019 there were more than 7,000 cases of dengue infection across the country with 25 deaths (Vientiane capital: 6, Borikhamxay: 1, Khammuane: 2, Savanakheth: 8, Saravane:3, and Champasack: 5). Vientiane has the second highest number of people with dengue disease with a total number of 2,374 from the end of December 2018 to the beginning of July 2019 (see Figure 1.6). It is known that dengue is not curable, but it is a preventable disease and the best method used to effectively prevent the disease transmission is to control the breeding sites. It is claimed that “good knowledge, attitudes and practices (KAP) among public are required to successfully prevent or minimize dengue outbreaks.” However, few people are aware of the severity of dengue (Mayxay et al. 2013).

Therefore, the aim of this current study is to examine the relationship between changes of surface water as a source of breeding habitats to dengue vectors and dengue incidence in 2017 which was declared to be the largest epidemic since 2013.

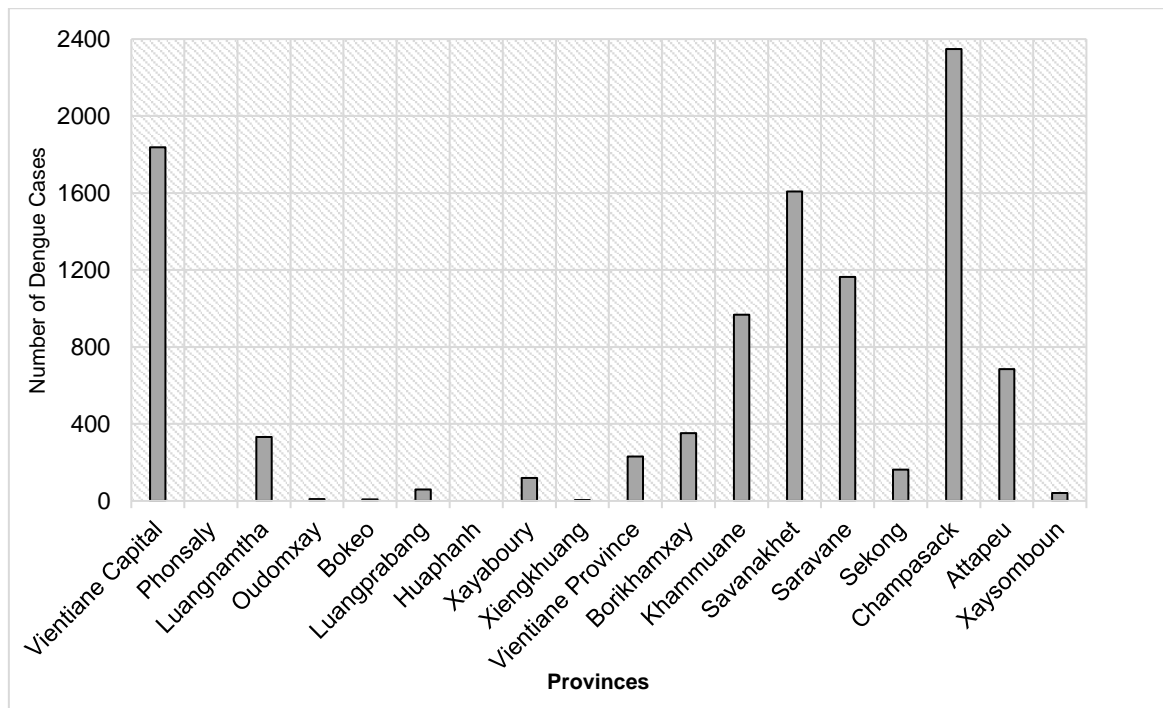


Figure 1.6: Current Dengue Epidemic (29/12/2018 to 01/07/2019) by Province

In short, this chapter determined possible aspects that are associated with the emergence of dengue fever disease by conducting the systematic literature review. According to the review, water bodies seem to influence dengue cases, so that applying advanced technologies such as Geospatial information system (GIS), and Remote Sensing (RS) in examining surface water was considered. To achieve the objectives provided in this study, further investigation of appropriate techniques, as well as factors correlated with the disease cases, will be implemented in the next chapter.

CHAPTER TWO: RESEARCH METHODS

This chapter presents the methodologies used throughout this research project. Three main sections are included in this chapter: 1) Ethics Approval, 2) sources of data, and 3) methods used in carrying out this current study in order to extract surface water areas and find out the relationship between water areas and dengue incidence.

2.1. Ethics Approval

This study followed the application form of the Social and Behavioural Research Ethics Committee (SBREC), Flinders University, and it fulfilled the criteria for negligible risk research under the Risk and Benefit of the National Statement on Ethical Conduct in Human Research (March 2007). It was approved by the Executive out-of-session on the basis of the information contained in the application with approval notice No. 8359, approved on 20 May 2019.

2.2. Data Collection

2.2.1. Image Dataset Selection for Surface Water Extraction

Four sets of image data – Sentinel-2 optical imageries, Sentinel-1 SAR, PlanetScope 3B, and RapidEye level 3A – were tested in order to obtain the most suitable images used in this present study, regarding the availability of data at different times and spatial resolutions. These image datasets are the free of charge images which are freely provided for those who are interested in applying satellite data in fields of interests, except PlanetScope and RapidEye.

Indices concerned to be the most used for extracting surface water such as normalized vegetation index (NDVI), normalized difference water index (NDWI), normalized difference moisture index (NDMI), were also evaluated and compared in order to achieve more accurate results of surface water.

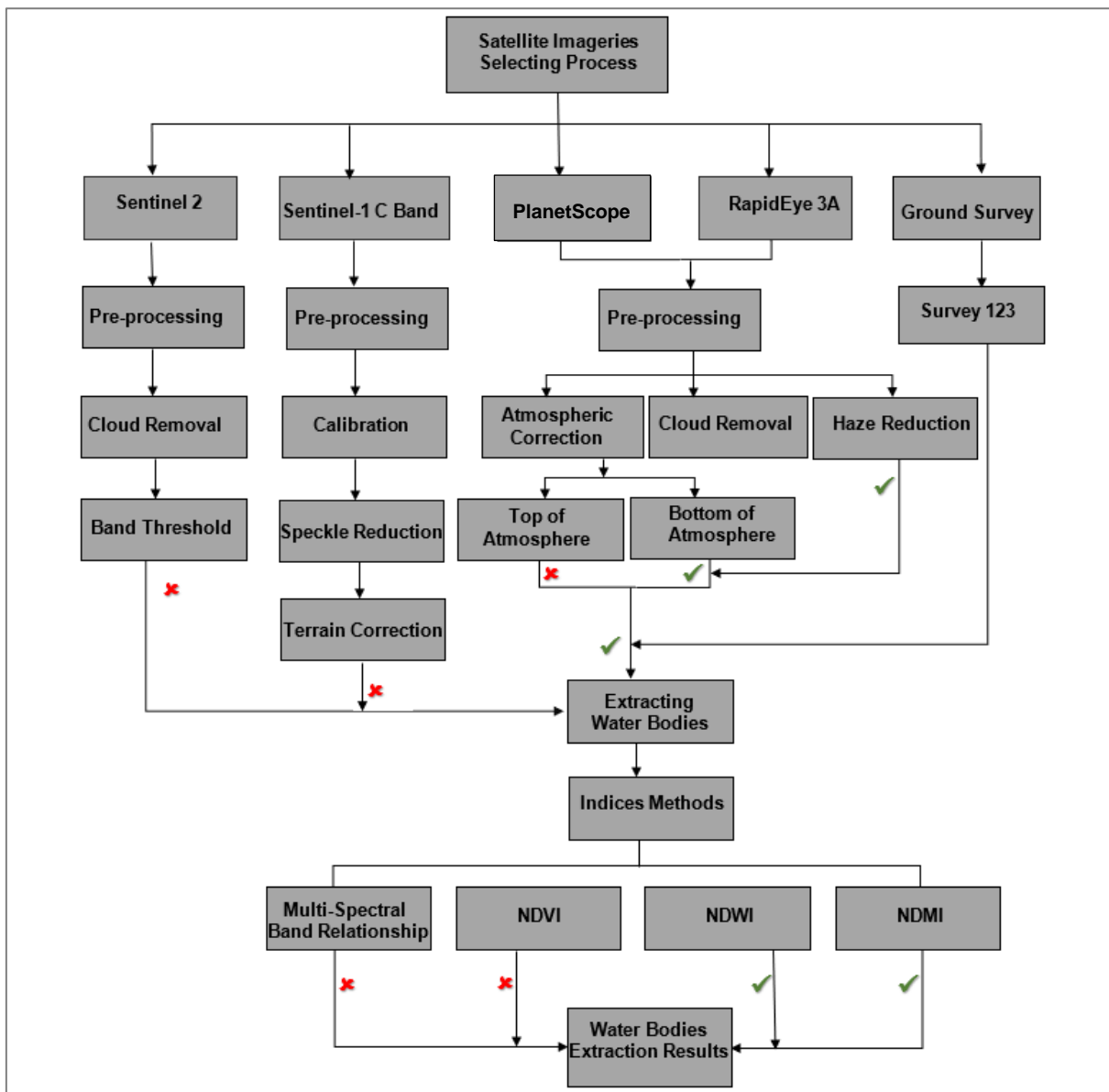


Figure 2.1: Flowchart method process of extracting surface water data

Sentinel-2 Multispectral Instrument (MSI)

Sentinel-2 MSI is freely available funded by the European Space Agency (ESA). The Sentinel-2 mission was launched with the purpose of observing the over earth surface with a high revisit of five days using a bi-satellite system which is highly beneficial for mapping the dynamics of land cover over time. Thirteen spectral bands are carried by this instrument ranging from visible (Red, Green, Blue – RGB) channel and near-infrared (NIR) to Short-wave infrared (SWIR) channels with a ground resolution from 10 m to 60 m (Drusch et al. 2012) (See Table 2.1).

Table 2.1: Sentinel-2 satellite sensor specifications

Sentinel-2 Bands	Central Wavelength (μm)	Resolution (m)
Band 1 – Coastal aerosol	0.443	60
Band 2 – Blue	0.490	10
Band 3 – Green	0.560	10
Band 4 – Red	0.665	10
Band 5 – Vegetation Red Edge	0.705	10
Band 6 – Vegetation Red Edge	0.740	20
Band 7 – Vegetation Red Edge	0.783	20
Band 8 – NIR	0.842	20
Band 8A – Vegetation Red Edge	0.865	20
Band 9 – Water vapour	0.945	60
Band 10 – SWIR – Cirrus	1.375	60
Band 11 – SWIR	1.610	20
Band 12 – SWIR	2.190	20

Source: Adopted from ESA (2019)

Many researchers have applied Sentinel-2 MSI in discriminating water features. Yang and Chen (2017) attempted to map urban surface water by using moderate resolution remote sensing which is freely available. Sentinel-2 was used as a main image data source applying methods of normalized difference water index (NDWI), the modified NDWI combined with the automated water extraction index (AWEI). It was found that a Kappa coefficient of 0.92 could be achieved. Similarly, Chen et al. (2018) had used Sentinel-2 MSI imagery to detect urban surface water bodies with high accuracy, as well as Kulinkina et al. (2018) who compared three satellites imageries Landsat 8, Sentinel-2, and RapidEye and found that Sentinel-2 was the most accurate data source. Thus, this study explored the advantages of Sentinel-2 MSI in extracting water information in the study area.

Sentinel-2 MSI imageries were downloaded from <https://scihub.copernicus.eu>. Image data were acquired for two dates (see Table 2.2). These dates were selected according to seasonality as March represents the dry season (December to April) and October represents the wet season (May to November). Figure 2.2 shows Sentinel-2 imageries in true-colour composite.

Table 2.2: Sentinel-2 MSI image dataset

Dates	Number of Images	Acquisition Date
18 March 2018	1	20 May 2019
28 March 2018	2	20 May 2019
04 October 2018	3	20 May 2019

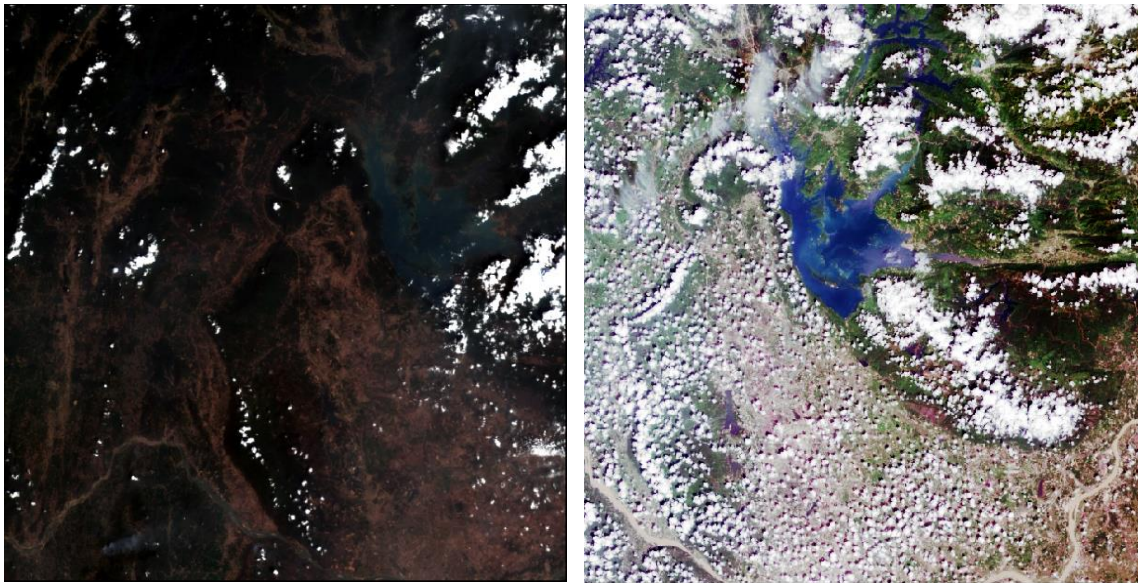


Figure 2.2: Sentinel-2 MSI in true-colour composite with radiometry adjust—Equalised Percentage (March 2018-left) and Histogram Equalisation (October 2018-right)

The presence of cloud was the major challenge so removing cloud was implemented using spatial modeler. A cloud removal model was created by applying Spatial modeler, Toolbox, ERDAS Imagine 2018. Figure 2.4 shows the spatial model built as an attempt to mask out the cloud. Band 2 (Blue) was used to threshold the cloud reflectance due to its high reflectance of dense cloud (ESA 2019). The threshold value used to detect cloud was examined by using the Inquire tool, ERDAS Imagine. The threshold value was set to be greater than 15,00; and with the use of Either/Or function (Figure 2.3) where the test is converted to binary, and the Output Otherwise is returned. All values of clouds were converted to zero, however, most of the areas covered ground features such as water bodies, settlements, and roads were lost (see Figure 2.5).

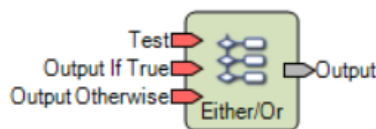


Figure 2.3: Either/Or Function used in Spatial Model

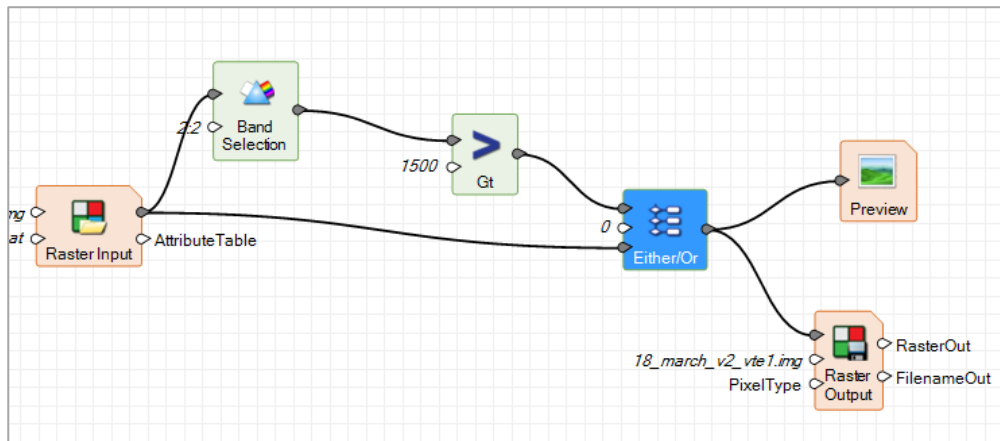


Figure 2.4: Cloud removal model

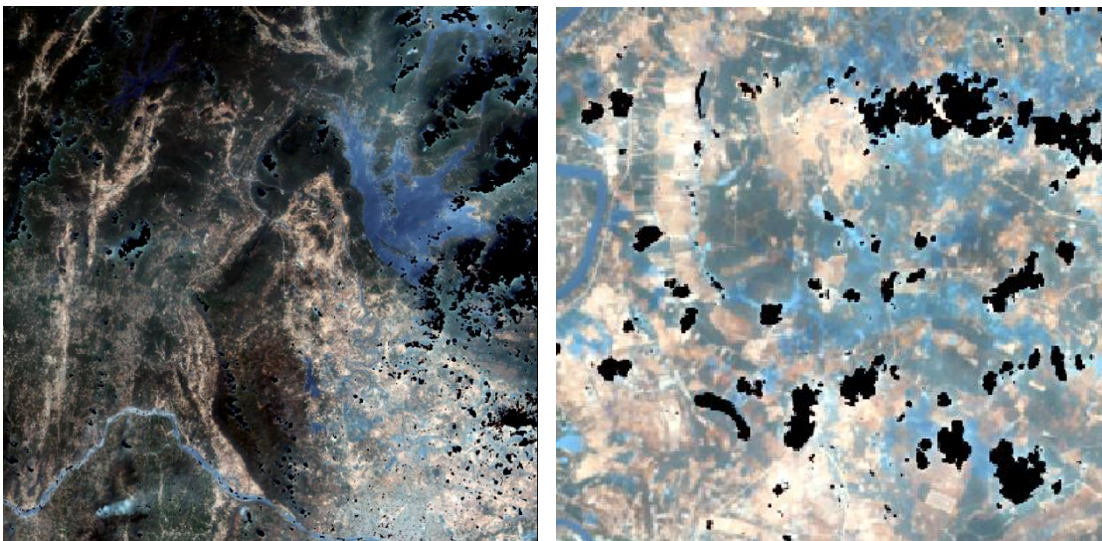


Figure 2.5: Cloud masked image in March 2018 displayed in true-colour composite

Even though cloud was masked out from the study area, most of the surface features, especially surface water, were removed. In addition, although the spatial resolution of this Sentinel-2 MSI has been improved up to 10 m, the resolution is still not at the best option to use in extracting small ponds and surface water in this study site. Hence, Radar image data became another option.

Sentinel-1 SAR

Sentinel-1A SAR is operating at 5.405 GHz with four modes – Interferometric Wide Swath Mode (IW), Extra Wide Swath Mode (EW), Strip Map (SM), and Wave (WV) (for more detail see <https://sentinel.esa.int/documents/Sentinel-1-Product-Definition>). In this current study, Interferometric Wide Swath (IW) mode was selected for the initial experiment. This mode is suitable for investigating the ground surface with the ability of capturing the highly dynamic nature of several aquatic habitats with a swath width of 250 km and 400 km at ground resolution of 5 m x 20 m, and a moderate geometric resolution of 10 m (see detail in Table 2.3). IW is predominantly used for systematic monitoring large land and coastal areas (Pham, Prigent & Aires 2017; Yagüe-Martínez

et al. 2016) with dual polarisation (VV+VH or HH+HV) capacity which provide more ground surface information (Zeng et al. 2017). It is commonly used in detecting and monitoring surface water with relatively high accurate results in detecting water regions under poor weather conditions (Twele et al. 2016). IW mode consists of two different types of format – ground range, multi-look, detected (GRD) and single look complex (SLC). From a review of previous studies, between these two products, it was found that a number of studies have been carried out applying Sentinel-1 C bands to detect water bodies: for instance, Huang et al. (2018) employed Sentinel-1 data IW mode, GRD format cooperating with Landsat optical data to extract the water extent by using automated extraction. Similarly, Hardy et al. (2019) used Sentinel-1 with Sentinel-2 and Pleiades optical imageries to help detect open and vegetated water bodies to map African Malaria vector mosquito breeding habitats. Also, Cazals et al. (2016) deployed Sentinel-1A with a C band sensor to acquire data derived from GRD mode at dual polarisation (VV/VH) to map and characterise hydrological dynamics in a coastal marsh.

Table 2.3: Sentinel-1C band, Interferometric Wide swath mode nominal measurement modes

Characteristic	Value
Swath width	250 km
Incidence angle range	29.1° – 46.0°
Sub-swaths	3
Azimuth steering angle	± 0.6°
Polarisation options	Dual HH+HV, VV+VH Single HH, VV
Maximum Noise Equivalent Sigma Zero (NESZ)	-22 dB
Pixel size	10 m

Source: sentinel.esa.int/user-guide/sentinel-1-sar/acquisition-modes

The Sentinel-1A, IW mode, in GRD formats can be downloaded from Sentinel Scientific Data Hub (<https://scihub.copernicus.eu/dhus>). GRD (Figure 2.6.) was downloaded for a primary examination in March 2018. Sentinel Application Platform toolbox (SNAP) was used to process the image analysis – pre-processing – before observing surface water. During pre-processing of image analysis, SAR images had been through three processes, 1) Calibration, 2) Speckle reduction, and 3) Geometric correction.

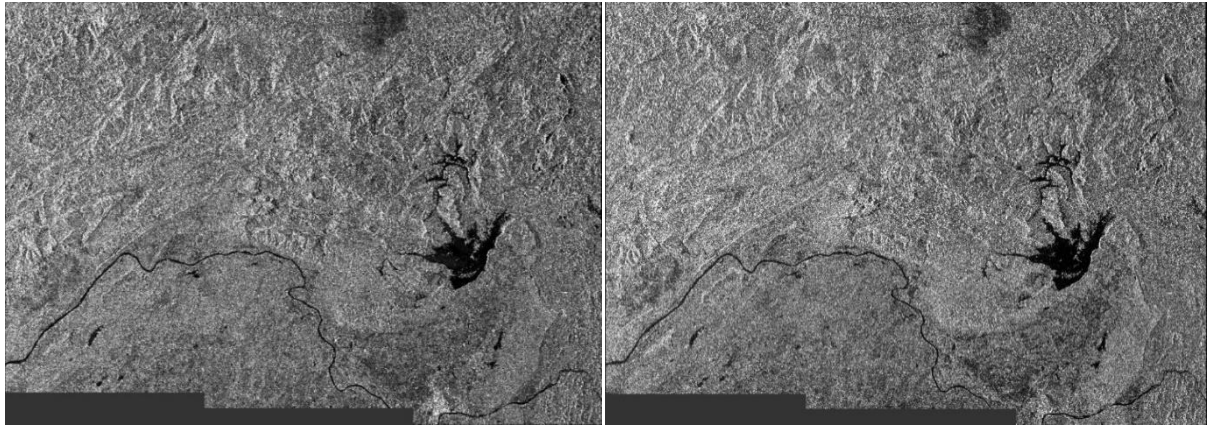


Figure 2.6: Original image of SAR from amplitude VV (left) and VH (right)

Calibration: Digital images were calibrated by applying radiometric correction under the Radar function. This calibration converts amplitude digital pixel values into radar brightness which contains returned backscatter information from the objects (Dong et al. 2011; Frulla et al. 1998).

Speckle Reduction: De-speckle is necessary when dealing with SAR sensors. This type of sensor performs in the microwave electromagnetic channel causing a noise effect which degrades the accuracy of image analysis (Frulla et al. 1998). To reduce noise effects, speckle filtering on SNAP was used. There are many techniques used to reduce noise in SAR images, and the choice of selecting a specific filter depends on the study area figures (Li 1988). It is suggested that however, “regions with large variations in greys show fine details in the image, small filter window size is preferred, whereas homogeneous regions where little variation in greys are typical, a large window size to preserve homogeneity is preferable” (Frulla et al. 1998). In this study, the study area is likely to contain large area of greys so that window size 3 x 3 and 5 x 5 of Lee Filter were tested in Single Product Speckle Filter under Speckle Filter function, SNAP. To display the de-speckle outputs in RGB image (Figure 2.7), bands Sigma0_VH and VV were converted to decibel (dB). Apparently, window size 3 x 3 of Lee Filter visually presents clearer ground features than the 5 x 5 window size (Figure 2.8).

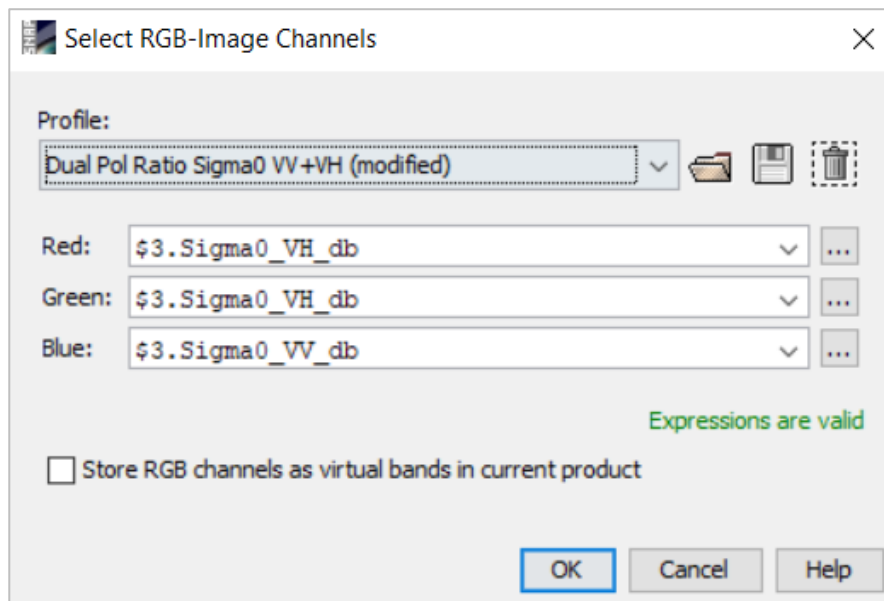


Figure 2.7: Red, Green, Blue image channels

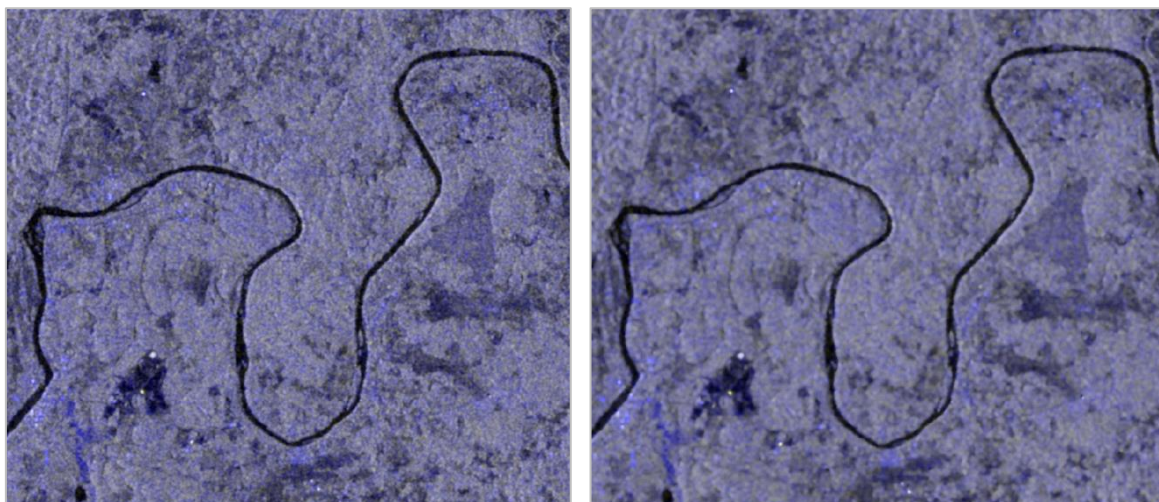


Figure 2.8: A combination of VH-dB, VH-dB, VV-dB Lee filter 3x3 (left) and 5x5 (right) displayed in RGB

Terrain Correction: This SAR data was obtained in the form of a GRD product which is in a multi-look from the original Single Look Complex (SLC) with no terrain correction. To obtain ortho-image correction, a digital elevation model (DEM) or a polynomial correction which assumes that surface is flat can be used (Frulla et al. 1998). In this present research, the digital terrain model SRTM 1arc-second with approximately 30 metres derived from Global dem from <https://earthexplorer.usgs.gov> was used. The study area shown in SAR data is mostly covered by a long river, a dam and the Mekong River. These water features were detected using SAR imaging. This data is useful when dealing with flood events during the rainy seasons as during this time there is high cloud coverage. In this study, however, detecting water areas where dengue mosquitoes are likely to breed is the main purpose. Favourable sites of breeding for mosquitoes are small sized surface water, and areas

where small amounts of water are accumulating. Therefore, with the issue of spatial resolution, PlanetScope and RapidEye imageries seemed to be better options to use in extracting surface water information with small sizes of less than 10 metres.

Field Survey

Field survey was implemented to observe surface water areas in the study site, and to obtain dengue incidence data from ECOMORE 2 project, Institut Pasteur du Laos (IPL). Ground surveys were conducted over six days in July and August 2019, and 33 ground points were collected (see Appendix 1). However, due to the time constraints and the large amount of water around the study site (more than 3,000 square kilometres), this survey was begun from the areas where IPL has determined to be the most prevalent dengue areas in Vientiane, at the village level, based on dengue incidence data in 2017. The observed areas were the targeted regions where the team from the Medical Entomology and Biology of Disease Vectors Laboratory, ECOMORE 2, IPL has frequently been to collect mosquito vectors.

The tool used in this field survey was the application of Survey 123. It is a GIS application which has been created for collecting data by forms with a provision of skip logic, defaults and support for multiple languages. Users can use these functions to create a form to be used during a field survey in web or mobile devices and it can be used even when there is no internet connection during the field observation. To log in, an ArcGIS organisational account is required (ESRI n.d). This current study, Survey 123 was performed under the Flinders University account. The survey form (See Appendix 2) was created from the application installed in a mobile phone (iPhone 8 Plus). From field observations, it was found that many surface water areas appear smaller than 10 metres and some of them are approximately 10 metres or bigger than that, as shown in Figure 2.9. Numbers of areas are properties which are not able to be identified, so the observer collected the data as close to the area as possible, and during surveying, internet connection was activated. From this field survey, Sentinel-2 and Sentinel-1 SAR were considered as inappropriate choices of imagery data to use in this current study due to their low spatial resolution to detect small surface water regardless of the ability of penetrating cloud cover.

Therefore, relatively high-resolution imaging data, such as PlanetScope and RapidEye, with 3 m and 5 m, respectively, were used as another option for examining surface water.

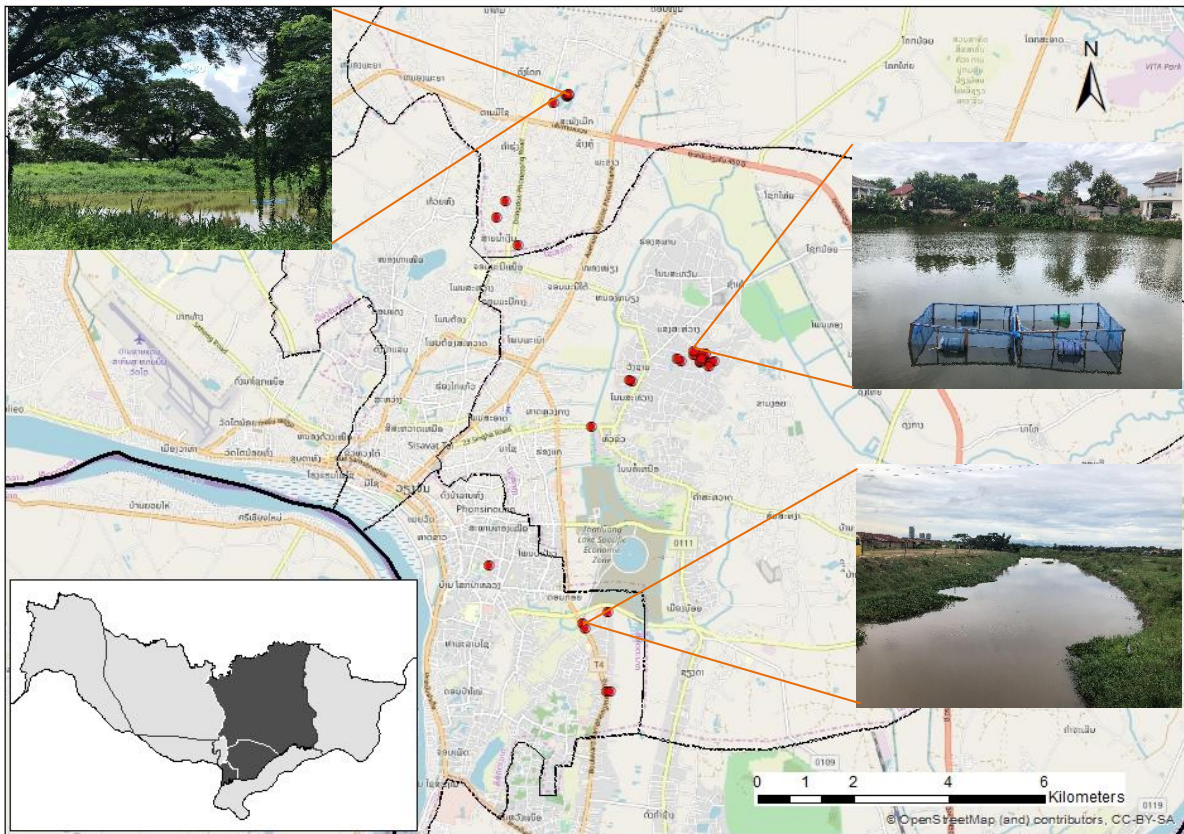


Figure 2.9: Ground point data collected from Survey 123 overlaid on Open Street Map

Relatively High-Resolution Satellite Imageries

PlanetScope datasets were the main data chosen in this current study. Twelve dates from January to December 2017 were expected to be acquired. In order to obtain PlanetScope with 3 m spatial resolution, an application under their Education and Research Program is required. Planet provides access to Planet data for students and faculty who are conducting research into fields such as the world's ecosystems, climate, humanitarian crises, markets and global challenges in real-time. A certain amount of image data (10,000 km² per month) in a specific region can be downloaded under personal research licenses and students need to apply under the University account.

A Flinders University student account was used to register under the Planet program and the download quota for this research was 10,000 km² per month in the study area. However, due to the presence of cloud in a large area study site and unavailability of PlanetScope, only PlanetScope image data from January to May, and August to December 2017 were derived. The image in March was RapidEye, while June, July and September were not able to be downloaded because the cloud cover over the study area was more than 50%. Although an attempt was made to access RapidEye data from other sources such as Earth Online operated by European Space Agency (ESA) the data was not freely accessible.

PlanetScope Ortho Tile Product Level 3B

PlanetScope is the new high spatial resolution satellite image which captures the earth's surface area of up to 150 million km² per day (Planet 2018). The images can be produced daily with a high ground resolution of 3 m. There are four bands provided ranging from visible bands (Blue, Green, Red), to near-infrared (NIR) (Table 2.6). The PlanetScope analytic ortho tile product is orthorectified, multispectral data derived from the satellite constellation. The products (Table 2.4) are projected in a Universal Transverse Mercator (UTM) cartographic projection and calibrated which allow analysts to use data for scientific analysis. Throughout the processes, distortion caused by terrain is removed as well as the perspective effect on the ground being eliminated. Orthorectified visual imagery is optimal for image processing with an enhancement of radiometric correction. With this correction, any sensor artefacts and transformation to at-sensor radiance are corrected, thus image processing such as vegetation indices, and land cover classification can be effectively analysed (Planet 2018).

Table 2.4: PlanetScope 3B analytic ortho tile product attributes

Product Information	Description
Analytic Bands	Four band multispectral image (blue, green, red, near-infrared)
Ground Sample Distance	3.7 m (at reference altitude 475 km)
Pixel Size (orthorectified)	3.125 m
Bit Depth	16-bit
Geometric Corrections	Sensor-related effects are corrected using sensor telemetry and a sensor model, bands are co-registered, and spacecraft-related effects are corrected using altitude telemetry and best available ephemeris data. Orthorectified using GCPs and fine DEMs (30 m to 90 m) to <10m RMSE positional accuracy
Positional Accuracy	Less than 10 m RMSE
Radiometric Calibration	
Accuracy	Initial availability <ul style="list-style-type: none">• No correction applied• Pixel values are digital numbers

Source: Adopted from Planet (2018)

RapidEye Ortho Tile Product Level 3A

The RapidEye product is orthorectified data derived from a constellation of five identical earth observation satellites. The product is multispectral data which provides five bands and frequent

revisits of approximately five days, and 5 m of ground resolution (Table 2.6). The distortion which is caused by terrain has been removed and the perspective effect on the ground has also been eliminated. Radiometric correction has been corrected for any sensor artefacts and transformed to at-sensor radiance (Table 2.5). This orthorectified imagery can optimise the results of image processing such as vegetation indices and land cover classification.

For this research project, PlanetScope images at the 3B level, and RapidEye images at the 3A level downloaded from the Planet (<https://www.planet.com/explorer>) were used. Forty-nine tiles of PlanetScope (45 tiles) and RapidEye (4 tiles) were used in this present study (Table 2.7). PlanetScope and RapidEye have already made the products of surface reflectance so atmospheric correction on the orthorectified images is not needed (Collison & Wilson 2017; Wicaksono & Lazuardi 2018).

Table 2.5: RapidEye analytic ortho tile products attribute

Product Information	Description
Analytic Bands	Five band multispectral image (blue, red, red edge, near-infrared)
Pixel Size (Orthorectified)	5 m
Bit Depth	16-bit
Geometric Corrections	Effects at sensor are corrected using sensor telemetry and a sensor model, bands are co-registered, and effects from spacecraft are corrected using altitude telemetry and available ephemeris data.
Positional Accuracy	Orthorectified using GCPs and fine DEMs (30 m to 90 m) to <10 m RMSE positional accuracy. Less than 10 m RMSE
Radiometric Correction	<ul style="list-style-type: none"> • Correction of relative differences of the radiometric response between detectors • Non-responsive detector filling which fills null values from detectors that are no longer responding • Conversion to absolute radiometric values based on calibration coefficients

Source: Adopted from Planet (2018)

Table 2.6: PlanetScope and RapidEye sensor specifications

Satellites	Band	Wavelength (nm)	Spatial Resolution (m)
PlanetScope	1 (VIS) Blue	455 – 515	3
	2 (VIS) Green	500 – 590	3
	3 (VIS) Red	590 – 670	3

Satellites	Band		Wavelength (nm)	Spatial Resolution (m)
	4 (NIR)	Near-Infrared	780 – 860	3
	1 (VIS)	Blue	440 – 510	5
	2 (VIS)	Green	520 – 590	5
RapidEye	3 (VIS)	Red	630 – 685	5
	4 (VIS)	Red Edge	690 – 730	5
	5 (NIR)	Near-Infrared	760 – 850	5

Source: Planet (2018)

Table 2.7: Image datasets used in this study

Satellite Images	Dates	Number of Tiles
	04 January	4
	16 January	4
	17 February	3
	04 April	4
	10 May	4
PlanetScope	June	-
	July	-
	23 August	6
	September	-
	17 October	8
	14 November	5
	24 December	7
RapidEye	13 March	4

2.2.2. Dengue Incidence Data

To obtain dengue incidence data and other dengue related data, a Memorandum of Understanding (MoU) was established between Flinders University and the ECOMORE 2 Project, Institut Pasteur du Laos (IPL). Two main datasets which included dengue incidence (georeferenced point data), and *Aedes* mosquito populations (*Aedes aegypti*, *Aedes albopictus*) collected in 2017 were obtained from IPL, under the ECOMORE 2 Project, and used in this study.

Dengue incidence in 2017 collected from hospitals that have a partnership with IPL's surveillance system was obtained from ECOMORE 2, IPL (see Appendix 3). The data were mainly collected using a smartphone via a link developed by IPL – <https://geo.pasteur.la/> – for direct data transfer.

Spatial data were recorded in a link server by patients whose cases were confirmed positive, and by district volunteers and the team members of Arboviral and Emerging Disease Laboratory team, IPL, who normally contact patients for collecting data. The data collected were geocoded indicating locations of the dengue cases (Appendix 4). Other information such as patients' information, including symptoms – onset date, village, and district – were collected using questionnaires completed by medical doctors. For clinical information, reverse transcription polymerase chain reaction (RT-PCR) and non-structural protein antigen 1 (NS1 antigen) were used to confirm dengue infection which was tested by the laboratory team members.

Georeferenced data indicating dengue cases in specific locations were firstly performed on data from 2015 until the present. However, past collection of this spatial data between in 2012 to 2014 were able to be collected and stored as *.xml/Excel* files. Clinical data was recorded in the system known as Pathogen Asset Control System (Pacs).

This study only used data from 2017, due to the availability of clinical data at village and district levels and spatial data (GPS). Despite the fact that spatial and clinical data has been collected and stored according to the proper methods, the GPS data and the clinical data still needed to be verified before they were used in this study. To verify the data, two files (Pacs and GPS) were compared by matching patients' identification (ID) codes attached in the files. During this matching task, some issues were found, for instance, some ID codes for patients in the GPS file did not exist in the Pacs file. Some dengue incidence dates were recorded as 2017 data in the GPS file, but in the Pacs file those data belong to data in 2018. The ID codes which were not found in the Pacs file had been checked by the Lab team members because when the cases were too large, it is likely that all GPS data could not be collected. Furthermore, when the Pacs file was updated, the GPS data file was rarely checked for an update. Thus, only the matched ID codes from GPS and Pacs were used in this study. To solve the problem with the dates of incidence, the onset date of dengue fever recorded in clinical data was used as a reference. For example, if the data was in 2018, but the onset date was in 2017, such data will be included in the 2017 dataset.

From this validation, total dengue numbers used in this study equalled 354 cases (GPS points projected in Geographic Coordinate Systems, World WGS 1984) or around 33% of total confirmed cases of 1,076 with all clinical data attached.

2.2.3. Meteorological Data

Daily and monthly rainfall data from 2016 to 2018 was derived from the Department of Meteorology, Ministry of Natural Resource and Environment (MoNRE), Laos (Figure 2.10). The monthly rainfall data helped visualise the trends in rainfall in 2017 and provided data to be compared with dengue incidence data in order to initially analyse the relationship between dengue prevalence and rainfall.

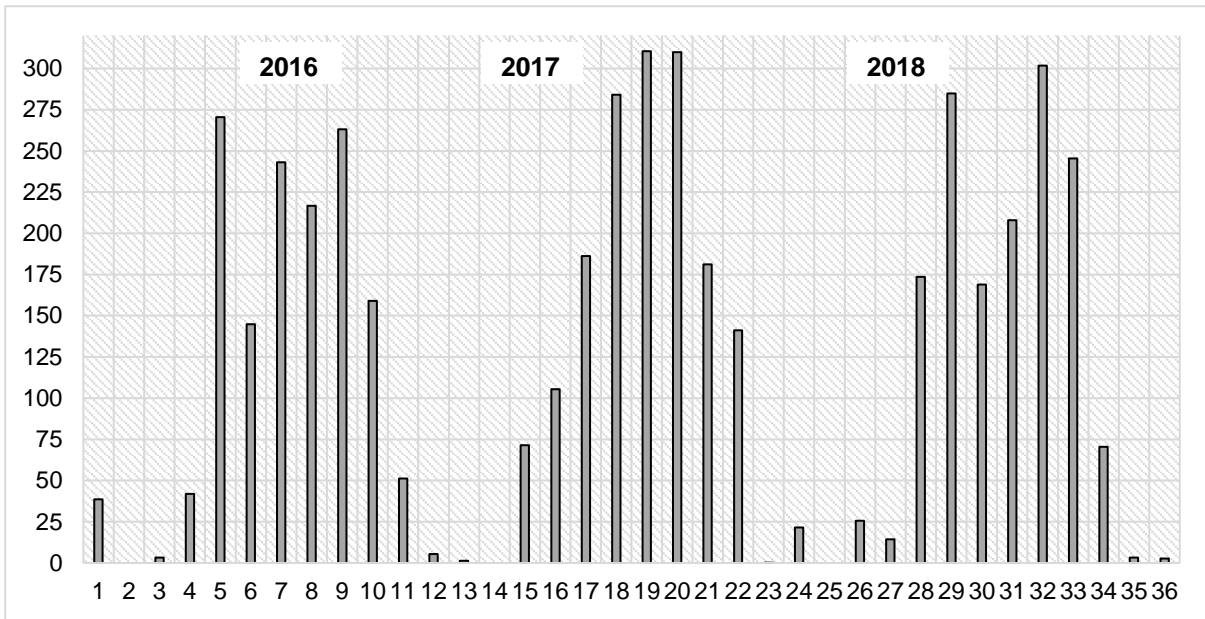


Figure 2.10: Monthly precipitation data from 2016 to 2018

2.3. Software Used

2.3.1. Earth Resource Data Analysis System (ERDAS) Imagine 2018

ERDAS Imagine is a software generated by Hexagon Geospatial company. It is a tool used to perform advanced remote sensing analysis and spatial modelling 2 Dimensional and 3 Dimensional views with high quality map compositions.

In this project, the processes of image analysis from pre-processing, surface water detection generated by using spatial modeller, Toolbox, were performed using this software. In this version, the ERDAS 2018 62-bit was used for examining the PlanetScope images and RapidEye to identify water bodies.

2.3.2. ArcGIS Version 10.6

ArcGIS software is a system designed to work with maps and geographic information in a field of architecture, geographic information. It was developed by the Environmental System Research Institute (ESRI) – an international supplier of geographic information systems software, web GIS and geodatabase management systems.

This study used ArcGIS version 10.6.1 under the licence of the College of Science and Engineering, Flinders University. It was applied to image analysis to separate surface water through a method of water indices from non-water features, and to generate maps in different series. This software was also used for accuracy assessment to produce confusion matrix of Kappa coefficient.

2.3.3. Google Earth Pro

Google Earth Pro is a geospatial software application that is used to explore features on the ground, capture geographical data as well as display a virtual globe. With these various abilities, it enables users to analyse data in the field of interest.

This software was used as a tool to help visualise the area of interest by linking it with ERDAS Imagine software to view and compare particular spots between satellites imageries and aerial imageries from Google Earth. Additionally, it was used as a base map to create ground truth points in the process of accuracy assessment once the digital image analysis had been performed.

2.3.4. Statistical Package for the Social Sciences (SPSS)

The Statistical Package for the Social Sciences is the software registered trademark of International Business Machines (IBM) which has been developed for the use of statistical data analysis. It has been widely used in the field of business and research solving problems by quantitative and qualitative analysis with the capacity of testing hypothesis and predicting analysis tools.

This study used IBM SPSS software version 25 under the register of Flinders University for analysing the association between surface water and dengue incidence. The main statistical models used in this software are correlation and regression analysis to experiment whether there is a relationship between variables, and to find out the association and predictions from the regression model.

2.4. Areas of Interest (AOI)

The whole area of the study site is approximately 3,583 square kilometres, however, due to the limited amount of satellite image data downloaded from the Planet, the specific areas of interest which were considered as the most prevalent dengue fever areas were selected. Figure 2.11 presents the sample area used to investigate the monthly surface water in 2017. AOI was created by the Create Features using the Editor Tool in ArcMap in Shapefile format. A polygon was drawn according to the selected areas of interest on the top of PlanetScope covering the study site. This AOI was then used as the feature mask data to mask the surface water output by Extract by Mask under Spatial Analyst tool, ArcMap.

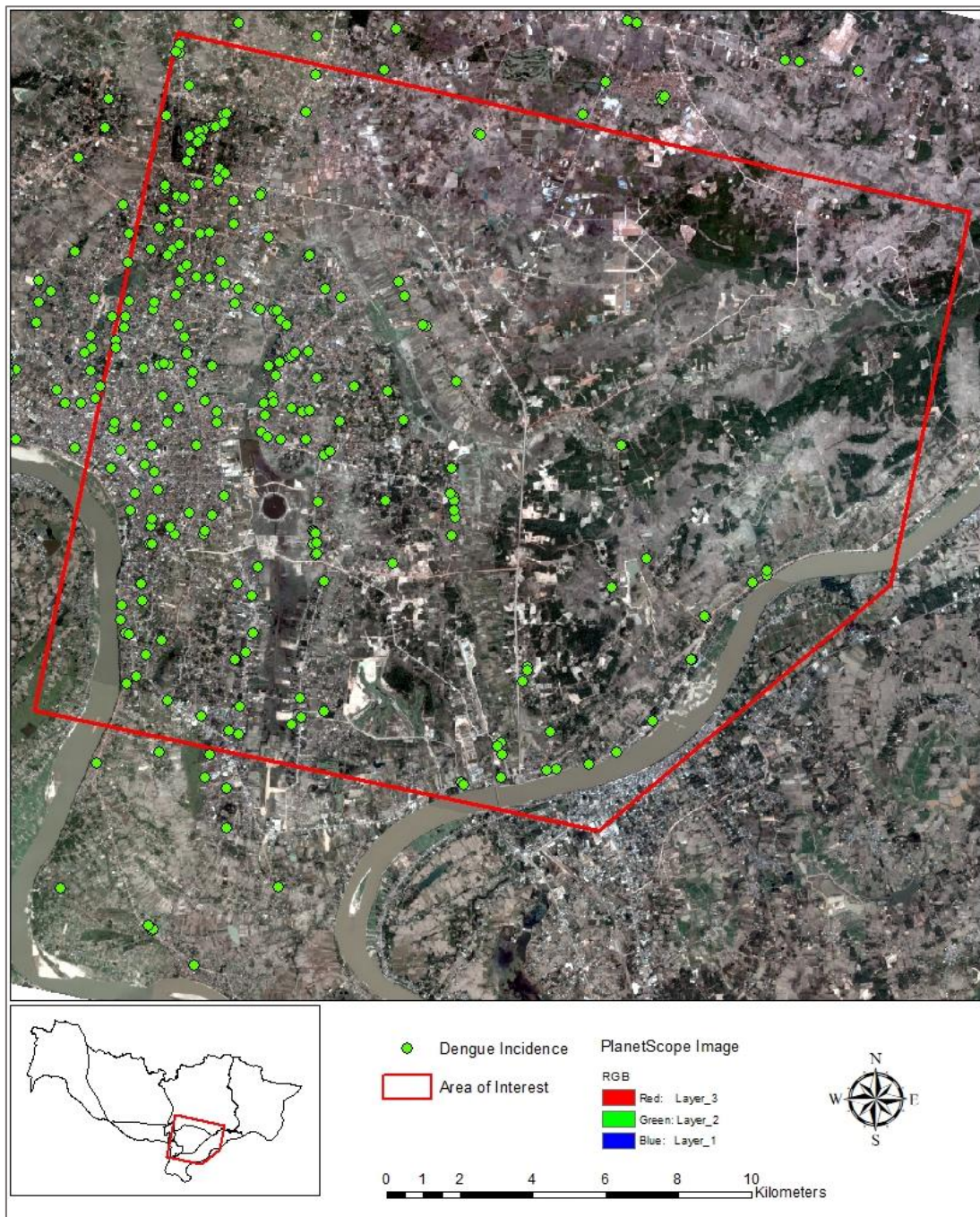


Figure 2.11: Area of interest and dengue incidence in the study site overlaid on PlanetScope image in January 2017 displayed in true-colour composite

2.5. Image Correction

2.5.1. Atmospheric Correction

The atmospheric effect at remotely sensing sensors caused by variable atmospheric conditions, solar illumination and view angles must necessarily be corrected. This correction removes radiometric distortions, and the true reflectance can be retrieved (El Hajj et al. 2008). Typically, sensors that detect electromagnetic radiance from ground surface by using visible and near-visible

radiance will record pixel locations which fail to represent the true ground features at particular points. The effects caused by the interference of the atmosphere on satellite imageries are mostly found in the visible or NIR bands (Figure 2.12) (Hadjimitsis et al. 2010). Thus correcting atmospheric effects enhances the quality of the reflectance radiance values of image data (Themistocleous & Hadjimitsis 2008).

In this study, the main source of satellite imageries used were PlanetScope and RapidEye images which include visible (Blue, Green Red), and NIR. In order to obtain more accurate results of image analysis, the disturbance from atmosphere needed to be corrected. To correct for the atmosphere in image data, image values were converted to surface reflectance by calibrating radiometric which involves the conversion of digital number values to radiance and to top of atmosphere (TOA) radiance. Bottom of atmosphere is another step needed to perform the correction (Chen & Cheng 2012). To process this, the top of the atmosphere radiance is converted to surface reflectance. The bottom of the atmosphere correction is performed by applying a simple correction of Dark Object Subtraction (DOS) method which can be applied to obtain BOA (Gautam et al. 2015). This method is considered to be a simple and reasonable approach used to correct atmospheric effects (Chavez 1988) and can provided better results compared with many complex atmospheric correction methods (Hadjimitsis, Clayton & Hope 2004).

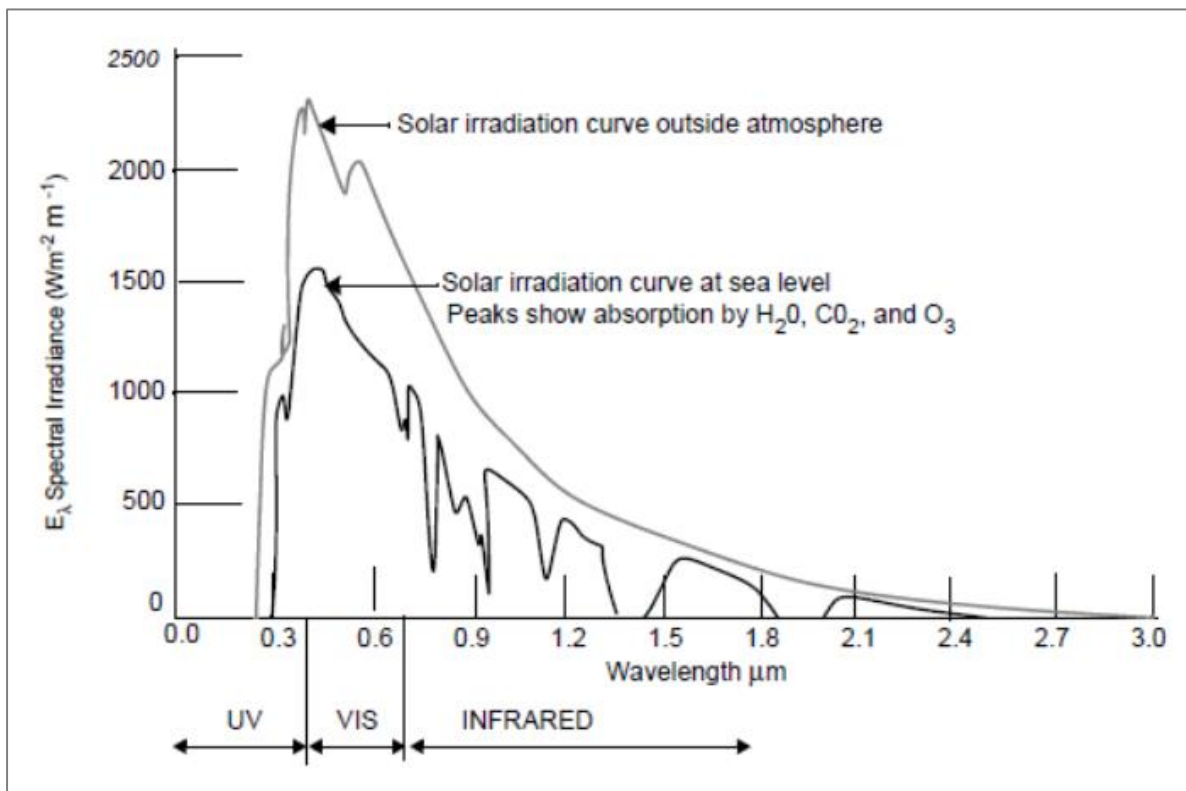


Figure 2.12: Spectral radiance at the Earth's surface

Source: Modified from Chahine et al (1983)

PlanetScope Images

PlanetScope products have already been orthorectified and the pixel values have been scaled to Top-of-Atmosphere (TOA) radiance (Planet 2018). However, atmospheric correction reflectance was required to be performed for image data in January 2017 (04 January and 16 January) as they were captured at different times and under different atmospheric conditions. Hence, atmospheric correction was attempted. To process this correction, Spatial Model Editor from ERDAS Image was used to create the spatial model for TOA (Figure 2.13). Digital number (DN) values of each band were converted to TOA by multiplying them with reflectance coefficients (Table 2.8) provided by the PlanetScope stored in the metadata file *.xml*. Reflectance output rasters were then multiplied by 10,000 to obtain final outputs. Reflectance is generally in a floating-point number between 0 and 1, whereas image file formats are defined as unsigned integers. A common performance of converting floating numbers to unsigned integers is to multiply the reflectance outputs by 10,000 (Planet 2019).

To obtain BOA reflectance, dark object subtraction was performed by using the dark ground features which had no effects from sunglint: the objects that are mostly free from sunglint tend to be the optically deep-water pixels as they are likely to highly absorb the reflectance (Wicaksono & Lazuardi 2018). In this study, surface water which appears dark had been observed, and minimum and maximum values of each band were also examine in order to find out the darkest values. Those obtained dark pixel values then were subtracted from each band performing in the spatial model created in ERDAS Imagine (Figure 2.14).

Not all images went through this process as the products of PlanetScope have already been atmospherically corrected. However, an investigation of image data with BOA and without BOA process was performed in order to obtain the highly accurate outputs of water index images.

Table 2.8: Reflectance coefficient of 04 January and 16 January 2017

Dates	Band 1 - Blue	Band 2 - Red	Band 3 - Green	Band 4 – NIR
04 January	$2.60489507083 \times 10^{-5}$	$2.75171253034 \times 10^{-5}$	$3.07292547872 \times 10^{-5}$	$4.64466548288 \times 10^{-5}$
	$2.60203983282 \times 10^{-5}$	$2.74869636502 \times 10^{-5}$	$3.06955723033 \times 10^{-5}$	$4.63957444273 \times 10^{-5}$
	$2.59919487701 \times 10^{-5}$	$2.74569106141 \times 10^{-5}$	$3.06620111158 \times 10^{-5}$	$4.63450173626 \times 10^{-5}$
	$2.59635994985 \times 10^{-5}$	$2.74269635168 \times 10^{-5}$	$3.06285682335 \times 10^{-5}$	$4.62944691141 \times 10^{-5}$
16 January	$2.55464525586 \times 10^{-5}$	$2.70393385863 \times 10^{-5}$	$3.01624442414 \times 10^{-5}$	$4.54993037045 \times 10^{-5}$
	$2.55204736053 \times 10^{-5}$	$2.70118414723 \times 10^{-5}$	$3.01317711477 \times 10^{-5}$	$4.54530340987 \times 10^{-5}$
	$2.5494586734 \times 10^{-5}$	$2.69844418216 \times 10^{-5}$	$3.01012067744 \times 10^{-5}$	$4.54069284949 \times 10^{-5}$
	$2.54687934713 \times 10^{-5}$	$2.69571412498 \times 10^{-5}$	$2.69571412498 \times 10^{-5}$	$4.53609896121 \times 10^{-5}$

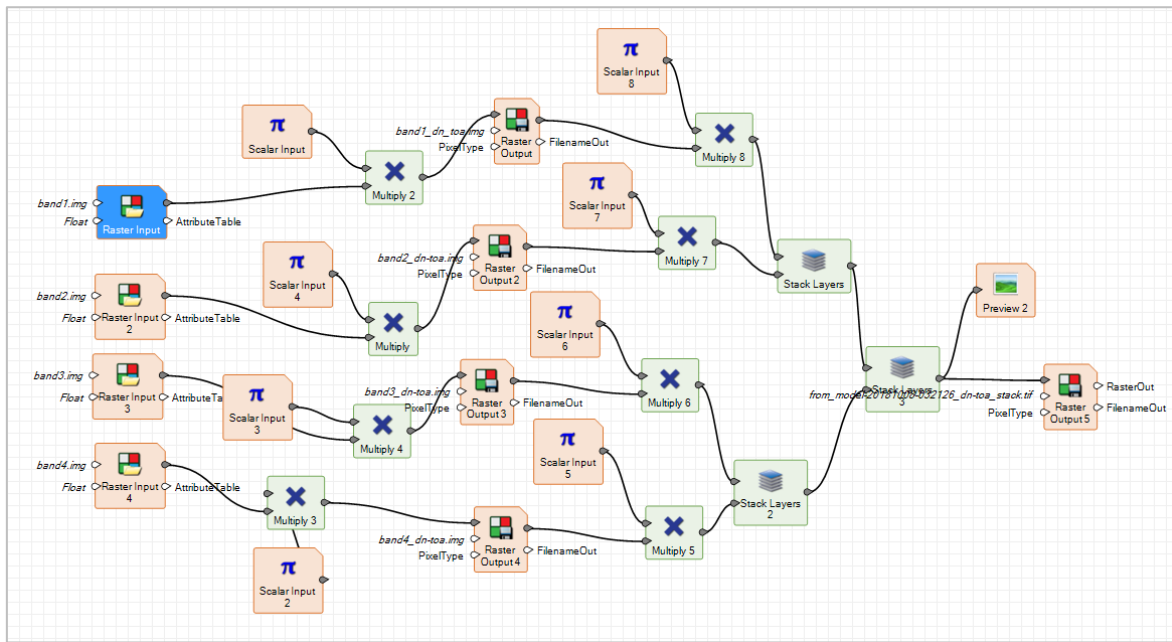


Figure 2.13: Spatial model of atmospheric correction to obtain TOA reflectance

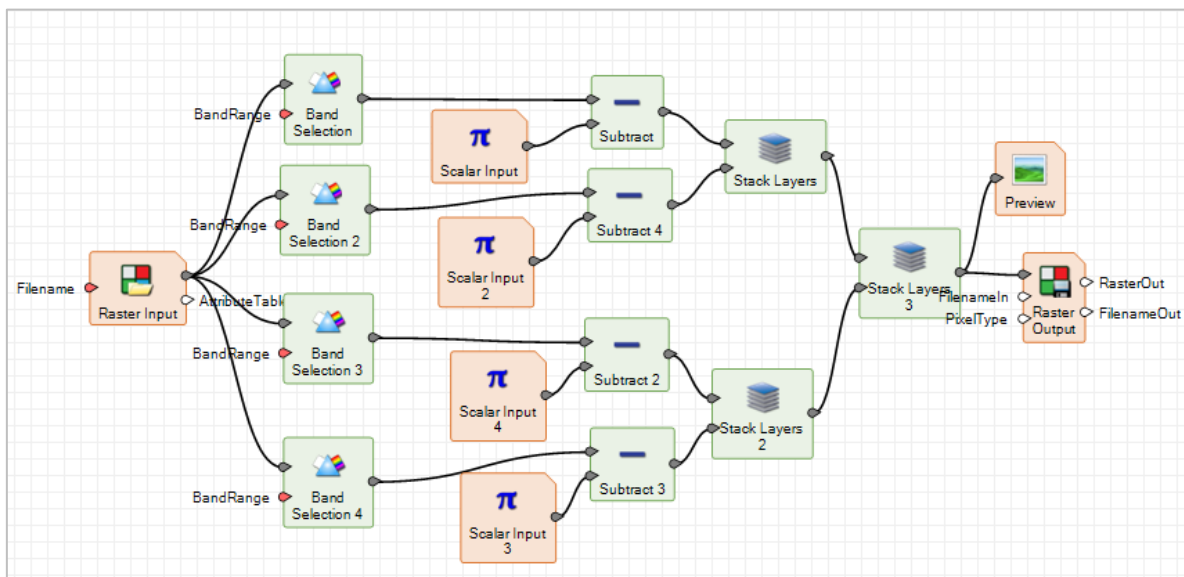


Figure 2.14: Spatial model of dark object subtraction to obtain BOA

RapidEye Images

To remove the influence of atmospheric effects, Rapid Atmospheric function provided on ERDAS Imagine was adopted and created by the Spatial Model Editor tool (Figure 2.15). Rapid Atmospheric function is used to compute the radiometric transform from DN values of satellite images to corrected values which truly represent ground reflectance. The process of Rapid Atmospheric correction used the information from the metadata *.xml* file attached with the image products to perform the calibration which converts DN to radiance, and TOA.

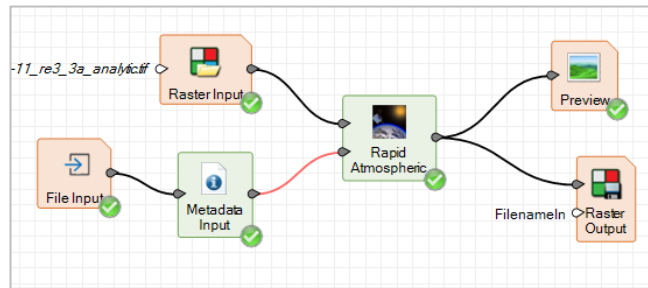


Figure 2.15: Atmospheric correction spatial model used to correct atmospheric effect on RapidEye

2.5.2. Haze Reduction

The presence of haze and cloud have become the main challenges to optical remote sensing, which blocks ground features from remotely sensed detection and creates the uncertainty of spectral reflectance from sensors (Kaufman & Sendra 1988). Many algorithms have been developed such as dark object subtraction (Kaufman & Sendra 1988), frequency filtering (Du, Guindon & Cihlar 2002), and transformation approaches (Moro & Halounova 2007). However, a problem of most methods is to select haze values independently from each spectral band, but haze values are strongly correlated and highly scattered in the visible wavelength of the electromagnetic spectrum. Therefore, to reduce haze, multispectral image data is needed for correction depending on spectral band (Chavez 1988). The tasselled cap transformation (TCT) approach developed by Kauth and Thomas (1976) was found to be the most promising to use for haze reduction. TCT can help visualise the three-dimensional surface phenomena and the important variables such as bare soil, view angle, and atmospheric haze in the separated spectral band. So, this transformation is able to estimate and correct atmospheric haze and moisture effects by using the specific measurable pattern elements of the TCT structure.

This study attempted to reduce haze on image data by adopting the haze reduction function in ERDAS Imagine: due to the unviability of index values of PlanetScope used in TC. Raster Radiometric function in ERDAS Imagine was adopted. To create a haze reduction spatial model, the Spatial Model Editor tool was used. The custom matrix function was applied with the nearest neighbour method for raster interpolation with 5 x 5 convolution kernel (Figure 2.16).

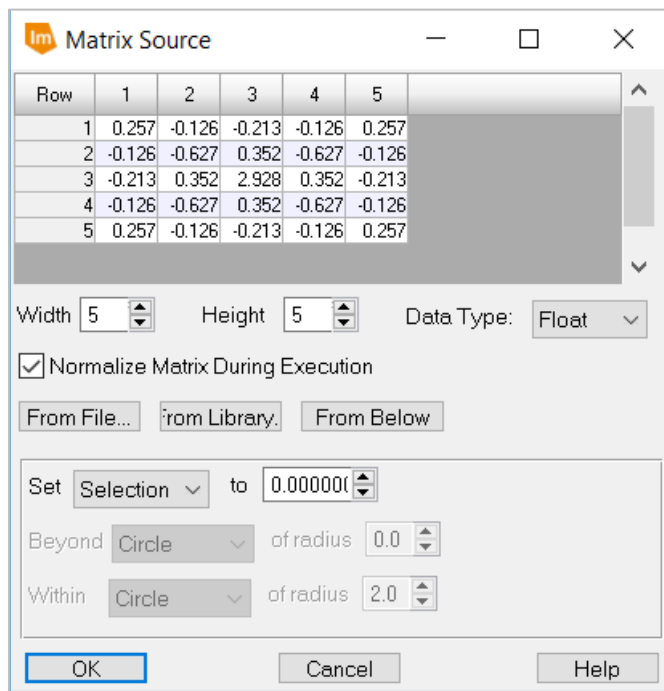


Figure 2.16: 5 x 5 Convolution Kernel

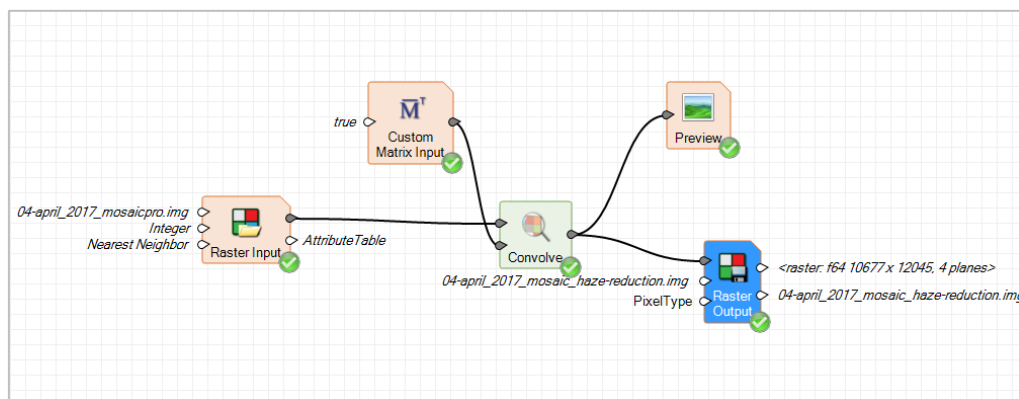


Figure 2.17: Haze reduction spatial model

2.5.3. Cloud Masking

To obtain the water index result, cloud cover and shadow which block radiance reflected from the ground surface needed to be removed. PlanetScope image data in August 2017 was captured during the wet season in the study area when one of the main obstacles is the presence of cloud. Automated cloud and shadow detection algorithm to mask out the cloud coverage was not available for PlanetScope images (Cooley et al. 2017). To mask out cloud, PlanetScope imageries bands to be assessed cloud cover are band 2, band 3, and band 4 (Red, Green, and NIR respectively) (Planet 2016). Band thresholding and unsupervised classification were applied.

Unsupervised classification, ERDAS Imagine, was assigned as a tool to classify cloud and shadow. Three hundred classes were set using Isodata, and 20 maximum iterations. Cloud and shadow were classified and recoded as 0 for new values and 1 for non-cloud and shadow by using the Recode

function applicable in ERDAS Imagine. To mask out the cloud and shadow from the imagery, a spatial model of cloud mask was created from the Spatial Model Editor (Figure 2.18). The mask of cloud and shadow was multiplied with the original spectral image in order to retrieve a cloud mask image.

Band 2 (Green) was used for cloud pixel value inspection in order to find the best threshold values for masking cloud from the image. The selected pixel value used for thresholding cloud masking was 10,000 as it can best detect cloud cover in most of the cloud covered areas. Spatial model for cloud masking from Spatial Model Editor, ERDAS Imagine was developed (Figure 2.19) for cloud removing implementation.

The performance of cloud masking showed that a lot of areas covered by cloud and shadow were poorly detected by unsupervised classification if compared with the thresholding method, regardless of its ability to detect shadow. Hence, to improve cloud and shadow masking, cloud mask images from the threshold method was multiplied with the cloud mask image generated from unsupervised classification using Spatial Model Editor (Figure 2.20). However, the result from this attempt (Figure 3.5, Chapter 3) shows that by combining these two methods, many water areas were classified as shadow due to the overestimation of deep-water bodies. Therefore, in this study, only cloud mask by a single band threshold method was performed.

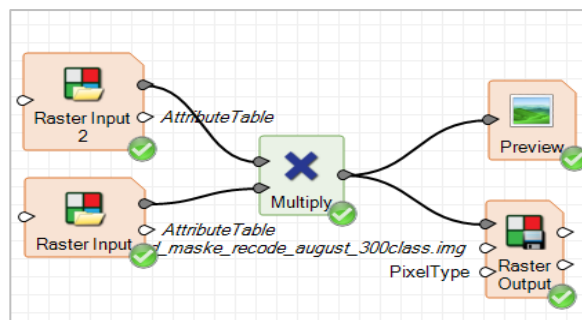


Figure 2.18: Spatial model for cloud and shadow masking multiplied with image data

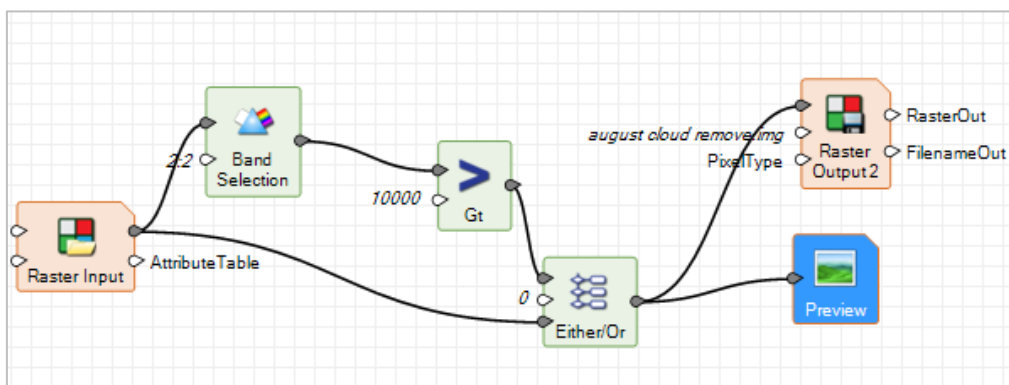


Figure 2.19: Spatial model for cloud masking image obtained from a single band threshold method

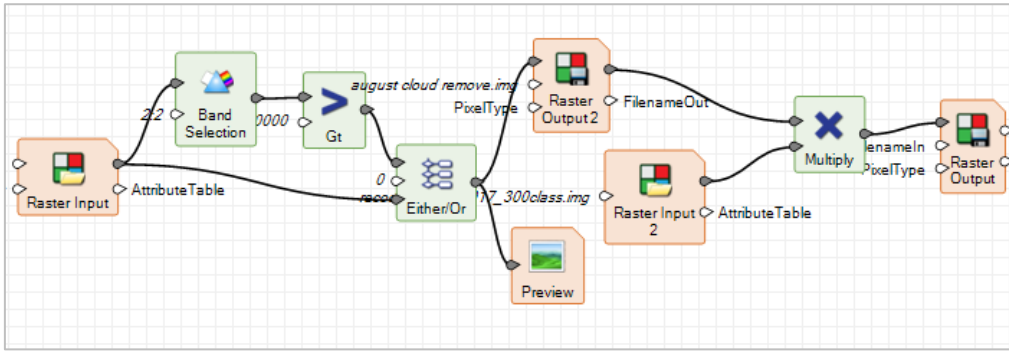


Figure 2.20: Combining cloud masked binary image produced from classification method with the cloud mask image from a single band threshold method

2.5.4. Mosaicking

The mosaic is the process that allow multi-images to be stitched together in order to create one large and cohesive image of an area of interest. The output images contain the same number of layers as the original image data (Hexagon n.d).

In this study, the mosaic process was performed after the image correction, tiles (Figure 2.21, Figure 2.22) for each date were stitched by the Mosaic function in ERDAS Imagine in order to generate new images that cover the study site.



Figure 2.21: PlanetScope image tiles displayed in true-colour composite

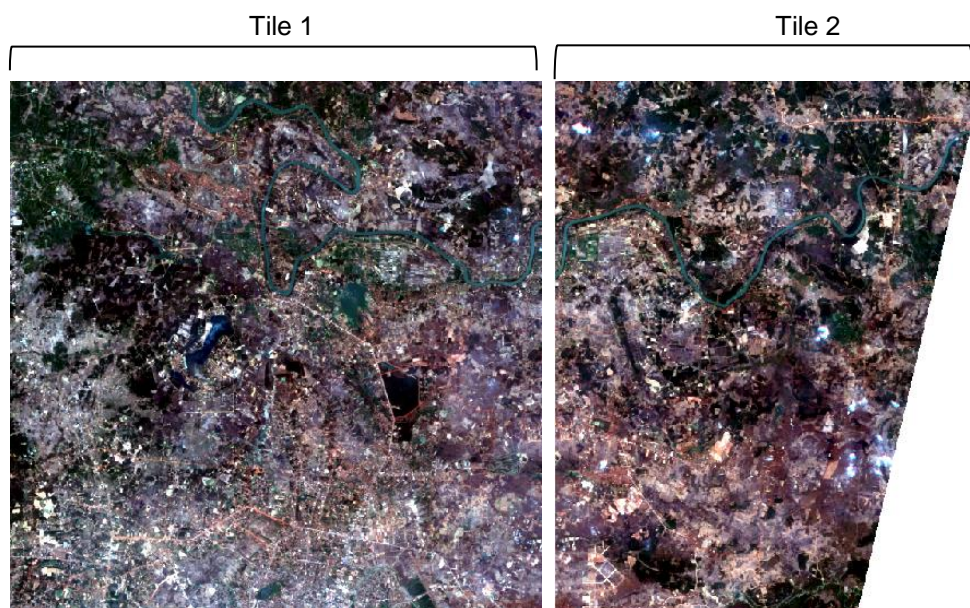


Figure 2.22: RapidEye image tiles displayed in true-colour composite

2.6. Water Body Extraction

Water body data can generally be extracted by two methods, firstly, supervised and unsupervised classification using single band or multiple bands, and secondly, the water spectral index (Huang, Chen & Wu 2014; Sheng, Shah & Smith 2008). It has been noted however that the water index algorithm “seems to be an essential approach for rapid performance of water bodies extraction in large scale areas” (Du et al. 2014).

To extract water body features, analysing and observing spectral features in the specific study area was needed before applying water extracting algorithms. Spectral Profile in ERDAS Imagine was used to visualise the reflectance spectrum of ground features through bands. Observation of spectral reflectance from PlanetScope shows that the reflectance of water bodies is higher in the visible part of the spectrum, especially in Blue and Green (455 – 515 nm, 500 – 590 nm), with low reflectance in Red and NIR where the light is mostly absorbed by surface water, as indicated in Figure 2.23. In the RapidEye spectral profile, water reflectance shows high absorption in Red, Red Edge and NIR bands and high reflectance in Blue and Green at the visible channel (440 – 501 nm, 520 – 590 nm) (Figure 2.24). For both satellite imageries, the spectral reflectance illustrates that shallow surface water contains a larger amount of pixel values when compared with the river and deep still water bodies.

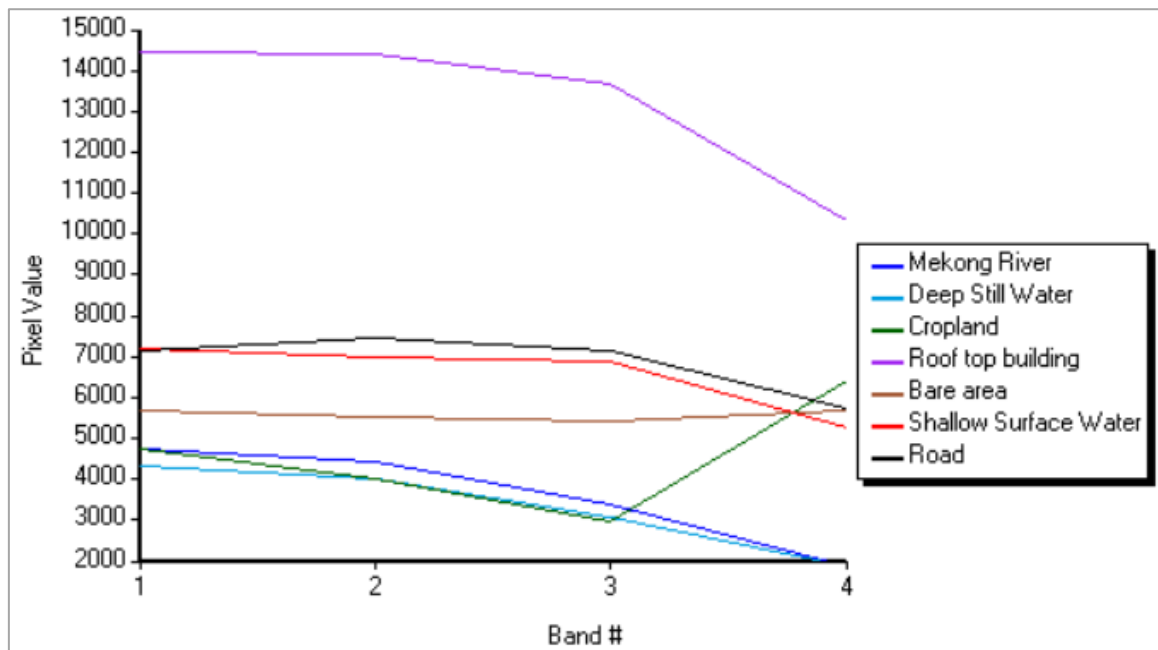


Figure 2.23: PlanetScope spectral profile

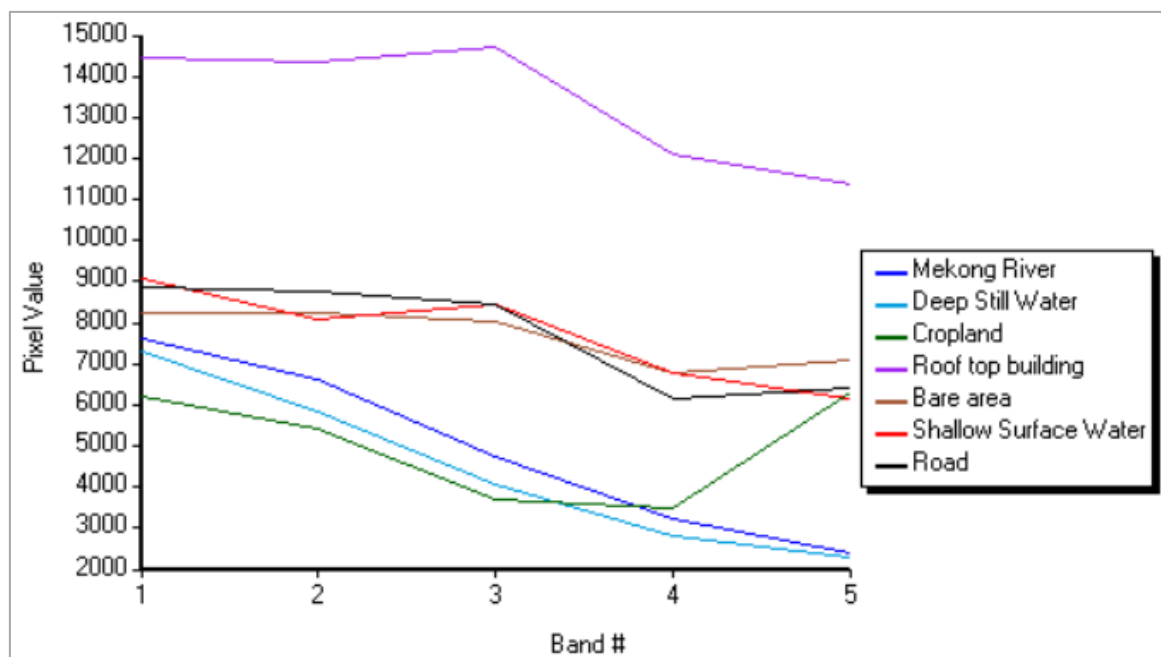


Figure 2.24: RapidEye spectral profile

2.6.1. Multi-band Spectral Relationship Method

According to the curve analysis of the spectral reflectance, on the basis of this test, Chen et al. (2004) introduced the water extraction model $(Green + Red) - (NIR + MIR) > T$ where T is defined as a threshold used to extract water information and non-water information. This study adopted this model with the change of band selection. Instead of using Red and MIR due to the limitation of sensor wavelength in PlanetScope and RapidEye, an effort to create a water extraction model used in this study area was performed in Spatial Model Editor, ERDAS Imagine (Figure 2.25), and the

model was defined as (Blue + Green) - (Red + NIR), where threshold values of the water feature is greater than zero. This model was created according to the spectral band analysis as it is found that Blue and Green bands show higher reflectance, whereas the low reflectance level was in Red and NIR. It was thought that this method could identify water areas, however it was falsely detecting large built-up areas and roads as surface water areas compared to normalized difference water index (NDWI) (McFeeters 1996), and normalized difference moisture index (NDMI) (Gao 1996) (Figure 3.4, Chapter 3).

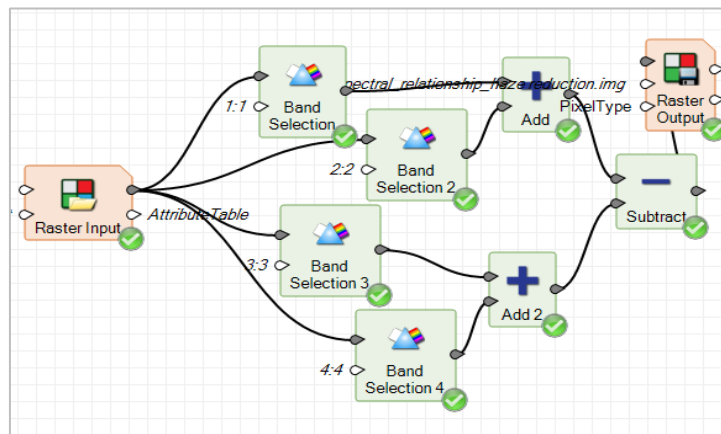


Figure 2.25: Spatial model of multi-band spectral relationship method

2.6.2. Normalized Difference Vegetation Index (NDVI)

Normalized Difference Vegetation Index (NDVI) proposed by Rouse Jr et al. (1974) was tested to determine whether it could help distinguish vegetation areas from water bodies in the study area. Many previous studies have applied NDVI as a model to extract water information from high resolution spectral remotely sensed imagery (Zhang, Wang & Shinohara 2007), and using NDVI with multispectral image data to achieve sufficient resolution to identify surface water (Carrasco-Escobar et al. 2019). PlanetScope imagery in February 2017 was used in this investigation carried by Spatial Model Editor, ERDAS Imagine (Figure 2.26). NDVI formula is displayed in Equation 2.1, where;

$$NDVI = \frac{(NIR - Red)}{(NIR + Red)} \quad \text{Equation 2.1}$$

Green = reflectance in Green wavelength

NIR = reflectance in near-infrared wavelength

The values of this range are from -1 to +1. Positive values are interpreted to be vegetated areas, while negative values are non-vegetated areas

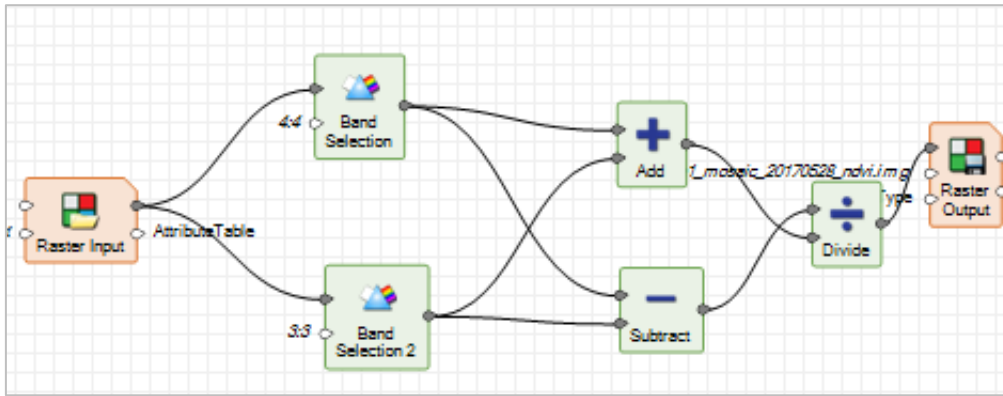


Figure 2.26: NDVI spatial model

2.6.3. Normalized Difference Water Index (NDWI)

Normalized difference water index was originally derived from the normalized difference vegetation index developed by McFeeters (1996). The typical form of this water index employs Green and NIR bands, however, several water indices modified from this originality have been developed, for instance, Gao (1996) used NIR and SWIR, and Rogers and Kearney (2004) had developed a water index formula by using Red and SWIR bands.

In this research project, the normalized difference water index was used based on comprehensive analysis of each band, the multi-band spectral relationship, for example. The NDWI developed by McFeeters (1996) was used due to its ability to improve the accuracy of water information extraction. It is suggested that this NDWI enhances water spectral signals by contrasting the highest reflectance and lowest reflectance to remove noise in wavelength regions so that NIR is used because water has a strong absorption in this range (Gao et al. 2016). To derive water features, NDWI was examined for generating surface water from PlanetScope images (January, February, April, May, August, October, November and December), and RapidEye image (March).

This index model is illustrated in Equation 2.2 where;

Green = reflectance in Green wavelength, 500 – 590 nm for PlanetScope; and 520 – 590 nm for RapidEye

NIR = reflectance in near-infrared wavelength, 780 – 860 nm for PlanetScope, and 760 – 850 nm for RapidEye

$$NDWI = \frac{(Green - NIR)}{(Green + NIR)} \quad \text{Equation 2.2}$$

The values of water index results produced from NDWI ranged between -1 to +1 where the pixel value which is closer to +1 is water information, while the pixel values toward -1 indicate the areas

of non-water. To acquire water index results, a spatial model was built using Spatial Model Editor in ERDAS Imagine (Figure 2.27).

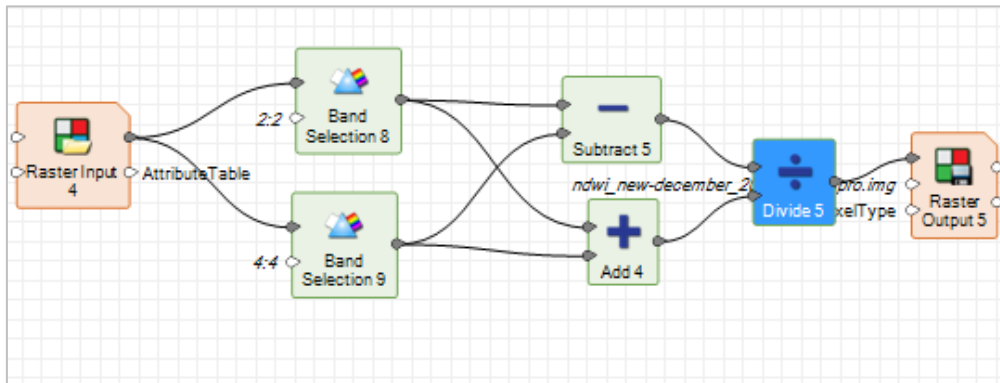


Figure 2.27: NDWI spatial model

2.6.4. Normalized Difference Moisture Index (NDMI)

Normalized difference moisture index (NDMI) was adopted from Gao (1996) as defined in Equation 2.3; where NIR and SWIR, which their wavelength was highly absorbed by that water, were exploited. From this development, it is found that the NDMI is likely to perform better in detecting low water and other objects which contains moisture (Ogilvie et al. 2018).

In this study, however, due to the limitations of remote sensing sensors which only contain visible bands and NIR band, Red and NIR bands of PlanetScope and RapidEye which show the lowest reflectance and high absorption from water were used. Multi-temporal images were applied to extract surface water during the time where water surface appeared less. NDMI modified is indicated in Equation 2.3.

$$\text{NDMI} = \frac{(\text{Red} - \text{NIR})}{(\text{Red} + \text{NIR})} \quad \text{Equation 2.3}$$

Where;

Red = reflectance of Red wavelength (band 3 for PlanetScope, and band 3 for RapidEye)

NIR = reflectance of NIR wavelength (band 4 for PlanetScope, and band 5 for RapidEye)

Values of this index range from -1 to +1, where values are close to one is considered as water and values are closer to -1 are non-water.

From this analysis, it is found that NDMI performed well in detecting low surface water during the dry season (February and March) and bare areas were less overestimated compared with the NDWI.

Therefore, NDMI was used to detect surface water from the image data in February and March. This water index model was created using Spatial Model Editor, ERDAS Imagine as represented in Figure 2.28.

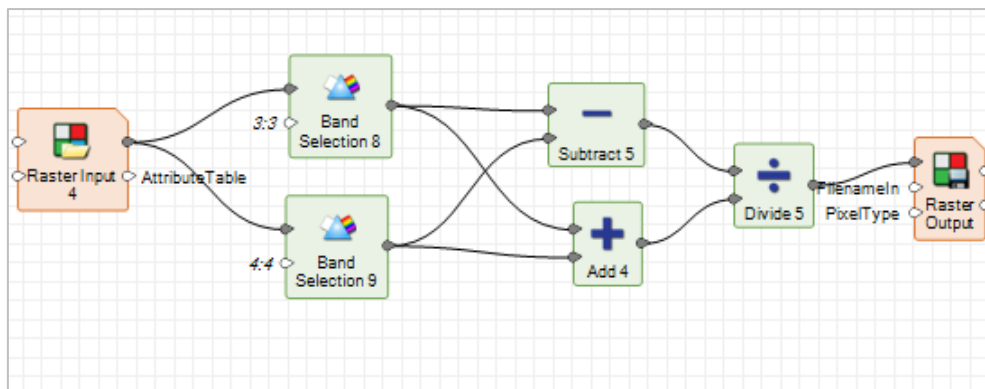


Figure 2.28: NDMI spatial model

2.6.5. Threshold Values

To extract surface water from other land cover types, manual thresholding was applied to select specific thresholds in order to classify two classes – water and non-water. In doing so, the identifying tool in ArcMap was used to inspect pixel values of water areas, and adjustments to the spectral histogram were applied to identify water from non-water (Figure 2.29). To classify surface water from other types of land cover, the Raster Calculator under Spatial Analyst Tool, ArcMap facilitated by the Condition function was used (Figure 2.30).

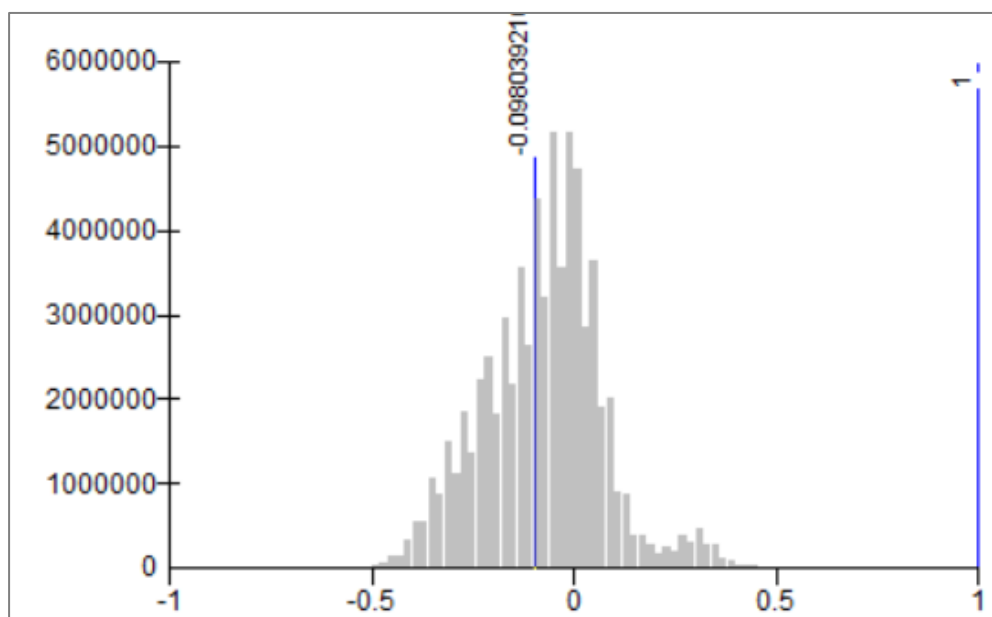


Figure 2.29: Spectral histogram

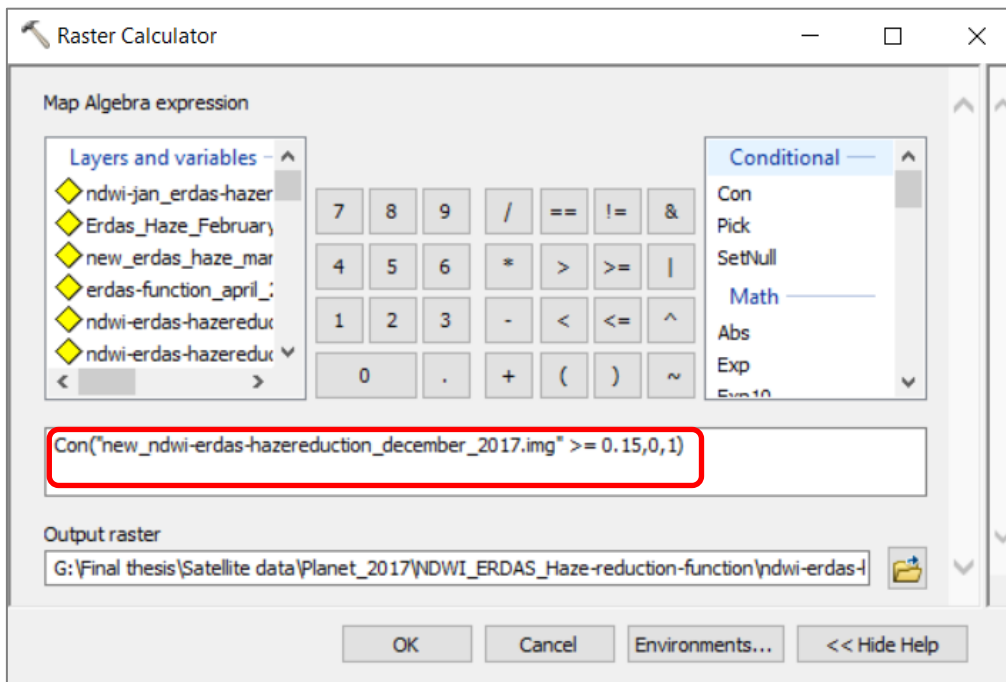


Figure 2.30: Conditional function used to classify surface water and non-surface water

2.7. Post-Image Analysis

NDWI and NDMI results were reclassified using the Reclassify tool under the Spatial Analyst tool, ArcMap to generate new water and non-water values which originally were 0 and 1 respectively. For this generation, water and non-water values were set to be 1 for water and 2 for non-water (Figure 2.31).

Extract by Mask function, Spatial Analyst Tools in ArcMap was applied to extract all pixel values from raster data within areas of interest. This study used this function to generate all water index results for all dates corresponding to the AOI (Figure 2.32). To obtain an estimate of the total amount of surface water for each date, the number of pixels counted was derived and calculated as a percentage. This is because this study used two different imageries which have different spatial resolutions (3 m for PlanetScope and 5 m for RapidEye) so that calculating the total water as a percentage was the most appropriate way to show the amount of water.

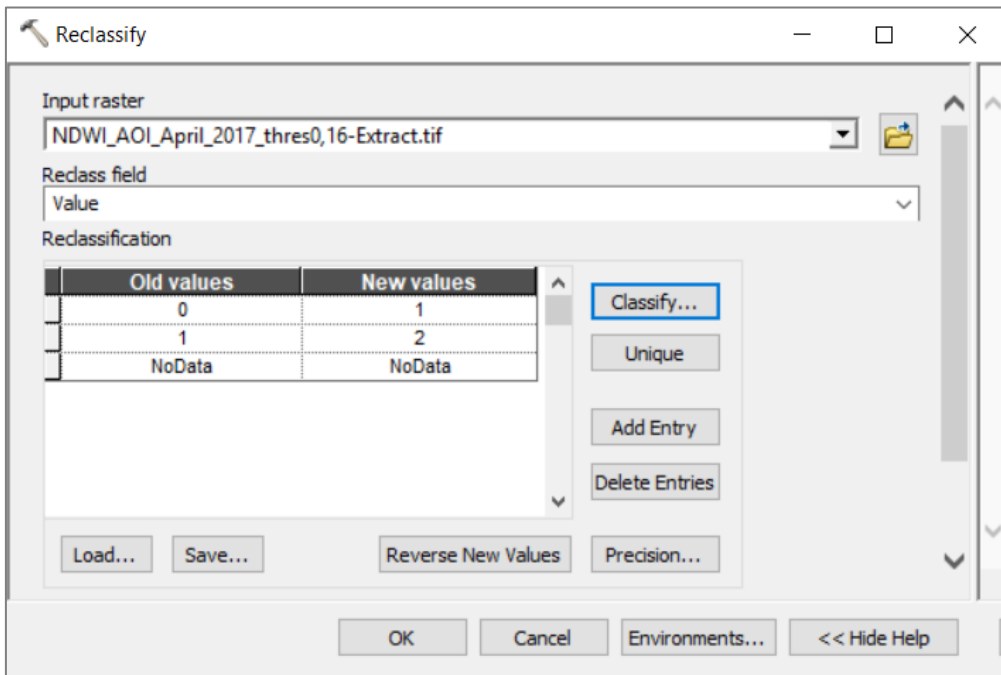


Figure 2. 31: Reclassify function

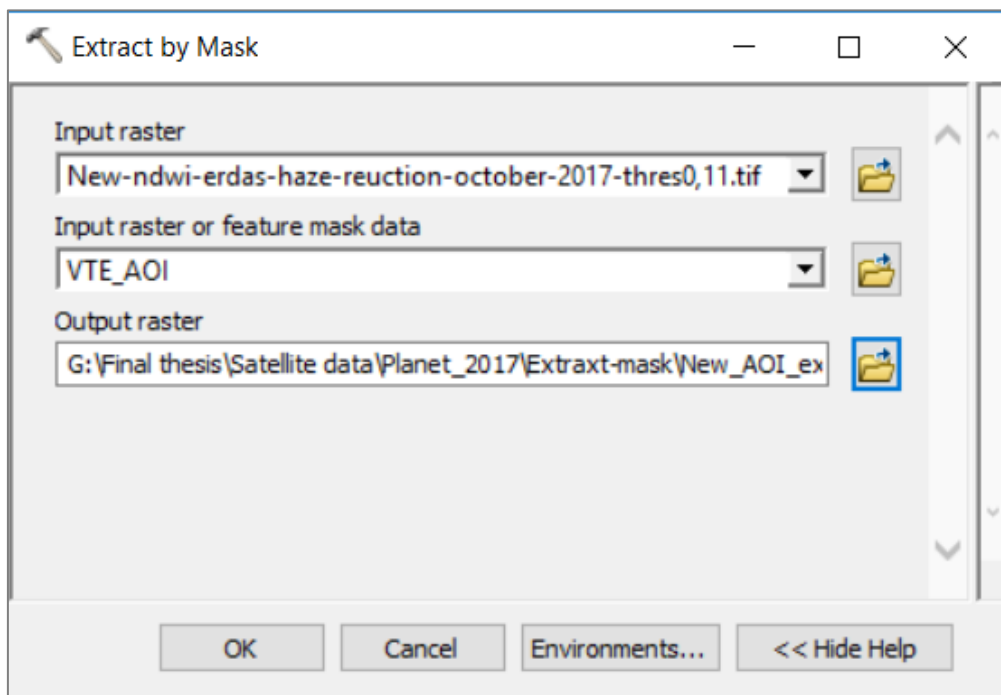


Figure 2.32: Extract by Mask

2.8. Accuracy Assessment

For quantifying the accuracy of the image processing, a statistic mechanism is needed to assess the output of surface features after the process of image analysis (Lillesand, Kiefer & Chipman 2015). The procedure of accuracy assessment is to apply confusion matrix which consists of a number of classes representing classified classes and ground truth. The Kappa statistic is calculated based on

the differences between the classified features and ground features to observe the degree of agreement and disagreement between the two. From this statistical analysis, overall classification accuracy (OA), Kappa coefficient, user's accuracy (UA) which represents the classified features categorised as the actual ground feature, and producer's accuracy (PA) which represent how well ground data are represented classified features, are produced. The Kappa statistic is shown in Equation 2.4, where;

$$\text{Kappa} = \frac{P_o - P_e}{1 - P_e} \quad \text{Equation 2.4}$$

P_o is the observed agreement

P_e is the expected agreement

Table 2.9 explains the Kappa confusion matrix, where, (a) and (d) are representative of the number of agreements between the two observations, while (b) and (c) represent the number of disagreements between the two. If there is no conflict the observations (b, c) will be 1 or 100%, and if there is no agreement the observed agreements (a, d) will be zero. n_1 , m_1 are the total counts of agreement, n_0 , m_0 are the total counts of disagreement, and n is the total number of the counts (Viera & Garrett 2005).

To calculate P_o and P_e , the Equation 2.5 and 2.6 are illustrated.

$$P_o = \frac{a+d}{n} \quad \text{Equation 2.5}$$

$$P_e = \left[\left(\frac{n_1}{n} \right) \left(\frac{m_1}{n} \right) \right] + \left[\left(\frac{n_0}{n} \right) \left(\frac{m_0}{n} \right) \right] \quad \text{Equation 2.6}$$

Table 2.9: Variation observation

		Observed 1 Results		
		Yes	No	Total
Observed 2 Results	Yes	a	b	m_1
	No	c	d	m_0
	Total	n_1	n_0	n

Adopted from Viera and Garrett (2005)

The Kappa coefficient ranges from -1 to $+1$ with six agreement levels – from poor agreement to almost perfect agreement as is shown in Table 2.10.

Table 2.10: Interpretation of Kappa coefficient

Coefficient Values	Level of Agreement
< 0	Poor Agreement
0.01 – 0.20	Slight Agreement
0.21 – 0.40	Fair Agreement
0.41 – 0.60	Moderate Agreement
0.61 – 0.80	Substantial Agreement
0.81 – 0.99	Almost Perfect Agreement

Adopted from Viera and Garrett (2005)

For this study, accuracy assessment was performed in ArcMap. 500 ground truths (Appendix 5) were created from the Accuracy Assessment Point tool using a stratified sampling strategy. Stratified is suggested as the better strategy as it can reduce sampling error with adequate sampling points in small scale areas. It can reduce bias of a single sample (Montello & Sutton 2012). Ground truth points were checked with the high-resolution aerial imagery in Google Earth Pro. The water index in March 2017 was used as the feature input for this assessment due to less cloud cover in the study area in the aerial imagery in Google Earth Pro.

2.9. Association of Surface Water and Dengue Incidence

2.9.1. Spatial Distribution of Dengue Cases

Dengue incidence data derived from ECOMORE2, IPL, was used as the main data for determining the dengue cases in the study area, and to investigate the potential relationship between dengue fever and water bodies. To understand the spread of dengue fever in 2017, easting and northing locations were performed in Data Analysis, Microsoft Excel, and the pattern of data distribution was conducted by using the Statistic Analysis Average Nearest Neighbour in ArcMap.

The F-Statistic was applied as an estimator to measure within the population with a provision of Mean, Variance, F and F critical values at confidence interval which can avoid bias (Goudet 1995). The F-Test Two Sample for Variance analysis tool compares two variables in order to compare these with the null hypothesis that these two groups of population are equally distributed (Microsoft Office 2019).

In this study, to acquire Mean and Variance values, F-Test two sample for variances with 0.05 confidence level was performed in Microsoft Excel.

Nearest Neighbour (NN) was applied to determine the dispersion of the data as it is normally used to investigate the quantitative analysis spread of data. This spatial analysis tool has been widely used to test the pattern of data distribution to determine whether it is clustered or dispersed. The basic principle of this analysis is that the distance between each feature centroid and its nearest neighbour's location is measured in order to find the average distance between them. The ratio index used in this determination is provided in Equation 2.7, where;

$$ANN = \frac{D_O}{D_E} \quad \text{Equation 2.7}$$

ANN = Average Nearest Neighbour ratio

D_O = Observed Distance between the given features and their nearest neighbour

D_E = Expected distance of the given features random pattern

The index of ANN is defined as 1. If the resulting index is less than 1, the pattern of data distribution is clustering, while if the value is greater than 1 the spread of data is in a dispersed way. Figure 2.33 illustrates the pattern of dispersion and clustering data spread.

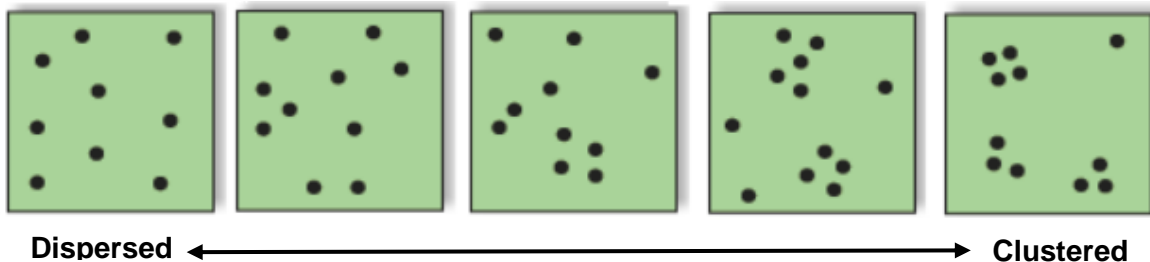


Figure 2.33: An illustration of data distribution pattern

Source: Adopted from Arc Toolbox, Average Nearest Neighbour

To examine the pattern of data spread, the Nearest Neighbour Analysis tool in ArcMap was used (Figure 2.34). The input used was georeferenced dengue incidence (354 points) data with a method of Euclidean Distance within the given study area size of approximately 3,640,256,266 square metres calculated from the spatial data.

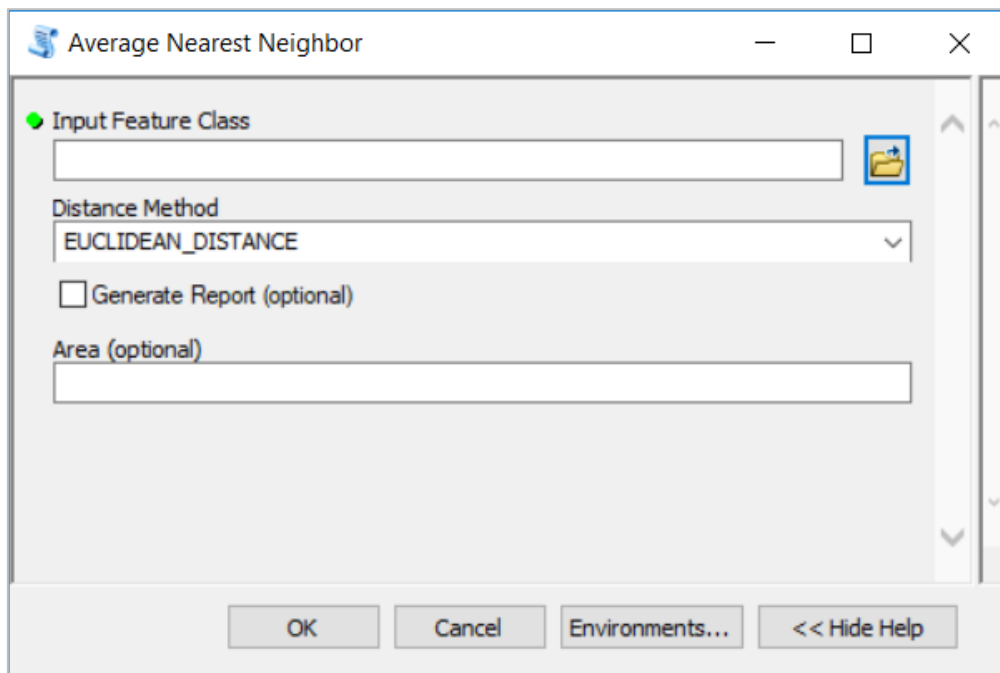


Figure 2.34: Average Nearest Neighbour analysis

2.9.2. Analysis of Dengue Incidence Associated with Water Bodies

The *Aedes* mosquito has four life stages; egg, larva, pupae and adults (Figure 2.35). It takes around seven to ten days to develop. Water is an essential breeding habitat for female mosquitoes to lay eggs. This can be anywhere where it is wet, including the wet walls of containers, and also small water areas (CSIR 2011). Eggs can survive being dried for up to eight months and have been shown to live throughout winter time in the southern United States, and they will then hatch once they are exposed to water (EPA 2017). Various external components affect the time taken for them to fully develop into adult flying mosquitoes. These include air temperature, water and relative humidity, which are the key factors that support development (Nasir et al. 2017; Shang et al. 2010). Reducing the vector breeding sites is a necessary component in the process of preventive disease occurrence to control the disease (Jayawardene et al. 2011).

In this study, of dengue cases in 2017, surface water extracted from satellites imageries, and rainfall data were used to analyse the relationship between dengue vectors and water. To explore the emergence of dengue fever, the onset date was used to determine the expected date of when a person was bitten by an infected mosquito. The egg development into an adult, based on the incubation period after the bite from an infected mosquito, and its life cycle, were also considered. According to World Health Organization (2019), the disease symptoms will appear in 4 to 10 days, and it will last for 2 to 7 days after a bite from an infected vector. Therefore, to estimate exposure date, a 10-day period was subtracted from the onset date. This was defined as Lag2. The estimated time of mosquito developing into an adult was defined as Lag1, derived by subtracting 8 days for the mosquito development time (see Figure 2.36). Data of mosquito populations collected in 2017 was also used to determine the adult development time (see Table 2.10).

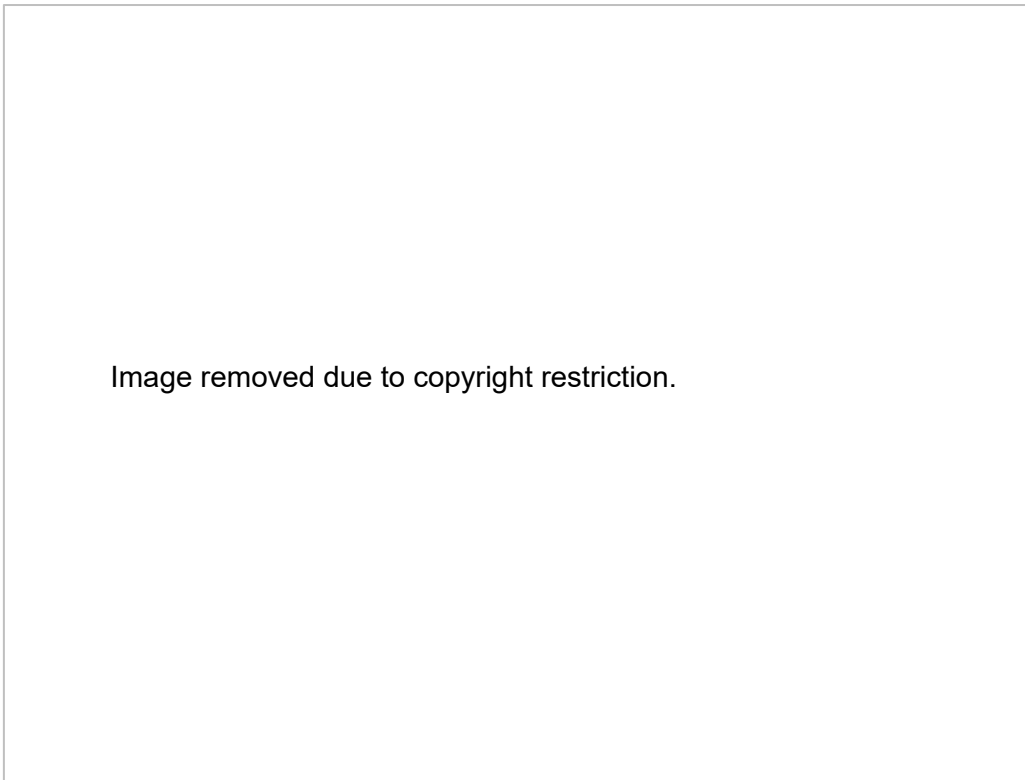


Figure 2.35: *Aedes* mosquito life cycle

Source: CSIR 2017 (http://ictervis.nic.in/KidsCentre/Mosquito_1501.aspx)

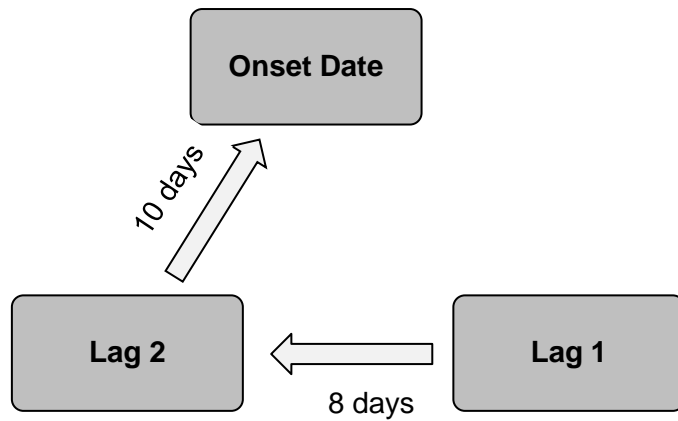


Figure 2.36: The estimated time of patients contracting the disease (Lg2), and the estimated time of mosquitoes developing into adults (Lg1) based on the onset time

Correlation coefficient and regression statistics in SPSS were used in this study to examine the relationship between dengue incidence and surface water. Exploring whether the data was parametric and non-parametric can help the operator decide on a suitable tool. Parametric data are assumed to be normally distributed and consist of independent observations, and a large sample size which is normally greater than 30. On the other hand, non-parametric data are assumed to be

not normally distributed, with a smaller sample size. This is not based on the numbers of samples but on ranking order (Gibbons & Fielden 1993).

Spearman rank order correlation and Linear Regression Model in IBM SPSS Statistics version 25 were applied in this study due to the small sample size (less than 30) used in this study (see Table 2.11). The Spearman's correlation is a non-parametric analysis which does not require normally distributed data, and is suitable for small datasets (Artusi, Verderio & Marubini 2002). It measures the relationship between two variables determined on ordinal scale (Gravetter & Wallnau 2013). Spearman's correlation values range from -1.00 to +1.00 used to determine the strength of the association of one variable to another variable. A value of 0.00 shows no relationship between two variables, whereas +1.00 indicates a strong relationship between the two variables which positively influence each other. The -1.00 indicates a perfect correlation of the two variables, but in a negative way – the decrease of one variable will cause the other to increase (Rafieyan 2016). R^2 is the squared values acquired from the correlation coefficient. To interpret this Cohen (1988) defined the range of values for the interpretation ranged from 0.00 to 1.00 (Table 2.12).

Table 2.11: Sample datasets

Month	Dengue Cases			Surface Water (%)	Rainfall (mm)	Number of <i>Aedes</i> Mosquitoes
	Onset Date (N)	Lag1	Lag2			
December 2016	-	8	5	-	-	-
January	18	14	13	6.9	143	143
February	5	5	6	5.49	89	89
March	4	1	4	7.16	42	42
April	3	9	7	6.87	22	22
May	11	15	17	8.34	41	41
June	25	46	33	-	103	103
July	63	78	64	-	157	157
August	71	72	81	9.54	93	93
September	77	58	62	-	83	83
October	40	26	34	9.53	72	72
November	28	21	25	7.33	84	84
December	9	1	3	8.45	82	82

Table 2.12: Range of strength relationship and squared correlation

Correlation Values	Squared Correlation Values	Interpretation
0.10 – 0.29	0.01	Small Correlation
0.30 – 0.49	0.09	Medium Correlation
0.50 – 1.00	0.25	Large Correlation

The Linear Regression Model is used to determine the best predictor of the dependent variables by involving one or more independent variables. The outputs provided by this model consist of regression coefficient, correlation matrix, multiple R and R^2 , and adjust R^2 standard error of the estimate, the predicted values as well as 95% confidence intervals or each regression coefficient.

In this current study, a 95% level of confidence interval was applied. Surface water and rainfall data were used as the independent variables to test the dependent variables – lag1, lag2, *Aedes* mosquito population – in order to examine their relationship. Lag 1 was used as an independent variable to test the association with number of *Aedes* mosquitoes.

In conclusion, this chapter outlined the selection process of satellite image data used to detect surface water in this study, and the experiment of approaches used enhance image quality in extracting water bodies. Indices methods used to extract surface water from image data were also examined. Statistical analysis of correlation and regression used to investigate the relationship between surface water and dengue incidence. In the next chapter, findings derived from these methodologies will be presented, and then some points of indices method selection will also be briefly discussed.

CHAPTER THREE: RESULTS

This chapter presents the results including the pre-processing of images analysis of PlanetScope and RapidEye images, water indices methods used to extract surface water and the post-image analyses. The section assessing the suitable satellite imageries used in this study is not included in this chapter as they were already presented and discussed in the chapter 2.

3.1. Pre-processing of Image Analysis

3.1.1. Atmospheric Correction

Top of Atmosphere (TOA)

Image data from 04 and 16 January 2017 were atmospherically corrected by conversion of TOA reflectance. The histograms (Figure 3.1, Figure 3.2) show the results illustrating a range of pixel values data from band 2 and band 4 (Blue and NIR) from the darkest to the brightest on the X axis, and frequency ranges of the data value on the Y axis. Atmospheric correction images show a higher range of value frequency in band 1 (Blue) compared with the non-atmospheric correction images, while the range of frequency values derived from the atmospheric correction in band 4 (NIR) shows a lower frequency than that of the image with no correction for atmosphere effects.

An improvement in the high frequency of pixel values in band 1 (Blue) indicates that spectral reflectance of pixels in this band channel is significantly affected by atmosphere on electromagnetic radiance (Hadjimitsis et al. 2010), and typically was able to be enhanced by applying the TOA. Nevertheless, when applying the results obtained from TOA in the NDWI model, it was found that several areas of water surfaces appear as false negatives (Table 3.1), (normally water pixel values would be higher than zero) (McFeeters 1996). A consequence of this was the overestimation of surface water containing negative values as roads and built-up areas. Because of this result, the conversion of TOA reflectance in the January images was not applied in this study.

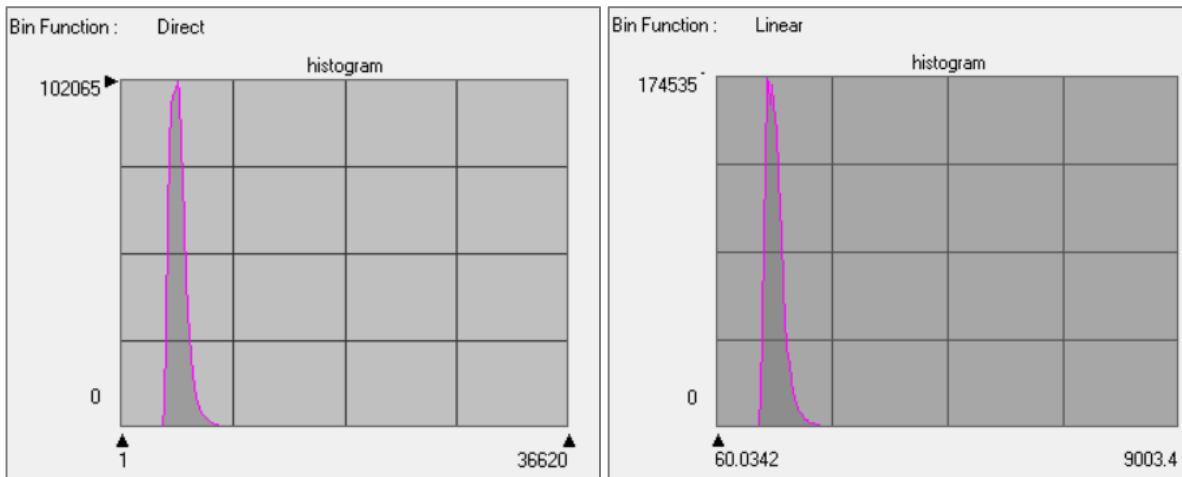


Figure 3.1: Histogram showing data values for January images in band 1 (Blue) with non-atmospheric correction (left) and with atmospheric correction (right)

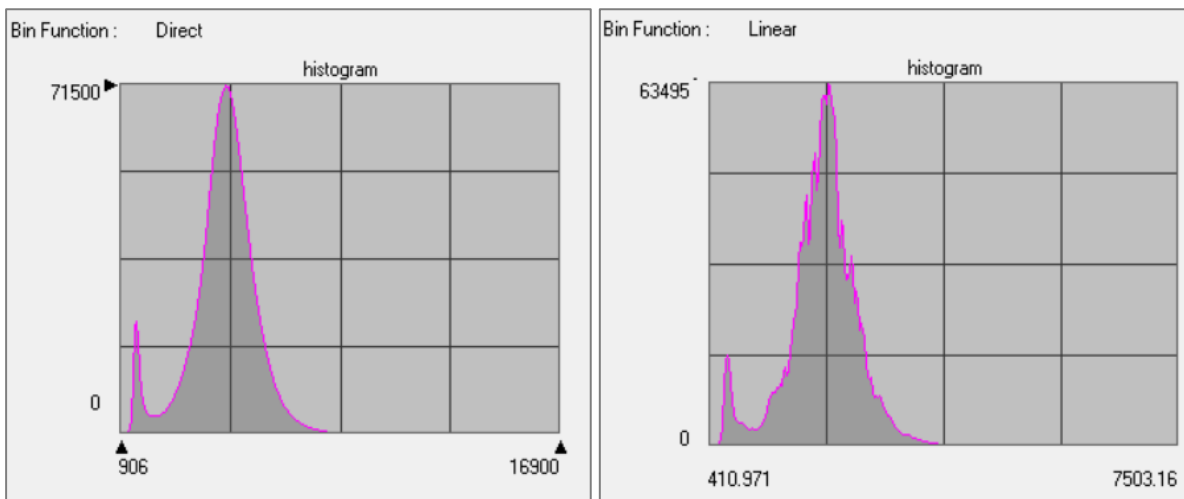


Figure 3.2: Histogram showing data values for January images in band 4 (NIR) with non-atmospheric correction (left) and with atmospheric correction (right)

Table 3.1: Statistical values of NDWI and water values obtained from TOA and non-TOA

	NDWI Images			Water Pixel values
	Min	Max	Mean	
Non-TOA	-0.52	0.7	-0.029	> 0.19
TOA	-0.68	0.6	-0.27	> -0.071

Bottom of Atmosphere (BOA)

Dark Object Subtraction (DOS) was applied to investigate the quality of images for extracting surface water. October image data was used in the process and dark pixel values were derived from deep water bodies in the study area, and the minimum values of each band (Table 3.2). Table 3.3 presents the values from statistical analyses derived from DOS compared with the values before the DOS process. The dark pixel object used the darkest pixel value from deep water shows that the minimum values of each band contain negative values. The mean values are substantially different from the non-DOS image values. The results of the darkest pixel values used minimum values of each band, the mean values were smaller than those of the non-DOS. Only the minimum values of Green, Red, and NIR bands were smaller than those of the non-DOS.

Table 3.2: Dark pixel values used for dark object subtraction

Band	Dark Pixel values from Deep Water	Minimum values
Band 1 – Blue	4,928	1,031
Band 2 – Green	4,202	2,891
Band 3 – Red	3,252	1,082
Band 4 – Near-Infrared	2,766	1,831

Table 3.3: Statistical information of PlanetScope satellite image derived from DOS

Band	Non-DOS			With DOS (deep water pixel)			With DOS (band min values)		
	Min	Max	Mean	Min	Max	Mean	Min	Max	Mean
Blue	1,031	34,365	5,433.707	-1,001.3	25,903	505.666	2,895.8	29,800	4,402.666
Green	2,891	25,549	4,981.321	-682.38	19,042	779.272	628.63	20,353	2,090.272
Red	1,082	32,507	3,924.416	-1,215.5	25,400	672.364	954.69	27,570	2,842.364
NIR	1,831	28,451	6,606.832	-863.19	23,457	3,840.815	71.813	24,392	4,775.815

To examine the effectiveness of the DOS method in extracting surface water, images generated from DOS were assessed using the normalized difference water index (NDWI). Table 3.4 presents the values from statistical analyses obtained from NDWI. The range of values of the water index of the non-DOS method were between -0.46 to 0.62, while that of NDWI generated from DOS using the deep-water pixels was beyond the range of NDWI (-1 to +1). The NDWI values acquired from DOS using the minimum values of each band ranged from -0.77 to 0.89. Only NDWI values derived from non-DOS and DOS that used the minimum values of bands were compared. Comparison of water pixel values of these two images shows that many areas of surface water appear similar

(Figure 3.3). Hence, in this study, as the non-DOS and DOS images generated similar water index results, bottom of atmosphere correction using DOS was not applied.

Table 3.4: Statistical values of NDWI with non-DOS and with DOS and water pixel values

NDWI Images	Min	Max	Mean	Pixel Values			
				Point 1	Point 2	Point 3	Point 4
Non-DOS	-0.46814	0.6228	-0.134	0.22	0.23	0.52	0.55
DOS (deep water pixel values)	-402.83	381.13	-0.65	-	-	-	-
DOS (min and max values)	-0.77406	0.89039	-0.380	0.21	0.23	0.54	0.57

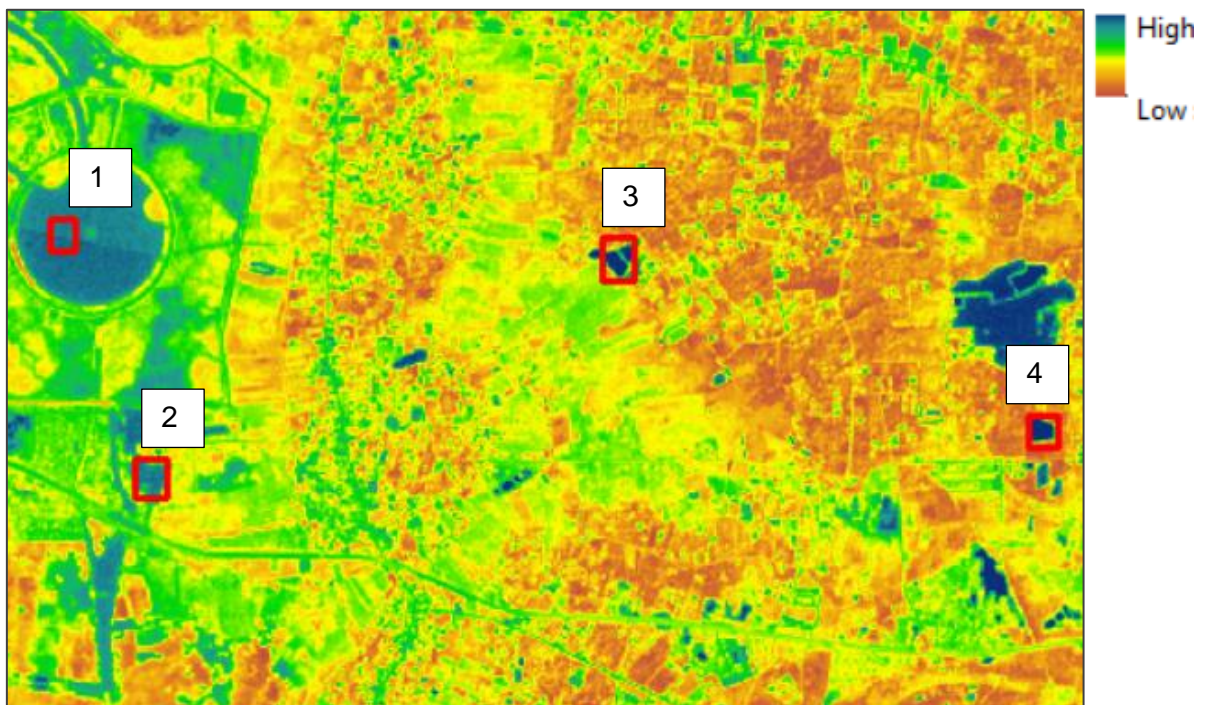


Figure 3.3: Water areas spots for pixel values inspection

The RapidEye Image was atmospherically corrected by applying the Rapid Atmospheric Correction applicable in ERDAS Imagine 2018. The raw digital number (DN) values of the image were internally converted to ground reflectance. Figure 3.4 shows the minimum and maximum values of the image before and after the process of Rapid Atmospheric Correction. The frequency of values and DN values were extended and larger than those of the image before the correction. The outputs yielded from NDWI and NDMI show more spread of DN values with greater standard deviation values of 0.311 and 0.295 for NDWI and NDMI respectively (Table 3.5).

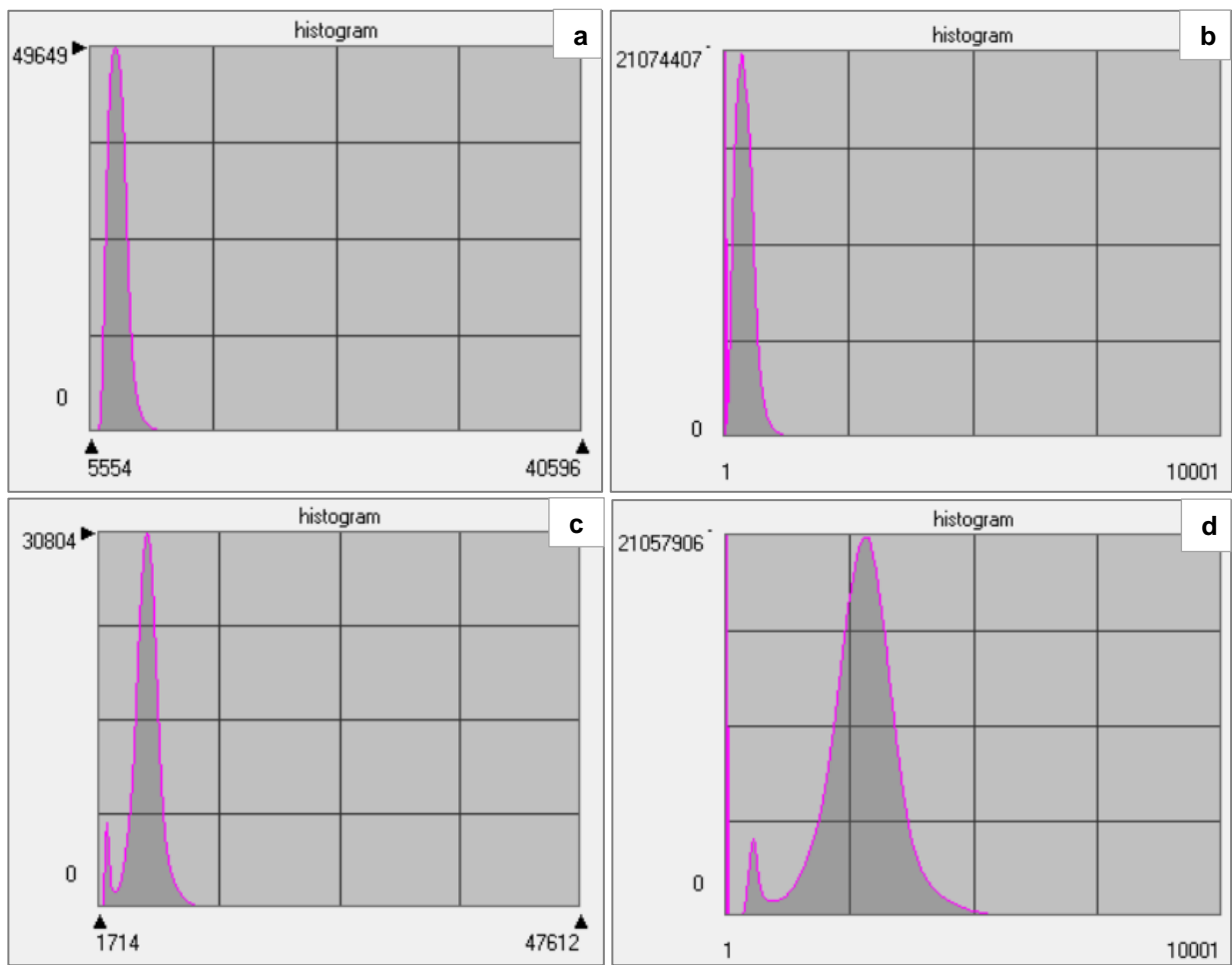


Figure 3.4: Histograms showing the minimum and maximum values of Blue band, before the correction (a), and after the correction (b); and NIR band, before the correction (c), and after the correction (d)

Table 3.5: Statistical values of NDWI before and after Rapid atmospheric correction

	Min	Max	Mean	Std. Dev
Before Correction	-0.43	0.59	0.018	0.125
After Correction NDWI	-0.99	0.52	-0.49	0.311
After Correction NDMI	-0.99	0.40	-0.42	0.295

3.1.2. Haze Reduction

Haze reduction is another method that is used to correct atmospheric effects. It can improve the spectral reflectance by using the haze reduction model created in Spatial Model Editor, ERDAS Imagine. All images were processed in this process. The image in February was used in this experiment. It is noticed that visually the image undergoing the process shows clearer ground features compared with the original image (Figure 3.5).

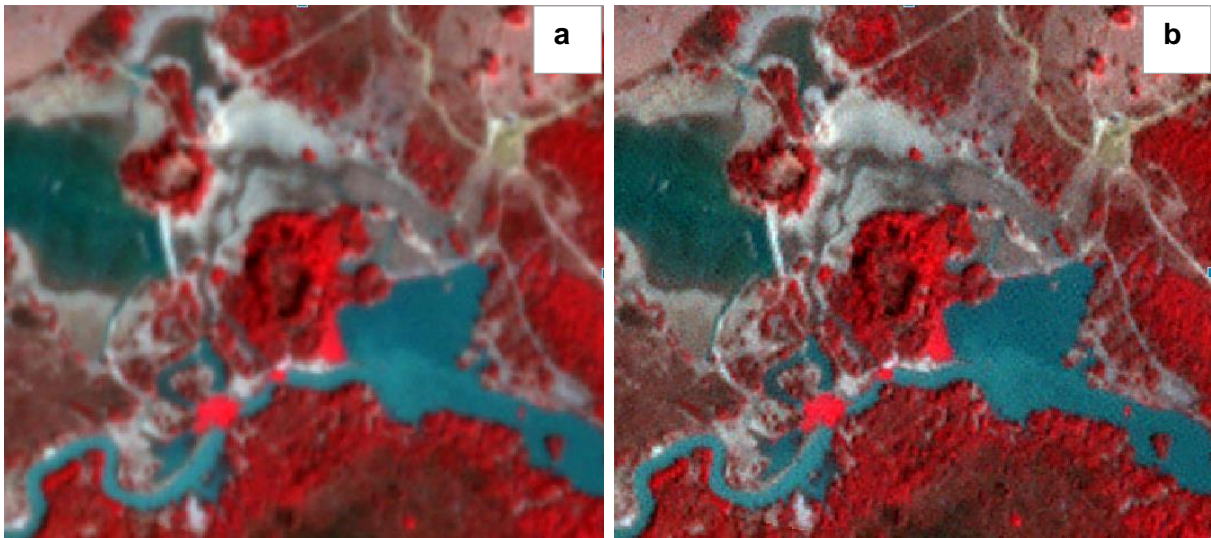


Figure 3.5: PlanetScope image in February before haze reduction (a) and after haze reduction (b) displayed in false-colour composite (RGB: band 4, band 3, band 2)

Statistically, the minimum and maximum values of the image after the haze reduction process were also improved with the improvement of standard deviation values (Table 3.6). The performance of this haze reduction method generating NDWI and NDMI outputs was assessed. Table 3.7 presents the minimum, maximum, mean, and standard deviation values of non-haze reduction and haze reduction values generated from NDWI and NDMI. The range of values of NDWI and NDMI were increased with a greater standard deviation. However, the mean values of the NDWI with non-haze reduction and the reduction of haze NDWI were similar (-0.003), and the standard deviation value of the haze reduction NDWI image shows only a minor difference from that of non-haze reduction NDWI.

Table 3.6: Statistical information for February image data

Band	Image with non-haze reduction				Image with haze reduction			
	Min	Max	Mean	Std. Dev	Min	Max	Mean	Std. Dev
1 – Blue	2,925	29,395	5,255.971	771.013	6	48,518	5,257.499	898.036
2 – Green	3,330	24,590	4,920.263	845.517	22	35,613	4,921.627	925.024
3 – Red	2,284	27,075	4,351.070	1,134.514	1	40,336	4,352.247	1,220.525
4 – NIR	1,394	17,176	5,024.227	1,082.307	3	26,586	5,025.663	1,161.951

Table 3.7: NDWI statistical values of non-haze and haze reduction images in February

	Min	Max	Mean	Std. Dev
Non-Haze reduction	-0.405	0.649	-0.003	0.120
With Haze reduction NDWI	-1	1	-0.003	0.123
With Haze reduction NDMI	-1	1	-0.071	0.142

Table 3.8 presents the statistical values generated from NDWI and NDMI of RapidEye (March image data). Both NDWI and NDMI yielded values of indices with minimum values of -1 and maximum values of +1, while the non-haze reduction was -0.405 and 0.64 for minimum and maximum values, respectively. When these values are compared with the NDWI and NDMI values generated from the Rapid Atmospheric Correction (Table 3.5), the range of values of NDWI and NDMI after using haze reduction outperformed those of NDWI and NDMI images using Rapid Atmospheric Correction. Thus, haze reduction was used to improve the spectral reflectance of the March data to extract water information.

Table 3.8: NDWI, NDMI Statistical information before and after de-haze of RapidEye image

	Min	Max	Mean	Std. Dev
Non-Haze reduction	-0.43	0.59	0.018	0.125
With Haze reduction NDWI	-0.89	1	0.020	0.134
With Haze reduction NDMI	-1	1	-0.082	0.163

3.1.3 Cloud Masking

Cloud masked images were produced by two different methods – unsupervised classification and a single band threshold method. Table 3.9 presents pixel values of cloud reflectance from band 2 (Green) and shadow reflectance values detected from band 4 (NIR). With an attempt at masking cloud and shadow from the PlanetScope (August image data), cloud and shadow derived from unsupervised classification method showed accurate result of cloud and shadow masking at moderate level. However, when comparing this with a single band threshold method, it was found that cloud cover was able to be masked out with less overestimation of the surface water than the classification method (see Figure 3.6).

Table 3.9: Threshold values used to detect cloud and shadow

Attribute	Pixel Vales
Clouds	Ranged from 12,084 to 18,624
Shadow	Range from 3,882 to 5,083



Figure 3.6: Cloud masking image from unsupervised classification (a), a single band threshold (b) and the combination of classification and a single band threshold methods (c) displayed in true-colour composite

3.2. Surface Water Extraction

The normalized difference water index (NDWI), and the normalized difference moisture index (NDMI) were deployed to discriminate water bodies. The use of the normalized difference vegetation index (NDVI) was also explored and compared with the NDWI and NDMI. From this comparison, it was found that NDWI and NDMI appeared to be the most suitable methods used to extract water information with less disturbance from other non-water areas (see 3.2.2).

3.2.1. Multi-band Spectral Relationship Method

Figure 3.7 shows the comparison output from the multi-spectral band method (a), and the result derived from NDWI (b). Generally, the multi-spectral band approach was able to delineate surface water in a similar way to the NDWI method. Some small water bodies were able to be detected as shown in Figure 3.6 (c) compared with the original image (d) (see the rectangle area). However, the multi-band spectral method was likely to largely interpret built-up features and bare areas as water features with a considerable amount of noise disturbance. As the area of this current research contains both urban and rural regions, lots of non-water pixels counted as water could decrease the accuracy of water extraction. With respect to this, Gao et al. (2016) pointed out in the investigation of multi-band spectral method that although this water detection algorithm could extract more water information, it mistakenly overestimated small shadow and built-up features as water bodies. Thus, this algorithm was not used in this study to extract surface water.

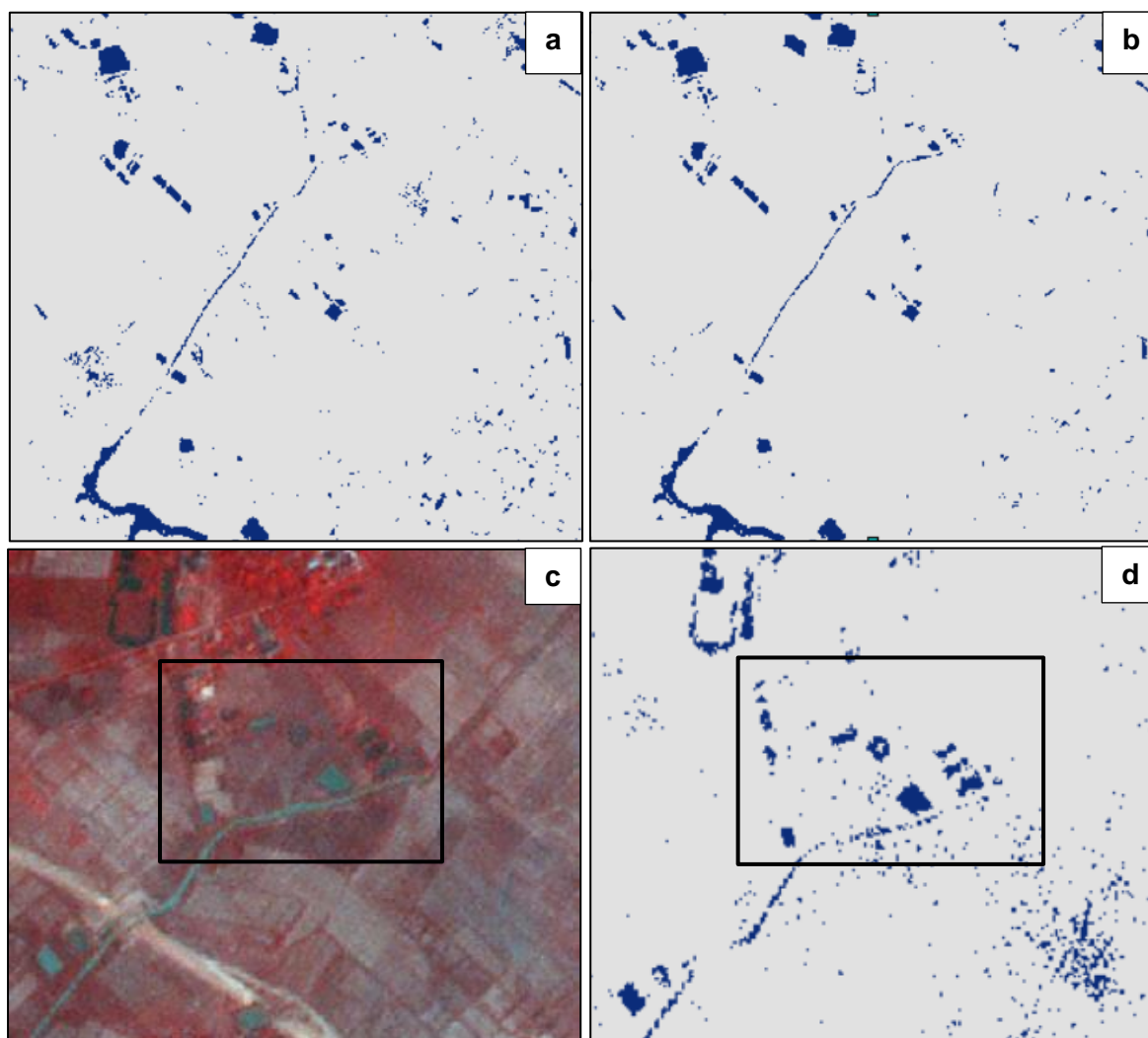


Figure 3.7: Multi-band spectral relationship method compared with NDWI and NDMI

3.2.2. Normalized Difference Vegetation Index (NDVI)

PlanetScope imagery data from February was used as an experiment of the normalized vegetation index (NDVI) model to generate water bodies. A binary image which distinguishes vegetation from other features including water features was produced. Threshold values of this vegetation index range from -1 to +1, where the values above zero indicate vegetated areas, while the values below zero indicate non-vegetated areas. Table 3.10 presents the minimum, maximum, and mean values of NDVI compared with those of NDWI and NDMI. Optimum threshold values were defined by manually adjusting the histogram to categorise water and non-water features.

Table 3.10: Statistical information for NDVI, NDWI, NDMI, and optimal threshold values

February	Min	Max	Mean	Threshold	Non-Water	Water
NDVI	-1	1	0.071	-0.15	> - 0.15	-1 to -0.15
NDMI	-1	1	-0.071	0.165	< 0.16	0.16 to 1

February	Min	Max	Mean	Threshold	Non-Water	Water
NDWI	-1	1	-0.002	0.18	< 0.18	0.18 to 1

Figure 3.8 shows the results produced from the NDVI, NDMI and NDWI. The vegetation index and moisture index outputs show almost identical results separating water from non-water areas, while the results of NDWI could also distinguish some surface water, but not shallow water. It has been said that NDVI might not be suitable to use in identifying surface water in this study area as NDVI is likely to differentiate land vegetation rather than the aquatic vegetation that mixes with small surface water (Kulinkina et al. 2018; Rokni et al. 2014). In this study, however, the results generated from NDVI appeared to do well in determining surface water in the dry season (February, March).

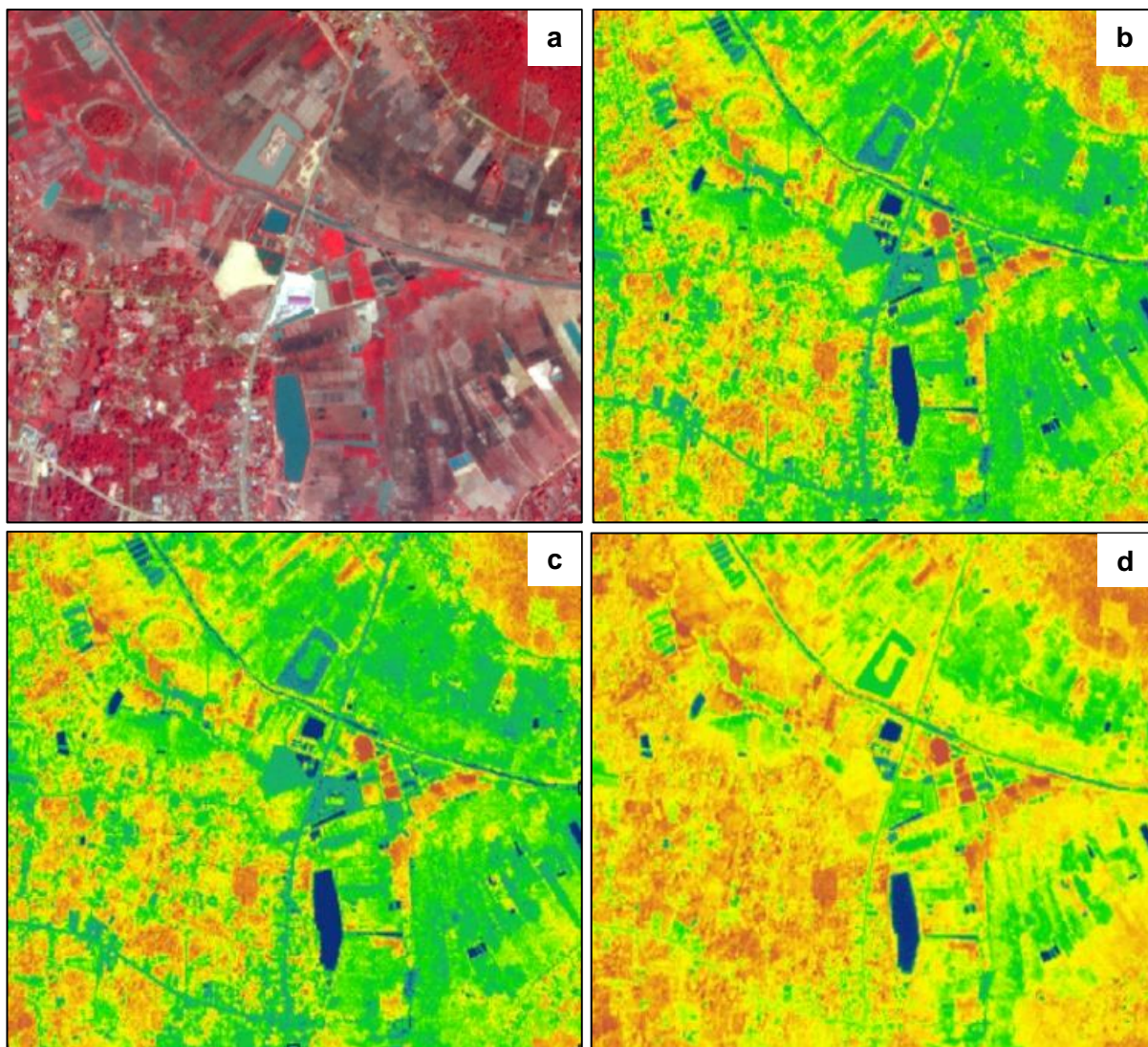


Figure 3.8: PlanetScope image (a) displayed in false-colour (RGB: 4,3,2), and indices of vegetation (b), moisture (c), and water (d) images displayed in the same colour ramp

Despite the ability of NDVI to differentiate water from vegetation, when thresholding the NDVI and MDMI images; NDMI seemed to effectively generate water regions with less disturbance of noise from other ground features compared with the NDVI, within the red rectangles in Figure 3.9 showing the areas where NDVI was interrupted by non-water features. Thus, NDMI produced the output image with less interference and was selected to use in this study with the image data in February and March.



Figure 3.9: Comparison of NDVI (a) and NDMI (b) used to extract water features

3.2.3. Normalized Difference Water Index (NDWI) and Normalized Moisture Index (NDMI)

Normalized difference water index (NDWI) was applied to extract water bodies from satellite images of PlanetScope (January, April, May, August, October, November, and December 2017). For the images from February and March 2017, surface water was derived using the normalized difference moisture index (NDMI). With the use of these indices, the optimum threshold was applied to separate water from non-water features. The optimum threshold of NDWI and NDMI was determined by visual observation and the adjustment of the histogram. The values of the optimum threshold used to delineate surface water and non-water derived from NDWI and NDMI are presented in Table 3.11.

Table 3.11: Threshold values used to extract surface water from water index images

Dates	Threshold		Statistics Information			Water		
	NDWI	NDMI	Min	Max	Mean	Deep water	Mixture of Water and others	Non-Water
January	0.22		-1	1	-0.027	> 0.22	-0.07 – 0.22	< -0.07
February		0.41	-1	1	-0.071	> 0.41	-0.16 – 0.14	< -0.16
March		0.15	-1	1	-0.265	> 0.15	-0.19 – 0.155	< -0.19

Dates	Threshold		Statistics Information			Water		
	NDWI	NDMI	Min	Max	Mean	Deep water	Mixture of Water and others	Non-Water
April	0.14		-1	1	-0.098	> 0.14	-0.04 – 0.14	< -0.04
May	0.125		-1	1	-0.034	> 0.125	-0.07 – 0.12	< -0.07
August	0.11		-0.68	0.51	-0.117	> 0.11	-0.15 – 0.11	< -0.15
October	0.11		-1	1	-0.130	> 0.11	-0.16 – 0.11	< -0.16
November	0.16		-1	1	-0.089	> 0.16	-0.12 – 0.16	< -0.12
December	0.155		-1	1	-0.046	> 0.155	-0.08 – 0.155	< -0.08

The outputs of water features were divided into three levels – high, medium and low. The range of high values was considered to be the area which NDWI and NDMI mostly interpreted as water areas, while the ranges of middle and low values include non-water features such as built-up areas and others with mixed water and vegetation (Figure 3.10).

From the results of NDWI and NDMI as shown in Figure 3.11, it can be seen that areas that contained less water in 2017 occurred in February, March, April and May, while in January, August, October, November and December a large number of water areas was clearly detected. Some spots of water index image for August appeared as No Data due to the result of cloud masking. When performing NDWI modelling, pixels presenting No Data values were not computed.

Figure 3.12 shows the amount of water in percentage extracted from NDWI and NDMI. August and October had more water areas compared with the other times, and the low surface water areas were in February, March, and April. Visually, although August appeared to contain surface water, as a result of cloud masking, the amount of surface water at this time was not very different from October.

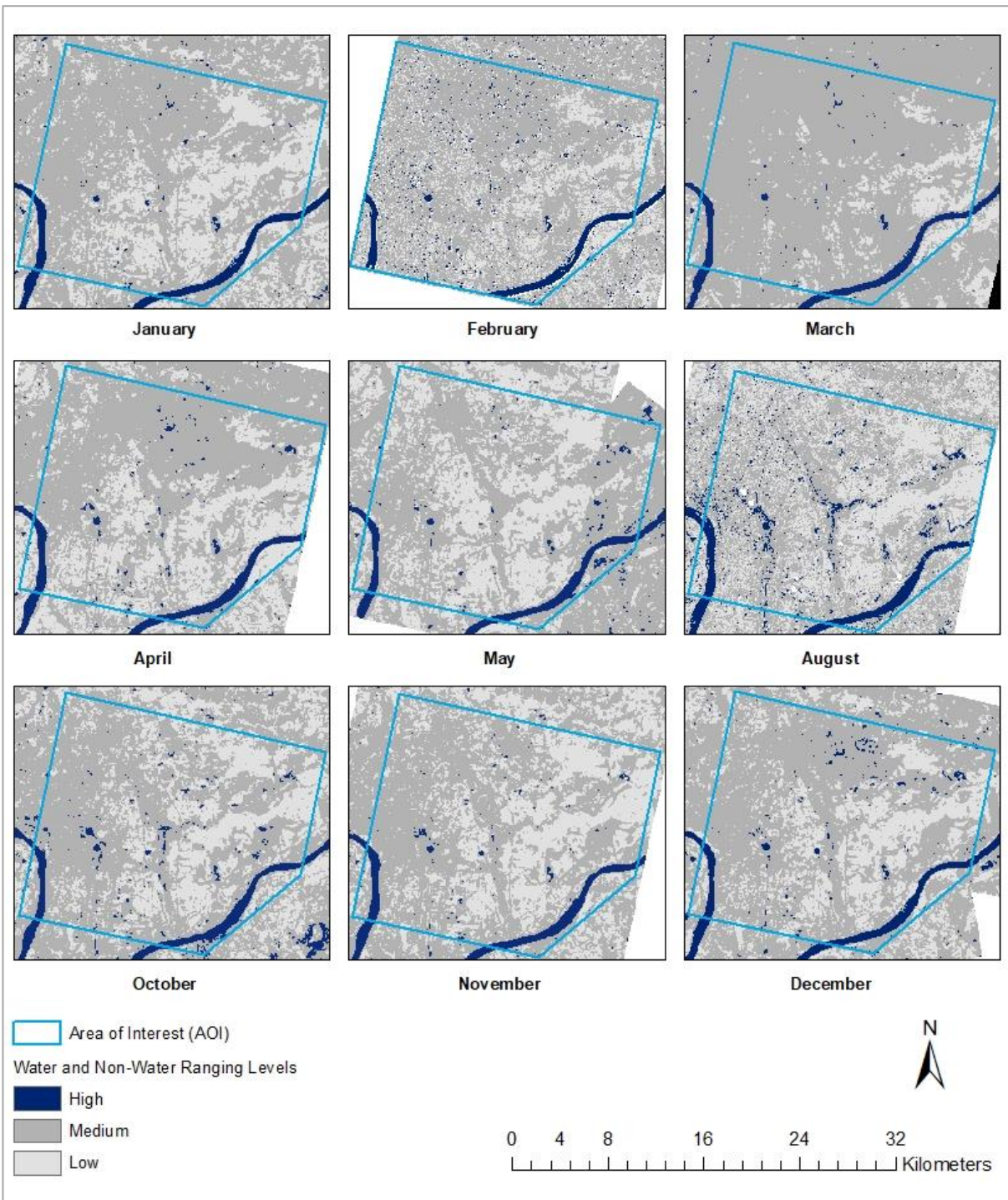


Figure 3.10: Surface water extraction from NDWI and NDMI

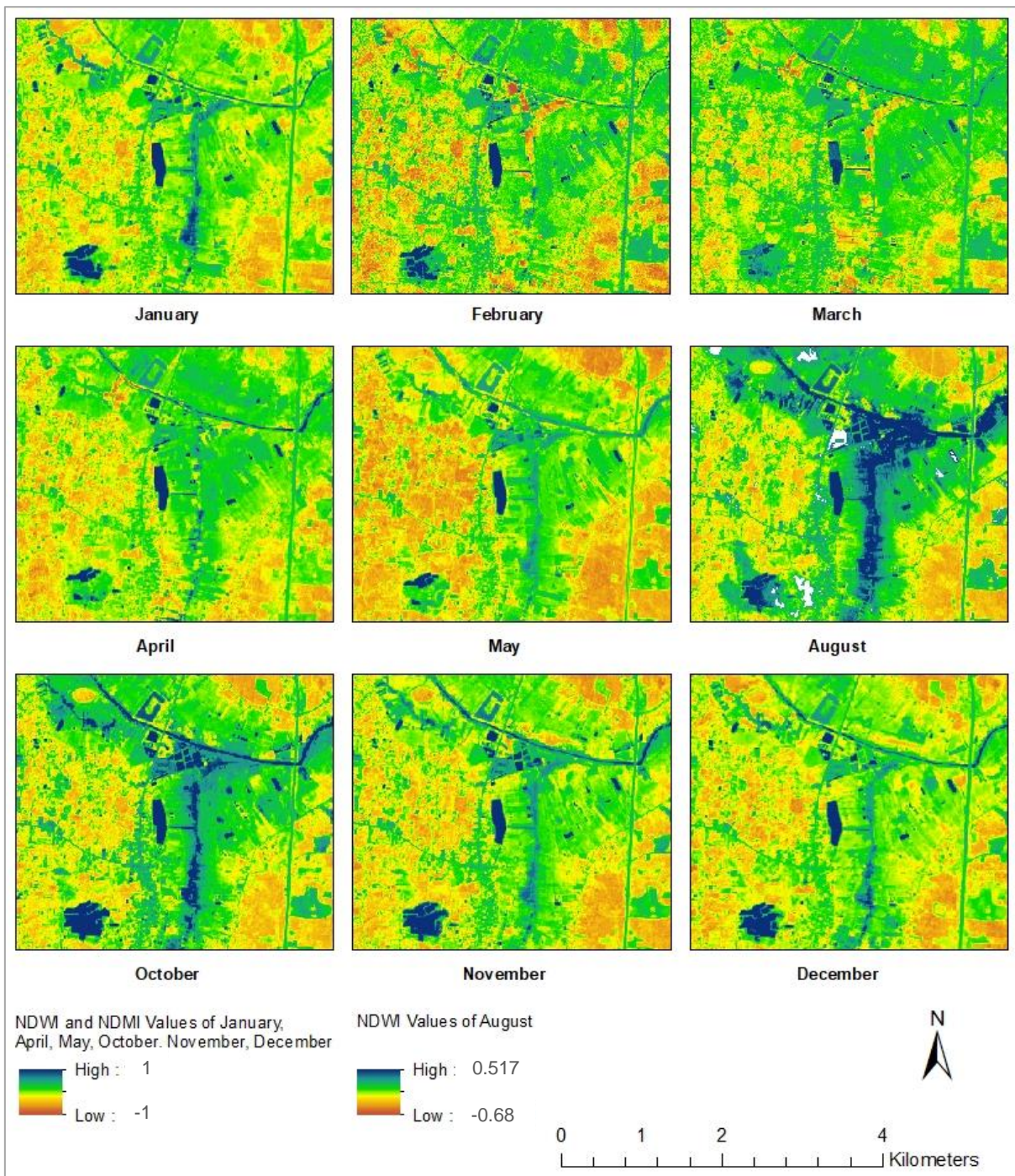


Figure 3.11: NDWI and NDMI results displayed in stretched colour ramp

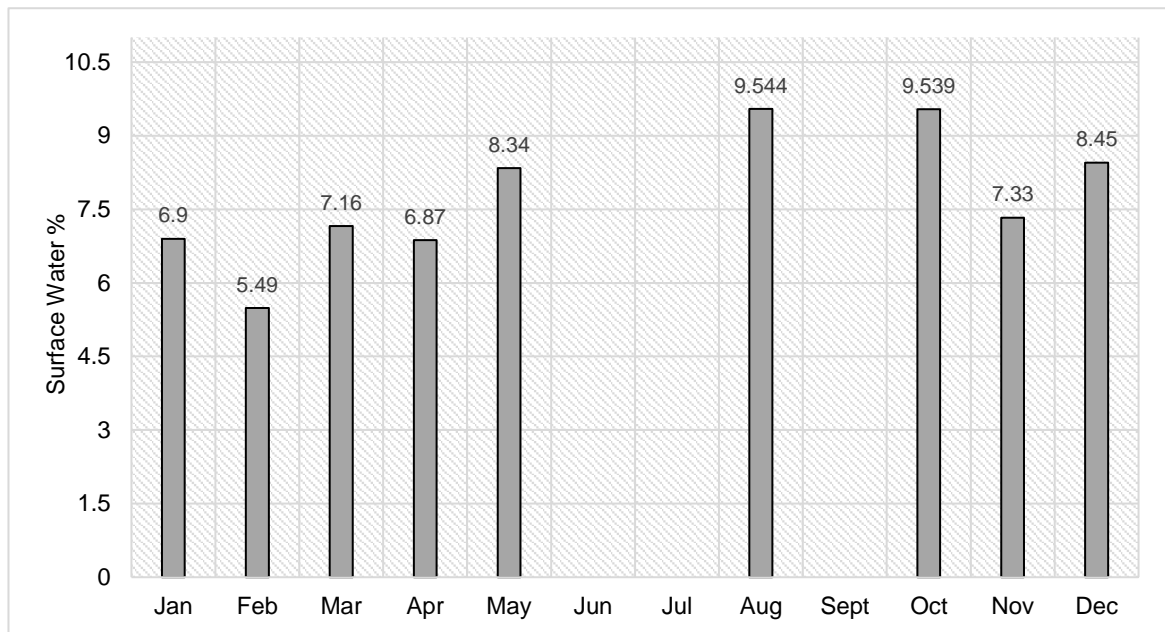


Figure 3.12: Surface water extraction in percentage

3.3. Accuracy Assessment

Accuracy assessment was implemented in order to evaluate the performance of water delineation results. Table 3.12 shows the results derived from Kappa statistical analysis used to measure the accuracy of the water index products. Overall, features that were interpreted as water were accurate at 0.69 from the User Accuracy (UA), while it was 0.42 from Producer Accuracy (PA). For features considered as non-water accuracy was at 0.93 of UA assessment and at 0.97 of PA assessment. Overall accuracy was 0.91 or around 91%, and the Kappa coefficient showed that the result of this water index was at 0.48, which was at a moderate level of agreement.

Table 3.12: Confusion matrix derived from Kappa statistics

Class Value	Water	Non-Water	Total	User Accuracy	Kappa
Water	23	10	33	0.69697	0
Non-Water	32	435	467	0.933476	0
Total	55	445	500	0	0
Producer Accuracy	0.425926	0.977528	0	0.917836	0
Kappa	0	0	0	0	0.486587

3.4. Association between Surface Water and Dengue Incidence

3.4.1. The Spatial Distribution of Dengue Cases

The incidence data geocodes were determine in order to explore the spatial distribution of the disease in the study site. From the initial analysis, the distribution of dengue cases showed a normal distribution as illustrated in Figure 3.13 and Figure 3.14. Examination of dispersion and self-clustering were performed to statically measure the distribution pattern of this incidence.

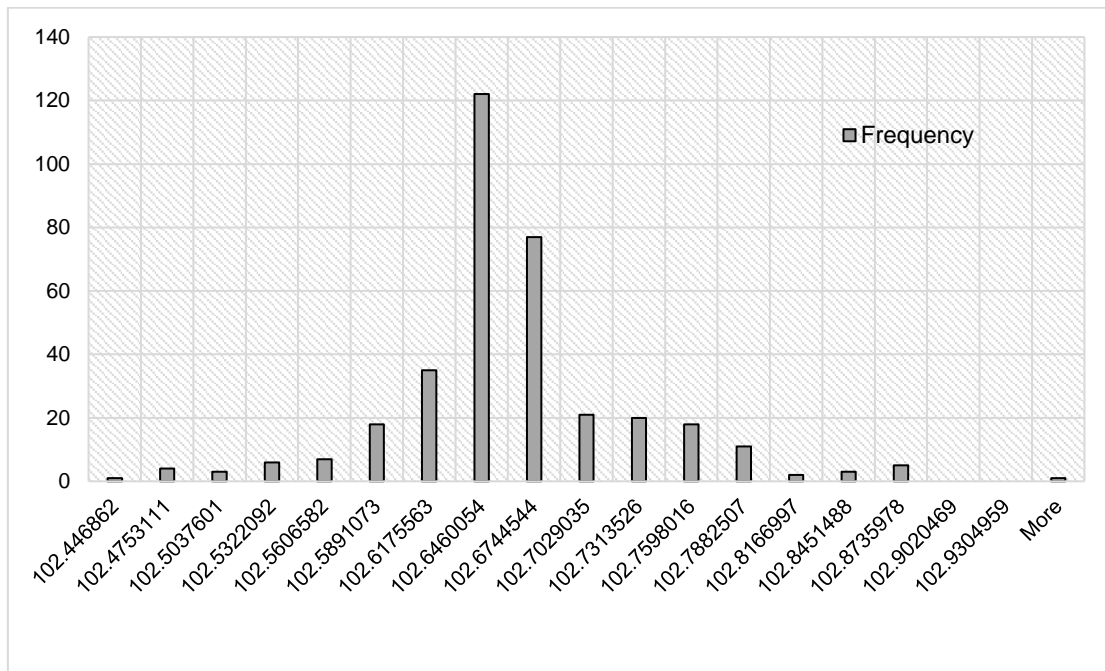


Figure 3.13: Frequency of dengue incidence spread in Easting

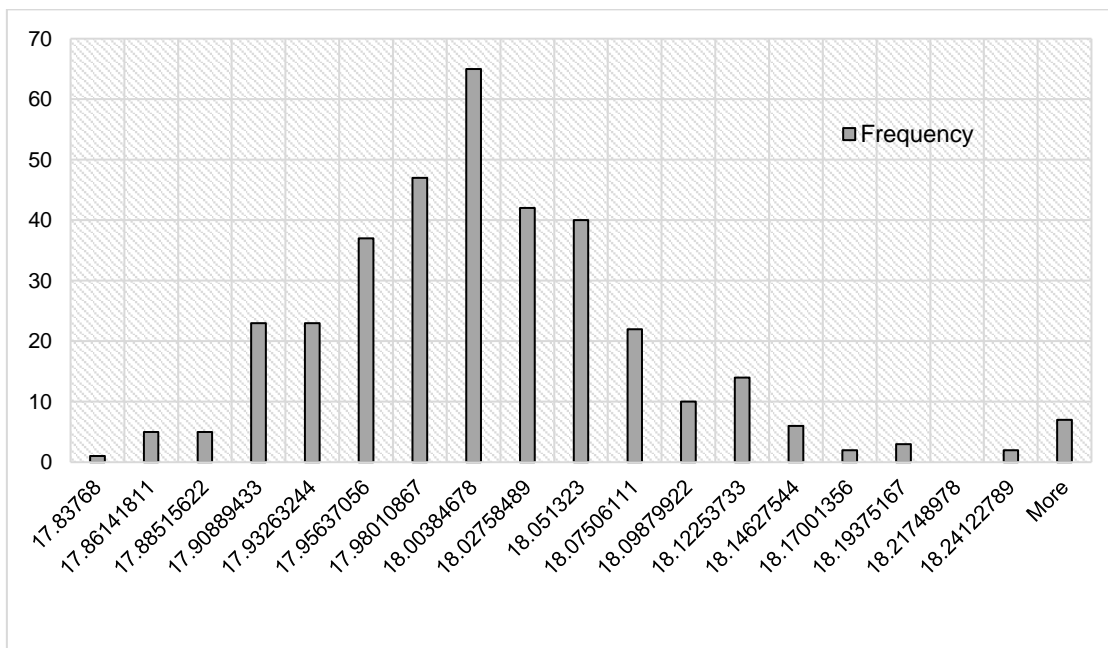


Figure 3.14: Frequency of dengue incidence spread in Northing

Table 3.13 presents the mean, variance, F values and F critical values derived from F-test. X (Easting) and Y (Northing) coordinates were defined as Variable 1 and Variable 2 respectively. Variance is considered to be an important aspect to measure the pattern of data distribution as well as their variability (Schumacker & Tomek 2013). The results from this analysis show that the variance values of X and Y were not very different, which indicates that the distribution in the eastern and northern direction in this study area were normally distributed. When observing the output values of F-test, the F-critical value was greater than the F value, which confirms that the distribution of the data in the east and the north were almost identical.

Table 3.13: F-Test two-sample for variances

	Variable 1	Variable 2
Mean	102.651425827684	18.0003793841808
Variance	0.0045042801900127	0.00566465799218626
Observation	354	354
df	353	353
F	0.79515483480659	
P(F<=f) one-tail	0.0157997545693054	
F Critical one-tail	0.839180457013118	

Average Nearest Neighbour (ANN) was performed based on the average distance between given features and their nearest neighbour features. From the analysis, the Nearest Neighbour index was 0.35611 with the mean values of expected distance and observed distance of 1603.37, and 570.97 respectively, and a P value of zero and -23.176 of Z Score (Table 3.14). The result shows that the NN ratio was smaller than 1 which indicates that the pattern of data distribution is clustered (see Appendix 6: Average Nearest Neighbour Summary Report).

Table 3.14: Average Nearest Neighbour analysis information

	Index Values
Nearest Neighbour Ratio	0.35611
Nearest Neighbour Expected	1603.37221
Nearest Neighbour Observed	570.976251
P Value	0
Nearest Neighbour Z Score	-23.176319

3.4.2. Analysis of Dengue Incidence Associated with Surface Water

To explore the emergence of dengue incidence throughout the wet and dry seasons, the number of dengue cases, lag2, lag1 and *Aedes* mosquito numbers were analysed graphically by comparing these with the surface water results extracted from satellite image data.

The trend of dengue incidence was initially compared with rainfall. Figure 3.15 shows that the highest number of dengue fever cases was found at the beginning of January and dropped in late January until April before it started to increase again in May and reached the peak point in September. It was found that the increase of disease incidence occurred after rainfall events.

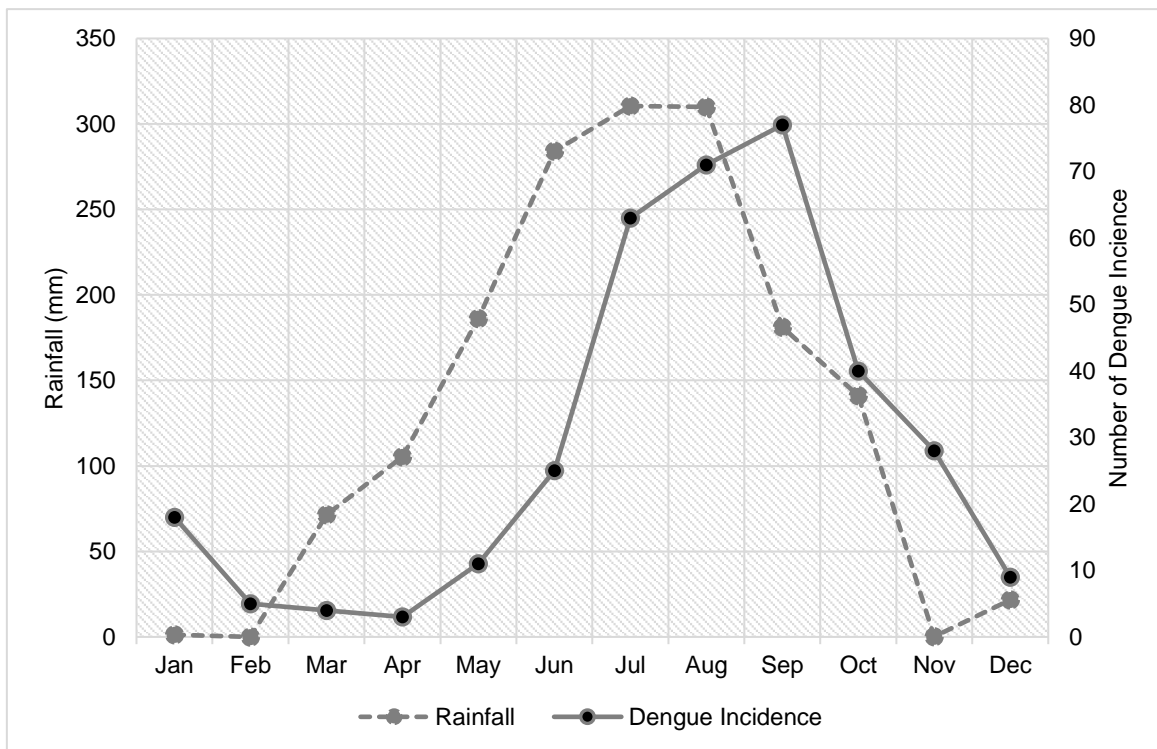


Figure 3.15: Dengue incidence compared with rainfall

Figure 3.16 shows the amount of surface water compared with disease incidence. Due to the unavailability of image data to generate surface water in June, July and September, only the first five months showed a continuous trend in the amount of water on the ground surface. Overall, the increase of the amount of water was not related to the increase of dengue although the large amount of surface water in August was consistent with the highest time of dengue cases found.

Surface water was compared with lag2 and lag1. Figure 3.17 presents the estimated counts of people contracting the disease (lg2). It was found that the infected people were detected from January and started to increase considerably in April and peaked in August with a large number of infected people. This high number of cases was at the time that surface water was at its peak (August), however, the number of infected people decreased in October and December when surface water was also high.

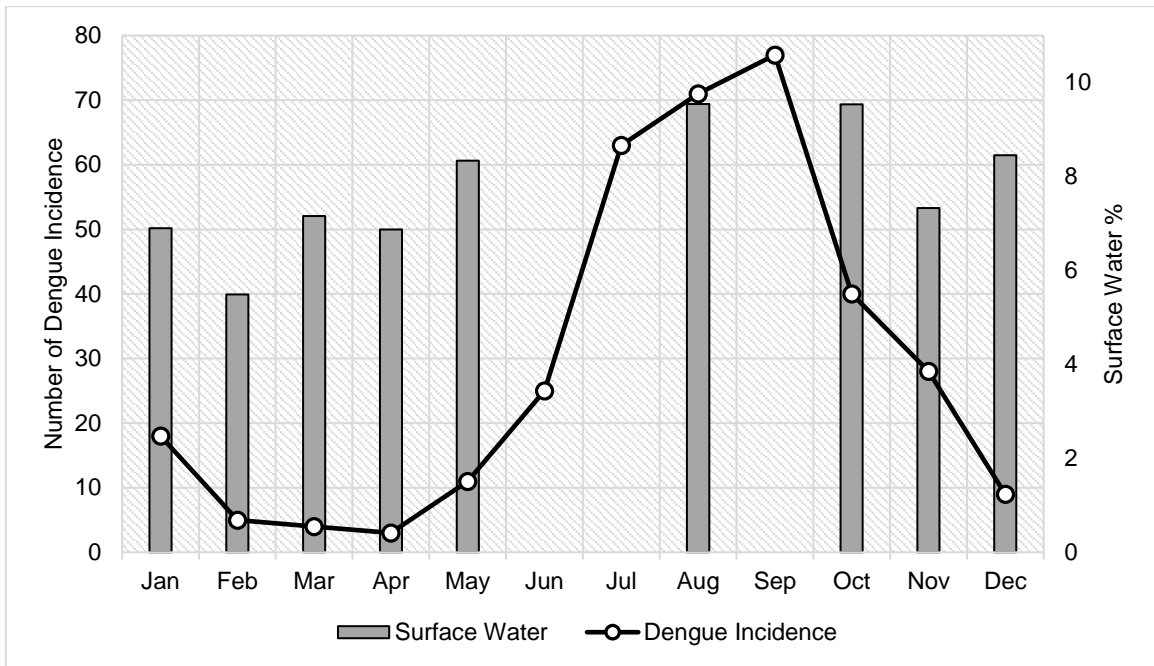


Figure 3.16: Dengue incidence compared with surface water

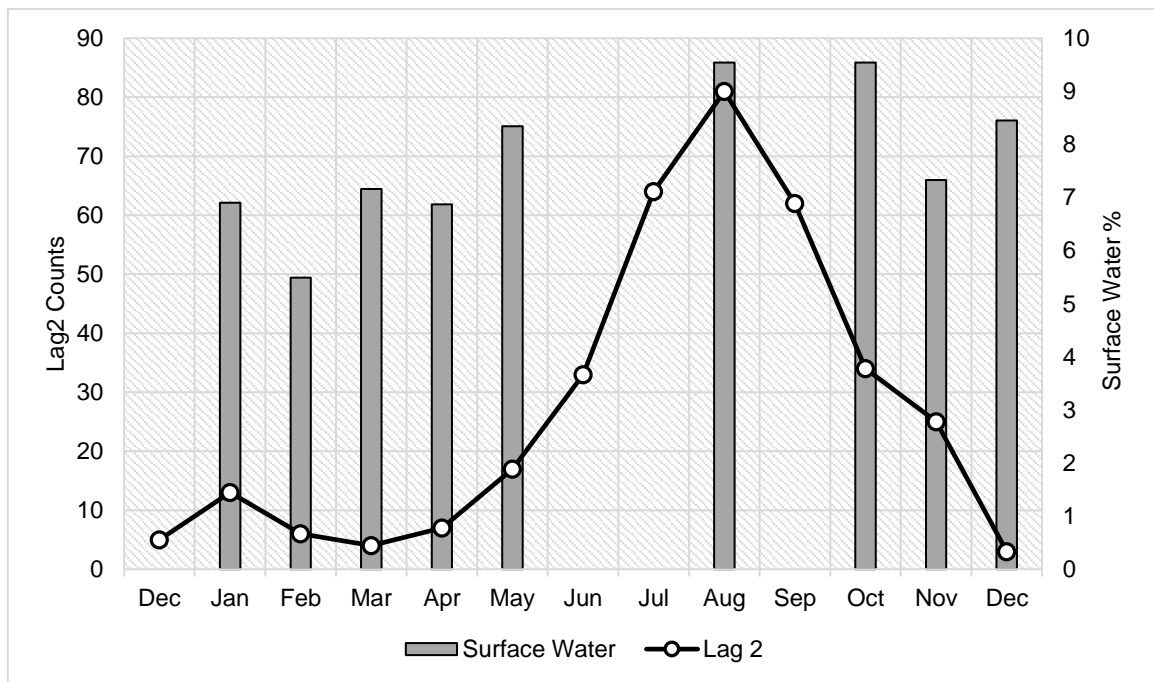


Figure 3.17: Surface water compared with Lag2 counts

Figure 3.18 illustrates the estimated time of a vector mosquito developing into an adult (lg1). Significant numbers of *Aedes* mosquitoes were found from the beginning of the year, and a high rate of adult mosquitoes was detected in July towards the end of the rainy season. This estimation was consistent with the data of the *Aedes* mosquito populations (*A. aegypti* and *A. albopictus*) collected in 2017, derived from IPL data (Figure 3.19). When comparing surface water data with the number of vector mosquitoes, it can be seen that at the beginning of the year adult mosquitoes were found

with the increase of surface water in January, and there were small numbers of mosquito populations during the low level of surface water only in February.

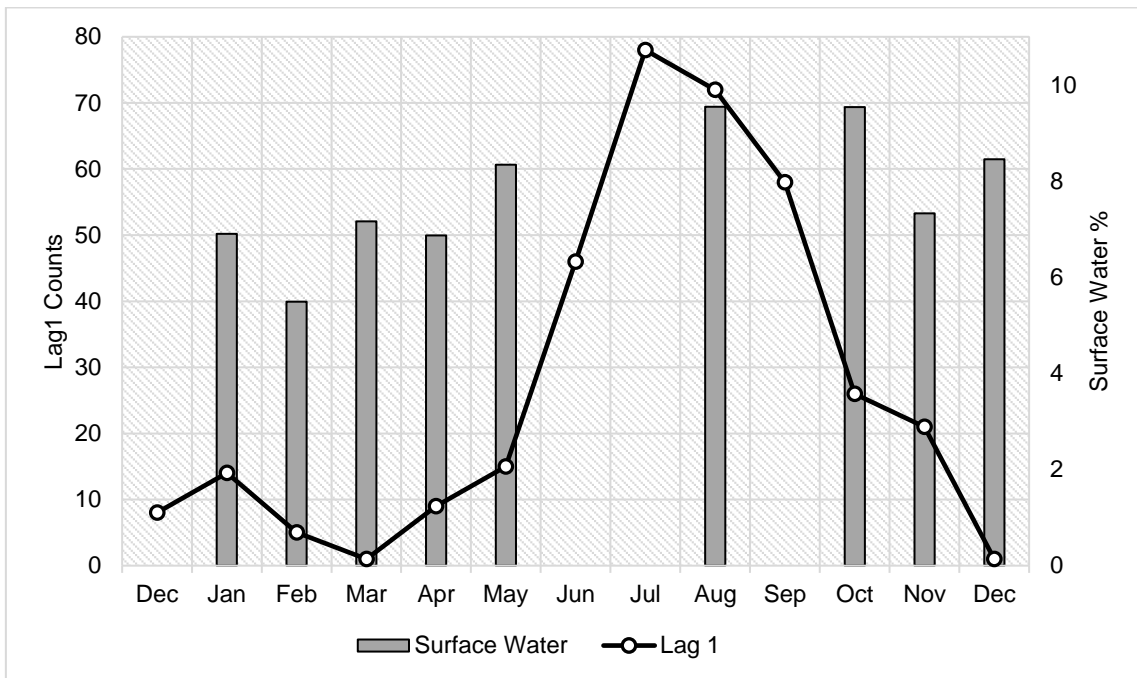


Figure 3.18: Surface water compared with Lag1 counts

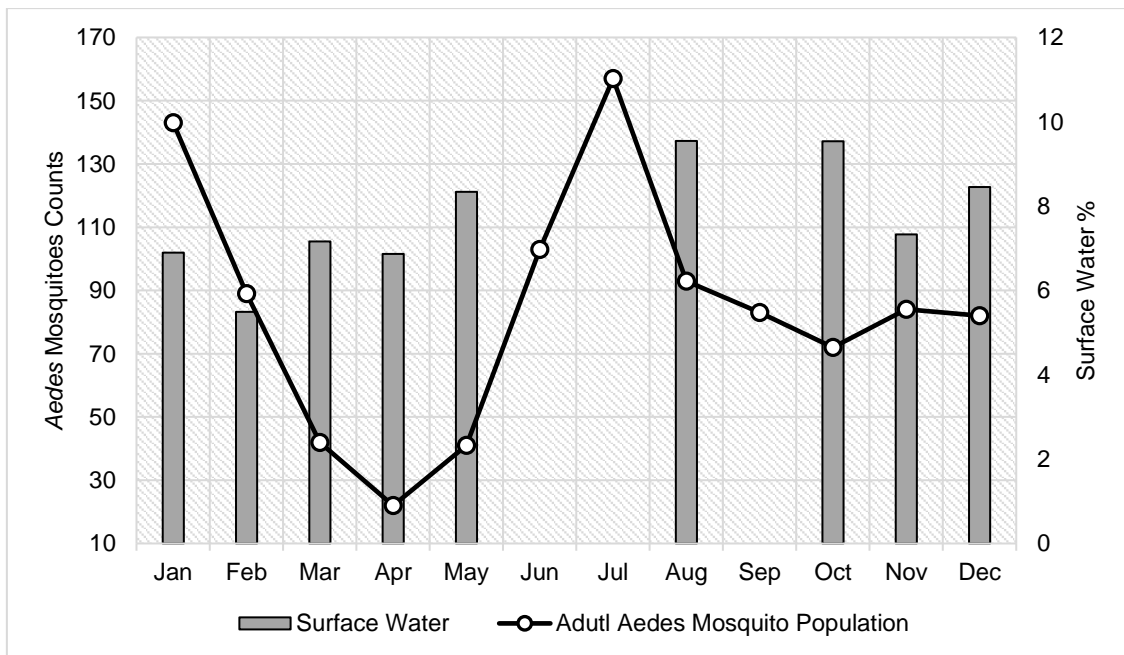


Figure 3.19: Surface water compared with Aedes mosquito population

Correlation Analysis

The analysis of the relationship between surface water and dengue incidence was performed by using Spearman’s correlation coefficient. Table 3.15 shows the values of the correlation coefficient derived from Spearman’s rho, with a value of $p < 0.05$ applied as the level of statistical significance. Surface water shows a positive correlation with dengue fever cases ($r = 0.7, p = 0.025$) with a

significant p value of less than 0.05. Similarly, the association of surface water with lag1 and lag2 shows a positive correlation ($r = 0.56, p = 0.1$; $r = 0.53, p = 0.1$ respectively), but these are not significant. The association of *Aedes* mosquito counts, and surface water shows no correlation with a very small coefficient value ($r = 0.067, p = 0.8$).

Rainfall shows a positive correlation with dengue incidence but not at a significant level ($r = 0.53, p = 0.071$), whereas with lag2 and lag1, rainfall appears positively correlated at a level of significance ($r = 0.72, p = 0.007$; $r = 0.75, p = 0.005$). There is a small correlation between rainfall and *Aedes* mosquito counts with no significance ($r = 0.18, p = 0.5$). Lag2 counts, which were cases of individuals contracting the disease, shows a positive correlation with *Aedes* mosquito numbers but that was not at a statistically significant level ($r = 0.4, p = 0.1$).

Table 3.15: Spearman's correlation coefficient analysis

Correlation		Surface Water (n = 9)	Rainfall (n = 12)	N Counts (n = 12)	Lag2 Counts (n = 13)	Lag1 Counts (n = 13)	<i>Aedes</i> Mosquito (n = 12)
Spearman's rho	Surface Water (n = 9)	Correlation Coefficient	1.00				
	Rainfall (n = 12)	Correlation Coefficient	.667 *	1.000			
	N Counts (n = 12)	Correlation Coefficient	.733*	.538	1.000		
	Lag2 Counts (n = 13)	Correlation Coefficient	.533	.727 **	.0902**	1.000	
	Lag1 Counts (n = 13)	Correlation Coefficient	.561	.753 **	.890**	.982 **	1.000
	<i>Aedes</i> Mosquito (n = 12)	Correlation Coefficient	.067	.182	.510	.448	.518

* Correlation is significant at the 0.05 level (2-tailed)

** Correlation is significant at the 0.01 level (2-tailed)

Linear Regression Model Analysis

Tables 3.16 to 3.18 illustrate the regression coefficient values derived from the Linear Regression Model. Surface water shows no significant association with lag1 counts with a p value of 0.072 despite the medium level regression coefficient value of 0.62. However, with an association between surface water and lag2 counts, there is a positive correlation with a significant level of 0.049, and a regression coefficient value of 0.66. For the relationship between *Aedes* mosquito counts and

surface water, the regression coefficient value shows no correlation with a negative value of 0.04 and p value is greater than 0.05.

Rainfall showed a strong relationship with lag1 counts of 0.84 with a significant value at 0.001, and with lag2 counts of 0.78 regression coefficient, and 0.003 significant value. Regression analysis of rainfall and *Aedes* mosquito counts, however, show a small value of coefficient of 0.21 at a non-significant level of 0.5.

The *Aedes* mosquito count was included in the analysis to examine its association with the lag1 counts. It was found that there is a positive correlation between these two, but that is not at significant level.

Table 3.16: Association between lag1 counts and surface water and rainfall from Multivariate Linear Regression

Model	Standardized Coefficients Beta	Sig.	95 % Confidence Interval		R Square	R
			Lower Bound	Upper Bound		
Surface Water	.625	.072	-1.183	21.652	.391	.625
Rainfall	.847	.001	.108	.280	.717	.65

Table 3.17: Association between lag2 counts and surface water and rainfall from Multivariate Linear Regression

Model	Standardized Coefficients Beta	Sig.	95 % Confidence Interval		R Square	R
			Lower Bound	Upper Bound		
Surface water	.668	.049	.045	24.641	.446	.668
Rainfall	.785	.003	.077	.269	.616	.785

Table 3.18: Association between *Aedes* mosquito counts and surface water, rainfall, and lag1 counts from Multivariate Linear Regression

Model	Standardized Coefficients Beta	Sig.	95 % Confidence Interval		R Square	R
			Lower Bound	Upper Bound		
Surface Water	-.040	.918	-25.053	22.891	.002	.040
Rainfall	.213	.507	-.154	.292	.045	.213

Model	Standardized Coefficients Beta	Sig.	95 % Confidence Interval		R Square	R
			Lower Bound	Upper Bound		
Lag1 Counts	.534	.074	-.088	1.600	.285	.534

To conclude, the image analysis results showed that haze reduction helped improve the range values of indices methods. NDWI, and NDMI presented more accurate results with less disturbance of non-water information. Correlation and regression results showed that there was a correlation between surface water and dengue incidence, but that had no relationship with vector population. Rainfall also appeared to be positively correlated with dengue incidence. These findings will be discussed further in chapter4 in which relevant literature will be used where it necessary in the discussion.

CHAPTER FOUR: DISCUSSION AND CONCLUSION

This chapter will begin with the discussion of spatial distribution of dengue incidence over the study area, and it will then discuss the findings of relationships between dengue fever cases and surface water, and rainfall; and compare these with the literature reviewed in chapter 1. Approaches used to extract surface water including pre-processing, post-processing of image analysis, and the factors that are likely to be the main influences on the results of water extraction will be outlined. Some of the methods used in the experiment to acquire more accurate results of surface water are not discussed in this section. Finally, aspects that should be considered when applying remote sensing and GIS in epidemiology are discussed. Limitations found in this study will be outlined, as well as further areas to be examined are also provided. This chapter will end with the conclusion section which highlights the key findings from this study, as well as the recommendations.

4.1. Analysis of Dengue Fever Occurrence

4.1.1. Spatial Distribution of Dengue Incidence

Dengue cases data from 2017 was spatially analysed in order to examine the frequency of the cases and its pattern of spatial distribution. Analysis showed cases were frequently found in the northern to northeast and expanded into the western part of the study area, with a frequency found in the east. The distribution of the incidence was normally distributed when simply plotted and analysed in the Data Analysis tool provided in Microsoft Excel. However, the result from dispersion data analysis showed that the data was in a clustered pattern according to the result derived from the Average Nearest Neighbour ratio (NN Ratio < 1). This clustering is assumed to be due to the influence of a higher density of population and urbanisation in the area. Figure 4.1 shows the areas where large numbers of dengue cases were found in the centre of the study site with a high population of more than 90,000. The disease incidence was found clustering within the densely populated areas as shown in Figure 4.2. Bohra and Andrianasolo (2001) investigated the risk factors causing dengue disease in India and found that in crowded areas where there is a high density of population, dengue transmission is more likely to happen. This illustrates that humans are the main source of blood for dengue vectors, therefore, where there is a denser population, the vectors are likely to be found. In this study, it is noted that the regions that appear to be attractive sites for dengue vectors are the core urbanisation areas in the study site with more than 90% development (see Figure 1.4, Chapter 1). Coker et al. (2011) stated that the emergence of vector-borne disease is associated with the rapid development of urbanisation, especially in areas where there is a mixture of urban and peri-urban areas in which storing water is implemented due to insufficient water supply and unreliable sanitation systems. However, although the density of population and urban development are the driving forces behind the disease, it is essential to investigate the distances between breeding sites and dengue cases. It has been pointed out that virus transmission is connected with the flight distance of vector

mosquitoes which is likely to be more than 50 metres for *Aedes aegypti* (Morlan & Hayes 1958; Reiter et al. 1995). So, in further analysis, in order to develop a risk or predictive model of dengue disease; approximate flight distance of the vectors, breeding sites and human settlement should be considered.

In this research, from the initial exploration of the spatial distribution of dengue over the study area, it appeared that the trend of dengue occurrence was influenced by the spatial distribution of population. However, there was a lack of data at the village level, which is necessary for the spatial evaluation to analyse whether the clustering pattern of dengue distribution is significantly correlated to population and urban development. Importantly, this is beyond the scope of this study, but it is critical that this should be considered in a further study.

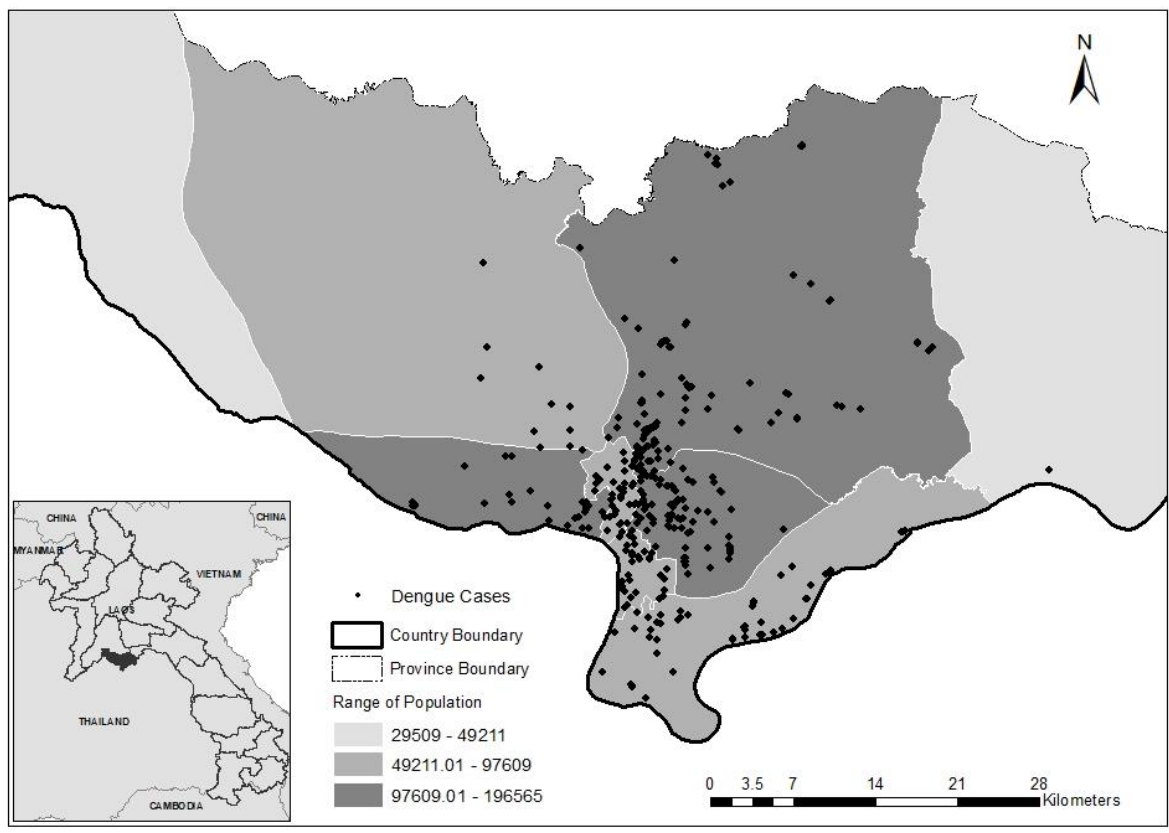


Figure 4.1: Study area by number of populations

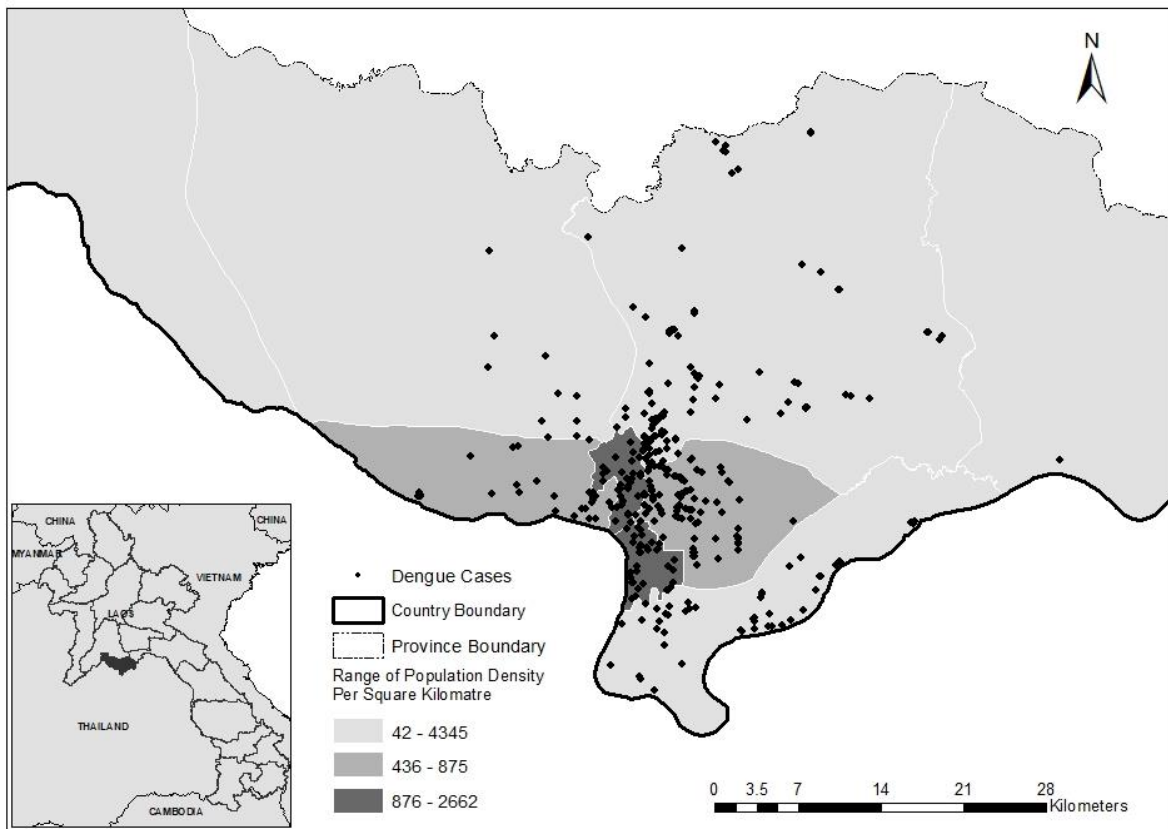


Figure 4.2: Population density per square kilometre

4.1.2. Analysis of the Association of Dengue Incidence and Water Bodies

Water bodies serve as the breeding sites for dengue mosquitoes, and play an important role in the spread of dengue fever (Hsueh, Lee & Beltz 2012). However, biologically, the cycle of virus transformation is complicated, so it is important to understand the delay time of virus transmission and its development. In this study, the number of dengue cases (N), lag1 – an estimation of an adult mosquito development time, lag2 – an estimated date of people who contracted the virus, as well as the *Aedes* mosquito population, were analysed against surface water and rainfall.

The correlation between surface water and dengue cases was positive at significant level, however, this study did not include the distance from the disease cases to water bodies in the analysis, so it cannot be definitively stated that the changes of water bodies throughout the year influenced the occurrence of dengue fever. Chadee, Williams and Kitron (2005) and Chowell and Sanchez (2006) highlighted that water bodies are found to be correlated with the occurrence of dengue fever in the areas where there is a high population density. However, it is important to note that Hsueh, Lee and Beltz (2012) emphasized the range of flight distance of mosquito vectors from the breeding sites to food sources as an important aspect that should be considered as it could affect the dengue disease cases. Thus, to effectively evaluate the significance of surface water associated with dengue cases, population density – a main food source for dengue vectors – and the proximity between water bodies and dengue cases should be focused on in a further study.

Surface water was found to have a positive correlation with lag1 and lag2, but not at a statistically significant level, and showed no correlation with *Aedes* mosquito population numbers. Regression analysis showed no significance between surface water and lag1 and the vector population, but with lag2 with a positive correlation at a significant level. Nevertheless, there was a relatively low correlation between the two with an R square value of 0.45 which means that surface water is only a moderate predictor of the numbers of mosquitoes. From a review of the literature, and the findings in this study, a suggestion for further studies is that investigating other aspects which could influence the number of dengue vector mosquitoes, not just only the amount of surface water, is encouraged. It is known that water bodies serve as the breeding habitats for mosquitoes, and many studies found that there is a significant correlation between dengue fever and water bodies (Nakhapakorn & Tripathi 2005; Raju & Sokhi 2008; Tian et al. 2016), and dengue prevalence was found in the areas located closest to water regions (Halstead et al. 1965; Li et al. 2017; Zheng et al. 2019). However, the biology of dengue mosquitoes is too complicated to just simply treat all water bodies as equal.

Types and sizes of water bodies are significant components in a study of breeding habitats for dengue mosquitoes – *Aedes aegypti* and *Aedes albopictus* – since they have different breeding behaviour. Water body type and size affect the size of dengue vector population causing the density of the mosquito populations to vary (Tian et al. 2016). In this study, many of the water body areas were big rivers, flowing streams and deep standing water bodies. These types of water might not be appropriate sites of breeding for dengue mosquitoes as Tiong et al. (2015) found that large water bodies were not an influence for dengue prevalence because they limit oxygen and light from the sun, which support the growth of dengue vectors. It was assumed that, however, there is a likelihood that water bodies like lakes link to dengue cases (Li et al. 2017), as they could provide breeding sites for *Aedes albopictus* mosquitoes which could lead to a higher numbers of disease carrying mosquitoes (Tian et al. 2016). This study did not classify types of surface water favourable for dengue vectors, therefore, to effectively evaluate the relationship between surface water and the occurrence of dengue fever, the characteristics of water including size of water bodies (Tiong et al. 2015), types of water (Nasir et al. 2017) (turbid, standing water, flow water), depth of water, cleanliness of water (Phuanukoonnon, Brough & Bryan 2006), organic matters to feed mosquito vectors, as well as water temperature (Tun-Lin, Burkot & Kay 2000), should be taken into consideration.

Surface water was found to be correlated with rainfall data with strong correlation being statistically significant, which indicates the interconnection between the two. Several factors were found to influence the quantity of surface water, such as the amount and intensity of rainfall, temperature, and topographical features (World Health Organization n.d-b). In this study, as surface water was positively correlated to rainfall, surface water is not suggested to be used as an independent factor to predict dengue incidence occurrence.

4.1.3. Analysis of the Association between Dengue Incidence and Rainfall

From the primary assessment, it was noticed that the trends in dengue cases and rainfall events showed some hidden relationships between them (Figure 3.13, Chapter 3). Correlation and regression analysis were performed. Rainfall showed a positive correlation with dengue prevalence, at non statistical significance, but with lag1 and lag2, while there was no relationship with the adult vector population. Regarding the association between rainfall and dengue incidence, it is important to note that precipitation is found to be highly correlated with the disease incidence only when there is a low level of precipitation and with less inundation (Angel & Joshi 2009; Bi et al. 1998) because heavy rain can wash away the eggs and larvae, while a decrease of rainfall creates flooded areas for mosquitoes. Several studies showed similar findings, for instance, Sirisena et al. (2017), Bi et al. (1998) and Zheng et al. (2019) explored how dengue incidence was associated with rainfall and the results were reported that precipitation was associated with dengue fever occurrence when there was an increase in average rainfall under favourable conditions. This research project found that there was less significance between rainfall and dengue incidence, and only included total amount of rainfall in the analysis. However, this finding suggested that a further exploring the different level of precipitation is suggested in order to clearly see how significantly dengue incidence and rainfall are related. Another aspect should be attentively looked at when examining the correlation between these two is that rainfall acts as an indirect factor that provides appropriate conditions for mosquitoes to breed in and to proliferate. Precipitation creates a condition of high relative humidity with the support of temperature for vector mosquitoes (Nasir et al. 2017). With these suitable conditions, the number of vector mosquitoes can be increased at any time throughout the year, even in the dry season. This is supported by the findings by Angel and Joshi (2009) who showed that mosquito infectivity was high in desert areas where there is rare precipitation. Additionally, Sirisena et al. (2017) also found that high vector populations were reported in dry zones not just in wet areas. It was also evident that in this study, dengue cases were reported following the dry season and increased in the rainy season. Thus, it is important to prepare action plans before the rainy season starts in order to effectively deal with the situation that frequently happens prior to and during the rainy season.

4.2. Image Correction

4.2.1. Atmospheric Correction

It is acknowledged that correcting the interference of atmosphere on sensors especially in visible and NIR radiance is necessary, so this study attempted to perform this correction by applying top of atmosphere (TOA) and bottom of atmosphere (BOA) corrections.

Top of Atmosphere Correction (TOA)

Image data (04 and 16 January 2017) were selected for the test of TOA: although this appeared to improve spectral reflectance of PlanetScope, when performed in normalized difference water index (NDWI) to generate water features, it was found that some water areas contain negative values which typically are considered to be non-water areas ($NDWI \geq 0$). As a result of this, many areas which had negative values, such as built-up areas and bare areas, were overestimated as water features. It was suspected that this problem occurred because the process of converting radiance to TOA reflectance was operated by multiplying the DN values of each band with the reflectance coefficient values provided by the Planet. According to Avnir and Cartosat (2018) in the process of indices calculation of vegetation for instance, reflectance data is required for extracting ground features, but if the input data is in digital number (DN) values, they will be internally converted to TOA for the calculation. On this basis, it is assumed that in this study, this issue happened due to the process of converting TOA reflectance that might be calculated twice; 1). From the conversion of radiance to TOA reflectance, and 2). The calculation of TOA reflectance through NDWI. Wicaksono and Lazuardi (2018) applied this method of converting radiance to obtain TOA reflectance data of two different dates in their study of mapping benthic habitat and seagrass species. Satellite image data used in the study was PlanetScope images but their study was not focusing on applying indices methods. Baloloy et al. (2018) also used PlanetScope images to examine the biomass of mangrove forest above ground by applying vegetation indices. The process of TOA reflectance acquisition was performed according to a guide provided in the Planet Labs python (www.planet.com/docs/guides/quick-startndvi). In this current study, TOA reflectance was implemented based on the guidance provided from the tutorial of converting PlanetScope imageries from radiance to reflectance (Planet 2019). In doing so, instead of using Python 2.7 or 3+ as recommended by the Planet developer, Spatial Model Editor in EDAS Imagine 2018 was built according to the Python scrips and formula provided in the guide. In order to justify this, a further experiment on the use of Python and simple spatial model from ERDAS Imagine generating TOA reflectance data based on the provided formula is suggested.

Bottom of Atmosphere Correction (BOA)

In this study, normalized difference water index (NDWI) values were obtained from the atmospheric correction of bottom of atmosphere (BOA) performed by applying the dark object subtraction (DOS) method. Hadjimitsis, Clayton and Retalis (2003) explained the principle process of dark object that "pixels from dark targets are indicators of the amount of upwelling path radiance in the affected bands". By using this method, surface radiance of the dark objects is added by the radiance atmospheric values, therefore resulting in zero surface radiance or reflectance.

The results of NDWI values obtained using the DOS method showed a varied range. Pixel values extracted from deep and clear water areas were the darkest values in the process in the DOS

method. The results showed a huge range of values of NDWI (402.83 to 381.13). Mather (1987) and Switzer, Kowalik and Lyon (1981) investigated the digital number (DN) values of water features on Landsat TM 5 and TM 7. Those authors found that areas in the short-wave infrared band were significantly affected by the additive effect of haze, and the darkest pixel in the Landsat TM band 4 (760 nm – 900 nm) was presumably influenced by atmospheric effect. In this study, there is a likelihood that band 4 (780 nm – 860 nm) of PlanetScope image might be affected by the presence of atmospheric noise. Hadjimitsis, Clayton and Toullos (2010) mentioned that water bodies are objects that highly absorb atmospheric effects, so in order to find the suitable dark pixel values; applying different methods and comparing them together to generate dark pixels is recommended.

Apart from selecting dark pixels from water areas, histogram minimum values of each band were applied in this study to extract dark pixel values. The result of NDWI showed more moderate values in the range -0.77 to 0.89 compared with those of the dark pixels from water areas. Hadjimitsis, Clayton and Toullos (2010) pointed out that although histogram minimum values for acquiring dark pixel is used, it is not always straightforward to obtain suitable values for dark pixels because the values are automatically generated. To acquire suitable minimum values in each band, when plotting a histogram of DN values of dark areas on image, the outliers, which are assumed to be influenced by noise and data error, should be ignored (Hadjimitsis, Clayton & Toullos 2010).

This study simply extracted dark pixel values by examining digital number values from each band and used them in the DOS method without applying various approaches. As a result of this it could be assumed that the effect of selecting pixels from the dark object might be disturbed by other factors such as the atmospheric contribution.

Song et al. (2001) suggested that, nevertheless, simple atmospheric corrections, such as the dark pixel method, might not be suitable for the applications needed to acquire surface reflectance, but it seems to be applicable in classification and change detection tasks to derive the best overall result. In contrast, Hadjimitsis, Clayton and Toullos (2010) compared numbers of atmospheric corrections for the needs of surface reflectance applications by applying them to the Landsat TM image and it was found that the darkest pixel or object subtraction correction outperformed the others with a reasonable correction provided in bands 1, 2, and 3. Nevertheless, from the operator point of view, the effectiveness of the atmospheric correction method might need further work to test it with different satellite image data, at a different area of interest in order to obtain consistency.

4.2.2. Haze Reduction

Haze reduction was designed based on the sensor-specific calculation of the Tasselled Cap (TC) transformation used only on Landsat 4 TM, Landsat 5 TM, and Landsat 7 TM imageries. However, in this study, after exploring the method used to correct atmospheric effects (TOA, BOA), haze reduction was used as another method for correcting the disturbance of atmosphere. Images with

haze reduction were improved both statistically and visually. Importantly, the range values of the normalized difference water index (NDWI), and the normalized difference moisture index (NDMI) in February and March were also improved up to -1 to +1. The image data derived in August was applied before the masking cloud process. It was found that the NDWI range values was also improved from -0.47 to -0.68 for minimum values, and from 0.505 to 0.517 with an improvement of 0.124 to 0.127 of standard deviation values. With this improvement, Ahmad et al. (2014) assume that in the nature of haze reduction process, the pixels that contain haze will be replaced with the mean values from the clear regions, and spectral reflectance of ground features is also enhanced.

However, due to the unviability of coefficient values of PlanetScope used for proceeding in the model of haze reduction, further experiments should be undertaken by exploring satellite sensors containing 4 spectral bands with a similar wavelength, such as SPOT, that the coefficient values are available. Coefficient values used to perform TC can be found at the index database (<https://www.indexdatabase.de/>). This would help operators decide which atmospheric correction models should be at best applying in improving the accuracy of image analysis results.

4.2.3. Cloud Removal

Cloud cover seems to be the main constraint to multispectral sensors to detect the surface reflectance in tropical areas. The study site was in a tropical region so this issue cannot be ignored. The images obtained from PlanetScope were also covered by haze and cloud, but the huge amount of cloud presented in the image was in August. Due to the unavailability of an automated cloud masking method, cloud and shadow were classified by using Unsupervised Classification, and a single band threshold method. These two methods were performed and compared in order to find the better result. It was found that although the classification approach was able to detect cloud cover and shadow, many ground features, especially water information, were classified as cloud and shadow. In contrast, the threshold method showed better results in detecting cloud and less overestimation of water surface. Sun et al. (2016) stated that the threshold method is the most widely applied method with high accuracy and stable results but finding the suitable threshold values from any wavelength is not straightforward especially if the cloud cover is in the complex land surface composition. The threshold used to detect cloud typically detects clear pixel values which are normally related to other features that contain similar pixel values as it is presented in Figure 4.3. This is evident that not only cloud was removed but also other objects, such as buildings and roads were also removed. Nevertheless, as this study only focuses on water features these losses have no impact on this study.

To enhance the quality of cloud detection, applying different cloud detection algorithms with a concerned remote sensor in a specific study area is recommended, otherwise information about the ground surface derived from pixels values that has inaccurately undergone the process of cloud and shadow removal, will decrease the accuracy of land cover classification (Wang, Xie & Liang 2008).



Figure 4.3: The effects of cloud and shadow removal on other ground surface features, PlanetScope displayed in true-colour composite

4.3. Surface Water Extraction

The classification method was initially considered as the method to be used in generating surface water data, however due to the large number of satellite images, a method, such as indices algorithms, which performs with less time with overall accuracy at an accepted level, was considered.

4.3.1. Normalized Difference Water Index (NDWI)

The normalized difference water index (NDWI) was suitable for water body mapping in the study site over the dates where there were relatively large amounts of surface water. Most of the area covered by water bodies such as small ponds, rivers and streams were detected. When applied in the dry season, especially at the time that there was less water, the water index was poor in discriminating surface water and was interrupted by other non-water features such as bare areas. Despite the ability to detect the surface water of NDWI, the main challenge in applying this method, especially in urban areas, is that it often shows significant numbers of false positives in built-up areas such as buildings, roads, and bare areas due to their similarity of spectral reflectance in the Green and NIR bands (Rokni et al. 2014; Zhou et al. 2017). As some parts of the study site cover urban zones the issue of overestimating surface water was found to be a main challenge. Xu (2006) suggested a modified normalized difference water index (MNDWI) which deploys SWIR instead of Green band as this can remove the disturbance from built-up signals. However, this study only used free of charge image datasets – PlanetScope and RapidEye – which only consist of 4 bands (Visible and NIR bands). To decrease numbers of false positives that occurred in the results, this study focussed on seeking suitable optimal threshold values to generate water information. Thresholding was implemented to obtain the most suitable values to detect water bodies with less interference from the non-water

features. Thus, this study divided water extraction results into three classes – high level refers to pure water, medium level refers to water mixed with grass, small vegetation, and low refers to non-water. By applying threshold values to generate water information from others, Zhou et al. (2017) pointed out that the threshold used to delineate water features might not guarantee that NDWI could completely remove unwanted features from the results. With the limit of sensors, combining NDWI with Principal Component (PC) might be another option. Rokni et al. (2014) suggested an integration of NDWI and the Principal Component Analysis (PCA) – a technique of transforming the composite image into a new PCA space to produce uncorrelated output bands. This proposed method, however, was only applied to examine the changes of surface water at two or three different times in open surface water such as lakes and rivers in their study. Using different methods and integrating them together would help improve the accuracy of water body extractions. For instance, Acharya, Subedi and Lee (2018) examined the methods used to best detect surface water in Nepal and found that using different water indices, such as the normalized difference water index (NDWI), modified NDWI, and automated water extraction index (AWEI), they could obtain high accuracy results of water delineation. By combining these approaches, surface water can be extracted with better accuracy up to 0.96 of overall accuracy and 0.89 of Kappa coefficient.

4.3.2. Normalized Difference Moisture Index (NDMI)

The Normalized difference moisture index used in this study was modified from the NDMI originally developed by Gao (1996) which typically deploys near-infrared (NIR), and short-wave infrared (SWIR). Due to the limitations of remote sensors used in this study, the Red and NIR bands were used instead. This modified index was selected to use only with the image that presented a small amount of surface water (February and March). Results from this modified index showed less disturbance from non-water feature signals such as bare areas when compared with NDWI and NDVI. With the use of NDMI, Ogilvie et al. (2018) compared different method of indices to extract water bodies from SPOT data, and found the NDMI moisture index performs better in detecting low surface water and small water bodies. However, it showed low user accuracy due to its inability to separate vegetated pixels from water features. In addition to this, Rokni et al. (2014) extracted surface water from Landsat data by deploying NDWI and NDMI and found that NDMI was not able to generate surface water if compared with NDWI. Regardless of these poor performances of NDMI, this study used this modified normalized moisture index, and it appeared that the NDMI was able to extract surface water with a small number of false positives with overall accuracy of 0.91, and user accuracy of 0.69 at medium agreement level of Kappa coefficient (0.48). However, the NDMI used in this study was modified from the original model due to the limitations of sensor wavelength. Further experiments that apply this with other sensors where SWIR is not provided are recommended.

To sum up the use of indices methods, in order to produce highly accurate water body detection, an operator might need to comprehend that different types of water bodies have different spectral

reflectance in different remote sensors (Fisher, Flood & Danaher 2016). For instance, in this study, PlanetScope image, deep and large water bodies showed high reflectance in Green and dropped in the Red and NIR bands, while shallow water showed slightly different reflectance between Green and Red bands. RapidEye image, deep water bodies and shallows show the peak point of reflectance was in Green band and low reflectance in the Red band. It is suggested that to optimise the progress of mapping water bodies in urban areas, exploring surface reflectance of ground feature, as well as the combining water indices methods with other object extraction techniques would be another option to consider (Jiang et al. 2014).

4.3.3. Optimum Thresholds for Indices Methods

Threshold selection is an integral to achieving detecting water pixels from water index images (Chen et al. 2018). The fix threshold was defined by McFeeters (1996) who firstly developed the NDWI, and Gao (1996) who developed NDWI which was later defined as NDMI by Xu (2006). The threshold of these indices is set at zero where the water feature is greater than zero ($NDWI > 0$) and non-water is smaller or equal to zero ($NDWI \leq 0$). In this study, however, the threshold was manually adjusted according to the study site. Xu (2006) stated that despite the values fixed from the NDWI and NDMI, a manual adjustment of threshold performs better and more accurately in identifying water. This study provided the threshold values used to delineate water features with the consideration of 1). Detecting surface water as much as possible in the study area, and 2). Fewer false positives were contained in the outputs. The threshold used in this study was between 0.11 and 0.22 where the values greater than these were considered to be water features. With this low threshold, Ogilvie et al. (2016) reported that a threshold which is close to zero is mostly found in wetlands. In this study, the study area is a lowland surrounded by wetlands with water accumulation during the rainy season and water storage for agricultural activities (Comte 2009). So, it might be assumed that threshold values were at this range as a consequence of the study site's characteristics.

Regarding the issue of applying threshold values, Ji, Zhang and Wylie (2009) commented that due to the mixture of large numbers of water and non-water pixels, when applying threshold values, water pixels can be reduced. To improve this water delineation output, it is required to evaluate the water indices in order to determine a suitable threshold for extracting water features, and defining a suitable threshold can also reduce the interferences of clouds and shadow (Ji, Zhang & Wylie 2009; Ogilvie et al. 2018). Importantly, field data is necessary to enhance the accuracy of water mapping (Ogilvie et al. 2018).

4.4. Accuracy Assessment

The Confusion matrix (Figure 3.12, Chapter 3) illustrated that the overall accuracy derived from this assessment was up to 0.917 or 91.7 %. The accurate interpretation of water from User and Producer was 0.69 or 69 %, and 0.42 or 42 %, respectively, whereas, the accuracy of non-water interpretation was 0.93 or 93 % for User, and 0.97 or 97 % for Producer. However, the Kappa coefficient showed only at a medium level of agreement between the reference data (ground truths) and interpreted data. Regarding the accuracy produced by User and Producer, Congalton (1991) explained that to interpret the result produced from accuracy assessment, each clarified field is interpreted according to the results generated by User Accuracy (UA) and Producer Accuracy (PA). As the focus of this study was surface water, the correct pixels considered to be water were only 69 % correctly identified from User, while only 42 % of water areas were correctly identified as water from Producer. Congalton (2007) highlighted factors affecting the results of accuracy assessment which can happen during the process of image analysis. The errors include sensor issues, geometric correction, image analysis processes, as well as the assumptions made during the process of assessment.

During the process of assessment in this study, although 500 points were generated to represent ground references on the study site, many areas show unclear features which made it difficult for the operator to determine whether it was surface water or not, as is shown in Figure 4.4 (a) image, within a red rectangle a ground truth point was classified as water but it was bare areas on the ground surface: (b) image, area in red rectangle with point was classified as non-water but it was actually a wet area covered by green algae. Regarding this, the observer used local knowledge, but the unclear aerial image was the main challenge to accurate interpretation. In this case, local knowledge alone was not enough but the field survey needed to be planned beforehand. Due to the time constraints and large size of the study area, the ground reference data was not collected properly, and this study mainly relied on the operator's knowledge and some ground data collected during field observation.

Apart from a lack of local knowledge and field data, the methods of NDWI and NDMI are considered to be simple with achievement of an accuracy at an accepted level when using it in the areas with less interruption from environmental noise with standard threshold values (Acharya, Subedi & Lee 2018; Jiang et al. 2014). However, in this study, noise from non-water, especially in the areas where there were artificial ponds in the urban zones, could lead to misclassifying, and resulting low accuracy of User and Producer. Another factor that was assumed to affect the image analysis accuracy in this study was the threshold values used for identifying surface water. This study applied threshold values to generate water bodies and at the same time the issues of signal disturbance from non-water features such as built-up areas, and shadow were considered. As a result of this, a lot of water pixels mixed with non-water pixels were misclassified. To address this problem, the combination of methods and selection of a suitable threshold based on study site's characteristics

and remotely sensed sensors with the assistance of field survey data are essential to improving the accuracy of water extraction.



Figure 4.4: Ground reference on aerial imagery, Google Earth Pro, displayed in true- colour composite

4.5. Factors affecting Surface Water Results

The main challenges to waterbody delineation from multispectral satellite images in this study were the limitations of sensor wavelength and spatial resolution, the presence of clouds, and the date of image data acquisition. Firstly, it was acknowledged that the normalized difference water index (NDWI) and normalized difference moisture index (NDMI), although they are widely used for generating water bodies with high overall accuracy, under urban conditions they fail to differentiate water information from built-up signals and small shadows. Hence this study put significant effort into investigating different methods for water delineation. Nevertheless, a large number of false positives were still found and lots of water pixels were lost. In order to reduce this issue, Yang et al. (2017) recommended using high resolution image data as this could help reduce the missed pixels and improve the accuracy of urban surface water allocation. Despite the use of high spatial resolution images, NDWI and NDMI methods were not able to identify the water areas where they were covered by green vegetation as is shown in Figure 4.5. Hardy et al. (2019) suggested that with the issue of vegetated water bodies, applying machine learning classification such as Extremely Random Forests to obtain water body data can help improve water mapping up to 92% of mean overall accuracy. Yang et al. (2015) deployed the advantages of normalized difference water index (NDWI), and modified NDWI to obtain water features for implementation in the machine learning method – Deep learning. It was found that the water delineation was successfully generated, however, shadow, buildings and clouds were still constraints (Nath & Deb 2010; Yang et al. 2015), so that to

detect water bodies in urban areas and vegetated water bodies with actual water information, requires performance by several algorithms to develop a method that can be accepted universally.

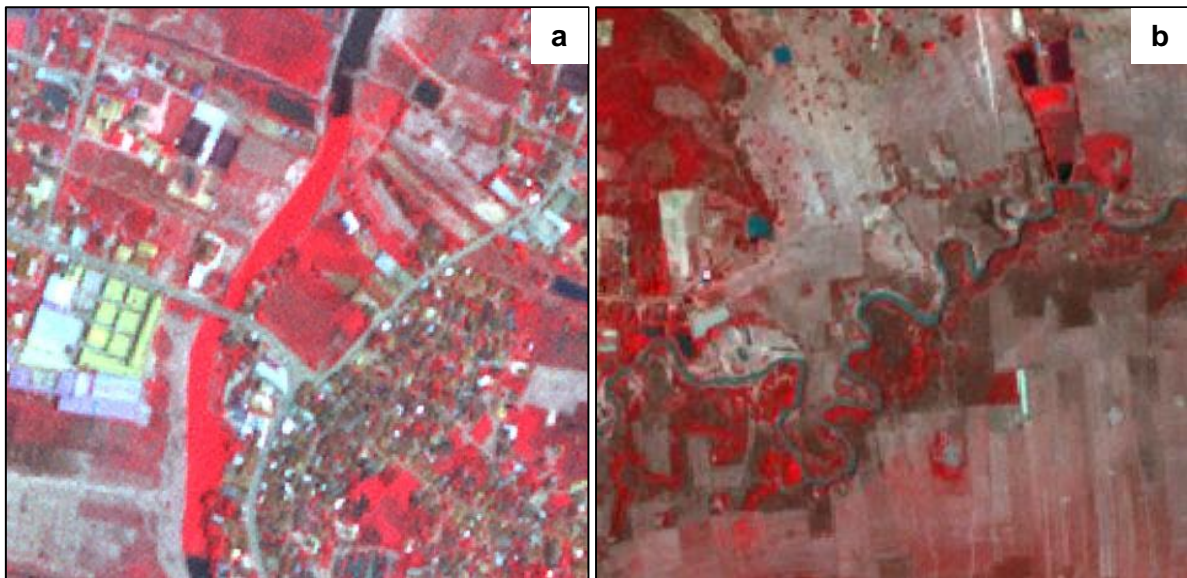


Figure 4.5: PlanetScope displayed in false-colour (RGB: 4,3,2), (a) shows water channel blocked by vegetation, and (b) small stream mixed with vegetation

Secondly, obtaining cloud-free images during the wet season in tropical regions from the optical satellite sensors is a considerable limitation. This research found that Radar image data such as Sentinel-1 Synthetic Aperture Radar (SAR) could penetrate cloud cover, however, due to the size of water bodies, less than ten metres, and the selection of free of charge image data which was a main focus, optical images data which contain less cloud coverage were selected. In this study, all dates of image data were obtained, only three dates image data – June, July, September – were unsuccessfully derived. The issue of cloud still remained on the image in August 2017. Surface water features were lost due to cloud masking. As a result of this, water pixels were reduced when compared with the rainfall data (Figure 4.6) in August which was supposed to be the highest time of surface water accumulation, the amount of water was almost the same amount as in October.

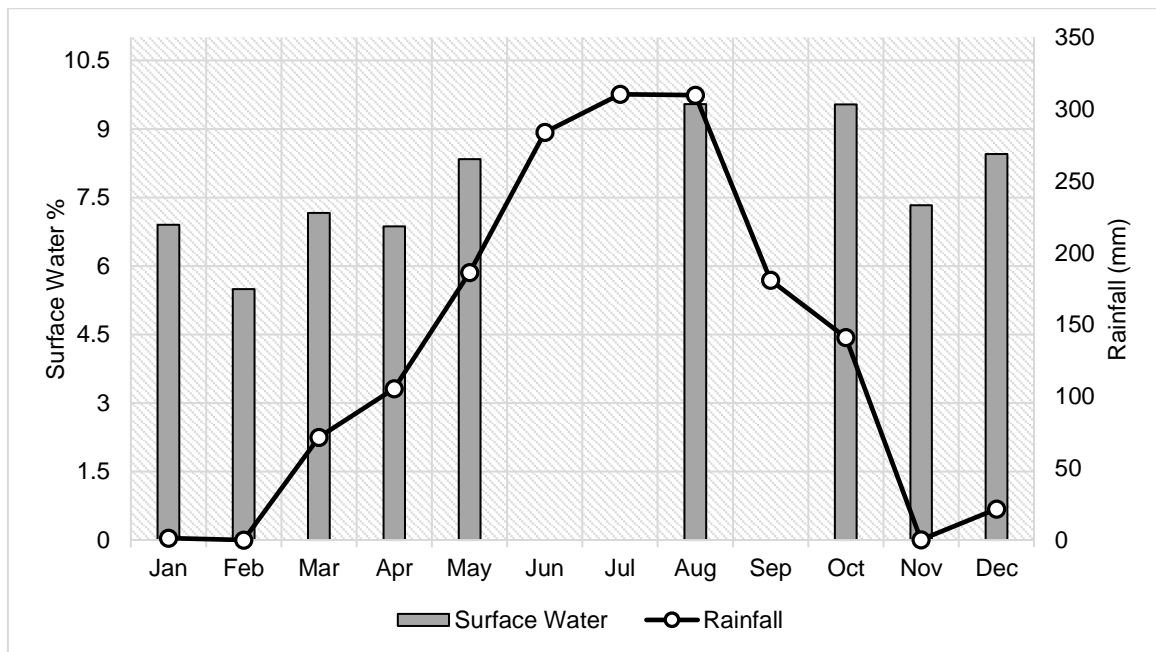


Figure 4.6: Rainfall data in 2017

Finally, the amount of surface water was compared with the rainfall data in order to visually examine the differences between the two data. Although surface water was affected by the method and the presence of cloud, time of image data acquisition also plays an important role in surface water results. Only in May, August and October image data was acquired close to rainfall events that continuously occurred for more than three days, while others were acquired at the time that there was a small amount of rain throughout the months (January, February, March, April, December) (see Appendix 7). However, in the dry season, in which there was less rainfall, artificial surface water was still found. According to the Lao Census of Agriculture 2014, Vientiane was ranked as the highest out of eight provinces that contributed to fish products across the country (19% of total 75%), and 43% of the area was covered by farm households with less than one hectare. Thus, during the dry season (December, January, March) surface water was still shown as being as high as in the rainy season (May, November). Other aspects that should be considered include the fact that the surface water can be affected from run-off, organic matter, climate, vegetation and soil types, as well as geographical characteristics (World Health Organization n.d-b). These aspects should be included to effectively examine the changing of surface level.

4.6. Aspects to be Considered When Applying RS and GIS in Dengue Epidemic

With respect to missing satellite image data, acquiring images for June, July and September was not possible, which is likely to be the peak rainy season. It might be thought that this could affect the extraction of surface water data used in the process of correlation and regression analysis. However, it was found that there was no trend in the correlation between surface water and disease

transmission, so that those missing dates of image data had no impact on the findings. In addition to this, it is suggested that to anticipate the occurrence of dengue incidence data, events of surface water and rainfalls before the rainy season should be a considered (M Grandadam 2019, online communication, 18 October). Figure 4.7 presents the five years of occurrence of dengue incidence (2014 to 2018) retrieved from Institut Pasteur du Laos (IPL). A higher prevalence was found not just during the rainy season but also at the beginning of each year in the dry season. This was consistent with the expected time for individuals contracting disease shown in this study. The pattern of dengue occurrence indicated that there is a need to work on the early rainy season or the late dry season in order to actively prevent the disease cases that will emerge during rainy season.

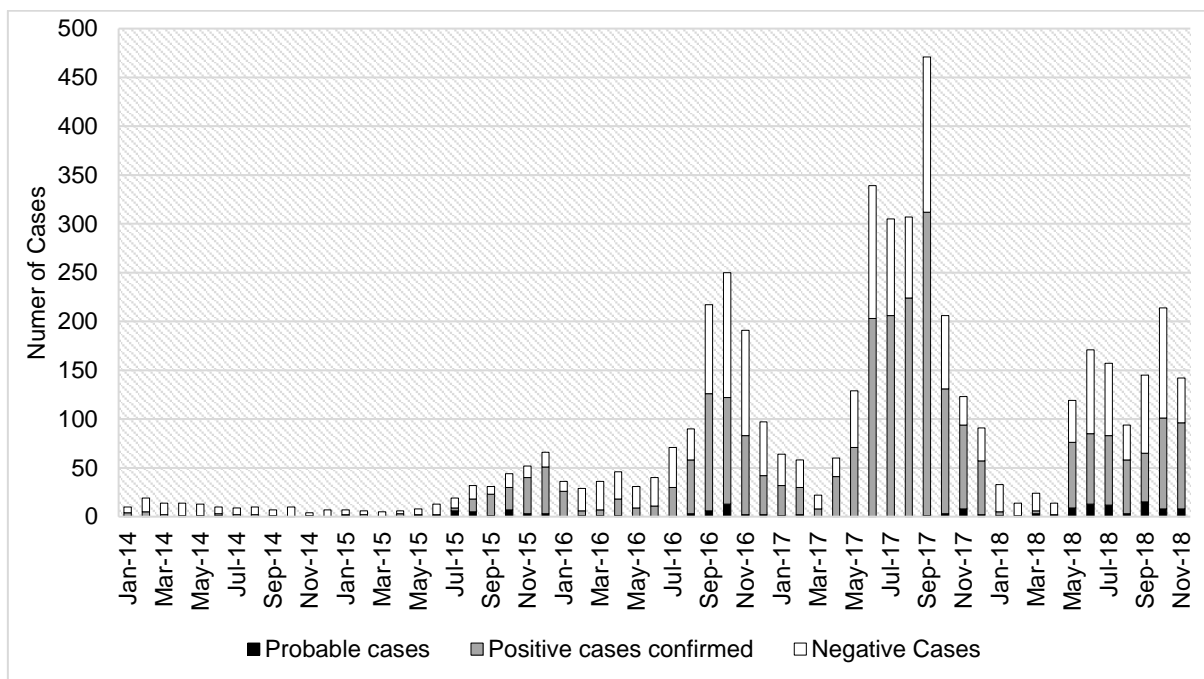


Figure 4.7: Dengue incidence in 2014 to 2018

Source: ECOMORE 2, IPL

The relationship between surface water and the epidemiology of dengue fever is complex compared with other mosquito borne illnesses such as malaria. Malaria is a vector-borne disease carried by *Anopheles* mosquitoes which are found in wetlands and has an association with vegetation, favourable conditions of water and distance to human populations (Sánchez-Ribas et al. 2015; Vittor et al. 2006). However, the malaria vector requires more stable water conditions and water movement which generally are not found in small water bodies. The breeding sites of this type of vector are likely to be in large, deep and clear water bodies such as swamps, lakes or large rivers (Rozendaal 1992) and the accumulation of water caused from rainfall (M Grandadam 2019, personal communication, 14 June). In contrast, dengue vectors like the *Aedes* mosquitoes behave differently from the malaria vector in terms of breeding behaviour. The breeding habitats are found in indoor areas such as water tanks and water containers for *Aedes aegypti*, and outdoors such as small sized

water bodies for *Aedes albopictus*. This biological diversity of dengue disease leads to limitations of the use of advanced technology such as remote sensing (hereafter RS) and Geographical Information Systems (hereafter GIS).

A significant constraint found in this study was the ability of satellite images to detect small water bodies accurately, and the inability to detect small scale surface water in construction sites. As this study used freely available image data with a relatively high spatial resolution, high spatial resolution image data facilitated by land use types, which will distinguish water types, land use types; and types soils, which will help examine the soil saturation with certain amount of water, might help to detect more accurate water information. Importantly, methods used to detect water features like indices approaches, still needed to be investigated more in order to produce better water-associated disease breeding sites (Kulinkina et al. 2018). GIS, on the other hand, showed the spatial distribution of the disease at the study site which allows the operator to further seek the factors influencing this clustering pattern. However, due to the lack of sufficient data necessary for analysis, this study could not provide results related to spatial analysis. To add to these points, Kitron (2002) stated that some critical issues should be considered when applying remote sensing and GIS in epidemiology, especially in applying it to vector-borne disease. These issues include lack of training data, quality and quantity data of epidemiologic and parasitological data, and tools for gathering data, as well as the limitations of understanding and knowledge on the complexity of epidemiology.

It has been suggested that when applying spatial information in epidemiology, specific use of analytical tools and methods should be focused in order to precisely detect factors that influence the occurrence of disease. Similarly, epidemiological studies should also include spatial locations in survey implementation in order to allow complete analysis of a disease outbreak phenomenon (Graham, Atkinson & Danson 2004). With the adequate integration of specific tools and laboratory and field observation tasks, more accurate models to predict the occurrence of disease can be developed, and preventive surveillance systems for disease control could be enhanced (M Grandadam 2019, online communication, 18 October).

4.7. Limitations

The challenges found to be the main constraints to this study included 1). The issue of spatial resolution to detect small water bodies for vector mosquitoes to breed in; 2). The limitation of wavelengths in satellite images for which only visible and near-infrared channels are available. A consequence of this leads to a limitation of applying different indices methods which can achieve high accuracy; 3). The issue of cloud coverage, especially in the wet season. Three dates for image data were not able to be obtained, and water features were lost due to the cloud masking process; 4). Spatial data of dengue incidence is too small to use for spatial analysis at the village level to determine spatial correlation within the area of study; 5). The limited time frame for this investigation

meant that an important aspect such as proximity of water bodies to dengue incidence was not included; and 6). Knowledge of applying remote sensing and GIS in the field of epidemiology was new to the operator, meaning that time constraints meant it was not possible to fully discover the biological phenomenon of dengue fever and vector mosquitoes.

4.8. Areas of Further Investigation

The areas of research that this study has determined should be investigated in the future include:

- 1) Different approaches used to extract surface water should be examined in a further study in order to optimise the result of accuracy.
- 2) The study area is in a tropical region where the presence of cloud is a significant challenge to extracting ground feature information, therefore integrating SAR images which can penetrate cloud cover with optical images should be examined.
- 3) Although surface water was found highly correlated with dengue incidence, it cannot be completely concluded that there is a strong relationship between them. So, if surface water was considered as one of the other important factors influencing dengue fever, further study might need to include the distance between the dengue incidence and the location of water. Exploring the average flight distance of dengue vectors will help define approximate distance between water bodies and the disease incidence.
- 4) In terms of health policy intervention, despite the lack of correlation between the surface water and dengue incidence, controlling factors and activities including small scale water bodies and accumulation of water on surfaces that support the growth of vector mosquitoes, should be implemented not only in the rainy season, but also in the dry season as how rainfall correlates with the disease incidence was clearly identified.

4.9. Conclusion

This study was conducted according to the findings from the review of the literature with the main aim of investigating whether there is a relationship between water bodies and dengue incidence. To achieve this objective, techniques of remote sensing (RS) and Geographical Information Systems (GIS), as well as statistical analysis were applied. Some key findings identified during this investigation are presented, as well as recommendations provided.

4.9.1. Key Findings

Surface water was found not to be a suitable independent factor to predict the occurrence of dengue prevalence as it acts as a marker of rainfall.

Rainfall was found to have a strong correlation with dengue cases, and lag1 (estimated time of dengue vector developing into an adult) and was correlated with the *Aedes* mosquito population. It is important to note that precipitation is not a direct factor that drives the emergence of dengue fever. Food supply vectors, water temperature, relative humidity, quality of surface water, and surrounding environment such as structure of urbanisation associated with size of population, are considered to be the main support of dengue prevalence.

The main findings from the literature review highlighted that water bodies have an association with dengue incidence as they provide sites of breeding for vector mosquitoes. Specifically, types of water such as standing water, level of water, size of water, temperature and nutrition within the water play an important part in the growth of dengue vectors. Several previous studies found dengue fever prevalence near surface water. Rainfall is one of the variables used to find the risk factors that affect dengue incidence and sizes of vector populations. A few studies compared the dengue incidence and density rate of vector mosquito in dry and wet areas and found that these two different zones have high rates of dengue incidence and mosquito populations.

Methods used for surface water extraction show accuracy at accepted level in detecting water features. Normalized difference moisture index (NDMI) was suitable for detecting water information in the dry season, while normalized difference water index (NDWI) was appropriate for detecting a high level of surface water. Threshold values used to differentiate water features from non-water features were found close to zero in the study area. Choice of selecting optimum threshold values affected the level of accuracy, so testing values with different methods before applying in indices images is recommended.

Haze reduction provided in ERDAS Imagine 2018 was found to spectrally and statistically enhance the results derived from NDWI and NDMI, while Top of atmosphere (TOA) reflectance derived from the conversion of TOA radiance showed false negatives in surface water areas. Bottom of atmosphere (BOA) images show less difference when compared with the non-BOA image in the results acquired from NDWI.

Cloud masking from a single band threshold method presented fewer overestimates in water surface and other features which have a similar spectral range as water, whereas unsupervised classification showed large areas of water information classified as cloud, regardless its ability in detecting shadow.

4.9.2. Recommendation

Analysis based on the perspectives of the biological phenomenon of dengue carrying mosquitoes must be taken into account. This would help define variables and suitable technical tools and materials to identify the factors that actually cause the emergence of the disease, not just to investigate their correlation.

The applications of remote sensing and GIS are useful in developing a reliable and accurate predictive model to help prevent disease outbreaks. Epidemiologists should acknowledge how important accurate spatial data is. Spatial data of disease incidence needs to be as accurate as possible because this can affect the accuracy and efficiency of spatial analysis. Similarly, RS and GIS specialists need to comprehend the dynamics of vector mosquitoes as they change and adapt according to the changes in surrounding environments.

Satellite image data which are able to detect small water bodies on construction sites, and areas which are susceptible to an expansion of vector populations, such as flat roofs and types of trees which are potentially holding small amounts of water are needed. This will allow visible generation and therefore detection of possible breeding sites for mosquitoes.

This study attempted to apply RS and GIS techniques in a field of epidemiology, examining the relationship between surface water and dengue incidence. Integration of these advanced technologies should be considered to be included as important aspects in national strategic plans to help control and prevent the debilitating and devastating dengue disease epidemic.

As urbanisation continues worldwide particularly in developing countries in Southeast Asia, and there is continuing pressure on resources within the newly developing areas, it is vital to find ways of predicting where diseases such as dengue fever are likely to emerge. This study has published that a combination of practical techniques can be applied as a major tool in future diseases prevention nationally and internationally.

REFERENCE LIST

- Acharya, T, Subedi, A & Lee, D 2018, 'Evaluation of water indices for surface water extraction in a Landsat 8 scene in Nepal', *Sensors*, vol. 18, no. 8, p. 2580.
- Ahmad, A, Ghani, MKA, Razali, S, Sakidin, H & Hashim, NM 2014, 'Haze reduction from remotely sensed data', *Applied Mathematical Sciences*, vol. 8, no. 36, pp. 1755-62.
- Angel, B & Joshi, V 2009, 'Distribution of dengue virus types in *Aedes aegypti* in dengue endemic districts of Rajasthan, India', *Indian Journal of Medical Research*, vol. 129, no. 6, pp. 665-8.
- Artusi, R, Verderio, P & Marubini, E 2002, 'Bravais-Pearson and Spearman correlation coefficients: meaning, test of hypothesis and confidence interval', *The International Journal of Biological Markers*, vol. 17, no. 2, pp. 148-51.
- Avnir, A & Cartosat, P 2018, *Parameter descriptions*, PCI Geomatics, viewed 16 October 2019, <<http://www.pcigeomatics.com>>.
- Baloloy, A, Blanco, A, Candido, C, Argamosa, R, Dumalag, J, Dimapilis, L & Paringit, E 2018, 'Estimation of mangrove forest aboveground biomass using multispectral bands, vegetation indices and biophysical variables derived from optical satellite imageries: Rapideye, PlanetScope and Sentinel-2', *ISPRS Annals of Photogrammetry, Remote Sensing & Spatial Information Sciences*, vol. 4, no. 3, pp. 29-36
- Banu, S, Hu, W, Hurst, C & Tong, S 2011, 'Dengue transmission in the Asia-Pacific region: impact of climate change and socio-environmental factors', *Tropical Medicine & International Health*, vol. 16, no. 5, pp. 598-607.
- Baumann, P 2010, *Introduction to remote sensing*, State University of New York, College of Oneonta, viewed 23 September 2019, <<http://employees.oneonta.edu/baumanpr/geosat2/RS-Introduction/RS-Introduction.html>>.
- Bhardwaj, A, Singh, MK, Joshi, P, Singh, S, Sam, L, Gupta, R & Kumar, R 2015, 'A lake detection algorithm (LDA) using Landsat 8 data: a comparative approach in a glacial environment', *International Journal of Applied Earth Observation and Geoinformation*, vol. 38, pp. 150-63.
- Bi, P, Wu, X, Zhang, F, Parton, KA & Tong, S 1998, 'Seasonal rainfall variability, the incidence of hemorrhagic fever with renal syndrome, and prediction of the disease in low-lying areas of China', *American Journal of Epidemiology*, vol. 148, no. 3, pp. 276-81.
- Bohra, A & Andrianasolo, H 2001, 'Application of GIS in modeling dengue risk based on sociocultural data: case of Jalore, Rajasthan, India', *Dengue Bulletin*, vol. 25.

- Bowatte, G, Perera, P, Senevirathne, G, Meegaskumbura, S & Meegaskumbura, M 2013, 'Tadpoles as dengue mosquito (*Aedes aegypti*) egg predators', *Biological Control*, vol. 67, no. 3, pp. 469-74.
- Bryant, R & Rainey, M 2002, 'Investigation of flood inundation on playas within the Zone of Chotts, using a time-series of AVHRR', *Remote Sensing of Environment*, vol. 82, no. 2-3, pp. 360-75.
- Carrasco-Escobar, G, Manrique, E, Ruiz-Cabrejos, J, Saavedra, M, Alava, F, Bickersmith, S, Prussing, C, Vinetz, JM, Conn, JE & Moreno, M 2019, 'High-accuracy detection of malaria vector larval habitats using drone-based multispectral imagery', *PLoS Neglected Tropical Diseases*, vol. 13, no. 1, p. e0007105.
- Cazals, C, Rapinel, S, Frison, P-L, Bonis, A, Mercier, G, Mallet, C, Corgne, S & Rudant, J-P 2016, 'Mapping and characterization of hydrological dynamics in a coastal marsh using high temporal resolution Sentinel-1A images', *Remote Sensing*, vol. 8, no. 7, p. 570.
- Chadee, DD, Williams, FL & Kitron, UD 2005, 'Impact of vector control on a dengue fever outbreak in Trinidad, West Indies, in 1998', *Tropical Medicine & International Health*, vol. 10, no. 8, pp. 748-54.
- Chavez, PS 1988, 'An improved dark-object subtraction technique for atmospheric scattering correction of multispectral data', *Remote Sensing of Environment*, vol. 24, no. 3, pp. 459-79.
- Chen, H-W & Cheng, K-S 2012, 'A Conceptual model of surface reflectance estimation for satellite remote sensing images using in situ reference data', *Remote Sensing*, vol. 4, no. 4, pp. 934-49.
- Chen, H, Wang, J, Chen, Z, Yang, L & Xi, W 2004, 'Comparison of water extraction methods in mountainous plateau region from TM image', *Remote Sensing Technology and Application*, vol. 19, no. 6, pp. 479-84.
- Chen, Y, Fan, R, Yang, X, Wang, J & Latif, A 2018, 'Extraction of urban water bodies from high-resolution remote-sensing imagery using deep learning', *Water*, vol. 10, no. 5, p. 585.
- Cheong, YL, Leitão, PJ & Lakes, T 2014, 'Assessment of land use factors associated with dengue cases in Malaysia using Boosted Regression Trees', *Spatial and Spatio-Temporal Epidemiology*, vol. 10, pp. 75-84.
- Chowell, G & Sanchez, F 2006, 'Climate-based descriptive models of dengue fever: the 2002 epidemic in Colima, Mexico', *Journal of Environmental Health*, vol. 68, no. 10.
- Cohen, J 1988, *Statistical power analysis for the behavioral sciences*, Hillsdale, NJ: Lawrence Erlbaum Association.
- Coker, RJ, Hunter, BM, Rudge, JW, Liverani, M & Hanvoravongchai, P 2011, 'Emerging infectious diseases in southeast Asia: regional challenges to control', *The Lancet*, vol. 377, no. 9765, pp. 599-609.

- Collison, A & Wilson, N 2017, *Planet surface reflectance product*, San Francisco, CA: Planet Labs.
- Comte, DL 2009, 'Global weather highlights 2008: Snow, flood, and drought', *Weatherwise*, vol. 62, no. 2, pp. 22-7.
- Congalton, RG 1991, 'A review of assessing the accuracy of classifications of remotely sensed data', *Remote Sensing of Environment*, vol. 37, no. 1, pp. 35-46.
- 2007, 'Thematic and positional accuracy assessment of digital remotely sensed data', in *In: McRoberts, Ronald E.; Reams, Gregory A.; Van Deusen, Paul C.; McWilliams, William H., eds. Proceedings of the seventh annual forest inventory and analysis symposium; October 3-6, 2005; Portland, ME. Gen. Tech. Rep. WO-77. Washington, DC: US Department of Agriculture, Forest Service: 149-154.*, vol. 77.
- Cooley, S, Smith, L, Stepan, L & Mascaro, J 2017, 'Tracking dynamic northern surface water changes with high-frequency planet CubeSat imagery', *Remote Sensing*, vol. 9, no. 12, p. 1306.
- Crétaux, J-F, Bergé-Nguyen, M, Leblanc, M, Abarca Del Rio, R, Delclaux, F, Mognard, N, Lion, C, Pandey, RK, Tweed, S & Calmant, S 2011, 'Flood mapping inferred from Remote Sensing data', *International Water Technology Journal*, vol. 1, pp. 48-62.
- Croner, CM, Sperling, J & Broome, FR 1996, 'Geographic information systems (GIS): new perspectives in understanding human health and environmental relationships', *Statistics in Medicine*, vol. 15, no. 18, pp. 1961-77.
- De La Rocque, S, Michel, V, Plazanet, D & Pin, R 2004, 'Remote sensing and epidemiology: examples of applications for two vector-borne diseases', *Comparative Immunology, Microbiology and Infectious Diseases*, vol. 27, no. 5, pp. 331-41.
- Derouich, M, Boutayeb, A & Twizell, E 2003, 'A model of dengue fever', *BioMedical Engineering OnLine*, vol. 2, no. 1, p. 4.
- Di, K, Wang, J, Ma, R & Li, R 2003, 'Automatic shoreline extraction from high-resolution IKONOS satellite imagery', in *Proceeding of ASPRS 2003 Annual Conference*, vol. 3.
- Dickin, SK, Schuster-Wallace, CJ & Elliott, SJ 2013, 'Developing a vulnerability mapping methodology: applying the water-associated disease index to dengue in Malaysia', *PLoS One*, vol. 8, no. 5, p. e63584.
- Dong, Y, Li, Q, Dou, A & Wang, X 2011, 'Extracting damages caused by the 2008 Ms 8.0 Wenchuan earthquake from SAR remote sensing data', *Journal of Asian Earth Sciences*, vol. 40, no. 4, pp. 907-14.
- Donoghue, DN 2000, 'Remote Sensing: sensors and applications', *Progress in Physical Geography*, vol. 24, no. 3, pp. 407-14.

- Drusch, M, Del Bello, U, Carlier, S, Colin, O, Fernandez, V, Gascon, F, Hoersch, B, Isola, C, Laberinti, P & Martimort, P 2012, 'Sentinel-2: ESA's optical high-resolution mission for GMES operational services', *Remote Sensing of Environment*, vol. 120, pp. 25-36.
- Du, Y, Guindon, B & Cihlar, J 2002, 'Haze detection and removal in high resolution satellite image with wavelet analysis', *IEEE Transactions on Geoscience and Remote Sensing*, vol. 40, no. 1, pp. 210-7.
- Du, Z, Li, W, Zhou, D, Tian, L, Ling, F, Wang, H, Gui, Y & Sun, B 2014, 'Analysis of Landsat-8 OLI imagery for land surface water mapping', *Remote Sensing Letters*, vol. 5, no. 7, pp. 672-81.
- Ebi, KL & Nealon, J 2016, 'Dengue in a changing climate', *Environmental Research*, vol. 151, pp. 115-23.
- El Hajj, M, Bégué, A, Lafrance, B, Hagolle, O, Dedieu, G & Rumeau, M 2008, 'Relative radiometric normalization and atmospheric correction of a SPOT 5 time series', *Sensors*, vol. 8, no. 4, pp. 2774-91.
- EPA 2017, *Mosquito life cycle*, viewed 18 October 2019, <<https://www.epa.gov/mosquitocontrol/mosquito-life-cycle>>.
- ESA 2019, *Technical guide, cloud masks*, viewed 20 September 2019, <<https://sentinel.esa.int/web/sentinel/technical-guides/sentinel-2-msi/level-1c/cloud-masks>>.
- ESRI n.d, *Survey123 for arcgis*, viewed 30 September 2019, <<https://survey123.arcgis.com/>>.
- Fisher, A, Flood, N & Danaher, T 2016, 'Comparing Landsat water index methods for automated water classification in eastern Australia', *Remote Sensing of Environment*, vol. 175, pp. 167-82.
- Frulla, L, Milovich, J, Karszenbaum, H & Gagliardini, D 1998, 'Radiometric corrections and calibration of SAR images', in *IGARSS'98. Sensing and Managing the Environment. 1998 IEEE International Geoscience and Remote Sensing. Symposium Proceedings. (Cat. No. 98CH36174)*, vol. 2, pp. 1147-9.
- Fukunaga, T, Phommasack, B, Bounlu, K, Saito, M, Tadano, M, Makino, Y, Kanemura, K, Arakaki, S, Shinjo, M & Insisiengmay, S 1994, 'Epidemiological situation of dengue infection in Lao PDR', *Tropical Medicine*, vol. 35, no. 4, pp. 219-27.
- Gao, B-c 1996, 'NDWI—A normalized difference water index for remote sensing of vegetation liquid water from space', *Remote Sensing of Environment*, vol. 58, no. 3, pp. 257-66.
- Gao, H, Wang, L, Jing, L & Xu, J 2016, 'An effective modified water extraction method for Landsat-8 OLI imagery of mountainous plateau regions', in *IOP conference series: Earth and Environmental Science*, vol. 34, p. 012010.

- Gautam, VK, Gaurav, PK, Murugan, P & Annadurai, M 2015, 'Assessment of surface water dynamics in Bangalore using WRI, NDWI, MNDWI, supervised classification and KT transformation', *Aquatic Procedia*, vol. 4, pp. 739-46.
- Gibbons, JD & Fielden, JDG 1993, *Nonparametric statistics: an introduction*, Sage, California, the United States of America.
- Githeko, AK, Lindsay, SW, Confalonieri, UE & Patz, JA 2000, 'Climate change and vector-borne diseases: a regional analysis', *Bulletin of the World Health Organization*, vol. 78, pp. 1136-47.
- Goudet, J 1995, 'FSTAT (version 1.2): a computer program to calculate F-statistics', *Journal of Heredity*, vol. 86, no. 6, pp. 485-6.
- Gould, E 1998, 'Dengue haemorrhagic fever: Diagnosis, treatment, prevention and control: Geneva: World Health Organization, 1997', *Transactions of the Royal Society of Tropical Medicine and Hygiene*, vol. 92, no. 4, p. 470.
- Gouveia, C & DaCamara, C 2006, 'Continuous mapping of the Alqueva region of Portugal using satellite imagery', in *Proceeding of the EUMETSAT Meteorological Satellite Conference, Helsinki, Finland*, pp. 12-6.
- Graham, AJ, Atkinson, PM & Danson, FM 2004, 'Spatial analysis for epidemiology', *Acta Tropica*, vol. 91, no. 3, pp. 219-25.
- Gravetter, F & Wallnau, L 2013, *Essentials of statistics for the behavioral sciences*. Belmont, CA: Wadsworth, Cengage Learning.
- Gubler, DJ 2011, 'Dengue, urbanization and globalization: the unholy trinity of the 21st century', *Tropical Medicine and Health*, vol. 39, no. 4supplement, pp. s3-s11.
- Hadjimitsis, DG, Clayton, C & Hope, V 2004, 'An assessment of the effectiveness of atmospheric correction algorithms through the remote sensing of some reservoirs', *International Journal of Remote Sensing*, vol. 25, no. 18, pp. 3651-74.
- Hadjimitsis, DG, Clayton, C & Retalis, A 2003, 'Darkest pixel atmospheric correction algorithm: a revised procedure for environmental applications of satellite remotely sensed imagery', in *Proceedings 10th international symposium on remote sensing*, pp. 8-12.
- Hadjimitsis, DG, Clayton, C & Toullos, L 2010, 'Retrieving visibility values using satellite remote sensing data', *Physics and Chemistry of the Earth, Parts A/B/C*, vol. 35, no. 1, pp. 121-4.
- Hadjimitsis, DG, Papadavid, G, Agapiou, A, Themistocleous, K, Hadjimitsis, M, Retalis, A, Michaelides, S, Chrysoulakis, N, Toullos, L & Clayton, C 2010, 'Atmospheric correction for satellite remotely sensed data intended for agricultural applications: impact on vegetation indices', *Natural Hazards and Earth System Sciences*, vol. 10, no. 1, pp. 89-95.

Hales, S, de Wet, N, Maindonald, J & Woodward, A 2002, 'Potential effect of population and climate changes on global distribution of dengue fever: an empirical model', *The Lancet*, vol. 360, no. 9336, pp. 830-4.

Halstead, SB, Voulgaropoulos, E, Tien, NH & Udomsakdi, S 1965, 'Dengue hemorrhagic fever in south Vietnam - report of 1963 outbreak', *American Journal of Tropical Medicine and Hygiene*, vol. 14, no. 5, pp. 819-830.

Hardy, A, Ettritch, G, Cross, DE, Bunting, P, Liywalii, F, Sakala, J, Silumesii, A, Singini, D, Smith, M & Willis, T 2019, 'Automatic detection of open and vegetated water bodies using Sentinel-1 to map African malaria vector mosquito breeding habitats', *Remote Sensing*, vol. 11, no. 5, p. 593.

Hexagon n.d, *Producer field guide contents*, viewed 02 October 2019, <https://hexagongeospatial.fluidtopics.net/reader/uOKHREQkd_XR9iPo9Y_ljw/0k4QSKUEnd_61z_nyN797g>.

Hii, YL, Rocklöv, J, Ng, N, Tang, CS, Pang, FY & Sauerborn, R 2009, 'Climate variability and increase in intensity and magnitude of dengue incidence in Singapore', *Global Health Action*, vol. 2, no. 1, p. 2036.

Hsueh, Y-H, Lee, J & Beltz, L 2012, 'Spatio-temporal patterns of dengue fever cases in Kaoshiung City, Taiwan, 2003–2008', *Applied Geography*, vol. 34, pp. 587-94.

Hu, Z, Gong, H & Zhu, L 2007, 'Fast flooding information extraction in emergency response of flood disaster', in *Proceedings of the ISPRS workshop on updating geo-spatial databases with imagery and the 5th ISPRS workshop on DMGISs, Urumchi*, pp. 28-9.

Huang, C, Chen, Y & Wu, J 2014, 'Mapping spatio-temporal flood inundation dynamics at large river basin scale using time-series flow data and MODIS imagery', *International Journal of Applied Earth Observation and Geoinformation*, vol. 26, pp. 350-62.

Huang, W, DeVries, B, Huang, C, Lang, M, Jones, J, Creed, I & Carroll, M 2018, 'Automated extraction of surface water extent from Sentinel-1 data', *Remote Sensing*, vol. 10, no. 5, p. 797.

Jayawardene, W, Lohrmann, D, Youssefagha, A & Nilwala, D 2011, 'Prevention of dengue fever: an exploratory school-community intervention involving students empowered as change agents*', *The Journal of School Health*, vol. 81, pp. 566-73.

Jetten, TH & Focks, DA 1997, 'Potential changes in the distribution of dengue transmission under climate warming', *The American Journal of Tropical Medicine and Hygiene*, vol. 57, no. 3, pp. 285-97.

Ji, L, Zhang, L & Wylie, B 2009, 'Analysis of dynamic thresholds for the normalized difference water index', *Photogrammetric Engineering & Remote Sensing*, vol. 75, no. 11, pp. 1307-17.

- Jiang, H, Feng, M, Zhu, Y, Lu, N, Huang, J & Xiao, T 2014, 'An automated method for extracting rivers and lakes from Landsat imagery', *Remote Sensing*, vol. 6, no. 6, pp. 5067-89.
- Joseph, G 2005, *Fundamentals of remote sensing*, Universities Press, Hyderabad, India.
- Kaufman, YJ & Sendra, C 1988, 'Algorithm for automatic atmospheric corrections to visible and near-IR satellite imagery', *International Journal of Remote Sensing*, vol. 9, no. 8, pp. 1357-81.
- Kauth, RJ & Thomas, G 1976, 'The tasseled cap--a graphic description of the spectral-temporal development of agricultural crops as seen by Landsat', in *LARS symposia*, p. 159.
- Khormi, HM & Kumar, L 2011, 'Modeling dengue fever risk based on socioeconomic parameters, nationality and age groups: GIS and remote sensing based case study', *Science of The Total Environment*, vol. 409, no. 22, pp. 4713-9.
- Kitron, U 2002, 'Remote Sensing and Geographic Information Systems in epidemiology', *Emerging Infectious Diseases*, vol. 8, no. 4, pp. 448-449.
- Kulinkina, AV, Walz, Y, Koch, M, Biritwum, N-K, Utzinger, J & Naumova, EN 2018, 'Improving spatial prediction of schistosoma haematobium prevalence in southern Ghana through new remote sensors and local water access profiles', *PLoS Neglected Tropical Diseases*, vol. 12, no. 6, p. e0006517.
- Lacaux, J, Tourre, Y, Vignolles, C, Ndione, J & Lafaye, M 2007, 'Classification of ponds from high-spatial resolution remote sensing: Application to Rift Valley Fever epidemics in Senegal', *Remote Sensing of Environment*, vol. 106, no. 1, pp. 66-74.
- Li, C 1988, 'Two adaptive filters for speckle reduction in SAR images by using the variance ratio', *Remote Sensing*, vol. 9, no. 4, pp. 641-53.
- Li, C, Wang, X, Wu, X, Liu, J, Ji, D & Du, J 2017, 'Modeling and projection of dengue fever cases in Guangzhou based on variation of weather factors', *Science of The Total Environment*, vol. 605-606, pp. 867-73.
- Li, W & Gong, P 2016, 'Continuous monitoring of coastline dynamics in western Florida with a 30-year time series of Landsat imagery', *Remote Sensing of Environment*, vol. 179, pp. 196-209.
- Lillesand, T, Kiefer, RW & Chipman, J 2015, *Remote Sensing and image interpretation*, John Wiley & Sons.
- Mather, PM 1987, 'Computer processing of remotely-sensed images: an introduction', *Geocarto International*, vol. 2, no. 4, p. 64.
- Mayxay, M, Cui, W, Thammavong, S, Khensakhou, K, Vongxay, V, Inthasoum, L, Sychareun, V & Armstrong, G 2013, 'Dengue in peri-urban Pak-Ngum district, Vientiane capital of Laos: a community survey on knowledge, attitudes and practices', *BMC Public Health*, vol. 13, no. 1, p. 434.

McFeeters, SK 1996, 'The use of the normalized difference water index (NDWI) in the delineation of open water features', *International Journal of Remote Sensing*, vol. 17, no. 7, pp. 1425-32.

Microsoft Office 2019, *Use the analysis toolpak to perform complex data analysis*, viewed 11 October 2019, <<https://support.office.com/en-us/article/use-the-analysis-toolpak-to-perform-complex-data-analysis-6c67ccf0-f4a9-487c-8dec-bdb5a2cefab6?NS=EXCEL&Version=90&SysLcid=1033&UILcid=1033&AppVer=ZXL900&HelpId=xladdin.chm1780&ui=en-US&rs=en-US&ad=US>>.

Montello, D & Sutton, P 2012, *An introduction to scientific research methods in geography and environmental studies*, Sage, Chennai, India.

Morin, CW, Comrie, AC & Ernst, K 2013, 'Climate and dengue transmission: evidence and implications', *Environmental Health Perspectives*, vol. 121, no. 11-12, pp. 1264-72.

Morlan, HB & Hayes, RO 1958, 'Urban dispersal and activity of *Aedes aegypti*', *Mosq News*, vol. 18, pp. 137-44.

Moro, GD & Halounova, L 2007, 'Haze removal for high-resolution satellite data: a case study', *International Journal of Remote Sensing*, vol. 28, no. 10, pp. 2187-205.

Murray, NEA, Quam, MB & Wilder-Smith, A 2013, 'Epidemiology of dengue: past, present and future prospects', *Clinical Epidemiology*, vol. 5, p. 299.

Nakhapakorn, K & Tripathi, NK 2005, 'An information value based analysis of physical and climatic factors affecting dengue fever and dengue haemorrhagic fever incidence', *International Journal of Health Geographics*, vol. 4, no. 1, p. 13.

Nasir, S, Jabeen, F, Abbas, S, Nasir, I & Debboun, M 2017, 'Effect of climatic conditions and water bodies on population dynamics of the dengue vector, *Aedes aegypti* (Diptera: Culicidae)', *Journal of Arthropod-Borne Diseases*, vol. 11, no. 1, pp. 50-9.

Nath, RK & Deb, SK 2010, 'Water-body area extraction from high resolution satellite images-an introduction, review, and comparison', *International Journal of Image Processing (IJIP)*, vol. 3, no. 6, pp. 265-384.

National Centre of Laboratory and Epidemiology 2010, 'Dengue surveillance data 2010', Ministry of Public Health, Laos.

Ogilvie, A, Belaud, G, Massuel, S, Mulligan, M, Le Goulven, P & Calvez, R 2016, 'Assessing floods and droughts in ungauged small reservoirs with long-term Landsat imagery', *Geosciences*, vol. 6, no. 4, p. 42.

——— 2018, 'Surface water monitoring in small water bodies: potential and limits of multi-sensor Landsat time series', *Hydrology and Earth System Sciences*, vol. 22, no. 8, p. 4349.

Pham, B, Prigent, C & Aires, F 2017, 'Surface water monitoring within Cambodia and the Vietnamese Mekong Delta over a year, with Sentinel-1 SAR observations', *Water*, vol. 9, no. 6, p. 366.

Phuanukoonnon, S, Brough, M & Bryan, JH 2006, 'Folk knowledge about dengue mosquitoes and contributions of health belief model in dengue control promotion in Northeast Thailand', *Acta Tropica*, vol. 99, no. 1, pp. 6-14

Planet 2016, *Planet imagery product specification: planetscope & rapideye*, viewed 08 September 2019, <https://www.planet.com/products/satellite-imagery/files/1610.06_Spec%20Sheet_Combined_Imagery_Product_Letter_ENGv1.pdf>.

— 2018, *Planet imagery product specification*, viewed 04 September 2019, <https://assets.planet.com/docs/Planet_Combined_Imagery_Product_Specs_letter_screen.pdf>.

— 2019, *Convert PlanetScope imagery from radiance to reflectance*, viewed 02 October 2019, <<https://developers.planet.com/tutorials/convert-planetscope-imagery-from-radiance-to-reflectance>>.

Prakash, A & Gupta, R 1998, 'Land-use mapping and change detection in a coal mining area—a case study in the Jharia coalfield, India', *International Journal of Remote Sensing*, vol. 19, no. 3, pp. 391-410.

Qi, X, Wang, Y, Li, Y, Meng, Y, Chen, Q, Ma, J & Gao, GF 2015, 'The effects of socioeconomic and environmental factors on the incidence of dengue fever in the Pearl River Delta, China, 2013', *PLoS Neglected Tropical Diseases*, vol. 9, no. 10.

Rafieyan, V 2016, 'Relationship between agiculturalization attitude and translation of culture-bound texts', *Journal of Studies in Education*, vol. 6, no. 2, pp. 144-56.

Rafiqui, PS & Gentile, M 2009, 'Vientiane', *Cities*, vol. 26, no. 1, pp. 38-48.

Raghavendra, K, Sharma, P & Dash, AP 2008, 'Biological control of mosquito populations through frogs: opportunities & constrains', *Indian Journal of Medical Research*, vol. 128, no. 1, pp. 22-5.

Raju, K & Sokhi, B 2008, 'Application of GIS modeling for dengue fever prone area based on socio-cultural and environmental factors—a case study of Delhi city zone', *International Archives of Photogrammetry Remote Sensing Spatial Information Science*, vol. 37, pp. 165-70.

Reiter, P, Amador, MA, Anderson, RA & Clark, GG 1995, 'Dispersal of *Aedes aegypti* in an urban area after blood feeding as demonstrated by rubidium-marked eggs', *The American Journal of Tropical Medicine and Hygiene*, vol. 52, no. 2, pp. 177-9.

Rogers, A & Kearney, M 2004, 'Reducing signature variability in unmixing coastal marsh Thematic Mapper scenes using spectral indices', *International Journal of Remote Sensing*, vol. 25, no. 12, pp. 2317-35.

- Rokni, K, Ahmad, A, Selamat, A & Hazini, S 2014, 'Water feature extraction and change detection using multitemporal Landsat imagery', *Remote Sensing*, vol. 6, no. 5, pp. 4173-89.
- Rouse Jr, JW, Haas, R, Schell, J & Deering, D 1974, 'Monitoring vegetation systems in the Great Plains with ERTS', *Proceeding of the 3rd Symposium on Significant Results Obtained from the first Earth Resources Technology Satellite*. Washington, D.C., USA, pp. 309-317
- Rozendaal, JA 1992, 'Relations between Anopheles darlingi breeding habitats, rainfall, river level and malaria transmission rates in the rain forest of Suriname', *Medical and Veterinary Entomology*, vol. 6, no. 1, pp. 16-22.
- Sánchez-Ribas, J, Oliveira-Ferreira, J, Rosa-Freitas, MG, Trilla, L & Silva-do-Nascimento, TF 2015, 'New classification of natural breeding habitats for neotropical Anophelines in the Yanomami Indian Reserve, Amazon Region, Brazil and a new larval sampling methodology', *Memórias do Instituto Oswaldo Cruz*, vol. 110, no. 6, pp. 760-70.
- Schmidt, W-P, Suzuki, M, Thiem, VD, White, RG, Tsuzuki, A, Yoshida, L-M, Yanai, H, Haque, U, Anh, DD & Ariyoshi, K 2011, 'Population density, water supply, and the risk of dengue fever in Vietnam: cohort study and spatial analysis', *PLoS Medicine*, vol. 8, no. 8, p. e1001082.
- Schumacker, R & Tomek, S 2013, 'Central tendency and dispersion', in *Understanding Statistics Using R*, Springer, New York, USA., pp. 75-105.
- Shang, CS, Fang, CT, Liu, CM, Wen, TH, Tsai, KH & King, CC 2010, 'The role of imported cases and favorable meteorological conditions in the onset of dengue epidemics', *PLoS Neglected Tropical Diseases*, vol. 4, no. 8, p. e775.
- Sharifi, A, Chiba, Y, Okamoto, K, Yokoyama, S & Murayama, A 2014, 'Can master planning control and regulate urban growth in Vientiane, Laos?', *Landscape and Urban Planning*, vol. 131, pp. 1-13.
- Sharma, O, Mioc, D & Anton, F 2007, 'Feature extraction and simplification from colour images based on colour image segmentation and skeletonization using the quad-edge data structure', *Václav Skala - UNION Agency*
- Sheng, Y, Shah, CA & Smith, LC 2008, 'Automated image registration for hydrologic change detection in the lake-rich Arctic', *IEEE Geoscience and Remote Sensing Letters*, vol. 5, no. 3, pp. 414-8.
- Sirisena, P, Faseeha, N, Harithra, K, Romesh, AT & LakKumar, F 2017, 'Effect of climatic factors and population density on the distribution of dengue in Sri Lanka: a GIS based evaluation for prediction of outbreaks', *PLoS One*, vol. 12, no. 1., pp. 1-14

- Song, C, Woodcock, CE, Seto, KC, Lenney, MP & Macomber, SA 2001, 'Classification and change detection using Landsat TM data: when and how to correct atmospheric effects?', *Remote Sensing of Environment*, vol. 75, no. 2, pp. 230-44.
- Spiegel, JM, Bonet, M, Ibarra, A-M, Pagliccia, N, Ouellette, V & Yassi, A 2007, 'Social and environmental determinants of Aedes aegypti infestation in Central Havana: results of a case-control study nested in an integrated dengue surveillance programme in Cuba', *Tropical Medicine & International Health*, vol. 12, no. 4, pp. 503-10.
- Sun, L, Wei, J, Wang, J, Mi, X, Guo, Y, Lv, Y, Yang, Y, Gan, P, Zhou, X & Jia, C 2016, 'A universal dynamic threshold cloud detection algorithm (UDTCDA) supported by a prior surface reflectance database', *Journal of Geophysical Research: Atmospheres*, vol. 121, no. 12, pp. 7172-96.
- Sutherst, RW 2004, 'Global change and human vulnerability to vector-borne diseases', *Clinical Microbiology Reviews*, vol. 17, no. 1, pp. 136-73.
- Switzer, P, Kowalik, W & Lyon, R 1981, 'Estimation of atmospheric path-radiance by the covariance matrix method', *Photogrammetric Engineering and Remote Sensing*, vol. 47, pp. 1469-76.
- Tabachnick, W 2010, 'Challenges in predicting climate and environmental effects on vector-borne disease epistystems in a changing world', *Journal of Experimental Biology*, vol. 213, no. 6, pp. 946-54.
- Themistocleous, K & Hadjimitsis, D 2008, 'The importance of considering atmospheric correction in the pre-processing of satellite remote sensing data intended for the management and detection of cultural sites: a case study of the Cyprus area', *Proceeding of the 14th International Conference on Virtual Systems and Multimedia*, Limassol, Greek, pp. 9-12.
- Tian, H, Huang, S, Zhou, S, Bi, P, Yang, Z, Li, X, Chen, L, Cazelles, B, Yang, J & Luo, L 2016, 'Surface water areas significantly impacted 2014 dengue outbreaks in Guangzhou, China', *Environmental Research*, vol. 150, pp. 299-305.
- Tiong, V, Abd-Jamil, J, Zan, MH, Abu-Bakar, R, Ew, C, Jafar, F, Nellis, S, Fauzi, R & AbuBakar, S 2015, 'Evaluation of land cover and prevalence of dengue in Malaysia', *Tropical Biomedicine*, vol. 32, no. 4, pp. 587-97.
- Tun-Lin, W, Burkot, T & Kay, B 2000, 'Effects of temperature and larval diet on development rates and survival of the dengue vector Aedes aegypti in north Queensland, Australia', *Medical and Veterinary Entomology*, vol. 14, no. 1, pp. 31-7.
- Twele, A, Cao, W, Plank, S & Martinis, S 2016, 'Sentinel-1-based flood mapping: a fully automated processing chain', *International Journal of Remote Sensing*, vol. 37, no. 13, pp. 2990-3004.
- Vallée, J, Dubot-Pérès, A, Ounaphom, P, Sayavong, C, Bryant, JE & Gonzalez, JP 2009, 'Spatial distribution and risk factors of dengue and Japanese encephalitis virus infection in urban settings:

the case of Vientiane, Lao PDR', *Tropical Medicine & International Health*, vol. 14, no. 9, pp. 1134-42.

Van Panhuis, W, Guha-Sapir, D & Oshitani, H 2005, 'Epidemiology of dengue in South East Asia: need for a new paradigm', *Tropical Medicine & International Health*, vol. 10, no. 2.

Viera, AJ & Garrett, JM 2005, 'Understanding interobserver agreement: the kappa statistic', *Family Medicine*, vol. 37, no. 5, pp. 360-3.

Vittor, AY, Gilman, RH, Tielsch, J, Glass, G, Shields, T, Lozano, WS, Pinedo-Cancino, V & Patz, JA 2006, 'The effect of deforestation on the human-biting rate of *Anopheles darlingi*, the primary vector of falciparum malaria in the Peruvian Amazon', *The American Journal of Tropical Medicine and Hygiene*, vol. 74, no. 1, pp. 3-11.

Wang, X, Xie, H & Liang, T 2008, 'Evaluation of MODIS snow cover and cloud mask and its application in Northern Xinjiang, China', *Remote Sensing of Environment*, vol. 112, no. 4, pp. 1497-513.

Wicaksono, P & Lazuardi, W 2018, 'Assessment of PlanetScope images for benthic habitat and seagrass species mapping in a complex optically shallow water environment', *International Journal of Remote Sensing*, vol. 39, no. 17, pp. 5739-65.

Wijayanti, SPM, Porphyre, T, Chase-Topping, M, Rainey, SM, McFarlane, M, Schnettler, E, Biek, R & Kohl, A 2016, 'The importance of socio-economic versus environmental risk factors for reported dengue cases in Java, Indonesia', *PLoS Neglected Tropical Diseases*, vol. 10, no. 9.

World Meteorological Organization 2019, *Weather information for Vientiane*, viewed 28 August 2019, <<http://worldweather.wmo.int/en/city.html?cityId=235>>.

World Health Organization 1986, *Dengue haemorrhagic fever: diagnosis, treatment, and control*, England.

— 2007, *WHO ALERT: Prompt action needed on dengue*. Press Release of the World Health Organization Southeast Asia Regional Office, New Delhi; 2007.

— 2008, *DengueNet: global surveillance of dengue and dengue haemorrhagic fever*, WHO, Geneva, viewed 23 September 2019.

— 2011, 'Comprehensive guideline for prevention and control of dengue and dengue haemorrhagic fever'.

— 2019, *Dengue and severe dengue*, viewed 13 October 2019, <<https://www.who.int/news-room/fact-sheets/detail/dengue-and-severe-dengue>>.

— n.d-a, *Dengue*, viewed 14 March 2019 2019, <<http://www.wpro.who.int/laos/topics/dengue/en/>>.

— n.d-b, *Surface water*, 5,

<https://www.who.int/water_sanitation_health/dwq/monograph42_chapter5.pdf>.

Wu, P-C, Lay, J-G, Guo, H-R, Lin, C-Y, Lung, S-C & Su, H-J 2009, 'Higher temperature and urbanization affect the spatial patterns of dengue fever transmission in subtropical Taiwan', *Science of The Total Environment*, vol. 407, no. 7, pp. 2224-33.

Xu, H 2006, 'Modification of normalized difference water index (NDWI) to enhance open water features in remotely sensed imagery', *International Journal of Remote Sensing*, vol. 27, no. 14, pp. 3025-33.

Yagüe-Martínez, N, Prats-Iraola, P, Gonzalez, FR, Brcic, R, Shau, R, Geudtner, D, Eineder, M & Bamler, R 2016, 'Interferometric processing of Sentinel-1 TOPS data', *IEEE Transactions on Geoscience and Remote Sensing*, vol. 54, no. 4, pp. 2220-34.

Yan, Y, Zhao, H, Chen, C, Zou, L, Liu, X, Chai, C, Wang, C, Shi, J & Chen, S 2018, 'Comparison of multiple bioactive constituents in different parts of *Eucommia ulmoides* based on UFLC-QTRAP-MS/MS combined with PCA', *Molecules*, vol. 23, no. 3, p. 643.

Yang, L, Tian, S, Yu, L, Ye, F, Qian, J & Qian, Y 2015, 'Deep learning for extracting water body from Landsat imagery', *International Journal of Innovative Computing, Information and Control*, vol. 11, pp. 1913-29.

Yang, X & Chen, L 2017, 'Evaluation of automated urban surface water extraction from Sentinel-2A imagery using different water indices', *Journal of Applied Remote Sensing*, vol. 11, no. 2, pp. 1-11, .

Yang, X, Zhao, S, Qin, X, Zhao, N & Liang, L 2017, 'Mapping of urban surface water bodies from Sentinel-2 MSI imagery at 10 m resolution via NDWI-based image sharpening', *Remote Sensing*, vol. 9, no. 6, p. 596.

Zeng, L, Schmitt, M, Li, L & Zhu, XX 2017, 'Analysing changes of the Poyang Lake water area using Sentinel-1 synthetic aperture radar imagery', *International Journal of Remote Sensing*, vol. 38, no. 23, pp. 7041-69.

Zhang, Q, Wang, C & Shinohara, F 2007, 'Automatic extraction of water body based on EOS/MODIS remotely sensed imagery', in *MIPPR 2007: Automatic Target Recognition and Image Analysis; and Multispectral Image Acquisition*, vol. 6786, p. 678642.

Zheng, L, Ren, H-Y, Shi, R-H & Lu, L 2019, 'Spatiotemporal characteristics and primary influencing factors of typical dengue fever epidemics in China', *Infectious Diseases of Poverty*, vol. 8, no. 1, p. 24.

Zhou, Y, Dong, J, Xiao, X, Xiao, T, Yang, Z, Zhao, G, Zou, Z & Qin, Y 2017, 'Open surface water mapping algorithms: a comparison of water-related spectral indices and sensors', *Water*, vol. 9, no. 4, p. 256.

Zhou, Yn, Luo, J, Shen, Z, Hu, X & Yang, H 2014, 'Multiscale water body extraction in urban environments from satellite images', *IEEE Journal of Selected Topics in Applied Earth Observations and Remote Sensing*, vol. 7, no. 10, pp. 4301-12.

Zhu, L, Suomalainen, J, Liu, J, Hyypä, J, Kaartinen, H & Haggren, H 2018, 'A Review: Remote Sensing Sensors', *Multi-purposeful Application of Geospatial Data. IntechOpen*, pp. 19-42.

APPENDICES

Appendix 1: Field Survey Collection Data

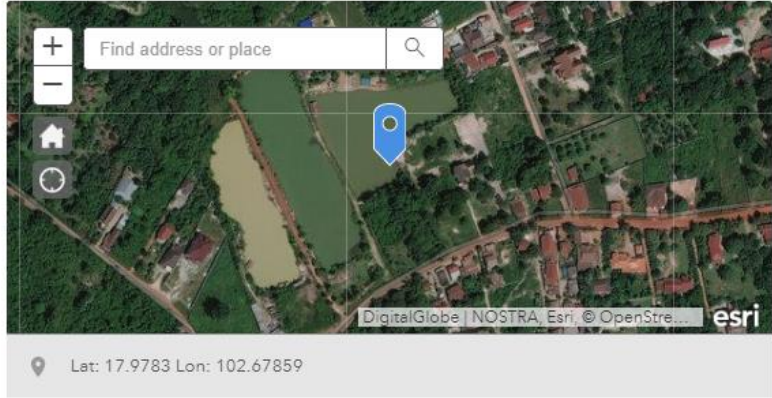
Object ID	Creation Date	Edit Date	Date and Time of Collecting Data	X	Y
1	18/07/2019 7:47	18/07/2019 7:52	18/07/2019 7:37	102.6705	17.9902
2	18/07/2019 8:18	18/07/2019 8:18	18/07/2019 8:12	102.6284	17.94953
3	22/07/2019 7:24	22/07/2019 7:24	22/07/2019 7:20	102.6682	17.98991
4	22/07/2019 7:35	22/07/2019 7:35	22/07/2019 7:31	102.6658	17.98862
5	22/07/2019 7:40	22/07/2019 7:40	22/07/2019 7:38	102.665	17.98896
6	22/07/2019 8:36	22/07/2019 8:36	22/07/2019 8:34	102.6563	17.98473
7	22/07/2019 8:40	22/07/2019 8:40	22/07/2019 8:37	102.6557	17.98486
8	22/07/2019 9:06	22/07/2019 9:15	22/07/2019 9:00	102.6483	17.97597
9	24/07/2019 7:35	24/07/2019 7:35	24/07/2019 7:31	102.6333	18.01025
10	24/07/2019 7:54	24/07/2019 7:54	24/07/2019 7:50	102.6705	17.9901
11	24/07/2019 8:28	24/07/2019 8:28	24/07/2019 8:21	102.652	17.94079
12	28/07/2019 2:17	28/07/2019 2:17	28/07/2019 2:15	102.6521	17.9259
13	28/07/2019 2:21	28/07/2019 2:21	28/07/2019 2:17	102.6528	17.92594
14	28/07/2019 2:36	28/07/2019 2:36	28/07/2019 2:31	102.6471	17.93859
15	28/07/2019 2:39	28/07/2019 2:39	28/07/2019 2:36	102.6477	17.93775
16	28/07/2019 5:39	28/07/2019 5:39	28/07/2019 5:35	102.6307	18.01853
17	28/07/2019 6:02	28/07/2019 6:02	28/07/2019 6:00	102.629	18.01545
18	8/08/2019 2:34	8/08/2019 2:34	8/08/2019 2:32	102.6716	17.98851
19	8/08/2019 2:34	8/08/2019 2:34	8/08/2019 2:30	102.6713	17.98843
20	8/08/2019 2:36	8/08/2019 2:36	8/08/2019 2:34	102.6717	17.98846
21	8/08/2019 2:41	8/08/2019 2:41	8/08/2019 2:37	102.6717	17.98846
22	8/08/2019 2:50	8/08/2019 2:50	8/08/2019 2:48	102.6724	17.98858
23	8/08/2019 3:25	8/08/2019 3:25	8/08/2019 3:23	102.6714	17.98772
24	8/08/2019 4:03	8/08/2019 4:03	8/08/2019 4:00	102.6697	17.98853
25	8/08/2019 4:09	8/08/2019 4:09	8/08/2019 4:06	102.6696	17.98865
26	8/08/2019 7:29	8/08/2019 7:29	8/08/2019 7:26	102.6696	17.99006
27	8/08/2019 7:47	8/08/2019 7:48	8/08/2019 7:43	102.6699	17.98904
28	8/08/2019 8:40	8/08/2019 8:40	8/08/2019 8:38	102.6684	17.99054
29	10/08/2019 3:28	10/08/2019 3:33	10/08/2019 3:26	102.64	18.03737
30	10/08/2019 3:43	10/08/2019 3:43	10/08/2019 3:40	102.6426	18.03863
31	10/08/2019 3:47	10/08/2019 3:47	10/08/2019 3:44	102.6428	18.03848
32	10/08/2019 3:49	10/08/2019 3:49	10/08/2019 3:47	102.6429	18.03873
33	10/08/2019 3:53	10/08/2019 3:53	10/08/2019 3:50	102.643	18.03901

Appendix 2: Survey 123 ArcGIS Form used for field surveying

Water map Survey

This survey will be used in the field work in VT for water bodies map out

1 **Locations***



2 **Photos of Features 1***

Press here to choose image file. (<10MB)

3 **Photos of Features 2***

Press here to choose image file. (<10MB)

4 **Photos of Features 3***

Press here to choose image file. (<10MB)

5 **Photos of Features 4***

Press here to choose image file. (<10MB)

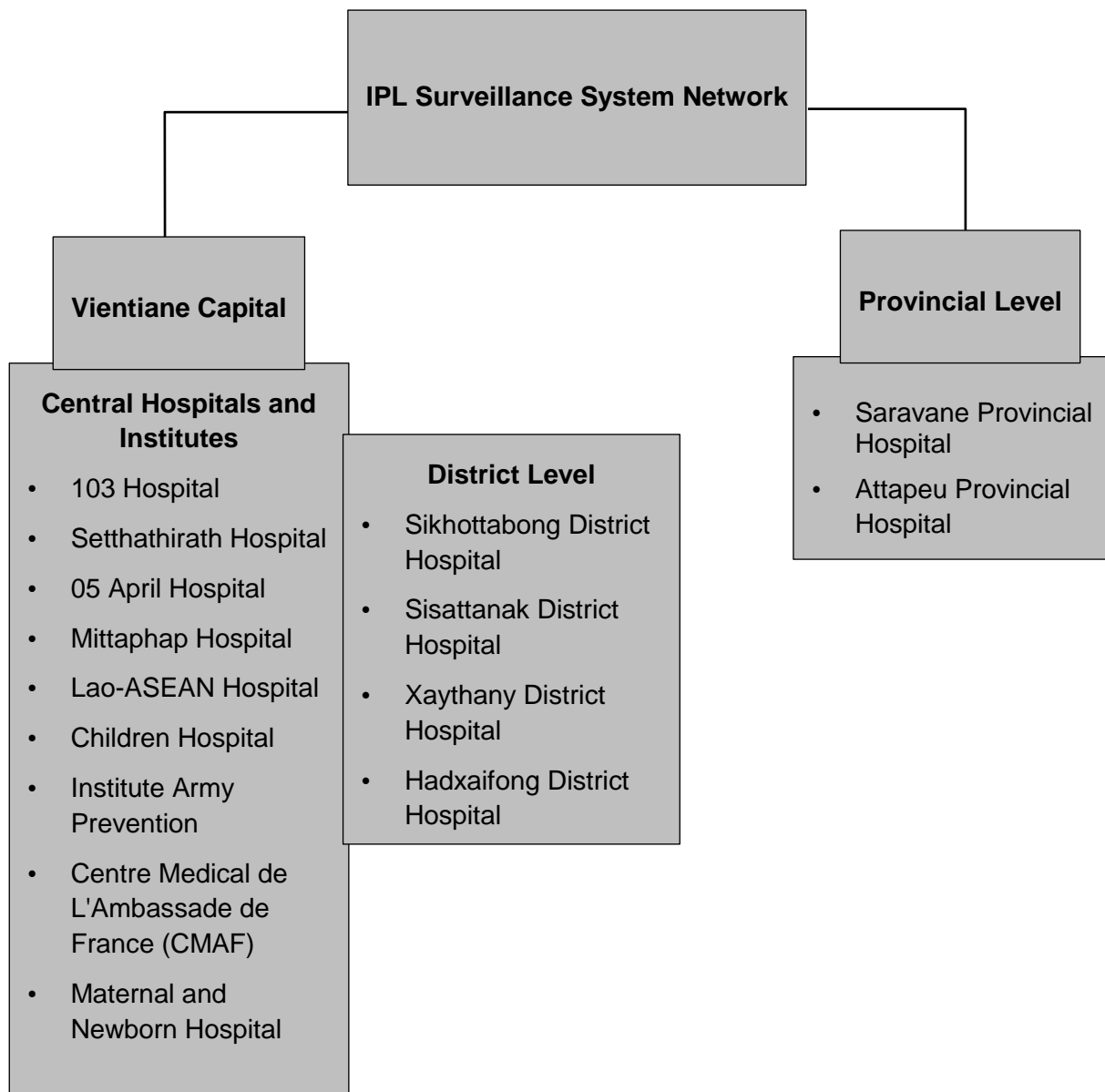
6 **Date and Time of Collecting Data***

9/30/19 3:09 PM

7 **Notes_Comments***

Submit

Appendix 3: Surveillance System, Institut Pasteur du Laos



Appendix 4: Georeferenced Points of Dengue Incidence

No	Patient Code	X	Y	Onset date	NS1 antigen	NS1 ELISA	Screening
1	5153	18.00313	102.6087	3/01/2017	Not tested	Not tested	Positive
2	5157	17.97033	102.6528	1/01/2017	Not tested	Not tested	Positive
3	5170	18.16423	102.7513	9/01/2017	Not tested	Not tested	Positive
4	5176	17.98011	102.5995	9/01/2017	Not tested	Not tested	Positive
5	5181	18.01262	102.6416	5/01/2017	Not tested	Not tested	Positive
6	5192	17.98676	102.6397	12/01/2017	Positive	Not tested	Negative
7	5195	17.99668	102.6309	15/01/2017	Not tested	Not tested	Positive
8	5196	17.97527	102.641	17/01/2017	Not tested	Not tested	Positive
9	5206	18.03167	102.6348	19/01/2017	Not tested	Not tested	Positive
10	5207	18.00229	102.6454	20/01/2017	Not tested	Not tested	Positive
11	5208	18.03427	102.6407	19/01/2017	Not tested	Not tested	Positive
12	5210	18.1126	102.6479	22/01/2017	Not tested	Not tested	Positive
13	5211	18.0437	102.6331	19/01/2017	Positive	Not tested	Positive
14	5215	17.90735	102.6185	25/01/2017	Not tested	Not tested	Positive
15	5217	18.1129	102.6501	19/01/2017	Not tested	Not tested	Positive
16	5218	18.00432	102.6301	19/01/2017	Not tested	Not tested	Positive
17	5219	17.97262	102.6412	26/01/2017	Not tested	Not tested	Positive
18	5220	17.87193	102.6451	26/01/2017	Not tested	Not tested	Positive
19	5221	17.89975	102.6641	30/06/2017	Not tested	Not tested	Positive
20	5234	17.9794	102.6555	30/06/2017	Not tested	Not tested	Positive
21	5250	17.98327	102.4489	12/02/2017	Not tested	Not tested	Positive
22	5251	17.98457	102.5558	13/02/2017	Not tested	Not tested	Positive
23	5252	17.96011	102.6252	10/02/2017	Positive	Not tested	Negative
24	5254	17.94226	102.624	13/02/2017	Not tested	Not tested	Positive
25	5272	17.98297	102.4469	26/02/2017	Not tested	Not tested	Positive
26	5279	17.88536	102.7161	1/03/2017	Not tested	Not tested	Positive
27	5287	17.98579	102.4473	12/03/2017	Not tested	Not tested	Positive
28	5288	17.98302	102.4476	14/03/2017	Not tested	Not tested	Positive
29	5314	17.98108	102.6852	18/03/2017	Not tested	Not tested	Positive
30	5371	18.11089	102.6459	24/04/2017	Not tested	Not tested	Positive
31	5372	18.11057	102.8638	10/04/2017	Not tested	Not tested	Positive
32	5373	17.95015	102.6343	19/04/2017	Not tested	Not tested	Positive
33	5379	17.92828	102.6225	6/05/2017	Not tested	Not tested	Positive
34	5388	18.10782	102.8612	7/05/2017	Not tested	Not tested	Positive
35	5390	17.98523	102.5887	9/05/2017	Not tested	Not tested	Positive
36	5400	18.12992	102.6161	10/05/2017	Not tested	Not tested	Positive
37	5426	18.00617	102.6689	12/05/2017	Not tested	Not tested	Positive
38	5428	17.9843	102.4489	18/05/2017	Not tested	Not tested	Positive
39	5544	17.94591	102.6665	4/06/2017	Not tested	Not tested	Positive
40	5546	17.84615	102.626	4/06/2017	Not tested	not finished	Positive
41	5548	17.90201	102.6481	2/06/2017	Not tested	Not tested	Positive
42	5550	18.23598	102.6993	2/06/2017	Not tested	Not tested	Positive
43	5551	18.12565	102.6651	4/05/2017	Not tested	Not tested	Positive
44	5554	18.12579	102.6652	24/05/2017	Not tested	not finished	Positive

No	Patient Code	X	Y	Onset date	NS1 antigen	NS1 ELISA	Screening
45	5556	18.26497	102.7568	31/05/2017	Not tested	Not tested	Positive
46	5557	18.11178	102.6461	31/05/2017	Not tested	Not tested	Positive
47	5558	18.26419	102.7564	4/06/2017	Not tested	Not tested	Positive
48	5560	18.25687	102.6811	30/05/2017	Not tested	Not tested	Positive
49	5573	18.0156	102.629	10/06/2017	Not tested	Not tested	Positive
50	5582	18.25407	102.6886	6/06/2017	Not tested	Not tested	Positive
51	5585	18.25003	102.6871	5/06/2017	Not tested	Not tested	Positive
52	5588	17.9457	102.6667	10/06/2017	Not tested	Not tested	Positive
53	5589	18.10973	102.6452	6/06/2017	Not tested	Not tested	Positive
54	5596	17.94547	102.6671	5/06/2017	Not tested	Not tested	Positive
55	5833	17.95469	102.7031	26/06/2017	Not tested	Not tested	Positive
56	5837	17.9545	102.6433	25/06/2017	Not tested	Not tested	Positive
57	5838	18.05023	102.735	28/06/2017	Not tested	Not tested	Positive
58	5839	17.95409	102.7029	28/06/2017	Not tested	Not tested	Positive
59	5840	18.26436	102.7567	24/06/2017	Not tested	Not tested	Positive
60	5842	18.23276	102.694	1/07/2017	Not tested	Not tested	Positive
61	5849	18.11369	102.8515	26/06/2017	Not tested	Not tested	Positive
62	5867	17.97658	102.6605	30/06/2017	Not tested	Not tested	Positive
63	5870	17.96204	102.7023	29/06/2017	Not tested	Not tested	Positive
64	5873	17.83768	102.6369	1/07/2017	Not tested	Not tested	Positive
65	5887	17.85657	102.6021	4/07/2017	Not tested	Not tested	Positive
66	5889	18.04616	102.6383	1/07/2017	Not tested	Not tested	Positive
67	5894	18.14462	102.7806	1/07/2017	Not tested	Not tested	Positive
68	5895	18.02021	102.6257	29/06/2017	Not tested	Not tested	Positive
69	5897	18.11328	102.8521	30-Jun-17	Not tested	Not tested	Positive
70	5898	17.99047	102.6647	30/06/2017	Not tested	Not tested	Positive
71	5900	18.11342	102.8519	30-Jun-17	Not tested	Not tested	Positive
72	5902	17.9734	102.673	4/07/2017	Not tested	Not tested	Positive
73	5907	17.96791	102.8407	1/07/2017	Not tested	Not tested	Positive
74	5926	17.93829	102.6872	10/07/2017	Not tested	Not tested	Positive
75	5941	17.92034	102.6511	3/07/2017	Not tested	Not tested	Positive
76	5954	18.01083	102.6314	8/07/2017	Not tested	Not tested	Positive
77	5957	17.9687	102.8435	8/07/2017	Not tested	Not tested	Positive
78	5968	18.18307	102.5796	7/07/2017	Not tested	Not tested	Positive
79	5976	17.94282	102.6665	2/07/2017	Not tested	Not tested	Positive
80	5983	17.93224	102.622	6/07/2017	Not tested	Not tested	Positive
81	5984	17.92342	102.6169	12/07/2017	Not tested	Not tested	Positive
82	5985	17.93645	102.7844	5/07/2017	Not tested	Not tested	Positive
83	5986	17.93749	102.7842	3/07/2017	Not tested	Not tested	Positive
84	5989	17.99674	102.5939	8/07/2017	Not tested	Not tested	Positive
85	6005	17.84648	102.6262	8/07/2017	Not tested	Not tested	Positive
86	6015	17.98201	102.6765	13-Jul-17	Not tested	Not tested	Positive
87	6022	17.97387	102.6897	10/07/2017	Not tested	Not tested	Positive
88	6030	18.00472	102.6894	11/07/2017	Not tested	Not tested	Positive
89	6031	17.95043	102.619	13/07/2017	Not tested	Not tested	Positive
90	6052	17.95562	102.6261	14-Jul-17	Not tested	Not tested	Positive

No	Patient Code	X	Y	Onset date	NS1 antigen	NS1 ELISA	Screening
91	6056	17.93995	102.6673	13/07/2017	Not tested	Not tested	Positive
92	6075	17.98533	102.5865	21/07/2017	Not tested	Not tested	Positive
93	6076	17.8575	102.6587	17/07/2017	Not tested	Not tested	Positive
94	6077	17.84754	102.6249	14/07/2017	Not tested	Not tested	Positive
95	6081	17.95562	102.7018	17/07/2017	Not tested	Not tested	Positive
96	6085	18.06155	102.5727	20/07/2017	Not tested	Not tested	Positive
97	6086	18.12215	102.6269	21/07/2017	Not tested	Not tested	Positive
98	6088	18.09117	102.547	14/07/2017	Not tested	Not tested	Positive
99	6089	18.02073	102.6255	15/07/2017	Not tested	Not tested	Positive
100	6093	18.01177	102.6327	13/07/2017	Not tested	Not tested	Positive
101	6097	18.04603	102.6389	19/07/2017	Not tested	Not tested	Positive
102	6098	18.01402	102.6279	18/07/2017	Not tested	Not tested	Positive
103	6118	18.00401	102.673	21-Jul-17	Not tested	Not tested	Positive
104	6119	18.01204	102.6175	21/07/2017	Not tested	Not tested	Positive
105	6125	17.95313	102.6675	22/07/2017	Not tested	Not tested	Positive
106	6132	17.90925	102.621	30/07/2017	Not tested	Not tested	Positive
107	6136	17.98685	102.5271	29/07/2017	Not tested	Not tested	Positive
108	6140	18.02824	102.5832	26/07/2017	Not tested	Not tested	Positive
109	6142	18.06433	102.6303	26/07/2017	Not tested	Not tested	Positive
110	6143	17.98551	102.6345	27/07/2017	Not tested	Not tested	Positive
111	6150	17.98892	102.6597	26/07/2017	Not tested	Not tested	Positive
112	6151	17.99264	102.6147	25/07/2017	Not tested	Not tested	Positive
113	6157	17.91844	102.6274	29/07/2017	Not tested	Not tested	Positive
114	6158	17.8905	102.6271	26/07/2017	Not tested	Not tested	Positive
115	6159	17.96785	102.5891	29/07/2017	Not tested	Not tested	Positive
116	6161	17.97553	102.6632	21/07/2017	Not tested	Not tested	Positive
117	6167	18.01942	102.6361	26/07/2017	Not tested	Not tested	Positive
118	6169	18.04518	102.708	26/07/2017	Not tested	Not tested	Positive
119	6170	17.98671	102.6285	29/07/2017	Not tested	Not tested	Positive
120	6171	18.02994	102.6518	29/07/2017	Not tested	Not tested	Positive
121	6175	17.9843	102.5869	29/07/2017	Not tested	Not tested	Positive
122	6180	17.96206	102.6225	27/07/2017	Not tested	Not tested	Positive
123	6183	17.89109	102.7163	25/07/2017	Not tested	Not tested	Positive
124	6185	17.89399	102.716	28/07/2017	Not tested	Not tested	Positive
125	6188	17.88763	102.6109	30/07/2017	Positive	Not tested	Negative
126	6189	17.99593	102.5417	30/07/2017	Not tested	Not tested	Positive
127	6190	18.12697	102.6658	1-Aug-17	Not tested	Not tested	Positive
128	6193	17.89312	102.715	1/08/2017	Positive	Not tested	Positive
129	6194	17.96747	102.8422	2/08/2017	Not tested	Not tested	Positive
130	6199	17.96668	102.6242	1/08/2017	Not tested	Not tested	Positive
131	6202	17.94458	102.6305	31/07/2017	Not tested	Not tested	Positive
132	6208	17.94304	102.6676	2/08/2017	Not tested	Not tested	Positive
133	6211	18.04905	102.6417	30/07/2017	Not tested	Not tested	Positive
134	6212	17.99086	102.6146	1/08/2017	Not tested	Not tested	Positive
135	6216	18.04594	102.6397	1/08/2017	Not tested	Not tested	Positive
136	6217	18.08088	102.7178	4/08/2017	Not tested	Not tested	Positive

No	Patient Code	X	Y	Onset date	NS1 antigen	NS1 ELISA	Screening
137	6219	18.03168	102.6357	30/07/2017	Not tested	Not tested	Positive
138	6239	17.9452	102.7025	4/08/2017	Not tested	Not tested	Positive
139	6241	17.98232	102.6343	4/08/2017	Not tested	Not tested	Positive
140	6244	17.94475	102.6379	6/08/2017	Not tested	Not tested	Positive
141	6245	17.89196	102.7458	4/08/2017	Not tested	Not tested	Positive
142	6246	17.96817	102.7462	6/08/2017	Not tested	Not tested	Positive
143	6256	17.95371	102.6851	3/08/2017	Not tested	Not tested	Positive
144	6274	17.99385	102.6081	4/08/2017	Not tested	Not tested	Positive
145	6275	17.98935	102.6603	7/08/2017	Not tested	Not tested	Positive
146	6277	17.96493	102.6689	8/08/2017	Not tested	Not tested	Positive
147	6321	17.98458	102.6563	13/08/2017	Not tested	Not tested	Positive
148	6322	17.93464	102.7807	12/08/2017	Not tested	Positive	Negative
149	6323	17.99835	102.6573	11/08/2017	Not tested	Not tested	Positive
150	6325	17.99371	102.6325	12/08/2017	Not tested	Not tested	Positive
151	6326	17.94639	102.6294	12/08/2017	Not tested	Not tested	Positive
152	6330	17.9456	102.6385	11/08/2017	Not tested	Not tested	Positive
153	6333	17.88745	102.7302	12/08/2017	Not tested	Not tested	Positive
154	6336	18.05516	102.7554	13/08/2017	Not tested	Not tested	Positive
155	6346	17.96593	102.6044	11/08/2017	Not tested	Not tested	Positive
156	6350	18.0737	102.7465	10/08/2017	Not tested	Not tested	Positive
157	6352	18.03034	102.627	10/08/2017	Not tested	Not tested	Positive
158	6354	17.99084	102.6082	10/08/2017	Not tested	Not tested	Positive
159	6356	17.9777	102.6531	12/08/2017	Not tested	Not tested	Positive
160	6358	17.96095	102.6137	13/08/2017	Not tested	Not tested	Positive
161	6359	17.97595	102.6651	15/08/2017	Not tested	Not tested	Positive
162	6368	18.00832	102.688	14/08/2017	Not tested	Not tested	Positive
163	6373	18.05462	102.7561	14/08/2017	Not tested	Not tested	Positive
164	6376	17.98602	102.5865	14/08/2017	Not tested	Not tested	Positive
165	6377	17.96571	102.6706	14/08/2017	Not tested	Not tested	Positive
166	6382	18.06202	102.8067	16/08/2017	Not tested	Not tested	Positive
167	6386	18.07204	102.6455	14/08/2017	Not tested	Not tested	Positive
168	6389	18.05016	102.6634	16/08/2017	Not tested	Not tested	Positive
169	6390	18.02503	102.6274	14/08/2017	Not tested	Not tested	Positive
170	6394	18.05256	102.6119	19/08/2017	Not tested	Not tested	Positive
171	6403	17.89619	102.6452	11/08/2017	Not tested	Not tested	Positive
172	6426	18.05413	102.7557	18/08/2017	Not tested	Not tested	Positive
173	6427	18.01461	102.4886	17/08/2017	Not tested	Not tested	Positive
174	6430	18.10842	102.6524	18/08/2017	Not tested	Not tested	Positive
175	6432	18.04607	102.6399	19/08/2017	Not tested	Not tested	Positive
176	6434	18.14537	102.7814	18/08/2017	Not tested	Not tested	Positive
177	6435	17.90922	102.7213	18/08/2017	Not tested	Not tested	Positive
178	6448	17.9709	102.6144	25/08/2017	Not tested	Not tested	Positive
179	6450	17.88405	102.7058	26/08/2017	Not tested	Not tested	Positive
180	6453	17.94681	102.6244	26/08/2017	Not tested	Not tested	Positive
181	6454	18.10825	102.6532	18-Aug-17	Not tested	Not tested	Positive
182	6457	17.97685	102.6017	24/08/2017	Not tested	Not tested	Positive

No	Patient Code	X	Y	Onset date	NS1 antigen	NS1 ELISA	Screening
183	6458	18.06625	102.6303	23/08/2017	Not tested	Not tested	Positive
184	6459	18.00125	102.6514	21/08/2017	Not tested	Not tested	Positive
185	6460	17.99601	102.6168	21/08/2017	Not tested	Not tested	Positive
186	6461	18.0871	102.6304	21/08/2017	Not tested	Not tested	Positive
187	6464	18.03729	102.6324	22/08/2017	Not tested	Not tested	Positive
188	6470	17.89977	102.6382	23/08/2017	Not tested	Not tested	Positive
189	6477	17.89016	102.6402	22/08/2017	Not tested	Not tested	Positive
190	6478	17.9137	102.6469	23/08/2017	Not tested	Not tested	Positive
191	6480	17.96789	102.5838	25/08/2017	Not tested	Not tested	Positive
192	6484	17.94028	102.6675	20/08/2017	Not tested	Not tested	Positive
193	6491	18.02555	102.6266	23/08/2017	Not tested	Not tested	Positive
194	6499	17.91478	102.6234	27/08/2017	Not tested	Not tested	Positive
195	6507	18.04515	102.6366	28/09/2017	Not tested	Not tested	Positive
196	6509	18.08466	102.6626	29/09/2017	Not tested	Not tested	Positive
197	6511	18.04495	102.6354	22/09/2017	Not tested	Not tested	Positive
198	6512	18.10596	102.5057	23/09/2017	Not tested	Not tested	Positive
199	6513	18.07748	102.6704	28/09/2017	Not tested	Not tested	Positive
200	6515	18.05922	102.6655	26/09/2017	Not tested	Not tested	Positive
201	6516	18.00886	102.6391	17/09/2017	Not tested	Not tested	Positive
202	6518	18.07948	102.6665	24/09/2017	Not tested	Not tested	Positive
203	6521	18.05493	102.7562	24/09/2017	Not tested	Not tested	Positive
204	6525	17.94947	102.6402	26/09/2017	Not tested	Negative	Positive
205	6557	17.97566	102.5779	1/09/2017	Not tested	Not tested	Positive
206	6562	18.00062	102.6241	29/08/2017	Not tested	Not tested	Positive
207	6572	18.07704	102.6685	29/08/2017	Not tested	Not tested	Positive
208	6597	18.01971	102.6387	1/09/2017	Not tested	Not tested	Positive
209	6598	17.97242	102.6283	1/09/2017	Not tested	Not tested	Positive
210	6603	17.99309	102.5253	3/09/2017	Not tested	Not tested	Positive
211	6615	17.94971	102.7031	31/08/2017	Not tested	Not tested	Positive
212	6618	18.07618	102.6687	2/09/2017	Not tested	Not tested	Positive
213	6619	17.98668	102.6259	1/09/2017	Not tested	Not tested	Positive
214	6621	17.99852	102.6137	1/09/2017	Not tested	Not tested	Positive
215	6622	18.00863	102.6388	30/08/2017	Not tested	Negative	Positive
216	6628	18.01871	102.654	1/09/2017	Not tested	Not tested	Positive
217	6630	17.9813	102.6109	30/08/2017	Not tested	Not tested	Positive
218	6637	17.99869	102.617	2/09/2017	Not tested	Negative	Positive
219	6644	18.02192	102.5216	8/09/2017	Not tested	Not tested	Positive
220	6653	18.02552	102.6267	6/09/2017	Not tested	Not tested	Positive
221	6657	18.02857	102.6302	5/09/2017	Not tested	Not tested	Positive
222	6659	17.88716	102.7279	2/09/2017	Not tested	Not tested	Positive
223	6660	17.92975	102.6507	5/09/2017	Not tested	Not tested	Positive
224	6661	17.91994	102.618	8/09/2017	Not tested	Not tested	Positive
225	6676	18.08214	102.501	6/09/2017	Not tested	Not tested	Positive
226	6695	17.99013	102.6612	6/09/2017	Not tested	Not tested	Positive
227	6696	17.91577	102.6494	10/09/2017	Not tested	Not tested	Positive
228	6697	17.98672	102.6544	10/09/2017	Not tested	Not tested	Positive

No	Patient Code	X	Y	Onset date	NS1 antigen	NS1 ELISA	Screening
229	6701	17.94229	102.6247	10/09/2017	Not tested	Not tested	Positive
230	6704	17.97621	102.6311	9-Sep-17	Not tested	Not tested	Positive
231	6705	17.97145	102.6202	8/09/2017	Not tested	Not tested	Positive
232	6706	17.90338	102.6294	7/09/2017	Not tested	Not tested	Positive
233	6713	18.06443	102.7873	8/09/2017	Not tested	Not tested	Positive
234	6715	17.95142	102.7031	7/09/2017	Not tested	Not tested	Positive
235	6727	18.02907	102.5496	8/09/2017	Not tested	Not tested	Positive
236	6728	18.04702	102.6419	5/09/2017	Not tested	Not tested	Positive
237	6735	17.98415	102.6669	9/09/2017	Not tested	Not tested	Positive
238	6737	18.04301	102.6362	7/09/2017	Not tested	Not tested	Positive
239	6739	17.97785	102.6558	11/09/2017	Not tested	Not tested	Positive
240	6753	17.91292	102.7226	13/09/2017	Not tested	Not tested	Positive
241	6761	17.98005	102.5858	14/09/2017	Not tested	Not tested	Positive
242	6768	17.90454	102.6636	12/09/2017	Not tested	Not tested	Positive
243	6769	18.00468	102.5975	12/09/2017	Not tested	Not tested	Positive
244	6770	17.98341	102.7033	10/09/2017	Not tested	Not tested	Positive
245	6777	17.98498	102.6347	12/09/2017	Not tested	Not tested	Positive
246	6778	17.98701	102.6271	13/09/2017	Not tested	Not tested	Positive
247	6793	18.04227	102.6351	14/09/2017	Not tested	Not tested	Positive
248	6794	18.04877	102.627	13/09/2017	Not tested	Not tested	Positive
249	6796	18.06417	102.7912	15/09/2017	Not tested	Not tested	Positive
250	6810	17.88893	102.7388	13/09/2017	Not tested	Not tested	Positive
251	6818	17.93251	102.6471	15/09/2017	Not tested	Not tested	Positive
252	6826	18.07303	102.7488	17/09/2017	Not tested	Not tested	Positive
253	6828	17.97585	102.5806	17/09/2017	Not tested	Not tested	Positive
254	6829	17.98814	102.5835	16/09/2017	Not tested	Not tested	Positive
255	6849	17.97222	102.6147	24/09/2017	Not tested	Not tested	Positive
256	6857	17.997	102.6591	19/09/2017	Not tested	Not tested	Positive
257	6858	18.02925	102.6518	19/09/2017	Not tested	Not tested	Positive
258	6859	17.96677	102.6358	17/09/2017	Not tested	Not tested	Positive
259	6860	18.00059	102.6554	17/09/2017	Not tested	Not tested	Positive
260	6861	17.96929	102.6544	21/09/2017	Not tested	Not tested	Positive
261	6862	18.01453	102.6037	21/09/2017	Not tested	Not tested	Positive
262	6886	17.96918	102.5718	23/09/2017	Not tested	Not tested	Positive
263	6889	18.00201	102.5945	23/09/2017	Not tested	Not tested	Positive
264	6892	17.99016	102.633	24/09/2017	Not tested	Not tested	Positive
265	6894	18.02548	102.6269	22/09/2017	Not tested	Not tested	Positive
266	6902	17.91509	102.7653	28/09/2017	Not tested	Not tested	Positive
267	6906	18.06891	102.6658	27/09/2017	Not tested	Not tested	Positive
268	6909	17.97457	102.6535	29/09/2017	Not tested	Not tested	Positive
269	6919	17.98972	102.6331	26/09/2017	Not tested	Not tested	Positive
270	6927	18.05858	102.7409	27/09/2017	Not tested	Not tested	Positive
271	6949	17.97825	102.6095	29/09/2017	Not tested	Not tested	Positive
272	6951	18.03132	102.6268	30/09/2017	Not tested	Not tested	Positive
273	6955	17.88333	102.7063	28/09/2017	Not tested	Not tested	Positive
274	6959	17.93696	102.6522	29/09/2017	Not tested	Not tested	Positive

No	Patient Code	X	Y	Onset date	NS1 antigen	NS1 ELISA	Screening
275	6962	17.97291	102.5569	26/09/2017	Not tested	Not tested	Positive
276	6969	17.91977	102.619	1/10/2017	Negative	Not tested	Positive
277	6985	17.98811	102.5865	2/10/2017	Not tested	Not tested	Positive
278	6987	18.045	102.7086	2/10/2017	Not tested	Not tested	Positive
279	6990	18.00739	102.631	30/09/2017	Not tested	Not tested	Positive
280	6999	17.90136	102.6699	7/10/2017	Not tested	Not tested	Positive
281	7002	17.91196	102.7226	8/10/2017	Not tested	Not tested	Positive
282	7003	17.91192	102.7226	9/10/2017	Not tested	Not tested	Positive
283	7015	18.01561	102.6233	3/10/2017	Not tested	Not tested	Positive
284	7020	18.03578	102.6409	5/10/2017	Not tested	Not tested	Positive
285	7022	17.98964	102.6064	9/10/2017	Not tested	Not tested	Positive
286	7035	17.95466	102.6203	7/10/2017	Not tested	Not tested	Positive
287	7041	17.96863	102.6577	14/10/2017	Not tested	Not tested	Positive
288	7042	17.93337	102.6695	10/10/2017	Not tested	Not tested	Positive
289	7044	18.04263	102.573	13/10/2017	Not tested	Not tested	Positive
290	7045	17.96882	102.6643	8/10/2017	Not tested	Not tested	Positive
291	7047	17.91366	102.6467	14-Oct-17	Not tested	Not tested	Positive
292	7050	18.00101	102.6521	7/10/2017	Not tested	Not tested	Positive
293	7052	18.04171	102.5446	13/10/2017	Not tested	Not tested	Positive
294	7055	18.03458	102.6426	9/10/2017	Not tested	Not tested	Positive
295	7058	17.98556	102.5051	16/10/2017	Not tested	Not tested	Positive
296	7070	17.98791	102.6573	16/10/2017	Not tested	Not tested	Positive
297	7076	18.0277	102.6447	14/10/2017	Not tested	Not tested	Positive
298	7081	18.07098	102.6862	12/10/2017	Not tested	Not tested	Positive
299	7087	17.98498	102.608	13/10/2017	Not tested	Not tested	Positive
300	7090	18.00053	102.6564	9/10/2017	Not tested	Not tested	Positive
301	7097	18.01935	102.6177	17/10/2017	Negative	Not tested	Positive
302	7108	17.88192	102.645	15/10/2017	Not tested	Not tested	Positive
303	7112	17.97889	102.6271	18/10/2017	Not tested	Not tested	Positive
304	7117	18.02656	102.6161	16/10/2017	Not tested	Not tested	Positive
305	7121	18.02788	102.6317	20/10/2017	Not tested	Not tested	Positive
306	7130	17.89993	102.755	23/10/2017	Not tested	Not tested	Positive
307	7135	18.04541	102.6112	18/10/2017	Not tested	Not tested	Positive
308	7137	17.99715	102.6951	20/10/2017	Not tested	Not tested	Positive
309	7144	17.92704	102.6171	22/10/2017	Negative	Not tested	Positive
310	7170	17.89681	102.7288	30/10/2017	Not tested	Not tested	Positive
311	7173	18.02208	102.6448	26/10/2017	Not tested	Not tested	Positive
312	7177	18.17502	102.6551	25/10/2017	Not tested	Not tested	Positive
313	7178	18.00602	102.6463	26/10/2017	Not tested	Not tested	Positive
314	7181	18.01725	102.9589	28/10/2017	Not tested	Not tested	Positive
315	7189	18.01417	102.6644	31/10/2017	Not tested	Not tested	Positive
316	7190	17.98213	102.5866	30/10/2017	Not tested	Not tested	Positive
317	7204	17.89776	102.6616	3/11/2017	Not tested	Not tested	Positive
318	7208	17.97691	102.6059	5/11/2017	Negative	Not tested	Positive
319	7210	18.00253	102.618	3/11/2017	Not tested	Not tested	Positive
320	7214	18.04945	102.6426	5/11/2017	Not tested	Not tested	Positive

No	Patient Code	X	Y	Onset date	NS1 antigen	NS1 ELISA	Screening
321	7215	18.03972	102.6333	3/11/2017	Not tested	Not tested	Positive
322	7216	17.98588	102.622	1/11/2017	Not tested	Not tested	Positive
323	7241	17.92563	102.7687	12/11/2017	Not tested	Not tested	Positive
324	7245	18.02228	102.5261	9/11/2017	Not tested	Not tested	Positive
325	7247	18.02836	102.6318	12/11/2017	Not tested	Not tested	Positive
326	7250	18.00229	102.6245	10/11/2017	Not tested	Not tested	Positive
327	7251	18.03788	102.6043	8/11/2017	Not tested	Not tested	Positive
328	7263	18.00887	102.6354	14/11/2017	Not tested	Not tested	Positive
329	7265	18.00748	102.5943	13/11/2017	Not tested	Not tested	Positive
330	7276	18.00705	102.6427	16/11/2017	Not tested	Not tested	Positive
331	7282	18.03065	102.5734	17/11/2017	Not tested	Not tested	Positive
332	7288	18.24879	102.689	20/11/2017	Not tested	Not tested	Positive
333	7295	17.89527	102.6477	23/11/2017	Not tested	Not tested	Positive
334	7302	18.03281	102.6406	21/08/2017	Not tested	Not tested	Positive
335	7303	18.02564	102.6266	25/11/2017	Not tested	Not tested	Positive
336	7306	18.07723	102.6677	24/11/2017	Not tested	Not tested	Positive
337	7309	18.06282	102.5576	25/11/2017	Not tested	Not tested	Positive
338	7312	17.91506	102.7648	20/11/2017	Not tested	Not tested	Positive
339	7313	17.94007	102.7531	20/11/2017	Not tested	Not tested	Positive
340	7316	17.92596	102.7683	26/11/2017	Not tested	Not tested	Positive
341	7322	18.02225	102.6306	26/11/2017	Not tested	Not tested	Positive
342	7323	18.01687	102.6309	22/11/2017	Not tested	Not tested	Positive
343	7324	18.0607	102.6833	26/11/2017	Not tested	Not tested	Positive
344	7325	17.96546	102.6162	30/11/2017	Not tested	Not tested	Positive
345	7327	17.94855	102.6247	25/11/2017	Not tested	Not tested	Positive
346	7329	17.933	102.7442	4/12/2017	Not tested	Not tested	Positive
347	7330	18.05627	102.6327	3/12/2017	Not tested	Not tested	Positive
348	7334	18.15798	102.7656	1/12/2017	Not tested	Not tested	Positive
349	7339	17.9974	102.6943	6/12/2017	Not tested	Not tested	Positive
350	7347	18.01445	102.6646	8/12/2017	Not tested	Not tested	Positive
351	7348	18.06472	102.6293	7/12/2017	Not tested	Not tested	Positive
352	7362	17.88442	102.6391	13/12/2017	Not tested	Not tested	Positive
353	7376	17.97783	102.638	17/12/2017	Not tested	Not tested	Positive
354	7380	18.17114	102.5011	22/12/2017	Not tested	Not tested	Positive

Appendix 5: Ground Reference

FID	Shape	Classified	Ground Truth	Easting	Northing
0	Point	2	2	249548.807	1999138.159
1	Point	2	2	249248.807	1998643.159
2	Point	2	2	249133.807	1997433.159
3	Point	2	2	248603.807	1997088.159
4	Point	2	1	249548.807	1997023.159
5	Point	2	2	248843.807	1996538.159
6	Point	2	2	249223.807	1995963.159
7	Point	2	2	249893.807	1995653.159
8	Point	2	2	249773.807	1995178.159
9	Point	2	2	249463.807	1994858.159
10	Point	2	2	250643.807	1998903.159
11	Point	1	1	251193.807	1998858.159
12	Point	2	2	250518.807	1998423.159
13	Point	2	2	252423.807	1998378.159
14	Point	2	2	252033.807	1998188.159
15	Point	2	2	250658.807	1997868.159
16	Point	2	2	254888.807	1997643.159
17	Point	2	2	253223.807	1997523.159
18	Point	2	2	255388.807	1997363.159
19	Point	2	2	253708.807	1997338.159
20	Point	2	2	251018.807	1997243.159
21	Point	2	2	252548.807	1997073.159
22	Point	2	2	250468.807	1996873.159
23	Point	2	2	252733.807	1996768.159
24	Point	2	2	251543.807	1996543.159
25	Point	2	2	252733.807	1996398.159
26	Point	2	2	253263.807	1996248.159
27	Point	1	1	252583.807	1996073.159
28	Point	2	2	251188.807	1995998.159
29	Point	2	2	252578.807	1995893.159
30	Point	2	2	253823.807	1995778.159
31	Point	2	2	251938.807	1995293.159
32	Point	2	2	254438.807	1995228.159
33	Point	2	2	250578.807	1995218.159
34	Point	2	2	255273.807	1995033.159
35	Point	2	2	252743.807	1994843.159
36	Point	2	2	252413.807	1994783.159
37	Point	2	2	254633.807	1994503.159
38	Point	2	2	256658.807	1997653.159
39	Point	2	2	258788.807	1997238.159
40	Point	2	2	257968.807	1997223.159
41	Point	2	2	256078.807	1997133.159
42	Point	2	2	259533.807	1996693.159
43	Point	2	2	257858.807	1996668.159
44	Point	2	2	256893.807	1996638.159

FID	Shape	Classified	Ground Truth	Easting	Northing
45	Point	2	2	255673.807	1996458.159
46	Point	2	2	257728.807	1996308.159
47	Point	2	1	257948.807	1996118.159
48	Point	2	2	257763.807	1995988.159
49	Point	1	1	257003.807	1995958.159
50	Point	2	2	257663.807	1995758.159
51	Point	2	2	258973.807	1995463.159
52	Point	2	2	257628.807	1995358.159
53	Point	2	2	258628.807	1995223.159
54	Point	2	2	256093.807	1995153.159
55	Point	2	2	258358.807	1994913.159
56	Point	2	2	259358.807	1994688.159
57	Point	2	2	257018.807	1994663.159
58	Point	2	2	256958.807	1994408.159
59	Point	2	2	261403.807	1996613.159
60	Point	2	2	263683.807	1996158.159
61	Point	2	2	263108.807	1995948.159
62	Point	2	2	260703.807	1995373.159
63	Point	2	2	261143.807	1995368.159
64	Point	2	2	263563.807	1995368.159
65	Point	2	2	261453.807	1995318.159
66	Point	2	2	263758.807	1995048.159
67	Point	2	2	262918.807	1994898.159
68	Point	2	2	264733.807	1994848.159
69	Point	2	2	261878.807	1994623.159
70	Point	2	2	264028.807	1994538.159
71	Point	2	2	266243.807	1995293.159
72	Point	2	2	266558.807	1995088.159
73	Point	2	2	269528.807	1994778.159
74	Point	2	2	267218.807	1994648.159
75	Point	2	2	266808.807	1994418.159
76	Point	2	2	249518.807	1994318.159
77	Point	2	2	248578.807	1994043.159
78	Point	2	1	247933.807	1993403.159
79	Point	2	2	248508.807	1993318.159
80	Point	2	2	247943.807	1993008.159
81	Point	2	2	247968.807	1992673.159
82	Point	1	1	247703.807	1992498.159
83	Point	2	2	248213.807	1992108.159
84	Point	2	2	249893.807	1992058.159
85	Point	2	2	248463.807	1991413.159
86	Point	2	2	247518.807	1991408.159
87	Point	2	2	247603.807	1990858.159
88	Point	2	2	250078.807	1990563.159
89	Point	2	2	249278.807	1990193.159
90	Point	1	2	249518.807	1989998.159
91	Point	2	2	250163.807	1989913.159

FID	Shape	Classified	Ground Truth	Easting	Northing
92	Point	2	2	250223.807	1989898.159
93	Point	2	2	249363.807	1989743.159
94	Point	2	2	254843.807	1994203.159
95	Point	2	2	254078.807	1994198.159
96	Point	2	2	252903.807	1993863.159
97	Point	2	1	251443.807	1993813.159
98	Point	2	2	255308.807	1993803.159
99	Point	2	2	251463.807	1993643.159
100	Point	2	2	251323.807	1993508.159
101	Point	2	2	253883.807	1993083.159
102	Point	2	2	250513.807	1992883.159
103	Point	2	2	254108.807	1992838.159
104	Point	2	2	253863.807	1992578.159
105	Point	2	2	254968.807	1992343.159
106	Point	2	2	252813.807	1992308.159
107	Point	2	2	250418.807	1992213.159
108	Point	2	2	252858.807	1992078.159
109	Point	2	2	253653.807	1991853.159
110	Point	2	2	252923.807	1991738.159
111	Point	2	2	253658.807	1991633.159
112	Point	2	2	255373.807	1991623.159
113	Point	2	2	251138.807	1991393.159
114	Point	2	2	251963.807	1991253.159
115	Point	2	2	254593.807	1991113.159
116	Point	2	2	254028.807	1990863.159
117	Point	2	2	251228.807	1990763.159
118	Point	2	2	254323.807	1990423.159
119	Point	2	2	254153.807	1990368.159
120	Point	2	2	252178.807	1990338.159
121	Point	2	2	254778.807	1990008.159
122	Point	2	2	252903.807	1989408.159
123	Point	2	2	251268.807	1989353.159
124	Point	2	2	260488.807	1994273.159
125	Point	2	2	259848.807	1994268.159
126	Point	2	2	255458.807	1994238.159
127	Point	2	2	257288.807	1994193.159
128	Point	2	2	259243.807	1994063.159
129	Point	2	2	259658.807	1993888.159
130	Point	2	2	255568.807	1993818.159
131	Point	1	2	259898.807	1993678.159
132	Point	2	2	259538.807	1993643.159
133	Point	2	2	256543.807	1993493.159
134	Point	2	1	260323.807	1993228.159
135	Point	2	2	256413.807	1993168.159
136	Point	2	2	256398.807	1992993.159
137	Point	2	2	256078.807	1992813.159
138	Point	1	2	259178.807	1992778.159

FID	Shape	Classified	Ground Truth	Easting	Northing
139	Point	2	2	257158.807	1992638.159
140	Point	2	2	256258.807	1992523.159
141	Point	2	2	259828.807	1992348.159
142	Point	2	2	255528.807	1992183.159
143	Point	2	2	257783.807	1991958.159
144	Point	2	2	257943.807	1991753.159
145	Point	2	2	257848.807	1991663.159
146	Point	2	2	260078.807	1991558.159
147	Point	2	2	256878.807	1991218.159
148	Point	2	2	257513.807	1991188.159
149	Point	2	2	259408.807	1991028.159
150	Point	2	2	259078.807	1990748.159
151	Point	2	2	260383.807	1990673.159
152	Point	2	2	256718.807	1990493.159
153	Point	2	2	258243.807	1990418.159
154	Point	2	2	258548.807	1990273.159
155	Point	2	2	259238.807	1990103.159
156	Point	2	2	256003.807	1989948.159
157	Point	2	2	255548.807	1989718.159
158	Point	2	2	256978.807	1989623.159
159	Point	2	2	257613.807	1989433.159
160	Point	2	2	255988.807	1989263.159
161	Point	2	2	264603.807	1994263.159
162	Point	2	2	264683.807	1994103.159
163	Point	2	2	261708.807	1993923.159
164	Point	2	2	261393.807	1993813.159
165	Point	1	2	261313.807	1993778.159
166	Point	2	2	264413.807	1993553.159
167	Point	2	2	260533.807	1993488.159
168	Point	2	2	265083.807	1993173.159
169	Point	2	2	264653.807	1992973.159
170	Point	2	2	261593.807	1992883.159
171	Point	2	2	263578.807	1992878.159
172	Point	2	2	264523.807	1992693.159
173	Point	2	2	260518.807	1992518.159
174	Point	2	2	261533.807	1992353.159
175	Point	2	2	265058.807	1992213.159
176	Point	2	2	264953.807	1991638.159
177	Point	2	2	264588.807	1991463.159
178	Point	2	2	262013.807	1991343.159
179	Point	2	2	260623.807	1991273.159
180	Point	2	2	263978.807	1991233.159
181	Point	2	2	260723.807	1991118.159
182	Point	2	2	264273.807	1990968.159
183	Point	2	2	262883.807	1990908.159
184	Point	2	2	264733.807	1990713.159
185	Point	2	2	262888.807	1990693.159

FID	Shape	Classified	Ground Truth	Easting	Northing
186	Point	2	2	261893.807	1990478.159
187	Point	2	1	264753.807	1990378.159
188	Point	2	2	261298.807	1990218.159
189	Point	2	2	265478.807	1990013.159
190	Point	2	2	262988.807	1989738.159
191	Point	2	2	263933.807	1989723.159
192	Point	2	2	260688.807	1989558.159
193	Point	2	2	261153.807	1989373.159
194	Point	2	2	265688.807	1994313.159
195	Point	2	2	268233.807	1994188.159
196	Point	2	2	266763.807	1993948.159
197	Point	2	2	270458.807	1993903.159
198	Point	2	2	265838.807	1993758.159
199	Point	2	2	269068.807	1993598.159
200	Point	2	2	266508.807	1993448.159
201	Point	2	2	269948.807	1993078.159
202	Point	2	2	266763.807	1992948.159
203	Point	2	2	270088.807	1992868.159
204	Point	2	2	266093.807	1992783.159
205	Point	2	2	267813.807	1992528.159
206	Point	2	2	266478.807	1992458.159
207	Point	2	2	269938.807	1992248.159
208	Point	2	2	266683.807	1991993.159
209	Point	2	2	266098.807	1991853.159
210	Point	2	2	267908.807	1991558.159
211	Point	2	2	267133.807	1991303.159
212	Point	2	2	267218.807	1991183.159
213	Point	2	2	266043.807	1991098.159
214	Point	2	2	268083.807	1990943.159
215	Point	2	2	268883.807	1990868.159
216	Point	2	2	267268.807	1990623.159
217	Point	2	2	267213.807	1990428.159
218	Point	2	2	269213.807	1990288.159
219	Point	2	2	267413.807	1990053.159
220	Point	2	2	266393.807	1989918.159
221	Point	2	2	267308.807	1989723.159
222	Point	1	2	248618.807	1989153.159
223	Point	2	2	249488.807	1989088.159
224	Point	2	2	247653.807	1988953.159
225	Point	2	2	249963.807	1988933.159
226	Point	2	2	249358.807	1988853.159
227	Point	2	2	249433.807	1988648.159
228	Point	2	2	250183.807	1988103.159
229	Point	2	2	248068.807	1987778.159
230	Point	2	2	247453.807	1987568.159
231	Point	2	2	249308.807	1987498.159
232	Point	2	2	247348.807	1987378.159

FID	Shape	Classified	Ground Truth	Easting	Northing
233	Point	2	2	248048.807	1987178.159
234	Point	1	2	247163.807	1986908.159
235	Point	2	2	249753.807	1986893.159
236	Point	2	2	248853.807	1986728.159
237	Point	2	2	248588.807	1986458.159
238	Point	2	2	246423.807	1986113.159
239	Point	2	2	246228.807	1985678.159
240	Point	2	2	248028.807	1985533.159
241	Point	2	1	247678.807	1985473.159
242	Point	1	1	246108.807	1985233.159
243	Point	2	2	249003.807	1985143.159
244	Point	1	1	247223.807	1985078.159
245	Point	2	2	247603.807	1984848.159
246	Point	2	1	249893.807	1984723.159
247	Point	2	2	249043.807	1984538.159
248	Point	2	2	250368.807	1989213.159
249	Point	2	2	253738.807	1989148.159
250	Point	2	2	253028.807	1989078.159
251	Point	2	2	252298.807	1988898.159
252	Point	2	2	253453.807	1988738.159
253	Point	2	2	251488.807	1988583.159
254	Point	2	2	254738.807	1988438.159
255	Point	2	2	251138.807	1988253.159
256	Point	2	2	253868.807	1988023.159
257	Point	2	2	251733.807	1987953.159
258	Point	2	2	250573.807	1987788.159
259	Point	2	1	251488.807	1987608.159
260	Point	2	2	253373.807	1987433.159
261	Point	2	2	253698.807	1987188.159
262	Point	2	2	253058.807	1987098.159
263	Point	2	1	251423.807	1986933.159
264	Point	2	2	252528.807	1986748.159
265	Point	2	2	255168.807	1986543.159
266	Point	2	2	253273.807	1986378.159
267	Point	2	2	250393.807	1986268.159
268	Point	2	2	252798.807	1986093.159
269	Point	2	2	253073.807	1985958.159
270	Point	2	2	251733.807	1985738.159
271	Point	2	2	254793.807	1985513.159
272	Point	2	2	253973.807	1985468.159
273	Point	2	2	252558.807	1985123.159
274	Point	2	1	253528.807	1985083.159
275	Point	2	2	251383.807	1984998.159
276	Point	1	1	251798.807	1984718.159
277	Point	2	1	255313.807	1984718.159
278	Point	2	2	253898.807	1984648.159
279	Point	2	2	252448.807	1984508.159

FID	Shape	Classified	Ground Truth	Easting	Northing
280	Point	2	2	251213.807	1984268.159
281	Point	2	2	255003.807	1984148.159
282	Point	2	2	260368.807	1989083.159
283	Point	2	2	259653.807	1989023.159
284	Point	2	2	256078.807	1988763.159
285	Point	2	2	260123.807	1988703.159
286	Point	2	2	258768.807	1988498.159
287	Point	2	2	257708.807	1988283.159
288	Point	1	2	259703.807	1988283.159
289	Point	2	2	256608.807	1987963.159
290	Point	2	2	259273.807	1987833.159
291	Point	2	2	258843.807	1987813.159
292	Point	2	1	257298.807	1987713.159
293	Point	1	1	259258.807	1987573.159
294	Point	2	2	258298.807	1987433.159
295	Point	2	2	255418.807	1987343.159
296	Point	2	2	259923.807	1987218.159
297	Point	2	2	257763.807	1987008.159
298	Point	2	2	260128.807	1986908.159
299	Point	2	2	259568.807	1986673.159
300	Point	2	1	257438.807	1986628.159
301	Point	2	2	258988.807	1986393.159
302	Point	2	2	258678.807	1986153.159
303	Point	2	2	255668.807	1986048.159
304	Point	2	2	258598.807	1985718.159
305	Point	2	2	259908.807	1985663.159
306	Point	2	2	257678.807	1985483.159
307	Point	2	2	259748.807	1985478.159
308	Point	2	2	255848.807	1985368.159
309	Point	2	2	256978.807	1985188.159
310	Point	2	2	258648.807	1984863.159
311	Point	2	2	260448.807	1984763.159
312	Point	2	2	257923.807	1984658.159
313	Point	2	1	257453.807	1984553.159
314	Point	2	2	262688.807	1989233.159
315	Point	2	2	260558.807	1989158.159
316	Point	2	2	262133.807	1989113.159
317	Point	2	2	263338.807	1989043.159
318	Point	2	2	263603.807	1988848.159
319	Point	2	2	265063.807	1988633.159
320	Point	2	2	264433.807	1988258.159
321	Point	2	2	265043.807	1988243.159
322	Point	2	2	264158.807	1988148.159
323	Point	2	1	265338.807	1988118.159
324	Point	2	2	261283.807	1987668.159
325	Point	2	2	265503.807	1987638.159
326	Point	2	2	260943.807	1987438.159

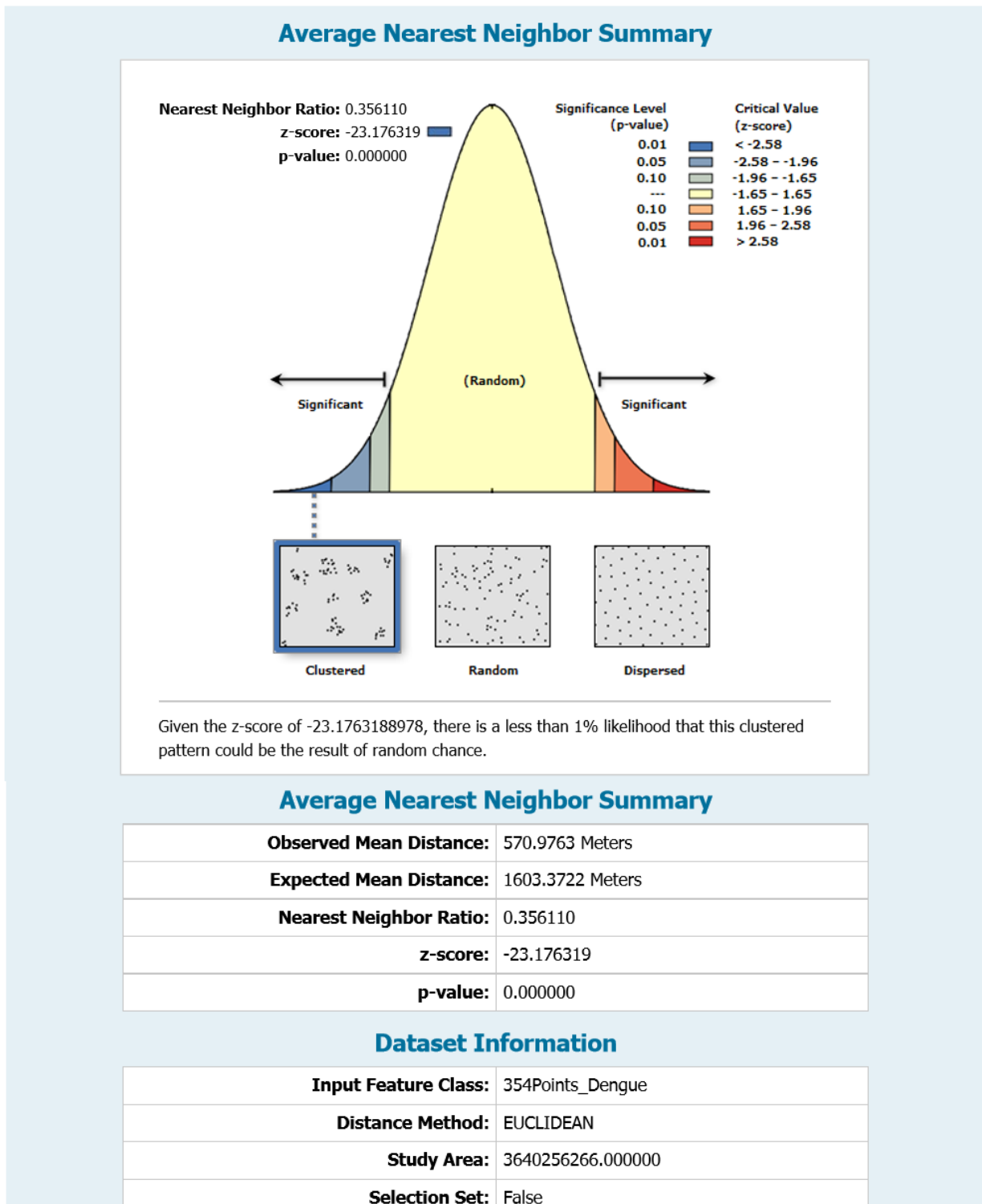
FID	Shape	Classified	Ground Truth	Easting	Northing
327	Point	2	2	264848.807	1987428.159
328	Point	2	2	261978.807	1987358.159
329	Point	2	2	260953.807	1987148.159
330	Point	2	1	264968.807	1987023.159
331	Point	2	2	262333.807	1986798.159
332	Point	2	2	263848.807	1986658.159
333	Point	2	2	261238.807	1986428.159
334	Point	2	2	262723.807	1986293.159
335	Point	2	2	260923.807	1986193.159
336	Point	2	1	265308.807	1986098.159
337	Point	2	2	263583.807	1985963.159
338	Point	2	1	264743.807	1985758.159
339	Point	2	2	261073.807	1985648.159
340	Point	2	2	262438.807	1985498.159
341	Point	2	2	265583.807	1985283.159
342	Point	2	2	261733.807	1985178.159
343	Point	2	2	262113.807	1984993.159
344	Point	2	2	260828.807	1984588.159
345	Point	2	2	263938.807	1984523.159
346	Point	2	2	263163.807	1984383.159
347	Point	1	1	261563.807	1984258.159
348	Point	2	1	264323.807	1984178.159
349	Point	2	2	269658.807	1989063.159
350	Point	2	2	266243.807	1988893.159
351	Point	2	2	268728.807	1988873.159
352	Point	2	2	266808.807	1988718.159
353	Point	2	2	269288.807	1988508.159
354	Point	2	2	267508.807	1988253.159
355	Point	2	2	267193.807	1988023.159
356	Point	2	2	266833.807	1987753.159
357	Point	2	2	267048.807	1987438.159
358	Point	2	2	266833.807	1987383.159
359	Point	2	2	267028.807	1987228.159
360	Point	2	1	268898.807	1986993.159
361	Point	2	2	266273.807	1986823.159
362	Point	2	1	269108.807	1986218.159
363	Point	2	1	268088.807	1986203.159
364	Point	2	2	268238.807	1986133.159
365	Point	2	2	267413.807	1985733.159
366	Point	2	1	266483.807	1985618.159
367	Point	2	2	266103.807	1985323.159
368	Point	1	1	268743.807	1984943.159
369	Point	2	2	268583.807	1984593.159
370	Point	1	1	266713.807	1984503.159
371	Point	2	2	268178.807	1984233.159
372	Point	2	2	246323.807	1984098.159
373	Point	2	2	249458.807	1983788.159

FID	Shape	Classified	Ground Truth	Easting	Northing
374	Point	2	2	248783.807	1983688.159
375	Point	1	1	247188.807	1983538.159
376	Point	2	2	246393.807	1983348.159
377	Point	2	2	246743.807	1983263.159
378	Point	2	2	250163.807	1983098.159
379	Point	2	1	245643.807	1982913.159
380	Point	2	2	248918.807	1982708.159
381	Point	2	2	246733.807	1982348.159
382	Point	1	1	247043.807	1982313.159
383	Point	2	2	246203.807	1982238.159
384	Point	2	2	245828.807	1981998.159
385	Point	2	2	249348.807	1981853.159
386	Point	2	1	248558.807	1981638.159
387	Point	2	2	246633.807	1981418.159
388	Point	1	1	246958.807	1981238.159
389	Point	2	2	247688.807	1980948.159
390	Point	2	2	247433.807	1980773.159
391	Point	2	2	247923.807	1980488.159
392	Point	2	1	248023.807	1980228.159
393	Point	2	2	248188.807	1980223.159
394	Point	1	1	248148.807	1980198.159
395	Point	2	2	248728.807	1980123.159
396	Point	2	2	251238.807	1984028.159
397	Point	2	2	254998.807	1983883.159
398	Point	2	2	255373.807	1983583.159
399	Point	2	2	253238.807	1983573.159
400	Point	2	2	255098.807	1983378.159
401	Point	2	2	253003.807	1983133.159
402	Point	2	2	253878.807	1983113.159
403	Point	2	2	254823.807	1982858.159
404	Point	2	2	254998.807	1982783.159
405	Point	2	2	255228.807	1982498.159
406	Point	2	2	253643.807	1982468.159
407	Point	2	2	253563.807	1982193.159
408	Point	2	2	252643.807	1981848.159
409	Point	2	2	250943.807	1981798.159
410	Point	2	2	252318.807	1981753.159
411	Point	2	2	252138.807	1981618.159
412	Point	2	2	251528.807	1981408.159
413	Point	2	2	253513.807	1981308.159
414	Point	2	2	254718.807	1980998.159
415	Point	2	2	250643.807	1980788.159
416	Point	2	2	255298.807	1980758.159
417	Point	2	2	253923.807	1980628.159
418	Point	1	1	255278.807	1980508.159
419	Point	2	2	253478.807	1980408.159
420	Point	2	2	253998.807	1980363.159

FID	Shape	Classified	Ground Truth	Easting	Northing
421	Point	2	2	253708.807	1980188.159
422	Point	2	2	253358.807	1980018.159
423	Point	2	2	250773.807	1979798.159
424	Point	2	2	251678.807	1979448.159
425	Point	2	2	252158.807	1979423.159
426	Point	2	2	253138.807	1979178.159
427	Point	2	2	259443.807	1984063.159
428	Point	2	2	259208.807	1983918.159
429	Point	2	2	256978.807	1983773.159
430	Point	2	1	256068.807	1983593.159
431	Point	2	2	255883.807	1983428.159
432	Point	2	2	257918.807	1983233.159
433	Point	2	2	260303.807	1983143.159
434	Point	2	2	258788.807	1982878.159
435	Point	2	2	260498.807	1982828.159
436	Point	2	2	257243.807	1982643.159
437	Point	2	2	259618.807	1982513.159
438	Point	1	2	256198.807	1982253.159
439	Point	2	2	256588.807	1982188.159
440	Point	2	2	260058.807	1982173.159
441	Point	2	2	258268.807	1982033.159
442	Point	2	2	256638.807	1981518.159
443	Point	2	2	256378.807	1981353.159
444	Point	2	2	256003.807	1981348.159
445	Point	2	2	258498.807	1981098.159
446	Point	2	2	260203.807	1981068.159
447	Point	2	2	260488.807	1980968.159
448	Point	2	2	256618.807	1980803.159
449	Point	2	2	257733.807	1980773.159
450	Point	2	2	257908.807	1980578.159
451	Point	2	2	258743.807	1980423.159
452	Point	2	2	256948.807	1980288.159
453	Point	2	1	260338.807	1980123.159
454	Point	2	2	256128.807	1979948.159
455	Point	2	2	255583.807	1979768.159
456	Point	2	1	257353.807	1979588.159
457	Point	2	2	257028.807	1979398.159
458	Point	2	2	259608.807	1979238.159
459	Point	2	2	256283.807	1979168.159
460	Point	2	2	262088.807	1984043.159
461	Point	2	1	263783.807	1983898.159
462	Point	2	2	261303.807	1983728.159
463	Point	1	1	264753.807	1983728.159
464	Point	2	2	265268.807	1983513.159
465	Point	2	2	260918.807	1983328.159
466	Point	2	2	262938.807	1983093.159
467	Point	2	2	263023.807	1982958.159

FID	Shape	Classified	Ground Truth	Easting	Northing
468	Point	1	1	264423.807	1982718.159
469	Point	2	2	265553.807	1982718.159
470	Point	2	2	261988.807	1982678.159
471	Point	2	2	260953.807	1982493.159
472	Point	2	2	262673.807	1982223.159
473	Point	2	2	262523.807	1982028.159
474	Point	2	2	264633.807	1981878.159
475	Point	2	2	265568.807	1981773.159
476	Point	2	2	262328.807	1981498.159
477	Point	2	2	262028.807	1981343.159
478	Point	2	2	260698.807	1981133.159
479	Point	1	1	263338.807	1981088.159
480	Point	2	2	263798.807	1980668.159
481	Point	1	1	260773.807	1980578.159
482	Point	2	1	260788.807	1980468.159
483	Point	2	2	262233.807	1980313.159
484	Point	1	1	262103.807	1980073.159
485	Point	2	2	261443.807	1979743.159
486	Point	2	2	262793.807	1979368.159
487	Point	1	1	261273.807	1979238.159
488	Point	1	2	266888.807	1983998.159
489	Point	2	2	267663.807	1983818.159
490	Point	2	2	267873.807	1983618.159
491	Point	2	2	265898.807	1983033.159
492	Point	2	2	265733.807	1982133.159
493	Point	2	2	255323.807	1978683.159
494	Point	1	1	258318.807	1978608.159
495	Point	2	2	259328.807	1978288.159
496	Point	2	2	259278.807	1977863.159
497	Point	2	2	260073.807	1977828.159
498	Point	2	2	261613.807	1978568.159
499	Point	1	2	261363.807	1978148.159

Appendix 6: Average Nearest Neighbour Summary



Appendix 7: Rainfall Data 2017

Date	Jan	Feb	Mar	Apr	May	Jun	Jul	Aug	Sep	Oct	Nov	Dec
1	0.0	0.0	0.0	0.0	0.0	0.0	3.6	0.0	6.4	23.6	0.0	0.0
2	0.0	0.0	0.0	0.0	0.0	0.0	0.0	0.3	0.0	1.3	0.0	0.0
3	0.0	0.0	0.0	0.0	1.7	0.0	22.4	0.0	2.7	3.0	0.0	0.0
4	0.0	0.0	0.0	0.0	1.0	0.0	13.1	0.5	3.4	46.4	0.0	0.0
5	0.0	0.0	0.0	0.0	0.0	0.7	0.0	80.6	0.5	7.6	0.0	0.0
6	0.0	0.0	0.0	0.0	15.5	4.5	2.2	1.0	4.6	13.0	0.2	0.0
7	0.0	0.0	0.0	0.0	0.0	79.7	13.8	1.2	6.8	0.0	0.0	0.0
8	0.0	0.0	0.0	0.0	0.0	0.6	2.9	11.1	0.0	0.0	0.0	0.0
9	0.3	0.0	0.0	0.0	0.0	9.7	0.0	3.8	4.7	0.0	0.0	0.0
10	0.4	0.0	0.0	0.0	0.0	30.4	2.1	0.0	0.0	10.0	0.0	0.0
11	0.0	0.0	0.0	0.0	0.0	0.5	0.2	0.0	0.0	0.0	0.0	0.0
12	0.6	0.0	0.0	15.4	0.0	0.4	5.5	0.0	0.0	9.9	0.0	0.0
13	0.0	0.0	0.0	0.0	3.0	3.9	0.0	0.0	2.4	0.0	0.0	0.0
14	0.0	0.0	0.0	0.0	49.1	1.1	36.2	0.0	0.8	5.0	0.0	0.0
15	0.0	0.0	0.0	82.5	0.0	1.3	2.5	3.0	41.7	10.3	0.0	0.0
16	0.0	0.0	1.0	0.0	22.2	0.0	9.3	54.8	47.1	5.7	0.0	0.0
17	0.0	0.0	20.0	0.0	15.9	0.0	18.7	17.8	7.0	4.9	0.0	0.0
18	0.0	0.0	0.4	0.0	45.2	4.9	2.5	4.0	0.0	0.0	0.0	0.0
19	0.0	0.0	0.0	0.0	0.0	18.3	6.6	26.4	0.0	0.0	0.0	0.0
20	0.0	0.0	0.0	0.0	0.0	0.2	68.0	17.1	0.0	0.0	0.0	0.0
21	0.0	0.0	0.0	0.0	0.0	0.0	17.0	0.0	25.7	0.4	0.0	0.0
22	0.0	0.0	0.0	0.0	30.6	0.0	0.8	0.0	2.6	0.0	0.0	0.0
23	0.0	0.0	0.0	0.0	0.0	1.0	1.0	0.0	0.0	0.0	0.0	0.0
24	0.0	0.0	0.0	7.5	2.1	0.0	0.0	10.3	0.0	0.0	0.0	0.0
25	0.0	0.0	0.0	0.0	0.0	5.8	13.3	9.3	3.3	0.0	0.0	0.0
26	0.0	0.0	35.2	0.0	0.0	19.5	1.8	2.3	0.0	0.0	0.0	13.7
27	0.0	0.0	0.0	0.0	0.0	2.4	15.6	0.0	0.0	0.0	0.0	7.9
28	0.0	0.0	0.0	0.0	0.0	61.0	32.7	26.5	20.6	0.0	0.0	0.0
29	0.0		0.0	0.0	0.0	38.0	17.5	24.2	0.0	0.0	0.0	0.0
30	0.0		14.9	0.0	0.0	0.2	1.2	0.0	0.8	0.0	0.0	0.0
31	0.0		0.0		0.0		0.0	15.7		0.0		0.0
Total	1.3	0.0	71.5	105.4	186.3	284.1	310.5	309.9	181.1	141.1	0.2	21.6
Max	0.6	0.0	35.2	82.5	49.1	79.7	68.0	80.6	47.1	46.4	0.2	13.7

Note: The yellow highlights are the dates of satellite image data acquired in each month